UNIVERSITÀ DEGLI STUDI DI PADOVA

Sede Amministrativa: Università degli Studi di Padova

Dipartimento di Fisica Tecnica

SCUOLA DI DOTTORATO DI RICERCA IN: INGEGNERIA INDUSTRIALE

INDIRIZZO: FISICA TECNICA

XXII CICLO

DEVELOPMENTS IN THERMAL MANAGEMENT FOR ELECTRONIC DEVICES IN AEROSPACE APPLICATIONS

Direttore della Scuola: Ch.mo Prof. Paolo Bariani

Coordinatore d'indirizzo: Ch.mo Prof. Luisa Rossetto

Supervisore: Dott. Ing. Claudio Zilio

Dottorando: Giovanni Schiochet

INDEX

Abstract.....5
Sommario.....7
1 State of the art.....9
1.1 Introduction.....9
1.2 Practical air cooling limit.....11
1.3 Fluids to be considered.....12
1.4 Possible approaches for electronic equipment thermal management.....13
1.5 ARINC 600 specifications.....14
1.6 ITRS prediction for power dissipation and maximum junction temperature.....20
2 New available cooling techniques for thermal management in avionics and in commercial applications.....22
2.1 Introduction.....22
2.2 Natural convection air cooling.....25
2.3 Forced air cooling.....26
2.4 Forced liquid cooling – Cold plates.....28
2.5 Heat pipes.....29
2.6 Immersion into refrigerant liquids.....30
2.7 Jet impingement.....31
2.8 Spray cooling.....32
2.9 Peltier coolers.....33
2.10 Stirling cycle coolers.....34
2.11 Mini vapor cycle systems (VCS).....35
2.12 Recent developments on aircraft cooling architecture.....37
3 Numerical simulation method for mini and micro channel cold plates.....45
3.1 Introduction.....45
3.2 General problem definition.....46
3.3 Elementary section in a cold plate.....51
3.4 Heat flux in the base plate element.....54
3.5 Conduction heat flux through side surfaces between adjacent elements.....55
3.5.1 Base plate.....55
3.5.2 Cover plate element.....57
3.5.3 Internal heat generation.....57
3.5.4 Cover plate convective heat flux.....58
3.6 Channel side walls.....59
3.6.1 General aspects.....59
3.6.2 Shape function.....59
3.6.3 Solution for Euler-Ostrogradskij equation.....61
3.7 Convection heat flux between fluids and plates.....69
3.8 Conductive heat flux between plates and vertical walls.....72
3.9 Total Thermal balance.....74
3.9.1 Gauss-Seidel procedure.....74
3.9.2 Total thermal balance on base plate element.....75
3.9.3 Cover plate cell thermal balance.....79

3.9.4 Composition of a matrix for an entire strip ... 82
3.10 Fluid sub-domain ... 85
3.10.1 General aspects ... 85
3.10.2 Elementary fluid cell ... 85
3.10.3 Convective heat transfer coefficient ... 87
3.10.4 Heat flux contributes ... 90
3.10.5 Heat flux over vertical walls ... 92
3.10.6 Convection over base and cover plate surfaces ... 95
3.10.7 Global thermal balance on a fluid cell ... 97
3.11 Global solution strategy ... 99
4 Fluids candidated to be used in aircraft applications ... 102
4.1 Introduction ... 102
4.2 Single-phase fluids ... 103
4.2.1 Fluid properties ... 103
4.2.2 Heat transfer efficiency factor ... 108
4.2.3 Electrical conductivity ... 110
4.2.4 Corrodibility ... 112
4.2.5 Environmental compatibility ... 112
4.3 Evaporation/boiling cooling ... 115
4.3.1 General aspects ... 115
4.3.2 Fluid selection for boiling/evaporation cooling ... 115
4.3.3 Ultra low-GWP fluids ... 120
5 Numerical simulations for cold plates working with single phase fluids ... 122
5.1 Introduction ... 122
5.2 Heat sinks for micro electronics ... 122
5.3 Numerical simulation for a micro channel heat sink ... 125
5.4 Simulation results – cold plate optimization ... 127
5.5 Simulation results – fluid assessment ... 134
5.6 Channel side walls efficiency ... 142
6 A new two-phase regrigerant proposed ... 146
6.1 Introduction ... 146
6.2 Fluids proposed to substitute R134a ... 147
6.3 Experimental apparatus ... 150
6.4 Test conditions ... 152
6.5 Results and discussion ... 153
Conclusions ... 161
Appendix ... 163
A1 Heat transfer through fins in a fin-and-tube gas-cooler ... 163
A2 Prediction of the mass flow rate of carbon dioxide through capillary tubes in transcritical cycles ... 177
Nomenclature ... 191
References ... 193
Acknowledgements ... 201

ABSTRACT

Recently, the electronic industry has had to face the issue of dissipation of high heat fluxes, as they have increased due to miniaturization of electronics devices, in order to keep chip junction temperature below a fixed value to guarantee reliability and to avoid damage.

This issue has also involved the aeronautics industry, which has for the most part favored air cooling systems; however, they are no longer suitable to meet avionics requirements and thus of power electronics. In fact, as avionics demands higher heat fluxes, power electronics, that is the set of transformers, converters, rectifiers etc., demands higher heat flow rates compared with traditional systems, as a consequence of the current design propensity for substituting hydraulic and pneumatic devices with electric systems, with accompanying increases in generated and transformed electric power in aircraft.

The present work proposes a review of cooling techniques which can be suitable to be employed in high flux electronic components, meeting the requirement for compact cooling systems. The study focuses on cold plate heat exchangers, in consideration of their versatility, moderate cost, and the cooling capacity which can be attained by using these types of systems. Particularly, mini and micro channel cold plates have been investigated, with parallel channel arrangement, which are easy to produce and cost effective, and which can be used both in liquid loops and in mini vapor compression systems, as evaporators.

To allow a careful and proper performance evaluation of such cooling systems, a new simulation model has been developed, as described in detail in the present work, which does not neglect the thermal conduction on the heat exchanger walls (unlike common numerical codes), then allowing a complete evaluation of the temperature profile along the cold plate base, on the surface in contact with the electronic component. Furthermore, this numerical code allows one to properly design cold plates in consideration of both heat flux and the fluid employed. In fact, the present work proposes a review of a large number of fluids, including saline solutions, hydrocarbon and aromatics blends (PAO) and fluorine compounds, both single phase and two phase, which have been considered for electronics cooling purposes, and whose properties have been taken from the open scientific literature or private communications with the manufacturers.

Among all the considered fluids, particular attention has been focused on a new low GWP refrigerant, the hydro flour olefin R1234yf, since it is proposed as a candidate

to substitute R134a in air conditioning systems in the automotive industry. As the more recent developments in the aeronautics industry consider the use of vapor compression systems aboard new aircrafts, mainly for air conditioning purposes but potentially also for electronics, test results are proposed in the present work, relating to several laboratory tests carried out to evaluate air conditioning system performance both with R134a and R1234yf.

Finally, the appendix reports laboratory test results for systems working with carbon dioxide, as it is still considered as a candidate substitute for traditional refrigerants. Two test campaign results are illustrated: in the first one, the thermal conduction effect along fins in a finned coil heat exchanger has been analyzed, and in the second one, capillary tube behavior has been assessed when used as a throttling device.

SOMMARIO

Nel corso degli ultimi anni l'industria dell'elettronica ha dovuto affrontare il problema della dissipazione di elevati flussi termici specifici, aumentati in seguito ai processi di miniaturizzazione che interessano tutti i dispositivi elettronici, in modo da contenere la temperatura dei chip entro limiti che ne garantiscano l'integrità e l'affidabilità.

Tale problema ha pertanto riguardato anche l'industria aeronautica, che fino a questo momento ha privilegiato sistemi di raffreddamento ad aria, attualmente non più in grado di rispondere alle esigenze non solo dell'avionica, ma anche dell'elettronica di potenza. In fatti, se l'avionica impone dei maggiori flussi termici specifici, l'elettronica di potenza, vale a dire il complesso dei sistemi di conversione e distribuzione della potenza elettrica, impone flussi termici complessivi maggiori rispetto a quelli tradizionali, in conseguenza dell'attuale ricerca di un maggior impiego di componenti elettici in sostituzione di quelli idraulici o pneumatici, con conseguente incremento di potenza elettrica generata e trasformata nel velivolo.

Il presente lavoro propone una sintesi delle tecniche di raffreddamento di possibile impiego per componenti elettronici ad alto flusso termico specifico, e che permettono inoltre di ottenere un sistema più compatto, in linea con le esigenze del settore. Particolare rilievo viene dato allo scambiatore di tipo cold plate, per la sua versatilità, il suo costo contenuto, e la capacità di raffreddamento che può essere conseguita con l'uso di tale sistema. In particolare, il tipo di cold plate considerato è a mini o micro canali, disposti e alimentati in parallelo, pertanto di realizzazione piuttosto semplice, e che sono utilizzati sia in sistemi ad anello liquido sia come evaporatori in cicli frigoriferi miniaturizzati. Per consentire una corretta e approfondita valutazione delle prestazioni di questa tipologia di scambiatori, è stato realizzato un modello di simulazione numerica, dettagliatamente descritto nel presente lavoro, che non trascura la conduzione termica lungo le pareti metalliche dello scambiatore, a differenza di quanto accade per i modelli tradizionali, e che pertanto permette di analizzare il profilo di temperatura che si realizza alla base dello scambiatore, vale a dire lungo la superficie di contatto con il componente elettronico. Grazie a questo modello è possibile inoltre eseguire un corretto dimensionamento in considerazione sia dei flussi termici imposti, sia del fluido da utilizzare. Infatti, il presente lavoro propone una vasta rassegna di fluidi, tra cui soluzioni saline, idrocarburi e miscele di composti aromatici (PAO) e composti fluorurati, sia monofase che bifase, presi in esame per il raffreddamento di

elettronica, e le cui principali proprietà sono state ricavate dalla letteratura scientifica o da comunicazioni private con i produttori.

Tra i vari fluidi considerati, è parso importante concentrare l'attenzione su di un nuovo fluido frigorigeno, R1234yf, in quanto candidato a sostituire R134a nelle applicazioni di condizionamento dell'aria nell'industria automobilistica. Poiché i recenti sviluppi dell'industria aeronautica prevedono l'impiego di cicli frigoriferi a bordo dei nuovi velivoli, utilizzati per il sistema di condizionamento ma potenzialmente anche per elettronica, si è ritenuto opportuno presentare i risultati di laboratorio conseguiti durante un'intensa campagna di prove condotte per valutare le prestazioni di un impianto di condizionamento, in cui è stato impiegato sia R134a sia R1234yf.

In appendice sono riportati infine i risultati conseguiti nello studio di sistemi ad anidride carbonica, fluido tuttora ritenuto potenziale sostituto di refrigeranti tradizionali. In particolare si riportano i risultati conseguiti in due distinte campagne di prove: nella prima è stato esaminato l'effetto della conduzione termica lungo le alette di uno scambiatore ad aria, mentre nella seconda è stato valutato il comportamento di un capillare utilizzato come organo di laminazione.

1 STATE OF THE ART

1.1 Introduction

The diffusion of electronics keeps continuously rising, relating also to the growing need to allow the optimization of plants of several sectors in terms of comfort, safety and consumption by means of complex control and regulation logic.
The integration of such electronic systems over the last decades is a constant effort to miniaturize electronics and to produce microprocessors with higher calculation capabilities and speed.
The problem of cooling electronic devices has been under investigation for years and is now a topical issue. It may represent a critical point to the success of next generation products, and it is one of the most important themes for the development of electronic systems which are to be integrated in sectors characterized by strict safety rules, as are found in the aeronautical industry.
From a technical point of view, the thermal control issue can be tackled by studying and analyzing several techniques to dissipate the thermal load generated by electronic systems, with the objective to contain its temperature within a suitable range to guarantee its integrity, functionality and stability of electrical output.
One of the most widespread techniques is to reject thermal fluxes directly to the ambient air, as is done in most consumer electronic appliances. This choice is certainly the cheapest among all the possibilities, and it is also very reliable, when the specific thermal flux is low. As for many appliances, natural convection could be considered suitable to guarantee a correct thermal flux, while other systems requires larger and enhanced surfaces, and also a higher heat transfer coefficient, thus imposing forced convection.
Anyway, in those cases characterized by higher specific thermal flux, air is not a suitable fluid mainly because of its low density and thus low specific mass flow achievable. Higher thermal capacity fluids need to be considered.
Single phase liquid or two-phase fluids could provide higher heat transfer coefficients, but several issues need to be considered, like the architecture to be adopted (which is more complex than simple fans used with air systems), economic matters about the system and fluid itself, reliability, integrability, and finally the system weight, which may present a problem in those devices projected to be as light as possible, such as laptops, or appliances for aircraft, where a higher mass means higher fuel consumption.

Several architectures need to be considered, both for single phase and for two phase fluids. Obviously fluids and architectures can be separately analyzed, but they have to be considered together to rank the solutions proposed for a particular device.
In 1986, the U.S. National Science Foundation organized a 3-day meeting to discuss "Research needs in electronic cooling". One of the purposes of the meeting was to identify areas of future research having the greatest potential to advance cooling technologies.
According to Incropera (1999), "at the workshop, considerable attention was given to air cooling, which was the predominant option of the day, and to identifying research initiatives that would enhance its efficacy". There was also recognition that very large scale integrated (VLSI) circuits would continue to become denser and faster, increasing power dissipation on a single chip and also, in cluster configurations, at a system level.
That workshop provided a "road map" for future research on the subject, and made distinction between single-phase liquid cooling and phase change cooling, and also between direct and indirect cooling, i.e. contact between liquid coolant and electronics is respectively permitted or not allowed.
Anyway, in the following years, some trends imposed themselves and inhibited diffusion of liquid cooling:

1) replacing of bipolar technologies with complementary metal oxide semiconductor (CMOS) devices, extending the applicability of air cooling and diminish incentives to seek alternatives (as illustrated in figure 1.1)
2) an intensely competitive market for electronic products and the attendant need to minimize production costs.

Nevertheless, miniaturization of electronic components is required to increase opportunities of implementation of such devices in several fields, higher heat flux needs to be rejected, therefore liquid cooling could be the only solution to guarantee a correct temperature field in particular systems.

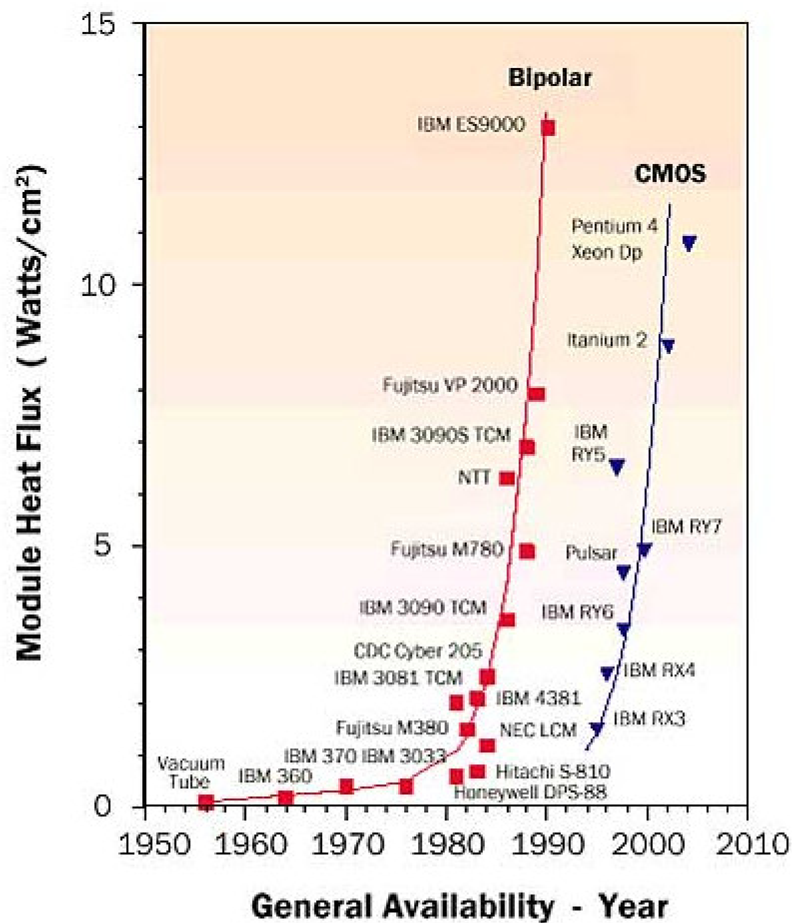

Fig. 1.1- Evolution of module level heat flux (Ellsworth et al., 2005)

1.2 Practical air cooling limit

Even if liquid cooling might be mandatory for certain applications, in order to allow more sophisticated electronic packages to be used, air remains the cheapest way to cool electronics. The matter is to understand when air cooling is no longer possible and thus liquid cooling needs to be adopted.

The air-cooling limit depends on a large number of factors:

- package configuration
- the desired chip temperature
- cooling air temperature
- volume available for a heat sink
- air flow and pressure drop available

- acoustic constraints
- cost of electronic device
- other factors.

It is clear that there is not a single answer to the question of when air cooling is no longer sustainable, since most of the time each single situation can be faced both with air cooling and liquid cooling.
What an engineer involved in designing these products can do is to evaluate what each solution implies in terms of reliability, noise, cost, volume and weight constraints, and thus there is the need to carry out accurate analyses of the heat exchanger which could be used.
Also, modeling of the heat exchanger can unequivocally provide a means to rank a list of fluids from a heat exchanging point of view.

1.3 Fluids to be considered

When considering the possibility of using liquid cooling systems, the designing process cannot refrain from considering several factors beyond thermophysical properties of a fluid.
Among factors to be taken into account are:

- toxicity
- flammability
- corrosion – compatibility with materials
- electric conductivity
- environmental aspects
- temperature at which the fluid will be subjected
- availability
- cost.

As it is for air cooling limits, there is not a single answer and each case needs to be carefully analyzed, in order to understand which factors may represent constraints in choosing the fluid.
Besides non-flammability and non-toxicity, which are mandatory features for most applications, environmental respect is definitely one of the most important issues to be

evaluated, since national regulations could forbid the use of fluids which don't meet requirements of low GWP, as is happening in automotive applications per European regulations. In particular, the European Union's F-gas regulations specify beginning on January 1, 2011 new models and January 1, 2017 new vehicles fitted with air cooling conditioning cannot be manufactured with fluorinated greenhouse gases having GWPs greater than 150.
The foregoing considerations lead to the need of evaluating the thermophysical properties of new refrigerants and their features in terms of efficiency and cooling capacity as drop in.

1.4 Possible approaches for electronic equipment thermal management

Avionics is one of the clearest examples of application in which heat flux is exceeding air cooling capacity, according to a general agreement in the scientific community, considering the available cooling area, air flow rate, fan power and noise constraints.
To understand the state of the art in avionics, and also to know airline goals, the standards published by ARINC are to be considered. Aeronautical Radio, Inc. (ARINC) is a privately-owned company (by major airlines and aircraft operators) dealing with the communications needs of the aeronautics industry. ARINC supports aviation industry committees and participates in related industry activities that benefit aviation at large by providing technical leadership and guidance and frequency management. The main objectives are to promote safety, efficiency, regularity, and cost-effectiveness in aircraft operations.

The Airlines Electronic Engineering Committee (AEEC) is an international body of airline technical professionals that leads the development of technical standards for airborne electronic equipment. The AEEC establishes consensus-based, voluntary form, fit, function, and interface standards that are published by ARINC and are known as ARINC Standards. ARINC Standards allow avionics interchangeability, and reduce avionics cost by promoting competition.
There are three classes of ARINC Standards:

A) ARINC Characteristics – Define the form, fit, function, and interfaces of avionics and other airline electronic equipment.

B) ARINC Specifications – Principally used to define either the physical packaging or mounting of avionics equipment, data communication standards, or a high-level computer language;

C) ARINC Reports – Guidelines or general information found by the airlines to be good practices, often related to avionics maintenance and support.

Since equipment described by ARINC is defined by shape, fit, function, and interfaces, they can actually be quickly replaced in case of failure by components stocked in inventory, at the flightline or airport ramp area. These devices are the so-called "LRUs", i.e. line replaceable units, and are treated by the end user as sealed black boxes, thanks to their interchangeability, as they are designed to common specifications. Electronic equipment is therefore included in a standard housing, the packaging, which assures correct interface with aircraft, both physical and electrical, it protects electronics and it supports handling to be easily replaced during maintenance.
Most of LRUs are defined by ARINC, but they can also be designed according to Boeing, Airbus, and the military.

Fig. 1.2- An ARINC600 packaging

1.5 ARINC 600 specifications

Among all the specifications defined in ARINC 600 (relating to shock, vibrations and accelerations) mainly considers the thermal management of avionics, since it represents more than 60% of stress sources and failure causes. It is a common agreement among avionics supplier that a reduction of 10 °C on the junction temperature is estimated to increase reliability by 50%.
Let us point out some definitions and assessments which will help to better understand how and why the aircraft cooling system architecture is to be modified.

Cooling medium

According to ARINC 600, “the cooling medium should be forced air […] moving through the LRU in the upward direction. The interface between the LRU and the thermal environment provided by the electrical/electronic equipment cooling system is via apertures located on the top and on the bottom surfaces of the LRU. Units which do not require forced air cooling will not have opening on any surface."

The only medium considered by ARINC to provide cooling is air. This solution was actually proper to supply the cooling capacity required by avionics, according to the power dissipation defined in the following, and hot spot issue was already considered a problem to be faced and solved with air cooling. In fact, according to ARINC 600, “the LRU designer must make efficient use of the cooling air supplied to the unit. To this end, internal air distribution systems, baffles, heat exchangers, cold plates, etc., should be judiciously employed to avoid hot spots. Particular attention should be directed to avoiding air leaks that allow coolant to bypass heat transfer surfaces.”

Cooling Air Interface

ARINC defines also how the cooling interface is to be designed. Top and bottom LRU apertures are design to minimize leakage and their location and size is pointed out in tables.

It is worth noticing that ARINC advises to screen cooling openings in order to avoid falling debris from passing through the interface. This is not a problem when using liquid cooling, where the system would be completely sealed. Even at the time ARINC published this document, some airlines expressed the desire for a top plenum, in order to enable an easy transition to a closed loop cooling architecture, yet based on air flowing.

It should also be noted that humidity and dust are consider to be relevant causes of failure, and thus a close loop is a more reliable solution.

Power Dissipation

Table 1.1, with limits for power dissipation, is given by ARINC, relating to the modular size.

Tab. 1.1- Limits for power dissipation according to ARINC600

LRU CASE SIZE (MCU = modular concept units, with fixed dimension)	MAX. PERMISSIBLE POWER DISSIPATION (WATTS)	MAX. PERMISSIBLE POWER DISSIPATION FOR EQUIPMENT WITHOUT COOLING OPENINGS (WATTS)
1 MCU	25	7
2 MCU	50	10
3 MCU	75	12
4 MCU	100	15
5 MCU	125	17
6 MCU	150	20
7 MCU	175	22
8 MCU	200	25
9 MCU	225	27
10 MCU	250	30
11 MCU	275	32
12 MCU	300	35

Electronic Part

"An electronic part […] is defined as an item not subject to further disassembly which is utilized in the fabrication of avionics equipment. For example: resistors, capacitors, filters, circuit breakers, switches, connectors (electrical), relays, coils, transformers, piezoelectric crystals, electron tubes, transistors, diodes, microcircuits, waveguides, synchros and resolvers."

Temperature Critical Parts

"Temperature-critical parts are electronic parts, whose surface temperatures are most likely to approach their maximum allowable temperature."

Maximum Steady State Heat Dissipation

"Maximum steady-state Heat Dissipation is the condition wherein the equipment is operated at the duty cycle which will yield the maximum heat dissipation (at rated voltage level)."

Ambient Temperature

"Ambient Temperature is the air temperature immediately surrounding the equipment rack."

Thermal Design Condition

"The Thermal Design Condition is the environmental and electrical operating mode to be used as the basic design condition for the equipment (not a worst case condition)." For avionics, "the Thermal Design Condition represents normal ground operation of the equipment as installed in the aircraft. For the test and design computational purposes herein, the Thermal Design Condition is defined as follows:

a. Equipment in the steady state thermal condition
b. Equipment in the electrical operating mode which will yield the Maximum Steady State Heat Dissipation.
c. Ambient pressure at 101.3 kPa (1013.25 mbar). The local ambient pressure is acceptable provided it is noted in the test report.
d. Ambient temperature […] at 50ºC.
e. Air velocities immediately surrounding the equipment not greater than those caused by air movement due to natural (free) convection effects.
f. Coolant air bulk inlet temperature at 40ºC.
g. Coolant airflow rate at 220 kg/(hr kW) based on actual heat dissipation at condition (b) above.
h. Inlet coolant air relative humidity not greater than 40%.
i. For test purposes, the equipment should be located in surrounding and supporting structure which stimulates a standard for in-service usage including adjacent units with surface temperatures of 60ºC and minimum emissivities of 0.85."

Electronic Part Application

To meet electro/thermal stress level requirements considering desired performance and reliability, electronic part temperature should be limited as follows:

a. "Electronic part temperatures for any anticipated operational mode should not exceed the component manufacturer's absolute maximum operating curve. (This temperature limit is usually expressed as a function of power dissipation but it may be a function of voltage, current, or other parameter of operation or combination thereof.) Anticipated operational modes include the start-up transient following a high temperature soak, the high continuous operating temperature, and continuous operation at reduced coolant flow. It is expected that all of these conditions may be encountered during the equipment lifetime but they do not represent normal operations and therefore are not the basis for a conventional reliability assessment. However, the probability of occurrence is considered high enough that electronic parts should be able to survive these

operating conditions without a drastic reduction of equipment life (as would be expected to occur when the component manufacturer's absolute maximum is exceeded).

b. During normal ground operation of equipment, defined by the Thermal Design Condition, Electronic Part temperature should not exceed a limit determined by the reliability number apportioned to that part based on the reliability number assessed against the equipment."

Finally, it should be noted that "part temperature" actually means part surface temperature and that measurement or calculation should relate to surface temperatures and not internal operating temperatures.

Coolant Air Flow Rate

"Cooling air is to be supplied to each equipment in proportion to the equipment's Steady State Heat Dissipation. The design air flow rate should 220 kg/(hr kW) at sea level. When the inlet cooling air temperature can be reduced, in ground or flight operation, the airflow rate can be expected to be reduced proportionally down to a minimum airflow rate of 136 kg/(hr kW) at a coolant air inlet temperature of 30ºC.

The use of internal blowers in equipment is not encouraged. When blowers are provided to meet the needs of non ARINC 600 cooled installations, then blower power should be wired through a separate pin on the rear connector. When such equipment is used in ARINC 600 cooled installations, the tray orifice should be sized to allow the standard airflow rate and power normally should not be provided for the blower." Furthermore, internal blowers could cause problems to adjacent LRUs, decreasing their airflow.

"The pressure drop at the design flow rate from inlet to exhaust must be 50 ±30 Pa (5 ±3mm of water) for 'Level 1' LRUs and 250 ± 50 Pa (25 ± 5mm of water) for "Level 2" LRUs under standard conditions 101.3 k Pa."

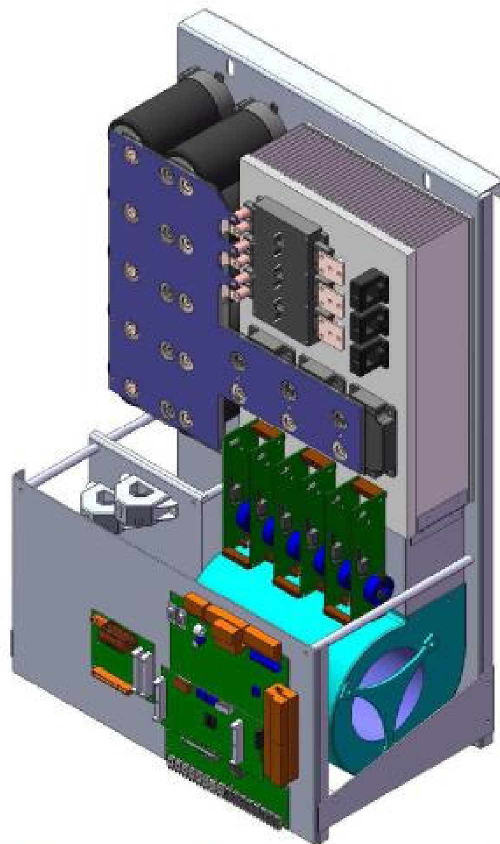

Fig. 1.3 Power part with internal blower

Thermal Interface Information

The following information should be supplied with the Equipment Installation and Control Drawing:

a. Total wattage input and actual heat dissipation for all modes of electrical operation for which the equipment was designed; e.g., standby, receiving, transmitting, etc.
b. Estimated in-flight and ground maximum duty cycle (when specified in the ARINC Characteristic)
c. Pressure drop through the unit in mm of water when the inlet coolant pressure is 101.3 kPa and,

1. Coolant inlet temperature is 40ºC at a flow rate of 220 kg/(hr kW)
2. Coolant inlet temperature is 30ºC at a flow rate of 136 kg/(hr kW)

Finally, also air quality is defined, in order to prevent detrimental effects on the life of avionics, and a centralized air cooling system is acceptable. Starting from the mentioned ARINC 600 specifications, the reader can easily figure that in case of an architecture

using liquid closed loop system, using cold plate as heat exchanger, there is no contact between the fluid and the electronics, and this can increase the reliability of the avionics. Furthermore, coolant mass flow rate can be set by valves, using just one pump for the whole electronic devices, allowing a great volume reduction and again an increase in reliability, since there is no need for individual blowers.

Another problem with air cooling could be represented by harsh conditions in military applications. In fact, military aircraft could operate unpressurized even at high altitudes, with a great reduction in cooling air availability.

Moreover, new integrated modular avionics present an important issue in terms of heat dissipation, since the latest technology processors impose a triplicate heat generation and hot spot heat to be dissipated more than five times higher than those occurring during the past. Air cooling could hardly ensure effective cooling, and can't assure reliability in the case of loss of cooling.

The International Technology Roadmap for Semiconductors indicated that the heat dissipation rate from a single chip package is expected to reach about 120 W and up to 220 W for a cost-performance and a high-performance single-chip packaging technology, respectively.

Air mass flow should be increased from five to ten times the standard one, fixed by ARINC 600, which is not only impracticable from a thermodynamic point of view, but it also lead to a intolerable noise level.

Therefore, a new liquid architecture could provide the cooling power required and allow a higher standardization level, meeting the needs of several field applications.

1.6 ITRS prediction for power dissipation and maximum junction temperature

The table here reported shows the projected design values for the ambient temperature, maximum junction temperature (the highest semiconductor temperature allowed), and heat dissipation for both cost-performance and high-performance components.

According to the International Technology Roadmap for Semiconductors (ITRS) projections, considering a higher on-chip interconnection level and that the "22 nanometre" (the CMOS process step following 32 nm) is expected to be reached by companies in the 2011–2012, volumetric heat generation rates will approach 3.3×10^4 W/mm^3 within the interconnect. Furthermore, new dielectrics (characterized

by lower thermal conductivity than SiO_2 or Si_3N_4,) are being introduced to reduce the interconnect delay problem, with the effect to amplify the thermal problem of on-chip interconnects.

When air in considered as the coolant medium, the required junction-to-ambient thermal resistance can be easily calculated as the ratio of the temperature difference between junction and air, and the chip thermal dissipation. The higher the thermal resistance, the lower package temperature, then a higher level of reliability (even considering low mechanical stress) and performance.

ITRS recommends to keep a constant junction temperature of 85°C, as reported in tab 1.2, then a lower temperature value can be considered as suitable to guarantee the reliability required.

Tab. 1.2- ITRS prediction (Gurrum et al., 2004)

Year of production	2003	2004	2005	2006	2007	2010	2013	2016
Maximum junction temperature [°C]								
Cost performance	85	85	85	85	85	85	85	85
High performance	85	85	85	85	85	85	85	85
Ambient temperature [°C]								
Cost performance	45	45	45	45	45	45	45	45
High performance	45	45	45	45	45	45	45	45
Power [W]								
Cost performance	81	85	92	98	104	120	138	158
High performance	150	160	170	180	190	218	251	288
Required thermal resistance [°C/W]								
Cost performance	0.49	0.47	0.43	0.41	0.38	0.33	0.29	0.25
High performance	0.27	0.25	0.24	0.22	0.21	0.18	0.16	0.14

2 NEW AVAILABLE COOLING TECHNIQUES FOR THERMAL MANAGEMENT IN AVIONICS AND IN COMMERCIAL APPLICATIONS

2.1 Introduction

In the past avionics and consumer electronics were considered totally different from a thermal management point of view, whereas, nowadays, this issue involves both avionics and consumer electronics in the same way, because of the low air efficacy in cooling the new high heat flux devices, and then cooling techniques developed for aerospace are becoming increasingly relevant to consumer electronics, and vice-versa.

In fact, as the air availability has also driven the development of airborne cooling systems, new compact consumer electronic devices, such as notebook computers, are incompatible with fan cooling systems, because of their constraints in volume and power consumption. Consequently, heat pipes and conduction methods, originally developed to cool avionics, are now common in commercial systems.

Furthermore, the need for low cost systems, even for aircraft applications, push toward a high standardization process, and then synergies between aerospace and other industries, the automotive and consumer electronics industries will be very important in the future, with the aim of using commercial off-the-shelf (COTS) components for different applications.

In this chapter, several cooling techniques are described, in order to provide a synthetic review of thermal management systems beyond “fins & fans”. Several cooling techniques can be suitable to both avionics, power electronics and consumer electronics, and some of them, ordered roughly by increasing cooling effectiveness and complexity, are listed and illustrated in the following:

- Natural convection
- Forced air cooling
- Forced liquid cooling - Cold plates
- Heat pipes
- Immersion into refrigerant liquids
- Jet impingement
- Spray cooling

- Peltier coolers
- Mini vapor cycle systems
- Stirling cycle coolers.

Each cooling method is characterized by advantages and disadvantages, which are to be carefully analyzed to optimize the cooling system for the particular application considered. Often, for most commercial cases, the simplest solution is used since it usually involves the lowest costs, while for aerospace applications the cooling system has also to guarantee a lightweight and reliable solution, with the best choice not necessarily being the cheapest one.

Thermal management techniques can be also conveniently grouped into passive and active. Passive methods, which do not require any input power, tend to be very reliable and relatively easy to implement. However, they are also performance limited and therefore inadequate for many high-power applications.

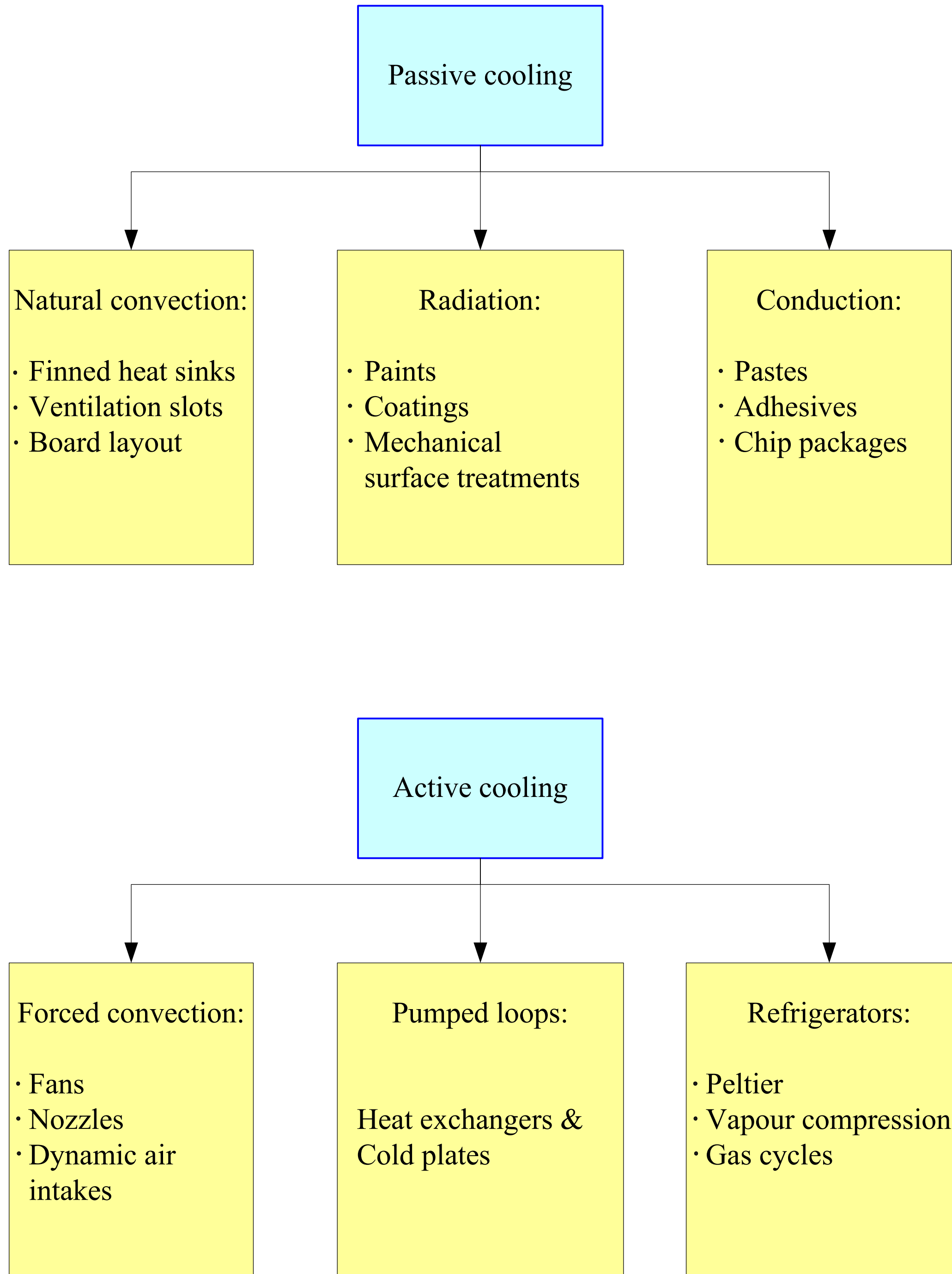

Fig. 2.1- Passive and active cooling methods

Active cooling techniques, which require electric power, provide increased cooling capacity and performance, but are generally more complex since they usually result from miniaturization of thermal management techniques to the micro-scale.

Since air is available on most applications, and it does not require complex and expensive sealing devices, the first techniques described herein refer to air direct cooling systems, also in order to better understand the air cooling limits.

2.2 Natural convection air cooling

A heat sink cooled by air natural convention is the simplest cooling technique, but it also has the lowest effectiveness and very often it is not suitable to meet the thermal management requirement.

To evaluate the heat flux associated with natural convection, the heat transfer coefficient α is to be calculated. The convective heat transfer can be expressed by Newton's law of cooling

$$Q = \alpha A (T_w - T_f) \tag{2.1}$$

where

- Q is the heat flow rate
- α is the heat transfer coefficient
- A is the heat transfer surface
- T_w is the wall-plate temperature
- T_f is the temperature of the surrounding fluid.

The heat transfer coefficient α generally depends on the heat transfer geometry and on the fluid and flow properties. It can be determined by finding the dimensionless Nusselt number according to

$$Nu = \frac{\alpha \cdot L}{k} \tag{2.2}$$

where

- L is the heated plate area divided by the plate circumference

- k the thermal conductivity of the fluid.

When considering a vertical isothermal plate representing the electronic packaging, the Nusselt number can be evaluated using several correlations. For example, it can be expressed as

$$\mathrm{Nu} = \begin{cases} 0.59\,\mathrm{Ra}^{1/4} & \text{for } \mathrm{Ra} < 10^9 \quad \text{laminar flow} \\ 0.138\,\mathrm{Gr}^{0.36}\left(\mathrm{Pr}^{0.175} - 0.55\right) & \text{for } \mathrm{Ra} > 10^9 \quad \text{turbulent flow} \end{cases} \tag{2.3}$$

where

- Ra is the dimensionless Rayleigh number
- Pr is the Prandtl number.
- Gr is the Grashof number

Furthermore, the performance of a possible fin heat sink depends on air density and fin efficiency, when considering an enhanced surface.

2.3 Forced air cooling

Forced convection is realized by air moving devices, such as fans.
Forced air cooling is widespread for many applications since it is a low-cost solution and is generally easily integrated.
In aircrafts, two situations for forced air cooling are possible:

- pressurized and controlled temperature environment
- non-pressurized and non-controlled temperature environment.

In the first case, the air to cool the avionics is taken from a separate environment in which temperature, pressure and humidity are controlled, as for the cockpit or the cabin. In this case, a proper air flow is bled from the total flow directed to the cabin and introduced into the avionics bay. Another choice is to cool the avionics by using the flow discharged from the cabin, in order to enhance the environmental control system efficiency. In these systems air is to be filtered and humidity controlled to avoid dust and moisture on the electronics (in the case there is any surface with a temperature below dew point).

Therefore, to avoid the complications and efficiency penalty introduced, forced air cooling in non pressurized and non temperature controlled compartments is chosen, when it meets the thermal management requirement. In this case, the cooling air, is

directly taken from the outside ambient, and then is blown by a dedicated fan or enters due to the dynamic effect of the flight, through an appropriate intake. Anyway, a few particular situations will be considered. For example, on a warm day, because of the combined effect of the static temperature and of the dynamic increase of the temperature, the air temperature could even be inadequate for the avionics. Another factor to be taken into consideration is the low availability of air associated with the high altitude operation where the air density and corresponding cooling capacity is reduced. An altitude compensating fan running at different speeds for different altitudes should be used, but it does not necessarily completely compensate for the air lower thermal capacitance.

Therefore, even air cooling, which represents the easiest choice, can require a particular caution in designing and optimizing the system.

2.4 Forced liquid cooling – Cold plates

In the present work, a cold plate is considered as a device in which the coolant flows through a circuit embedded in a metal block. The circuit channels could have several shapes and sizes and the fluid could be either single-phase or two-phase, according to the cooling capacity requirement.

The simplest configuration consists of a serpentine pipe embedded in an aluminum block, while for micro electronics cooling cold plate microchannels could be directly fabricated on the backside of the chip to be cooled (Kumari et al., 2007).
Actually, a cold plate is similar to a typical air cooled heat sink, as when rectangular channels are used, the vertical wall separating adjacent channels can be considered as a fin which extends the heat transfer surface. Examples of cold plates are illustrated in figure 2.2. On the left-hand side a simple cold plate is reported, as it consists of a single tube for liquid flow with multi-pass configuration. This solution allows leak-free operation and is associated with good thermal uniformity.
On the right hand side a more complicated cold plate is depicted, as it has brazed fins inside. The fins allow a high heat transfer surface, and a better liquid flow path with optimized thermal distribution, according to the avionics installation.

Furthermore, a cold plate could be the evaporator in a vapor compression cycle or it could be a component of a closed-loop liquid system, in which the fluid is cooled by air or by other loops.

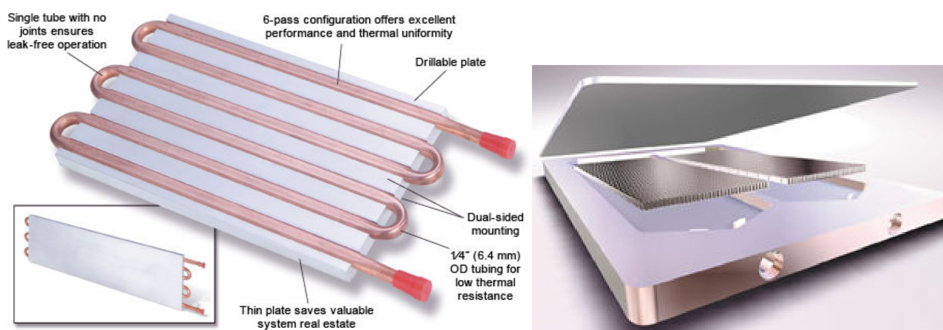

Fig. 2.2- Samples of cold plates

Despite the weight increase due to the fluid and to the piping, compared with air systems, a cold plate system can be more compact and lightweight thanks to the thermal properties of the fluid, such as high heat capacitance and thermal conductivity. Regardless, since a closed liquid loop, which is to be sealed in all situations, is required, the system is more complicated and expensive than a forced air cooling system.

Furthermore, fluids are to be carefully selected since, in case of leaks electronics could be damaged because of low dielectric strength and chemical properties not suitable, as it is anyway in all liquid systems.
A detailed analysis of cold plates was carried out and it is illustrated in the following chapters.

2.5 Heat pipes

The use of heat pipes has become extensive over last years in many electronic devices, such as notebooks and microelectronics. In fact, a remote heat exchanger is often used in order to allow a more compact design. The heat from the processor is transported by the use of heat pipes to the remote heat exchanger, usually an air cooled copper heat sink.

A heat pipe consists of a sealed metal shell, usually cylindrical, whose inner surface is lined with a capillary wicking material. The device is filled with a two-phase fluid, and the heat is removed thanks to evaporating and condensing processes. The liquid-phase, which is distributed along the surface thanks to the wicking material, boils at the hot end zone of the shell, and the vapor generated, because of its higher pressure, moves inside the pipe to the colder end zone, where condensation takes place. The fluid is then subjected to the capillary-driven flow, generating passive recirculation. Heat transfer given by heat pipes is several times higher than the one obtainable by thermal conduction using copper.

The main advantages of this system are its simplicity, the lack of moving parts, no electric power required, absence of noise and compactness. Regardless, it requires a careful design, since the wicking structure geometry is to be optimized in order to provide the required coolant flow rates under different thermal loads.

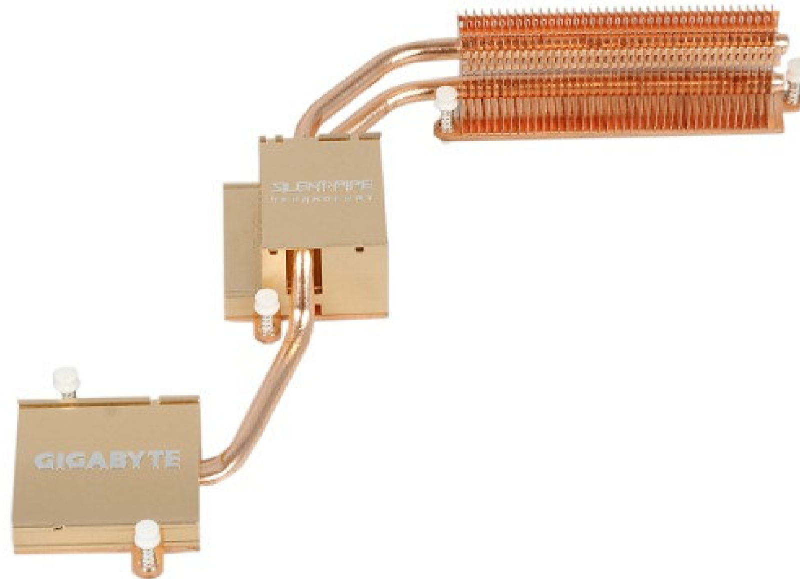

Fig. 2.3- Example of a heat-pipe used in a circuit board with two chips to be cooled

In the avionics environment, other forces than gravity have to be considered, and then careful investigation is to be conducted to understand the device behavior when subjected to strong vibration levels, various accelerations and also different orientations.

2.6 Immersion into refrigerant liquids

Although electronics cooling by direct immersion into boiling fluids had low diffusion in the 1980s and 1990s (for example, it was used in Cray-2 supercomputer), significant knowledge was developed and prospects for future use are good (Incropera, 1999). As a direct liquid cooling technique, the fluid has to be chemically inert, in order to be compatible with the chip package and printed circuit board materials, and its dielectric strength has to be as large as possible to ensure a proper electrical isolation. According to Bar-Cohen (2006), a few possible candidate fluids are reported together with the main properties in table 2.1.

Tab. 2.1- Thermophysical properties of the candidate fluids for direct liquid cooling (Bar-Cohen, 2006)

Fluid		FC-40	FC-72	HFE-7100	HFE-7200	Water
T_{sat}	[°C]	156	56	61	76	100
ρ_l	[kg/m³]	1870	1623	1500	1430	958.8
ρ_v	[kg/m³]	25	12.7	9.6	9.26	0.596
μ_l	[mPa]	3.54	0.457	0.61	0.61	0.279
c_{pl}	[J/(kg K)]	-	1097.8	1180	1210	4217
k_l	[W/(m K)]	-	0.052	-	-	0.68
i_{lv}	[kJ/kg]	711.6	84.8	125.6	122.6	2257
σ_l	[N/m]	0.016	0.0084	0.014	0.014	0.059
P_{cr}	[bar]	11.76	18.4	-	-	22.1

Direct immersion cooling is quite similar to air cooling, where air is substituted by a dielectric fluid, characterized by higher heat removal efficacy and thermal capacitance. In this cooling method both single-phase and two-phase fluids can be used, and fluid can be recirculated by using a pump, or relying upon buoyancy forces, in the case of a passive system, with no pumping power and moving parts. According to Mudawar (2000), surface micro-texturing or extended surfaces should be used in order to increase critical heat flux and to avoid the "incipient pressure drop", namely a sudden temperature decrease of the surface to be cooled which occurs when boiling begins on a surface highly superheated above the fluid saturation temperatures. For example, according to Reeber et al. (1980), bubble nucleation on a polished silicon heater surface in FC-72 was delayed to a surface temperature 46 °C higher than the fluid saturation temperature. According to Mudawar (2000), using surface enhancement allows to reach values as large as 105 W/cm^2 and 160 W/cm^2 in saturated and subcooled FC-72, respectively, compared to only 20 W/cm^2 for a bare surface in saturated FC-72.

2.7 Jet impingement

Jet impingement consists in a coolant single jet or an array of coolant jets directly impinging electronic components (chip packages on printed circuit boards). It could use either a single-phase fluid or a phase change fluid, and can be classified as a free surface or a submerged jet, in the case the ambient in which the fluid is discharged consists of gas or liquid of the same type.

Jet impingement is quite interesting because of the high heat transfer coefficient, thanks to the thin boundary layer, occurring at the impingement surface. Usually it is considered as a direct liquid cooling technique, then no thermal interface materials are to be used thanks to the direct contact between the dielectric liquid and the surface of the chip. Several high heat flux applications have used these cooling techniques, and according to Ing et al. (1993), this method was used in the SS-1 supercomputer, dissipating nearly 90 W/cm^2.

2.8 Spray cooling

Together with jet impingement, spray cooling has attracted the attention of many researchers dealing with high heat flux components. Also this method implies direct contact between fluid and electronics, then the fluid is to be dielectric.

According to Bar-Cohen (2006), spray heat transfer is much more effective than saturated pool boiling, as much higher peak heat fluxes, even several times higher than critical heat flux occurring in saturated pool boiling can be managed. However, spray cooling does require a significant pumping power investment, similar to jet impingement. In fact, it is generally agreed that both spray and jet impingement are characterized by similar heat transfer coefficients, critical heat flux values, and similar pumping power. However, spray cooling results in a more uniform temperature profile on the heater surface (Estes and Mudawar, 1995), which may be very important in order to avoid any thermal stress over chips and circuit boards.

2.9 Peltier coolers

A Peltier element (also called a thermoelectric converter or TEC) is a heat pump based on the Peltier effect, which can be used to cool components below ambient temperature. By applying an electric current, one side of the plate heats up while the other one cools down. The cold side is attached to the heat source while the warm side is to be connected to a heat sink (usually, a forced convection fin heat sink or to any other system to dissipate the heat flow rate coming from the Peltier element).

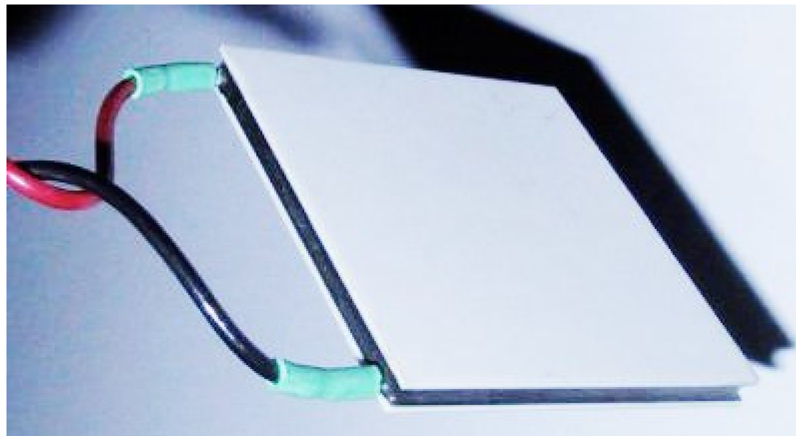

Fig. 2.4- Peltier cooling element

Anyway, a Peltier element introduces a new heat load to be dissipated, as the electric power needed adds to the total thermal load, and therefore the heat sink coupled to a Peltier element results in higher component temperatures than the heat sink by itself. For electronics cooling purposes, there exists very compact Peltier coolers, thanks to recent miniaturization efforts in last years, and as solid-state devices with no moving parts result in high reliability. However, there are some problems related to the Peltier elements to be considered in the design process. Depending on ambient temperature and air humidity, condensation may occur on the cold side (since temperature lower than the ambient one can be reached), which leads to problems on electronic components, and finally, TEC are characterized by a very low efficiency, so electric power consumption and heat flow rate increases.

2.10 Stirling cycle coolers

Microsystem Stirling coolers could offer good prospects for future use in volume-limited applications, such as electronics and avionics, and it also could provide cooling capacity below the ambient temperature.

A Stirling cycle for refrigeration consists of a traditional piston-bore geometry, filled with gas, and a regenerative heat exchanger. The pressure/volume behavior and the temperature-entropy diagrams are illustrated in figure 2.5.

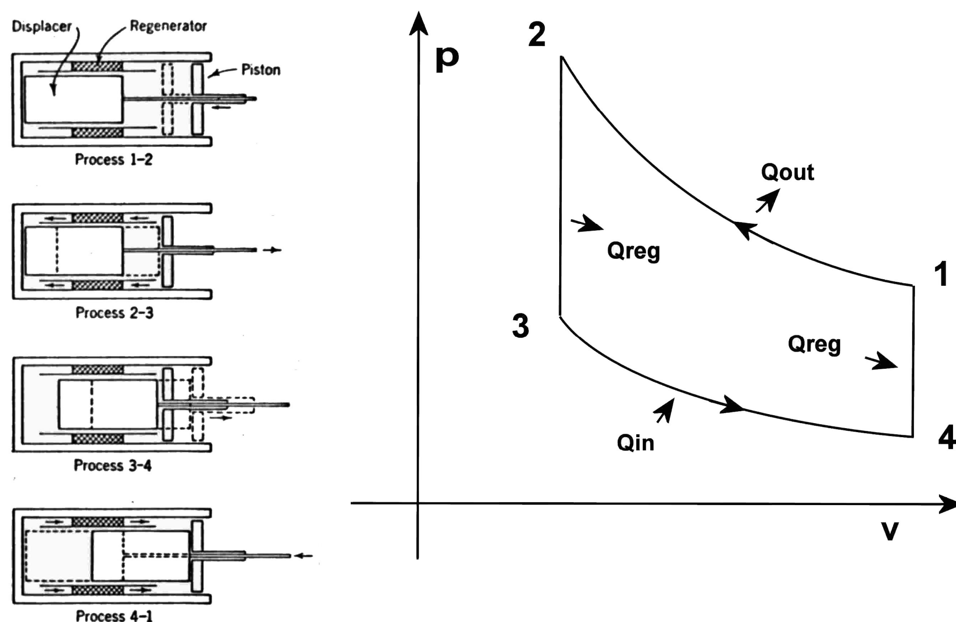

Fig. 2.5- Stirling cycle

Stirling refrigeration cycle has high thermal efficiency, being an order of magnitude higher than thermoelectric.

The Stirling cycle consists of a compression of the gas from state 1 to 2 in an ideally isothermal process, the cooling of the gas in a constant volume process as it is forced through the regenerator into the expansion space (state 2 to 3), the expansion of the gas (state 3 to 4, providing cooling capacity in the expansion zone) in an isothermal process and finally the gas returns to its original state (1) since it is heated in a constant volume process as it is forced back to the compression space through the regenerator.

In NASA Glenn research center (www.grc.nasa.gov) a patented micro system Stirling cooler has been developed for power generation and cooling over the last several decades; more recently they have developed micro systems capabilities initially focused on harsh environments using silicon carbide, and are now expanding to other areas, while development testing and fabrication of a prototype are still in progress at Johns Hopkins University Applied Physics Laboratory.

According to Moran (2004), the NASA system incorporates diaphragm actuators, which replace the pistons found in traditional-scale Stirling machines, to produce the Stirling refrigeration cycle within a planar configuration compatible with the thermal management of electronics. The use of diaphragms should eliminate the frictional losses and bypass leakage associated with pistons (one of the main problems in miniaturization process of the traditional-scale machines) while permitting reversal of the hot and cold sides of the device during operation to allow precise temperature control.

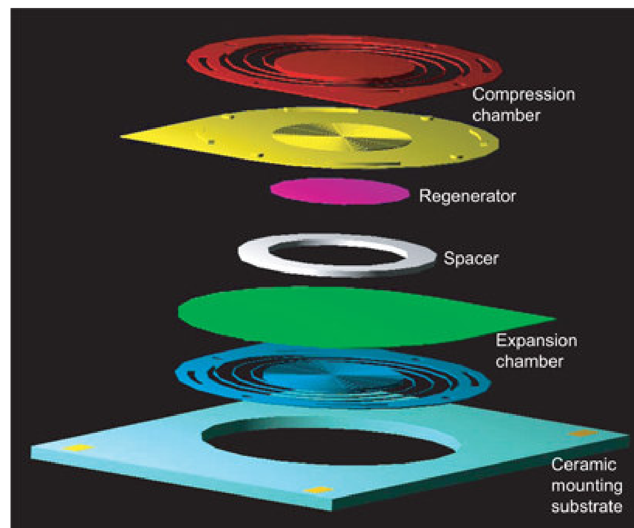

Fig. 2.6- Micro system Stirling machines developed by Nasa (http://www.grc.nasa.gov/WWW/RT/2004/RP/RPY-moran.html)

2.11 Mini vapor cycle systems (VCS)

Since the pioneering work of Scott (1974), researchers have only recently focused on the development of miniature refrigeration vapor cycle system (VCS) for electronics cooling. Trutassanawin et al. (2006) experimentally investigated a miniature refrigeration system obtaining a cooling capacity ranging from 121 to 268 W, with a

COP of 2.8 to 4.7, at pressure ratios of 1.9 to 3.2. The system developed used a microchannel cold plate as the evaporator, and the rotary compressor adopted was a small-scale hermetic reciprocating compressor (Hitachi Model XL0623D) working with R134a. Mongia et al. (2006) developed a small scale refrigeration system based on the vapor compression cycle to be integrated within a notebook computer, using a 12V Embraco compressor and a cold plate as the evaporator, obtaining high thermal efficiencies (COP > 2.25) for temperature rises of interest in mobile applications.
Finally, performance measurements on a prototype miniature rotary compressor were conducted by Sathe et al. (2008). The authors tested an Aspen hermetically sealed rolling piston compressor powered by a 24 V DC, working with R134a, which could potentially be used for electronics cooling applications, obtaining an estimated cooling capacity and a COP vary from 163 W to 489 W and 2.1 to 7.4, respectively.

The use of mini-VCS has proven to be a feasible solution for mobile electronics, but no application of mini-VCS for thermal management of electronics on-board aircraft is available at present, even if large VCS are already used on aircraft and helicopters, for galley cooling and in environmental control systems.

Fig. 2.7- Aspen miniature compressor (Sathe et al., 2008)

Anyway, besides the refrigerating system itself, the cold plate heat exchangers are to be carefully designed in order to provide the required cooling capacity and to be able to control the maximum electronics temperature, as it will detailed in the following chapters.

2.12 Recent developments on aircraft cooling architecture

As the ambient air is no longer a suitable medium to cool electronics, a more complex architecture needs to be designed, in accordance with the cooling techniques adopted. When using wither a liquid fluid or a two-phase fluid, it is to be used a loop, respectively a simple transfer liquid circulation, or a vapor cycle, depending on the cooling power to be supplied and on the temperature level that the user is to be maintained.

In addition to avionics, recent developments in the aeronautical field are leading to a completely new concept in power management aboard aircraft, in order to attain a considerable increase in efficiency, reliability, passenger comfort, together with cost reduction in maintenance and during the flight.

To achieve the foregoing objectives, according to ACARE (Advisory Council for Aeronautics Research in Europe, www.acare4europe.com) strategic agenda, new aircrafts will make extensive use of electrical devices, with substitution of hydraulic actuators by electro-mechanical ones, and new all electric air conditioning system. Therefore, more advanced approaches for power system management are being analyzed, with the aim of producing a new industrial standard for the whole electrical system design, with significant changes to electrical power generation capability and network techniques, as widely illustrated at MOET FORUM in Barcelona (www.eurtd.com/moet/home.html), September 2009.

Electrical components to be newly designed in an all electric aircraft concept can be summarized as follows:

- Electric engine start
- Electro-mechanical actuators
- Power electronics
- Electric wing ice protection
- All electric air conditioning
- ±270V DC power system
- All electric auxiliary power unit (APU)

This more electric technology concept requires a completely new thermal management system, with a full integration between environment temperature control system, avionics cooling, and power electronics cooling, with the possibility to reduce system volumes and noise, increase air quality and avionics reliability.

The most important issues discussed within the MOET project, can be summarized as follows:

- To define new electrical networks (full 230VAC, full +/-270VDC or mixed network for generation and distribution
- To propose all electrical solutions for air conditioning, wing ice protection, cooling and actuation systems
- To point out new installation constraints and opportunities for all the electronic devices.

At the moment, several industries are involved in designing new electrical power generation systems, up to 130 kW in mechanical power in starting mode, with different electrical characteristic, in order to investigate various architectures and possibilities.

According to the general industrial trend all these power generators are meant to be spray cooled with oil, supplied by external management system. However a deep analysis in cooling system standardization is yet to be done, but it appears as a key issue to make maintenance cheaper, and also to the complete integration of the whole thermal management system, with benefits for reliability and saving.

When considering regional aircrafts, business jets and helicopters, air cooling can still represent a suitable solution to provide the cooling needed, especially because the conditioned air can be channeled to electronics before being rejected outside the aircraft. Anyway, power electronic suppliers for this kind of aircrafts agree to evaluate liquid cooling systems as the most important factor to reduce the volume and the weight of the appliances.

Besides new power generation systems, new power converters are necessary to control frequency, voltage and current output.

This kind of power electronics is designed by suppliers to be liquid cooled, via a liquid closed loop, and the choice of the coolant liquid is to be made considering several characteristics, like weight, specific heat and flammability. Heat flux to be removed, coolant mass flow rate and maximum temperature allowed are to be defined by the power electronic suppliers.

The increasing amount of power has to be managed using higher voltage, 230VAC (HVAC) and 540VDC (HVDC), as illustrated by several industries in MOET Forum 2009, as Airbus France, ZODIAC-ECE, Thales Aes etc. This may necessitate using a liquid cooling system which keeps the liquid completely separated from the circuit to be cooled, and then a cold plate solution could represent the proper system to be applied. Industries involved in the production of these electric components did

actually use a liquid cooling system in their tests, thus considering air cooling not suitable and anyway difficult to be integrated in the cooling system architecture.

As mentioned, no bleed air will be anymore available for air conditioning, avoiding pneumatic power offtaken from the engines, and improving the air quality, since incidental presence of VOC would no longer be a problem for the comfort. As a consequence, the environmental control system (ECS) will be one of the largest consumers of electrical power. It will be made of a new stand alone system, and a new power system has to be supplied to drive and control the motorized turbo machined.

An ECS has to supply

- fresh air
- pressurization of the cabin
- temperature and humidity control of the cabin

which are functions related also to safety aspects, besides comfort for passengers.

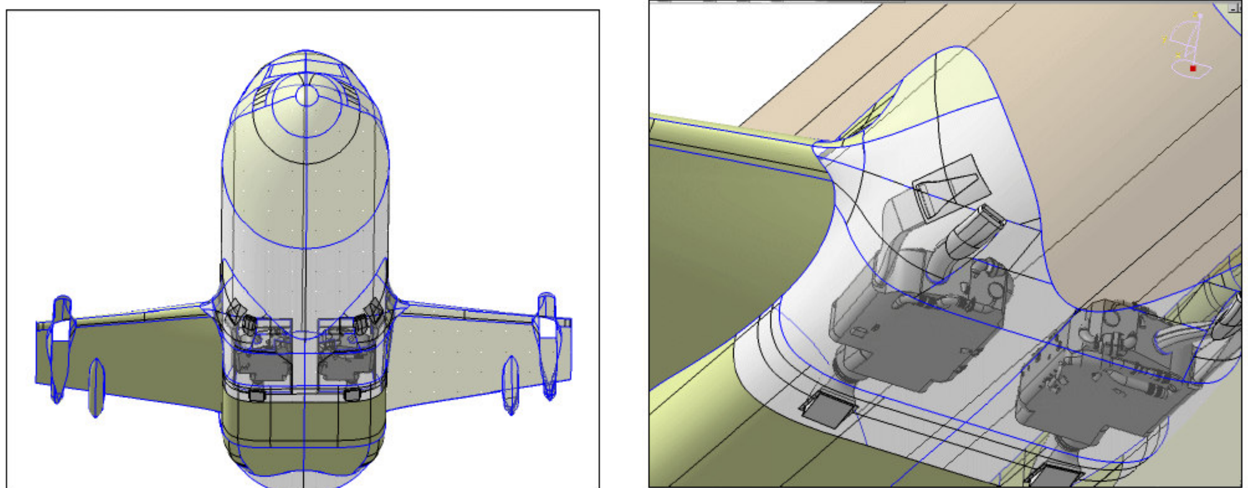

Fig. 2.8- Based pack installation (Galzin et al., MOET forum 2009)

The solution investigated at present consists of a vapor cycle system, while fresh air (needed to provide a suitable comfort) taken from external is as much as possible reduced, in order to decrease power consumption. Anyway, possible system weight increasing is to be taken into account, as well as electrical power offtake from the engines and ram fresh air demand (drag), as thoroughly investigated in POA (Power Optimized Aircraft, 5th Framework Program).

The conventional air system design can be represented as in figures 2.9.

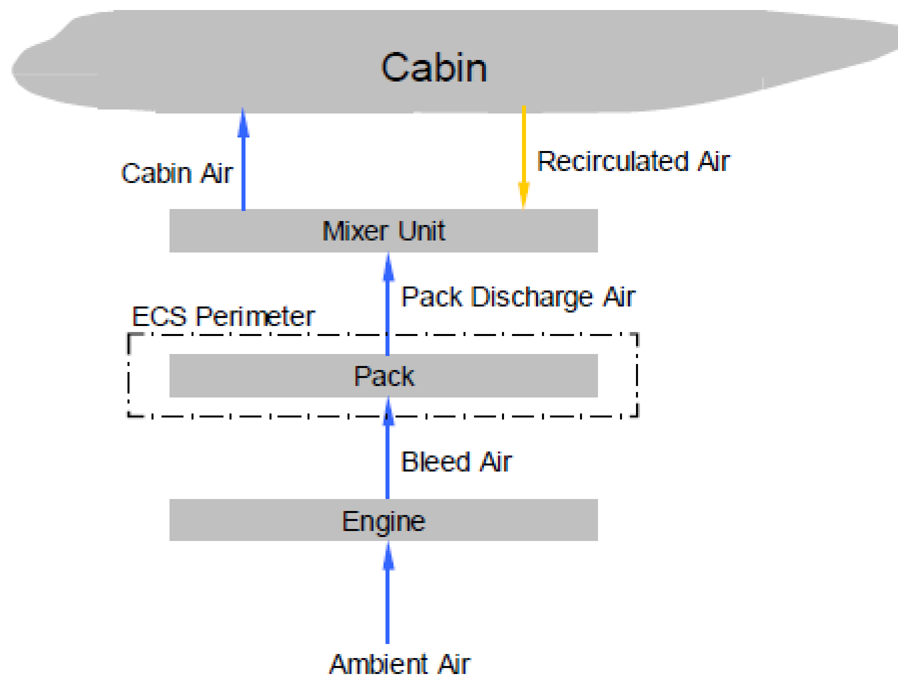

Fig. 2.9- Conventional air system design (Galzin et al., Moet forum 2009)

Since bleed air requires high energy consumptions because it has to be compressed, the first optimization introduced is an additional cooling system (vapor cycle) to manage the thermal load of the recirculated air.

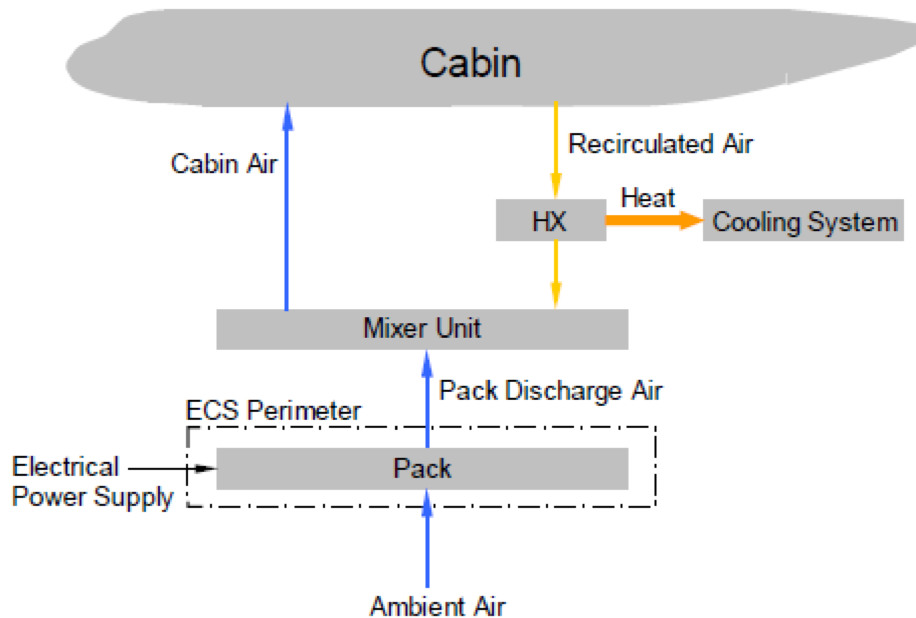

Fig. 2.10- Electrical system design (Galzin et al., Moet forum 2009)

In this electric bleedless air systems architecture, it is worth noticing that besides the electrical pack based on the air cycle technology, there is a vapor cycle system to condition the air extracted by the cabin and to be recirculated. The functions of the pack is the same as for conventional packs, i.e. fresh air supply, cooling and humidity control. It also provides pressurization to the cabin.

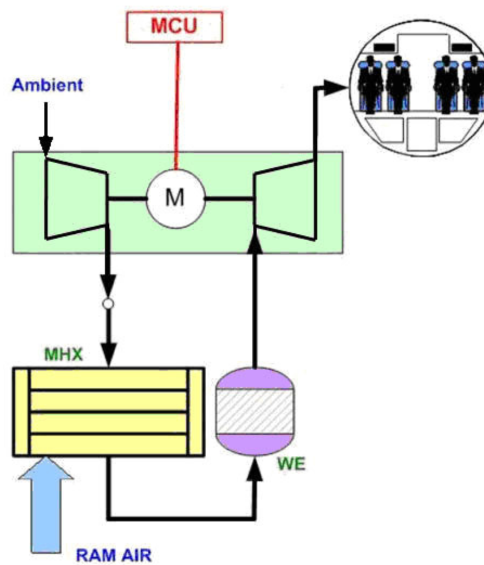

Fig. 2.11- Pack architecture

Referring to the outlined next generation ECS architecture, the function of the vapor cycle is to cool the air which is recirculated. However, it is to be pointed out that VCS is already in use for helicopter ECS and also for galley cooling in large aircrafts (as for A380). Thanks to recent developments in automotive systems, due to the need of replacing the old high GWP refrigerant R134a, technology adaptation could be implemented in the vapor cycle in order to use a new low GWP refrigerant (a hydro-flour-olefin) with competitive efficiency compared to the traditional ones, allowing thus a step forward in the environmental low impact technologies issue. In fact, according to SAE (Society of Automotive Engineers), "HFO-1234yf can be used as the global replacement refrigerant in future mobile air conditioning systems and it can be safely accommodated through established industry standards and practices for vehicle design, engineering, manufacturing, and service".

Designing the cooling system architecture is crucial to ensure saving and effectiveness of the project. It is to be designed in order to supply the cooling required by each electronic device and each generic power electric user, at the correct temperature level, which is quite different depending on the type of user. Specific temperature requirements are illustrated in the figure below:

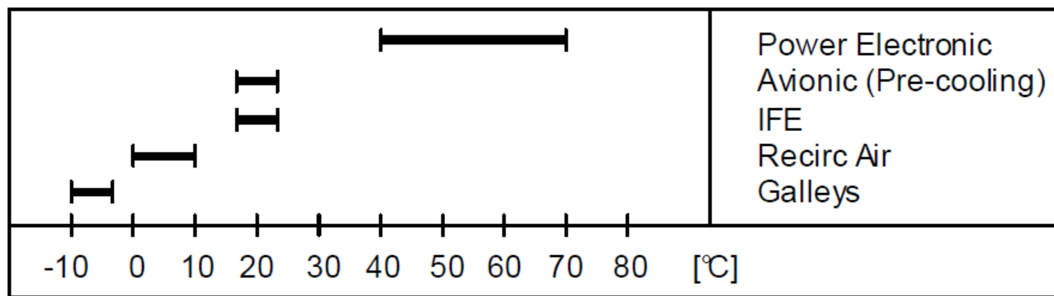

Fig. 2.12- Temperature levels for different users (Skuriat et al. 2009)

Furthermore, design ambient temperature conditions are different depending on the case: 55°C for power electronics and avionics, while for other users it is assumed as being 38°C.

According to Skuriat et al. (2009), the architecture will consist of two different loops: a hot loop to provide power electronic cooling, and a cold loop for all the other consumers.

Depending on reliability and efficiency assessment, galley cooling could be provided by a dedicated air chiller, or it could be served by cold loop.
The two cooling loops will be at different temperature levels.

Since power electronics are cooled with a temperature level higher than that of ambient air, hot loop has to absorb heat flow rate from a high temperature heat source to a lower temperature heat source. Liquid pumps are used to recirculate the coolant in the loop. Temperature is controlled by a 3-way valve for the loop and one control valve for each user.

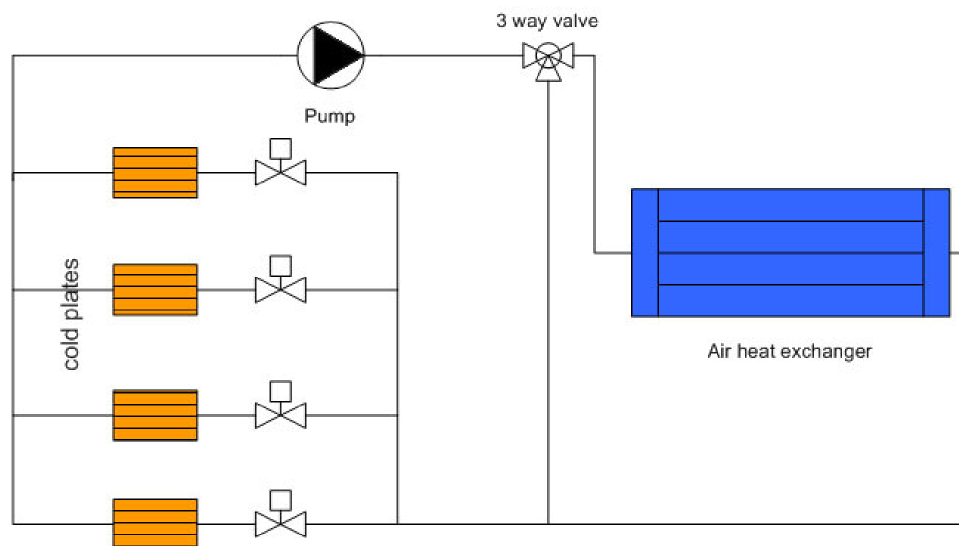

Fig. 2.13- Hot loop scheme

The cooling heat exchangers, the cold plates, are directly placed on power module base plates, interposing a layer of conductive thermal paste to reduce the thermal resistance between the two surfaces.

Liquid coolant can be either a single phase fluid or a two-phase fluid. When single phase is used, the liquid is pressurized in order to avoid any possibility of boiling phenomenon.

As the fluid flows in the heat exchangers (cold plates) to provide cooling power, its temperature increases between inlet and outlet. Therefore heat exchangers should be accurately designed to ensure a homogeneous temperature profile over the cold plates and then to reduce any thermal stress over the electronics.

In the following a numerical model will be described in detail, in order to provide a useful instrument to design and evaluate mini and micro channel cold plates. Furthermore, the numerical code developed allows to evaluate and rank several fluids considering the temperature profile, pressure drop and pumping power.

For cases where two-phase fluids are used as coolants, temperature is almost constant over heat exchangers, as the system is design for “negligible” pressure losses, then temperature difference is higher on average than for single-phase fluid. Moreover heat transfer coefficient during condensation is higher than for single-phase coolant, and therefore heat exchanger could be smaller, allowing a possible weight and volume reduction. However, it is well known that the heat exchanger design optimization should be carried out keeping in mind the conflicting effect of increasing pressure drop and increasing HTC through turbulence promotion. Despite the foregoing positive aspects, dry-out could occur over a hot spot surface, producing a local temperature increase due to a poor heat transfer coefficient. Thus the cold plate is to be carefully designed, so the model proposed in the following could be very helpful in geometry optimization, temperature profile assessment and fluid behavior along the heat exchanger.

According to Skuriat et al. (2009), two-phase fluid solution appears to be more complicated in regulation than single-phase loop, than liquid cooling seems to be more likely in a short-time project.

In relation to what was reported previously, new cooling solutions are to be investigated together with the novel design criteria in avionics, power electronics and other generic electrical users, in order to ensure high integration levels and thus cost reduction and reliability. This work aims at providing assessments and instruments to allow an accurate analysis on heat transfer on high density heat flux components, in agreement with the new design requirements.

3 NUMERICAL SIMULATION METHOD FOR MINI AND MICRO CHANNEL COLD PLATES

3.1 Introduction

It has previously been pointed out how the interest in modelling heat exchangers is increasing, since many applications, from automobiles to aircraft, require compact heat exchangers with large heat transfer surface, in which some effects neglected by classical theory, especially the longitudinal heat conduction on metal parts, can influence their performance. An accurate evaluation of the temperature field over the heat transfer surface is very useful when analyzing electronics cooling systems, as the temperature die can not exceed a threshold value defined by the supplier, in order to assure high reliability and proper component operation.

In this chapter, a new, reliable tool to analyze and simulate cold plate heat exchangers will be illustrated. This instrument was developed in order to design cold plates which could provide the required cooling capacity in general electronics applications and rank various fluids according to their pressure losses and cooling performance.

According to Asinari (2004), who used the same numerical method for a different heat exchanger, the code developed allows a lower computational time than general-purpose codes such as Fluent or Fidap, and furthermore it can be easily integrated in another code to simulate the entire cooling system, of which the cold plate is a part.

In this work, cold plates are intended as devices with a number of rectangular channels arranged in parallel. The interest in this arrangement is primarily the low cost for manufacturing or simplicity in channel machining on the cold plate.

Cold plate analysis is conducted according to the SEWTLE method (semi-explicit method for wall temperature linked equations), recently introduced by Corberan et al. (2001).

It is an iterative method, which allows to accurately model a heat exchanger, of any complexity, in order to calculate both fluid side temperatures and metal side temperatures, and therefore it is appropriate to analyze the temperatures of the interface between a generic cold plate and the electronics laid on it. This method allows de-coupling the metal side behavior and the fluid flowing inside each channel. Thus, for each iteration, the metal side temperatures are calculated on the base of the fluid

temperatures calculated in the previous step, and analogously fluid side temperatures are obtained using the metal side ones calculated in the preceding step.

It has to be pointed out that the analysis carried out with this method aims at evaluating the thermal conduction on the metal side, since it appears relevant to estimate the surface temperature profile of the electronic device to be cooled with microchannel cold plates.

3.2 General problem definition

Most of the solution methods to evaluate a heat exchanger are based on the elimination of the wall temperature from the equations to be solved, when longitudinal conduction is negligible. Wall temperature could finally be calculated when temperatures of fluids adjacent to the wall and heat flux are known.

Since electronics cooling is often characterized by high heat flux areas, namely hot spots, thermal conduction through metal parts becomes very important and thus the elimination of the wall temperature is not possible, and the SEWTLE method is used.

This is a general solution method in which fluid temperatures are only coupled with the global wall temperature field through equation 3.1

$$\Delta\Phi_i = \alpha_i \Delta S_i \left(T_{w,i} - T_{f,i}\right) \tag{3.1}$$

where $\Delta\Phi_i$ is the heat flow rate at a generic element *i* which surface is ΔS_i at a temperature $T_{w,i}$, in contact with a fluid at a temperature $T_{f,i}$ with a heat transfer coefficient α_i. The problem is therefore solving the wall temperature field and then the fluid temperatures can be evaluated integrating equation (3.1). For this reason Corberan et al. (2001) proposed the name of "Wall Temperature Linked Equations (WTLE)".

Assuming to analyze the fluid flow as a single phase 1D steady flow, then the governing equations along a channel of a cold plate are:

$$G = \rho u = constant \tag{3.2}$$

$$\frac{dp}{dx} = -\frac{d\left(\rho u^2\right)}{dx} - f\frac{1}{2}\rho\frac{u^2}{D_h} - \frac{d\left(\rho g z\right)}{dx} \tag{3.3}$$

$$\frac{d\left(i+\frac{u^2}{2}\right)}{dx}\cdot G\cdot A_c = \int_{perimeter}\alpha\ (T_w - T_f)\ dl \tag{3.4}$$

being (3.2) the continuity equation, (3.3) the momentum conservation equation, and (3.4) the energy conservation equation.

In the case of an evaporator, a 2-phase flow with phase change occurs. Separated fluid model is considered, and therefore the governing equations are:

$$G = \rho u = constant \tag{3.5}$$

$$-\frac{dp}{dx} = \frac{2f\cdot G^2(1-x_r)^2}{D_h\rho_l}\Phi_f^2 + G^2\frac{d}{dx}\left(\frac{x_r^2}{\rho_v\cdot\varepsilon_v} + \frac{(1-x_r)^2}{\rho_l\cdot(1-\varepsilon_v)}\right) + \\ + \left(\rho_v\varepsilon_v + \rho_l(1-\varepsilon_v)\right)\cdot g\cdot\sin\vartheta \tag{3.6}$$

$$\frac{\partial}{\partial x}\cdot\left[\left(i_v + \frac{G^2x_r^2}{2\rho_v^2\varepsilon_v^2}\right)\cdot x_r + \left(i_f + \frac{G^2(1-x_r)^2}{2\rho_l^2(1-\varepsilon_v)^2}\right)\cdot(1-x_r)\right]\cdot G\cdot A_c + \\ + \frac{\partial}{\partial x}(g\cdot z\cdot\sin\vartheta)\cdot G\cdot A_c = \int_{perimeter}\alpha\ (T_w - T_f)\ dl \tag{3.7}$$

The continuity equation (3.5) states the conservation of the mass flow rate along each channel. Fluid velocity, or mass flow rate, is given as an input to the code, then G is considered as a known constant in the following analysis. For each fluid cell, two equations are to be considered (energy and momentum), and assuming thermodynamic equilibrium, enthalpy and density both for liquid phase and for vapor phase are linked to the pressure, as it is for temperature which is assumed as the saturation one. Fluid quality can be calculated as the vapor and liquid phase enthalpy are known.

Finally, only void fraction remains to close the system. The equation (3.8) between the void fraction and the rest of the variables is to be added

$$\varepsilon_v = \frac{1}{1 + S\frac{1-x_r}{x_r}\frac{\rho_v}{\rho_l}} \tag{3.8}$$

where S, the slip ratio, is given by empirical correlations which can be found in the literature.

A second system is to be considered to analyze the metal plates and the vertical walls joining them. The general equation evaluating the balance of the heat exchanged in steady state condition with the surrounding fluids and the heat transferred by longitudinal conduction can be written as:

$$\int_{\Omega^S} -\nabla^3\left(k_w \nabla^3 T_w\right) dV = \int_{\Sigma^S} \mathbf{J_i} \bullet \mathbf{n}\, dS \tag{3.9}$$

where Ω^S is the solid metal domain, Σ^S is its border surface, and **J** is the specific thermal flux.

When considering an element with two surfaces in contact with different fluids, the effect of the longitudinal conduction is normally neglected and so the wall energy equation becomes the balance equation for the heat exchanged between fluids, differently from what illustrated in the following.

In order to write the equations already illustrated for the particular case here illustrated, let us point out the scheme adopted for the discretization. Since this method uses the thermal balance as convergence check, a conservative scheme for the discretization of involved equations, the Finite Volume Method (FVM), represents the most natural choice.

The fluid sub-domain is governed by ordinary differential equations characterized by first-order spatial derivative. Referring to the FVM, and considering a 1-D single-phase flow represented by equation (3.2), (3.3), and (3.4), centered grid point, referring to the fluid control volume, can be used and the first derivative are approximated by the corresponding finite-difference expression linking the values at the grid points (Corberan, 2000), applying up-wind techniques.

The base plate and the cover plate (figure 3.1), belonging to the solid domain, are actually analyzed by FVM, and then a control volume with a temperature value defined at its centre represents the easiest way to mesh each sub-domain and the most suitable configuration to evaluate second-order partial spatial derivatives. The

discretization of the Laplacian operator in equation (3.9) can be made by a classical finite difference approach (Corberan, 2000).

Anyway, according to Asinari (2004), in compact heat exchangers FVM could not be the most suitable method referring to wall sub-domain. In fact, to analyze vertical walls also Finite Element Method (FEM) can be used, and it involves a functional to be minimized over each element according to the calculus of variations. The FEM, applied on vertical walls, considers trial continuous temperature profiles as an approximate solution minimizing the functional. Each fin element is marked by four temperature values defined at the border and it is characterized by longitudinal conduction (along the fluid path) and by a detailed temperature profile in the transverse direction, i.e. from base plate to cover plate. As in Asinari (2004), the temperature values are set at the middle of the edges, and not at its corner as usual.

Considering two dimensional conduction and convective heat flux for the fluid, equation (3.9) can be written for a fin element as

$$\int_{\sigma^S} \left[\nabla^2 \left(k_w \nabla^2 T_w \right) s_w - \sum_i \alpha_i \left(T_{w,i} - T_{w,i} \right) \right] dA = 0 \tag{3.10}$$

Assuming the thermal conductivity does not depend on temperature, the resolution of equation (3.10) can be considered equivalent to the minimization of the functional

$$\Pi = \int_{\sigma^S} \left[\frac{1}{2} \left(\nabla^2 T_w \right) \bullet \left(\nabla^2 T_w \right) + \sum_i \frac{\alpha_i}{k_w s_w} \left(T_{w,i} - T_{w,i} \right) T_{w,i} \right] dA \tag{3.11}$$

and the temperature profile which gives the minimum value of the functional can be obtained solving the Euler-Ostrogradskij equation, as it will be thoroughly discussed in the following section (3.6.2).

Finite-volume description for base and cover plates and for fluid, and the finite-element description for vertical walls by means of intrinsically conservative elements can be adopted together with SEWTLE.

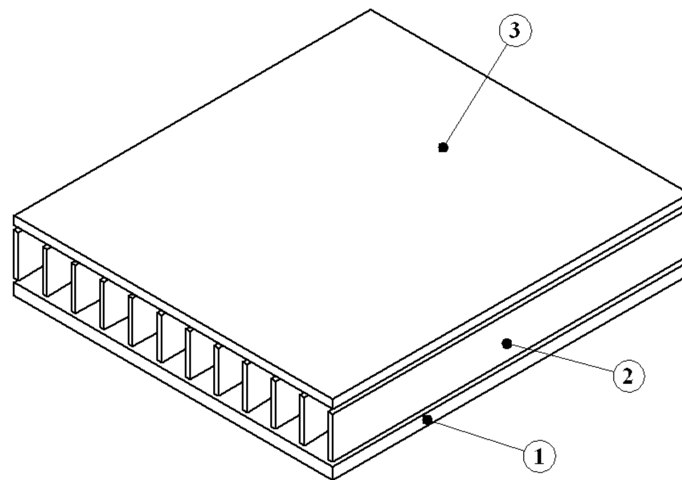

Fig. 3.1- Generic cold plate, 1) base plate; 2) cover plate; 3) fins, or vertical separating walls

3.3 Elementary section in a cold plate

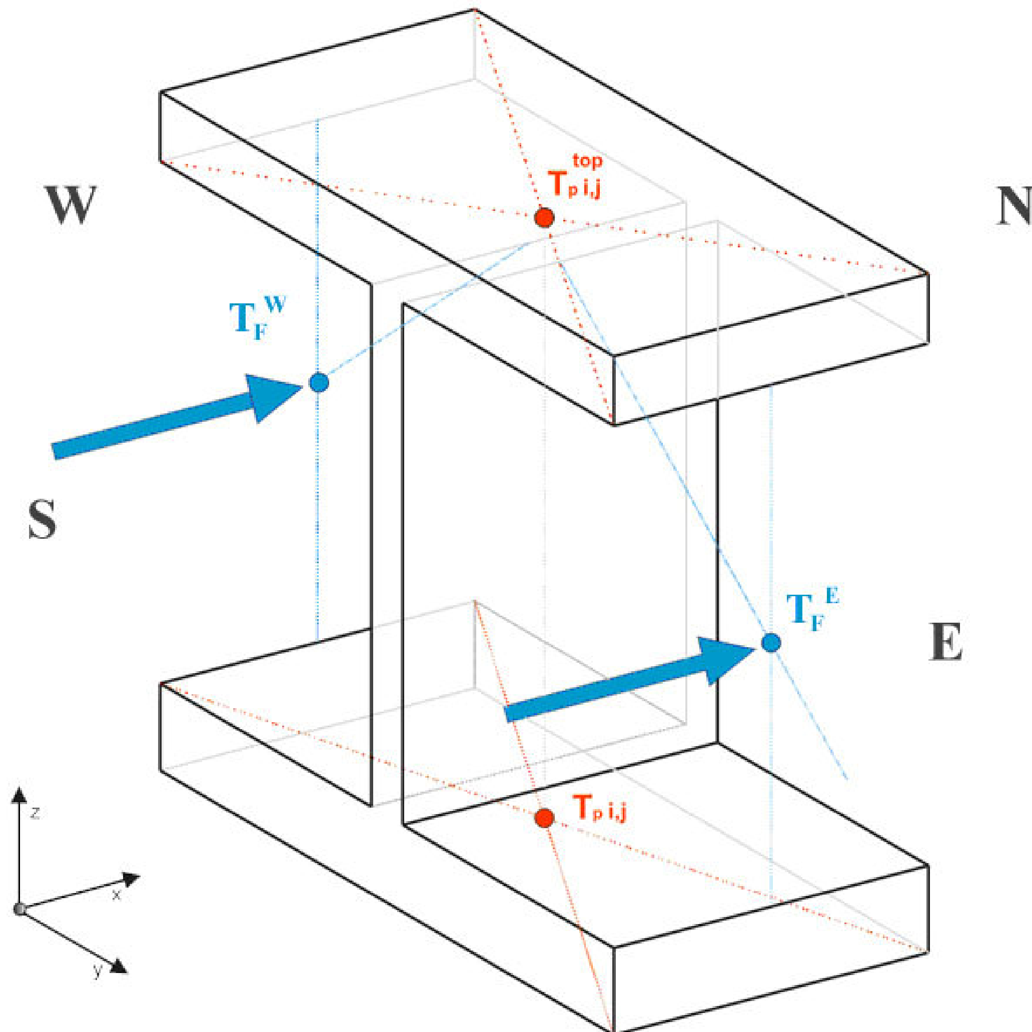

Fig. 3.2- elementary section, made of a base, separating wall and cover

In figure 3.2, it is represented the elementary portion of the cold plate solid sub domain. Placing side by side these elements on the *x-y* plane the entire heat exchanger can be obtained, having a little attention at the left hand side and right hand side edge of the plates, where the HX ends just with the vertical wall. Each element is indeed made of a part belonging to the base plate (in the above figure, it is marked by T_{pij}), a vertical wall, which can be considered as an extension of the plates, and finally a part belonging to the cover (marked with T_{pij}^{TOP}).

The figure illustrates also where the grid points are placed, in particular the red ones refer to the metal surface temperature, and the blue ones refer to the temperature of the two fluid cells coupled to every solid cell by the equations governing the heat flux, i.e. T_F^{EAST} e T_F^{WEST}.

As FVM is employed, fluid grid points are placed at the center of each fluid element and are representative of the whole volume.
The solution, i.e. the temperature field over the heat exchanger, can be obtained by the integration of the governing equations over the whole sub domain.

$$\Omega^{CP} = \Omega^{F} \cup \Omega^{S}$$
$$\Omega^{S} = \Omega^{base} \cup \Omega^{cover} \cup \Omega^{wall} \tag{3.12}$$

Figure 3.3 represents the mesh used for the solid sub-domain. Blue arrows indicate the fluid flow, the broken red line represents a single solid element and finally each grid point shows both base and cover element temperatures.

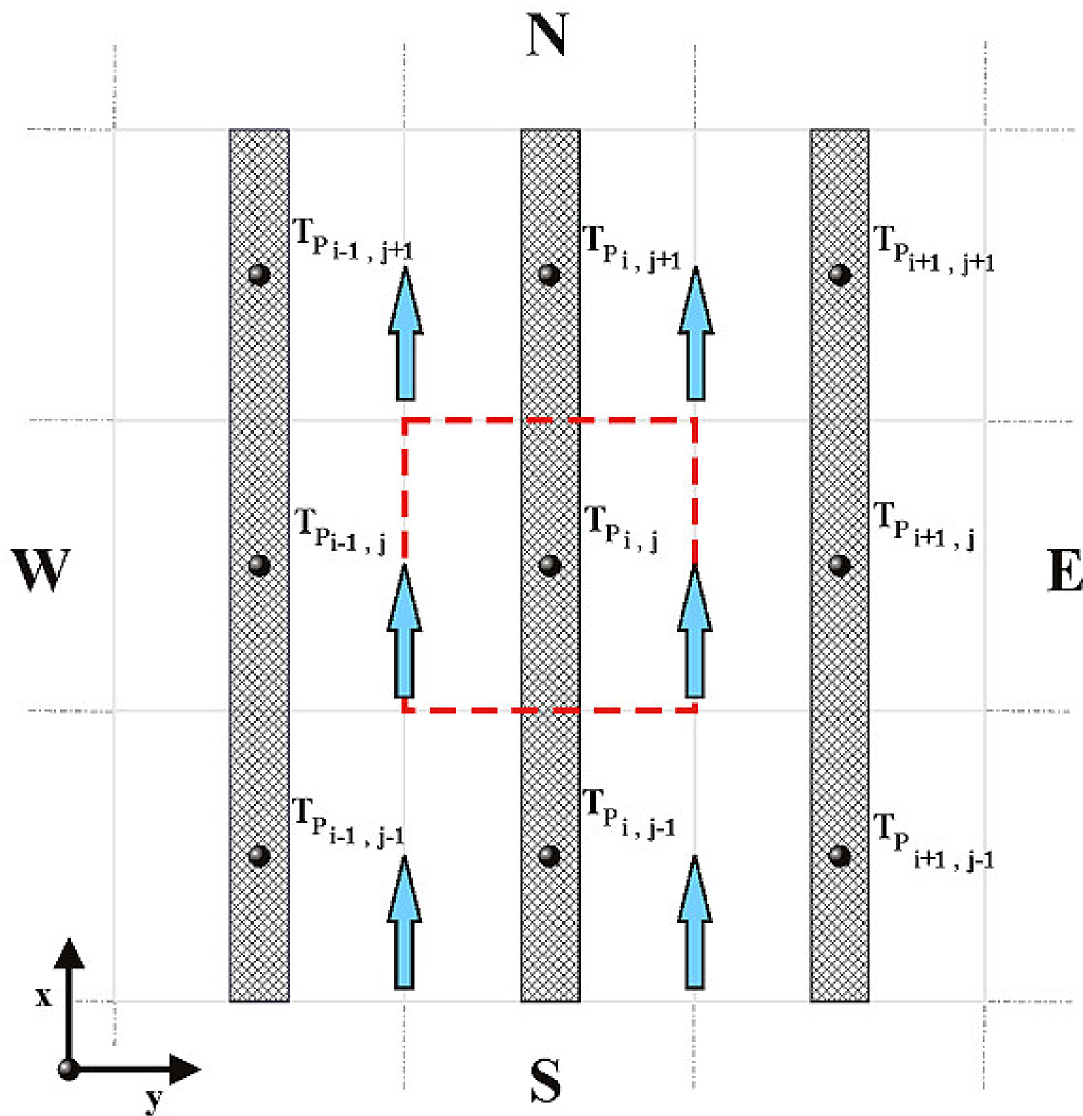

Fig. 3.3- Plan view of solid elementary cell.

Figure 3.4 shows the discretization cell for a generic fin, which has to be characterized by coherent description of thermal fluxes due to longitudinal conduction and by a detailed temperature profile in the transverse direction. It is suitable to locate the temperature values at the middle of the root edges. Finally, when using the proposed element instead of the classic element, it is possible to have two Dirichlet-type boundary conditions and two Neumann-type ones, and therefore the solution temperature profile for the entire fin, give by the Euler-Ostrogradskij equation can be uniquely determined, as will be detailed in the following discussion.

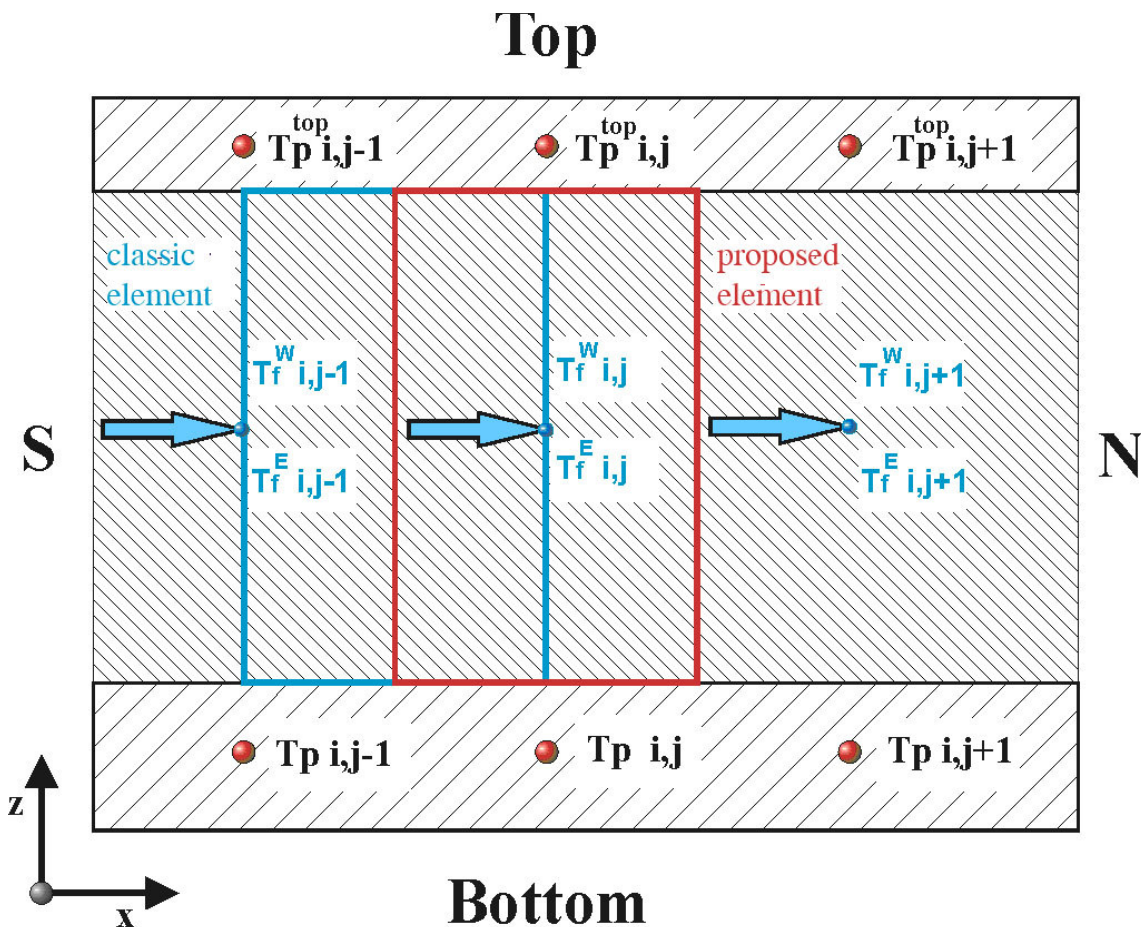

Fig. 3.4- lateral view, comparison between classic element and proposed one

3.4 Heat flux in the base plate element

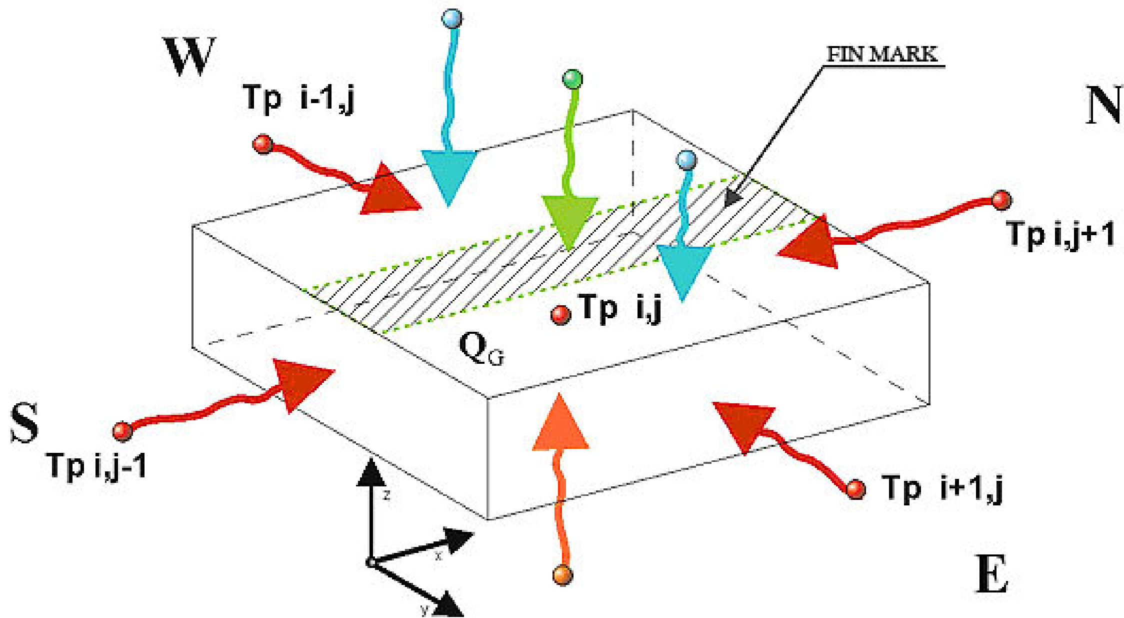

Fig. 3.5- base element and heat fluxes on it

A general base element is represented in figure 3.5. The grid point is located in the center of the volume and it is used to evaluate each heat flux, both with the base elements beside and with fluid cells and with the fin element. Each heat flux in the following equations is considered positive when entering the control volume.

Such figure can be easily adapted even to the cover element, with small differences which will be illustrated in the following. The base temperature will be considered as the bottom fin temperature and the temperature of the cover element will be considered as the temperature at the fin top. Therefore it is possible to solve base and cover temperatures at the same step of calculation, considering the whole elementary section of the cold plate.

From a geometrical point of view, general base element has dimensions Δx, Δy, and Δz, defined respectively as:

$$\Delta x = \frac{L_{COLD\,PLATE}}{N} \tag{3.13}$$

Total HX length by the number of elements each channel is divided (i.e. the distance between the grid point of adjacent elements, considering the N-S direction);

$\Delta y = channel\,width + fin\,thickness$ (i.e. the distance between the grid point of adjacent elements, considering the W-E direction);

and finally

$\Delta z = plate\ thickness$.

In the following heat flux contributes on each surface is reported both for a general base plate element and of a cover plate element.

3.5 Conduction heat flux through side surfaces between adjacent elements

3.5.1 Base plate

Considering figure 3.5, conduction heat fluxes are represented by red arrows, and are due to the temperature difference between the element temperature $Tp_{(i,j)}$ and adjacent elements temperature

- $Tp_{(i,j-1)}$, and $Tp_{(i,j+1)}$ for the thermal conduction respectively with the South element and the North element (according to figure 3.5);
- $Tp_{(i-1,j)}$, and $Tp_{(i+1,j)}$ for the thermal conduction respectively with the West element and the East element (according to 3.5).

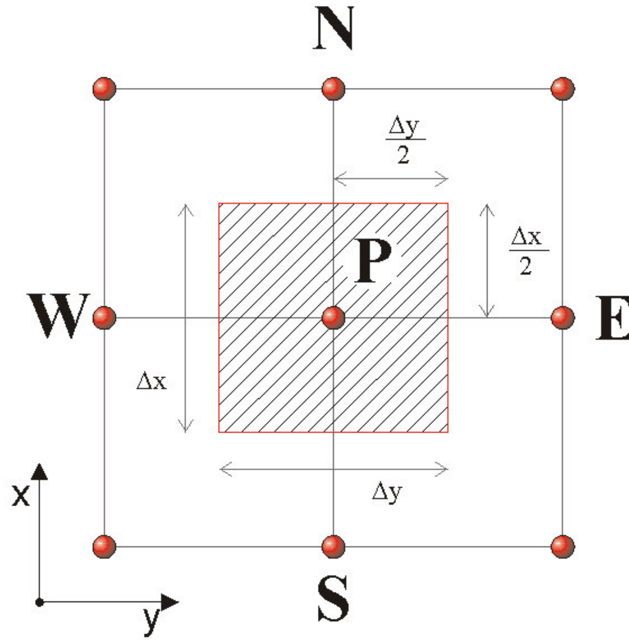

Fig. 3.6- Generic grid point P – plan view

According to the notation described by the above figures, each conduction heat flux with adjacent elements belonging to the same plate (base plate or cover plate) can be discretized and expressed as

$$\Delta\Phi_{i,j-1}^{COND} = a_{i,j-1}^{COND}(T_{P\ i,j-1} - T_{P\ i,j}) = k_P^X \frac{\Delta y \cdot \Delta z}{\Delta x}(T_{P\ i,j-1} - T_{P\ i,j}) \quad (3.14\ a)$$

$$\Delta\Phi_{i,j+1}^{COND} = a_{i,j+1}^{COND}(T_{P\ i,j+1} - T_{P\ i,j}) = k_P^X \frac{\Delta y \cdot \Delta z}{\Delta x}(T_{P\ i,j+1} - T_{P\ i,j}) \quad (3.14\ b)$$

$$\Delta\Phi_{i-1,j}^{COND} = a_{i-1,j}^{COND}(T_{P\ i-1,j} - T_{P\ i,j}) = k_P^Y \frac{\Delta x \cdot \Delta z}{\Delta y}(T_{P\ i-1,j} - T_{P\ i,j}) \quad (3.14\ c)$$

$$\Delta\Phi_{i+1,j}^{COND} = a_{i+1,j}^{COND}(T_{P\ i+1,j} - T_{P\ i,j}) = k_P^Y \frac{\Delta x \cdot \Delta z}{\Delta y}(T_{P\ i+1,j} - T_{P\ i,j}) \quad (3.14\ d)$$

It is to be pointed out that the present numerical analysis can consider different thermal conductivities depending on the direction, as it can be noticed by thermal conductivity k_P^X and k_P^Y for direction N-S and W-E respectively, even if most of materials used in HE have isotropic characteristics.

3.5.2 Cover plate element

The case of the cover plate is the same as the base plate element. The equations used to evaluate conduction heat fluxes are exactly of the same form.

Obviously the temperatures will be different from the base element ones, and thermal conductivity and plate thickness can be also different, while according to the figure above, Δx and Δy are the same as for the base plate element.

To distinguish these equations from the base plate ones, the terms different from base plate terms are marked with the notation "TOP".

$$\Delta\Phi_{i,j-1}^{COND,TOP} = a_{i,j-1}^{COND,TOP}(T_{P\ i,j-1}^{TOP} - T_{P\ i,j}^{TOP}) = k_P^{X\ TOP} \cdot \frac{\Delta y \cdot \Delta z^{TOP}}{\Delta x}(T_{P\ i,j-1}^{TOP} - T_{P\ i,j}^{TOP}) \quad (3.15\ a)$$

$$\Delta\Phi_{i,j+1}^{COND,TOP} = a_{i,j+1}^{COND,TOP}(T_{P\ i,j+1}^{TOP} - T_{P\ i,j}) = k_P^{X\ TOP} \cdot \frac{\Delta y \cdot \Delta z^{TOP}}{\Delta x}(T_{P\ i,j+1}^{TOP} - T_{P\ i,j}^{TOP}) \quad (3.15\ b)$$

$$\Delta\Phi_{i-1,j}^{COND,TOP} = a_{i-1,j}^{COND,TOP}(T_{P\ i-1,j}^{TOP} - T_{P\ i,j}^{TOP}) = k_P^{Y\ TOP} \cdot \frac{\Delta x \cdot \Delta z^{TOP}}{\Delta y}(T_{P\ i-1,j}^{TOP} - T_{P\ i,j}^{TOP}) \quad (3.15\ c)$$

$$\Delta\Phi_{i+1,j}^{COND,TOP} = a_{i+1,j}^{COND,TOP}(T_{P\ i+1,j}^{TOP} - T_{P\ i,j}^{TOP}) = k_P^{Y\ TOP} \cdot \frac{\Delta x \cdot \Delta z^{TOP}}{\Delta y}(T_{P\ i+1,j}^{TOP} - T_{P\ i,j}^{TOP}) \quad (3.15\ d)$$

3.5.3 Internal heat generation

There exist some applications in which the base plate is not an element separated from the electrical device, but it corresponds to the external surface of the device to be cooled, making the cold plate an integral part of the module itself. With heat-dissipating integrated circuit (IC) components on one side of a chip, microchannels may be precision machined or chemically etched on the opposite side (Incropera, 1999).

In this particular case, the heat source can be considered as coincident to the base plate and therefore an internal heat generation is assumed as the heat source, and temperature on the base plate will coincide with the electronic surface temperature.
In the following, internal heat generation is named as Q_G, and its values are given by

$$Q_G = Sc \cdot \Delta x \Delta y = Sc \cdot \Delta A \quad (3.16)$$

where Sc [W/m^2] is the specific internal heat generation.

From a numeric point of view, this heat flux is considered in the same way of an external heat flux, the only difference is that here interface thermal resistances are eliminated and therefore there is no difference between the base plate temperature and the surface device temperature, as said above.

When this happens, even fins are the same materials as the base plate (typically, a silicon substrate), so they will have the same thermal conduction, while the cover plate may be of any different material with its own thermal conductivity.

In the case there is a heat internal generation also in the cover plate, a further heat source has to be taken into account by the equation

$$Q_G^{\ TOP} = S_C^{\ TOP} \cdot \Delta x\, \Delta y = S_C^{\ TOP} \cdot \Delta A \qquad (3.17).$$

3.5.4 Cover plate convective heat flux

When not thermally insulated and not in contact with other electrical devices, the cover plate will be subjected to natural or forced convective heat flux with environment air at a certain temperature T_{EN} (*EN = environment*).

This heat flux will be evaluated using a suitable convective heat transfer coefficient α_{EN}, obtained from the literature, and considering the temperature difference between the environment and the generic cover plate element as the driving force for the heat exchange.

Heat flux is expressed as:

$$\Delta\Phi_{EN} = \alpha_{EN} \cdot \Delta x\, \Delta y (T_{EN} - T_{P\ i,j}^{TOP}) \qquad (3.18)$$

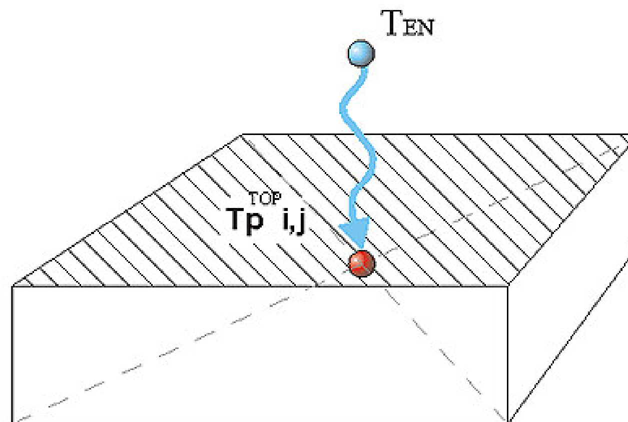

Fig. 3.7- convective heat flux on a generic cover plate element

The heat transfer coefficient could be set to 0 when the cold plate is thermally insulated from the surrounding environment.

3.6 Channel side walls

3.6.1 General aspects

The vertical separating walls (the fins, or dividers), which identify the microchannels, represent a special kind of extended surface and could be responsible for the whole device behavior, according to the fluid flowing through microchannels, to their geometrical characteristics and to their thermal conductivity. The distance between these vertical walls determines also the width of each solid element, as stated above.

Each separating wall is divided into the same number of elements as each fluid channel, so each base element has its corresponding fin, connected to a cover plate element, and it has two adjacent fluid cells, named as West and East fluid cells.

For this particular element, thermal conduction between surfaces in contact with the fluid is ignored (since fin thickness is usually very low), while internal thermal conduction from bottom to top and in the N-S direction (i.e. longitudinal heat conduction).

To describe the fin behavior, the finite element method is used, allowing to evaluate its temperature profile thanks to the Euler-Ostrogradskij equation, once bottom and top temperatures are known (Dirichlet-type boundary conditions) and ensuring a coherent description of the thermal fluxes due to longitudinal conduction (Neumann-type boundary condition).

3.6.2 Shape function

To analyze the fin behavior using the finite element method, it is useful to refer to the following annotation.

Let us consider the fin sub-domain, named as σ^m , and let us subdivide it in N elements, for which the thermal balance is expressed by the following equation:

$\forall m : 1 \leq m \leq N$

$$\int_{\sigma^S}\left[\nabla^2\left(k_w\nabla^2 T_w\right)s_w - \sum_i \alpha_i\left(T_{w,i} - T_{w,i}\right)\right]dA = 0 \tag{3.10}$$

Assuming the thermal conductivity as temperature invariant, the resolution of the previous equation can be considered equivalent to the minimization of the following functional:

$$\Pi = \int_{\sigma^S}\left[\frac{1}{2}\left(\nabla^2 T_w\right)\bullet\left(\nabla^2 T_w\right) + \sum_i \frac{\alpha_i}{k_w s_w}\left(T_{w,i} - T_{w,i}\right)T_{w,i}\right]dA \tag{3.11}$$

The use of Euler-Ostrogradskij equation leads to the following partial spatial derivative equation

$$P \in \sigma^m \qquad \frac{\partial^2 \vartheta}{\partial z^2} + \frac{\partial^2 \vartheta}{\partial x^2} = \frac{Bi}{h_0^2}\vartheta \tag{3.19}$$

where

$$\vartheta(y,z) = T_w(x,z) - \frac{\sum_{k=1}^{N}\alpha_k \cdot T_k}{\sum_{k=1}^{N}\alpha_k} \tag{3.20}$$

and

$$Bi = h_0^2 \frac{\sum_{i=1}^{N_f}\alpha_i}{k_w s} \tag{3.21}$$

The solution of the Euler-Ostrogradskij equation is the temperature profile which gives the minimum value of the functional. Assuming constant fluid temperatures for the considered element, an analytical solution can be found according to the classical theory for extended surface heat transfer

$$\vartheta(x,z) = C_1 e^{\omega x} + C_2 e^{-\omega x} + C_3 e^{\omega z} + C_4 e^{-\omega z} \tag{3.22}$$

where

$$\omega = \sqrt{\sum_{k=1}^{N}\frac{\alpha_k}{k_w \cdot s}} \tag{3.23}$$

The most natural choice for these elements is the surrounded quadratic element (classic element in figure 3.4). This is equivalent to considering four Dirichlet conditions for determining constants C_i. Since unfortunately these conditions are not linearly independent for function (3.16), they do not allow defining uniquely the set of constants. The basic idea is to “shift” or “move” the element, as shown in figure 3.4 (named as proposed element). In this case, two boundary conditions belong to Dirichlet-type while the other two to Neumann-type.

It is worth pointing out that the boundary conditions make the proposed finite element intrinsically conservative. This feature allows adopting the proposed element together with SEWTLE technique to describe finned surfaces because it does not compromise the convergence check based on exchanged thermal power. Furthermore, shifting the classical elements to the proposed element position, each fin element is placed at the same fluid cell and plate cell position.

3.6.3 Solution for Euler-Ostrogradskij equation

Referring to figure 3.8, red points represent the center of base plate elements, violet points represent the center of cover plate element, and blue ones correspond to fluid cell elements.

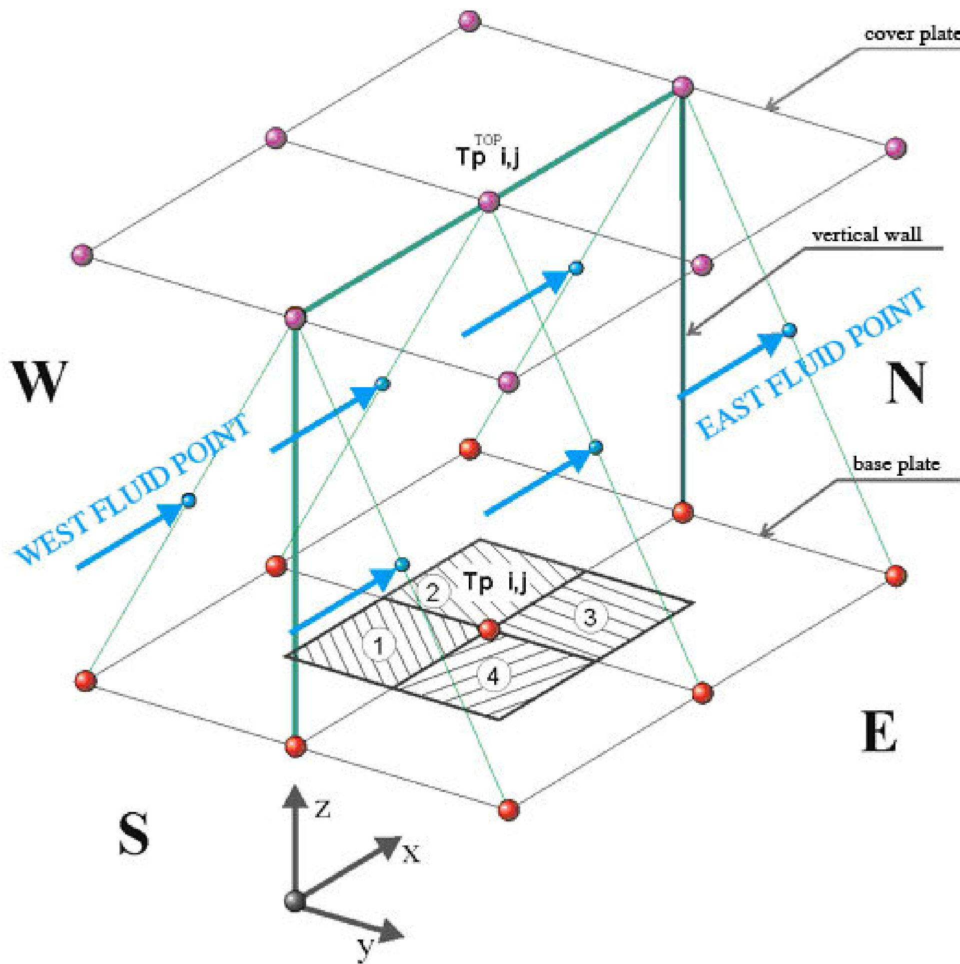

Fig. 3.8- Grid points and vertical wall

Base plate and cover plate grid points, belong both to the plates and also to the fin elements, as bottom and top temperatures.

Focusing on the above scheme, let us apply the thermal balance equations with regard to the thermal conduction, with the two corresponding plate elements (a base one and a cover one) and with two linked fins (the previous one and the next one), and to the convective heat flux with fluid flowing in the two adjacent channels (in the above figure, named as West fluid and East fluid).Therefore, the previously proposed equations are here adapted to the specific case described.

In Euler-Ostrogradskij equation,

$$\frac{\partial^2 \vartheta(x,z)}{\partial x^2} + \frac{\partial^2 \vartheta(x,z)}{\partial z^2} = \omega^2 \vartheta(x,z) \tag{3.24}$$

$\vartheta(x,z)$ links the local fin temperature (which is to be evaluated) with temperatures of the adjacent fluid cells, using an average value weighted on the convective coefficient associated,

$$\vartheta(x,z)=T_P(x,z)-\frac{\alpha_{i,j}^{E}\,T_{f\,i,j}^{E}+\alpha_{i,j}^{W}\,T_{f\,i,j}^{W}}{\alpha_{i,j}^{E}+\alpha_{i,j}^{W}} \tag{3.25}$$

The solution of the Euler-Ostrogradskij equation is represented by

$$\vartheta(x,z)=C_1e^{\omega x}+C_2e^{-\omega x}+C_3e^{\omega z}+C_4e^{-\omega z} \tag{3.26}$$

where ω accounts for convective heat transfer coefficients, for fin thermal conduction, and for its thickness

$$\omega=\sqrt{\frac{\alpha_{i,j}^{E}+\alpha_{i,j}^{W}}{k_w\cdot s}} \tag{3.27}$$

Finally, to have the temperature profile over the whole fin element, the for coefficients C_1 - C_2 - C_3 and C_4 are to be determined, by using the for boundary condition equations: two Dirichlet-type conditions and two Neumann-type conditions.

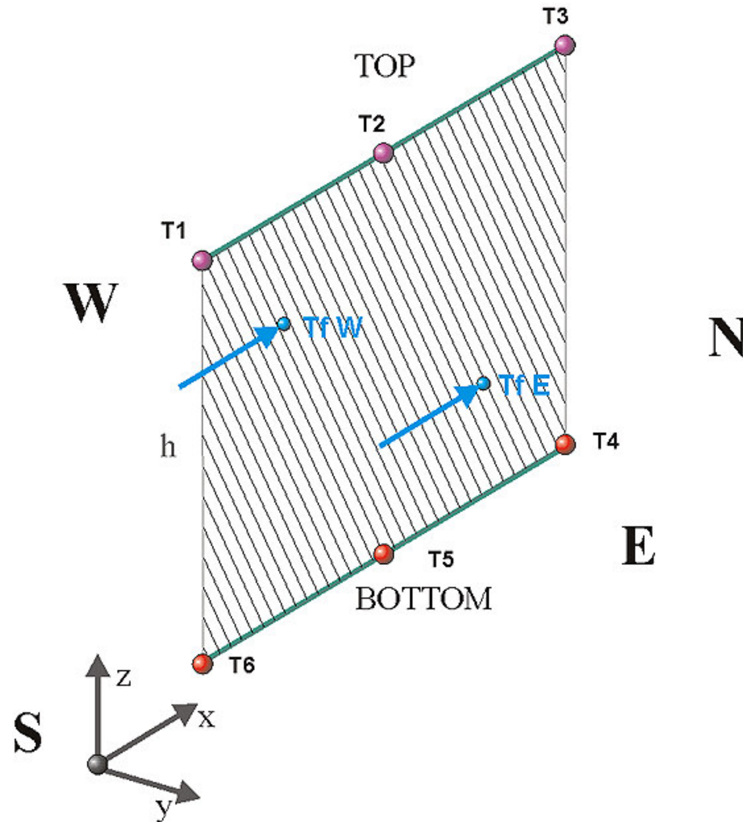

Fig. 3.9- Vertical wall, base and cover grid points, and fluid grid points

The first boundary conditions, the Dirichlet-type ones, are expressed setting the value of $\vartheta(x,z)$ in the center of the element at the fin bottom, i.e. $(0,0)$, and at the fin top, i.e. $(0,h)$, where h is the fin height, that is the internal microchannel height. Therefore the first condition lead to

$$\vartheta(0,0)_{i,j} = T_{P\,i,j} - \frac{\alpha_{E\,i,j}}{\alpha_{E\,i,j}+\alpha_{W\,i,j}} T^{E}_{f\,i,j} - \frac{\alpha_{W\,i,j}}{\alpha_{E\,i,j}+\alpha_{W\,i,j}} T^{W}_{f\,i,j} \tag{3.28}$$

$$\vartheta(0,0)_{i,j} = C_1 + C_2 + C_3 + C_4 \tag{3.29}$$

And the second one:

$$\vartheta(0,h)_{i,j} = T^{TOP}_{P\,i,j} - \frac{\alpha_{E\,i,j}}{\alpha_{E\,i,j}+\alpha_{W\,i,j}} T^{E}_{f\,i,j} - \frac{\alpha_{W\,i,j}}{\alpha_{E\,i,j}+\alpha_{W\,i,j}} T^{W}_{f\,i,j} \tag{3.30}$$

$$\vartheta(0,h)_{i,j} = C_1 + C_2 + C_3 e^{\omega h} + C_4 e^{-\omega h} \tag{3.31}$$

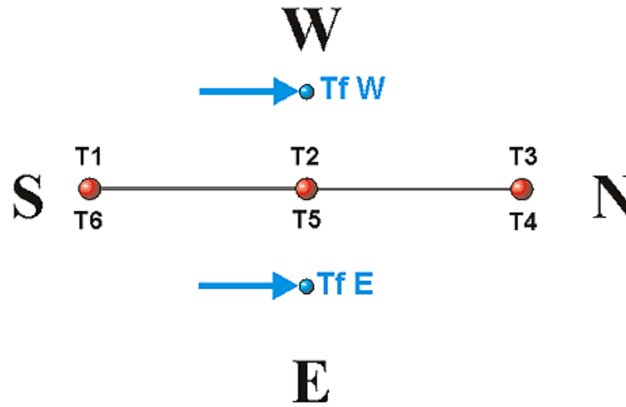

Fig. 3.10- Plan view for vertical wall

According to the figures here proposed, $T_{P\,i,j}$ corresponds to T_2 and $T^{TOP}_{P\,i,j}$ corresponds to T_5, while T_1 and T_6 represent bottom and top temperatures of the previous fin element, T_3 and T_4 are the temperatures of the next element.

$T_1=$	$T^{TOP}_{P\,i,j-1}$	$T_4=$	$T_{P\,i,j+1}$
$T_2=$	$T^{TOP}_{P\,i,j}$	$T_5=$	$T_{P\,i,j}$
$T_3=$	$T^{TOP}_{P\,i,j+1}$	$T_6=$	$T_{P\,i,j-1}$

As it has already been pointed out, fluid cell temperatures are placed in the same cross section of the fin temperature.

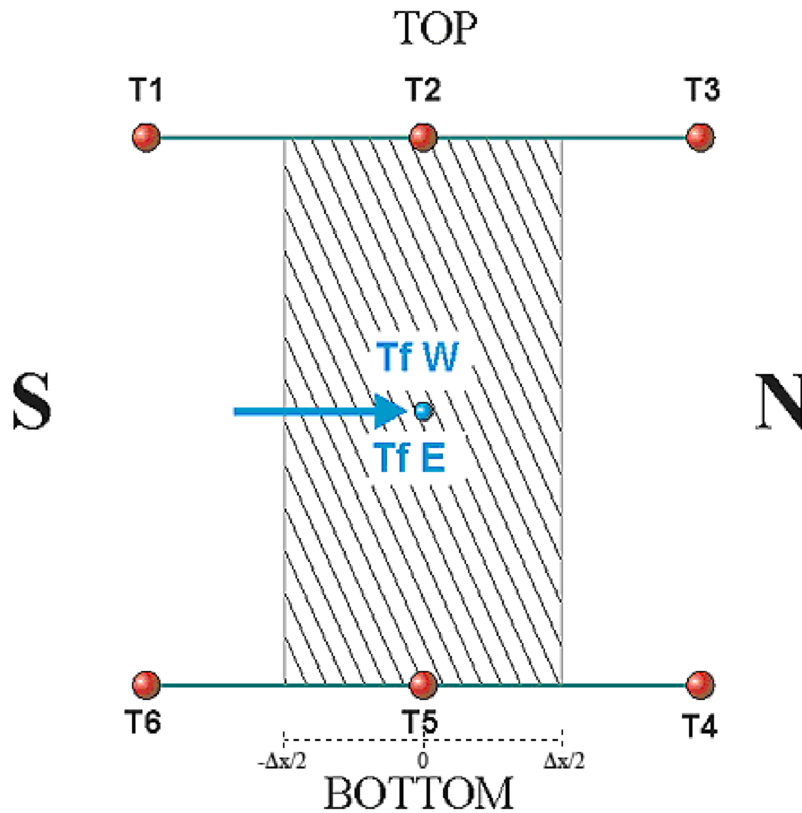

Fig. 3.11- side view for vertical wall

Let us introduce the other two boundary conditions in order to determine all the coefficients and to ensure a coherent description of the thermal fluxes due to longitudinal conduction. This longitudinal thermal flux between subsequent elements is calculated assuming a linear temperature profile on x direction.

$$\int_0^h k_w^z \cdot s \cdot \left.\frac{\partial \vartheta}{\partial x}\right|_{x=-\frac{\Delta x}{2}} dz = L_-(\vartheta_0, \vartheta_h) \tag{3.32}$$

$$\int_0^h k_w^z \cdot s \cdot \left.\frac{\partial \vartheta}{\partial x}\right|_{x=+\frac{\Delta x}{2}} dz = L_+(\vartheta_0, \vartheta_h) \tag{3.33}$$

where k_w^z is the fin thermal conductivity on z direction, and L- and L+ are linear correlation depending on bottom and top fin temperatures.

According to the general solution for the differential equation, the partial first derivative can be expressed as

$$\frac{\partial \vartheta}{\partial x} = \omega\left[C_1\, e^{\omega x} - C_2\, e^{-\omega x}\right] \tag{3.34}$$

To calculate thermal conduction heat flux at upstream edge and at downstream edge, the above expression is to be evaluated at $-\Delta x/2$ and at $+\Delta x/2$ respectively:

$$\left.\frac{\partial \vartheta}{\partial x}\right|_{\frac{-\Delta x}{2}} = \omega\left[C_1\, e^{-\omega\frac{\Delta x}{2}} - C_2\, e^{\omega\frac{\Delta x}{2}}\right] \tag{3.35}$$

$$\left.\frac{\partial \vartheta}{\partial x}\right|_{\frac{+\Delta x}{2}} = \omega\left[C_1 e^{\omega\frac{\Delta x}{2}} - C_2 e^{-\omega\frac{\Delta x}{2}}\right] \tag{3.36}$$

Finally heat flux can be easily calculate using the left-hand member of (3.24) and (3.25). The right-hand side of (3.24) and (3.25) is evaluated using the difference of average fin root temperatures, and the edge fin area is given by the product of thickness s and height h.

$$\int_0^h k_w^{\,z} \cdot s \cdot \left.\frac{\partial \vartheta}{\partial x}\right|_{x=-\frac{\Delta x}{2}} dz = k_w^{\,z} sh \frac{1}{2\Delta x}(T_2 + T_5 - T_1 - T_6) \tag{3.37}$$

$$\int_0^h k_w^{\,z} \cdot s \cdot \left.\frac{\partial \vartheta}{\partial x}\right|_{x=+\frac{\Delta x}{2}} dz = k_w^{\,z} sh \frac{1}{2\Delta x}(T_3 + T_4 - T_2 - T_5) \tag{3.38}$$

Finally C_1, C_2, C_3, C_4 can be obtained by solving the following linear system

$$\begin{cases} C_1 + C_2 + C_3 + C_4 = T_5 - \dfrac{\alpha_E}{\alpha_E + \alpha_W} T_f^E - \dfrac{\alpha_W}{\alpha_E + \alpha_W} T_f^W \\ C_1 + C_2 + C_3 e^{\omega h} + C_4 e^{-\omega h} = T_2 - \dfrac{\alpha_E}{\alpha_E + \alpha_W} T_f^E - \dfrac{\alpha_W}{\alpha_E + \alpha_W} T_f^W \\ C_1 e^{-\omega\frac{\Delta x}{2}} - C_2 e^{\omega\frac{\Delta x}{2}} = \dfrac{1}{2\omega\Delta x}(T_2 + T_5 - T_1 - T_6) \\ C_1 e^{\omega\frac{\Delta x}{2}} - C_2 e^{-\omega\frac{\Delta x}{2}} = \dfrac{1}{2\omega\Delta x}(T_3 + T_4 - T_2 - T_5) \end{cases} \tag{3.39}$$

where

h : fin height

Δx : fin length, equal to each element length

α^E and α^W : convective heat transfer coefficient for East fluid cell and West fluid cell respectively

$\omega = \sqrt{\dfrac{\alpha^E + \alpha^W}{k_w \cdot s}}$: correspond to square root of Biot number on fin height.

Fin elements use plate cell temperatures, therefore they do not introduce any new unknown value. Fluid cell temperatures to calculate the fin temperature profile are considered as known, when the solid sob-domain is analyzed: this step aims to completely solve the plates sub-domain, once the fluids sub-domain is solved. The forward step is to solve the fluid sub-domain, using the plates temperature profiles calculated in the previous step. The final solution is reached by means of an iterative procedure which is controlled by continuity of heat flow between hot-side thermal flux and cold-side one. At the beginning, each sub-domain is characterized by a guess temperature field, in order to supply known values to the really first step in the code.

Let us write the coefficient system in a matrix notation, in order to supply an easy way of implementation in any code.

Considering each matrix and vector element, the system can be written as

$$\begin{bmatrix} 1 & 1 & 1 & 1 \\ 1 & 1 & a & \frac{1}{a} \\ \frac{1}{b} & -b & 0 & 0 \\ b & -\frac{1}{b} & 0 & 0 \end{bmatrix} \cdot \begin{Bmatrix} C_1 \\ C_2 \\ C_3 \\ C_4 \end{Bmatrix} = \begin{bmatrix} 0 & 0 & 0 & 0 & 1 & 0 & -c & c-1 \\ 0 & 1 & 0 & 0 & 0 & 0 & -c & c-1 \\ -d & d & 0 & 0 & d & -d & 0 & 0 \\ 0 & -d & d & d & -d & 0 & 0 & 0 \end{bmatrix} \cdot \begin{Bmatrix} T_1 \\ T_2 \\ T_3 \\ T_4 \\ T_5 \\ T_6 \\ T_f^{\ E} \\ T_f^{\ W} \end{Bmatrix} \tag{3.40}$$

where

$$a = e^{\omega h} \tag{3.41}$$

$$b = e^{\omega \frac{\Delta x}{2}} \tag{3.42}$$

$$c = \frac{\alpha^E}{\alpha^E + \alpha^W} \tag{3.43}$$

$$1-c=\frac{\alpha^{W}}{\alpha^{E}+\alpha^{W}} \tag{3.44}$$

$$d=\frac{1}{2\omega\Delta x} \tag{3.45}$$

The system can be synthesized as

$$[A]\cdot\{C_i\}=[B]\cdot\{T\} \tag{3.46}$$

where temperatures are rearranged into vector $\{T\}$, constants are placed into vector $\{C_i\}$, and $[A]$and $[B]$ are matrix which contain all known coefficients, referring convection, conduction and geometrical properties
Therefore, the solution can be obtained as

$$\{C_i\}=[A]^{-1}[B]\cdot\{T\} \tag{3.47}$$

where

$$[A]=\begin{bmatrix} 1 & 1 & 1 & 1 \\ 1 & 1 & a & \frac{1}{a} \\ \frac{1}{b} & -b & 0 & 0 \\ b & -\frac{1}{b} & 0 & 0 \end{bmatrix} \tag{3.48}$$

$$[B]=\begin{bmatrix} 0 & 0 & 0 & 0 & 1 & 0 & -c & c-1 \\ 0 & 1 & 0 & 0 & 0 & 0 & -c & c-1 \\ -d & d & 0 & 0 & d & -d & 0 & 0 \\ 0 & -d & d & d & -d & 0 & 0 & 0 \end{bmatrix} \tag{3.49}$$

The system can be solved once for all, through the product of the matrix $[SF]$ by the temperature vector

$$[A]^{-1}[B]=[SF]=\begin{bmatrix} K & U & V & V & U & K & 0 & 0 \\ V & U & K & K & U & V & 0 & 0 \\ A & C & A & A & D & A & E & F \\ B & G & B & B & Z & B & H & L \end{bmatrix} \tag{3.50}$$

or, making each terms explicit,

$$[SF]=\begin{bmatrix} \frac{bd}{b^4-1} & \frac{-bd}{b^2-1} & \frac{b^3d}{b^4-1} & \frac{b^3d}{b^4-1} & \frac{-bd}{b^2-1} & \frac{bd}{b^4-1} & 0 & 0 \\ \frac{b^3d}{b^4-1} & \frac{-bd}{b^2-1} & \frac{bd}{b^4-1} & \frac{bd}{b^4-1} & \frac{-bd}{b^2-1} & \frac{b^3d}{b^4-1} & 0 & 0 \\ \frac{-bd}{(a+1)(b^2-1)} & \frac{2(a-1)bd+a(b^2-1)}{(a^2-1)(b^2-1)} & \frac{-bd}{(a+1)(b^2-1)} & \frac{-bd}{(a+1)(b^2-1)} & \frac{2(a-1)bd-(b^2-1)}{(a^2-1)(b^2-1)} & \frac{-bd}{(a+1)(b^2-1)} & \frac{-c}{a+1} & \frac{c-1}{a+1} \\ \frac{-abd}{(a+1)(b^2-1)} & \frac{2abd(a-1)-a(b^2-1)}{(a^2-1)(b^2-1)} & \frac{-abd}{(a+1)(b^2-1)} & \frac{-abd}{(a+1)(b^2-1)} & \frac{2abd(a-1)+a^2(b^2-1)}{(a^2-1)(b^2-1)} & \frac{-abd}{(a+1)(b^2-1)} & \frac{-ac}{a+1} & \frac{a(c-1)}{a+1} \end{bmatrix} \tag{3.51}$$

Therefore, to get the shape function for all fins there is no need to invert any matrix, since it can be done once for all. The matrix is just to be updated with the properties which represent the fin considered.

3.7 Convection heat flux between fluids and plates

Let us refer to the base plate elements, for notation convenience, also cover plate is analyzed in the same way. Each base plate element is subjected to a convection heat flux with fluid flowing in both channels adjacent to the separating wall, according to the particular kind of element chosen to discretize the metal sub-domain.

Referring to the general base plate element, marked by *(i,j)*, four heat transfer surfaces can be characterized, as shown in figure 3.12.

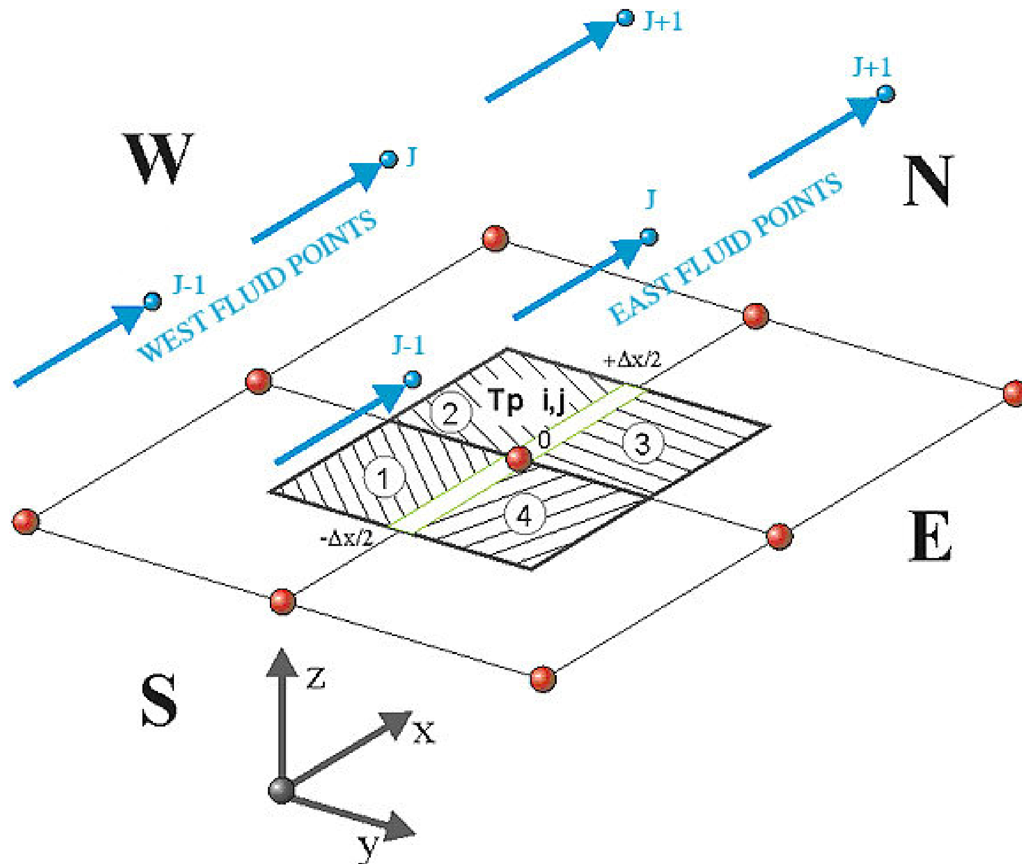

Fig. 3.12- Base plate element convective heat transfer surfaces (hatched)

Total convective heat flux on the base element is to be calculated by four surface integral on areas 1-2-3-4, which do not include the vertical wall projection on base element. Areas 1 and 2 are subjected to heat flux with west fluid channel, while areas 3 and 4 are in contact with East fluid channel. Furthermore, fluid temperature profile (which depends on specific heat capacity and flow rate) was assumed as linear, therefore to evaluate each base element convective flux, 6 fluid temperatures are to be considered: fluid cells corresponding to the base cell, the two previous fluid cells and the two following ones.

The generic fluid temperature is finally given by:

$$T^f_{j\div j+1}(x) = T^f_j + \frac{T^f_{j+1} - T^f_j}{\Delta x} \cdot x \qquad (3.52)$$

where T^f_j and T^f_{j+1} are the fluid grid point temperatures.

Thus fluid temperature used to calculate heat flux at areas 1 and 4 is different from the one used at the areas 2 and 3 respectively as shown in figure 3.13.

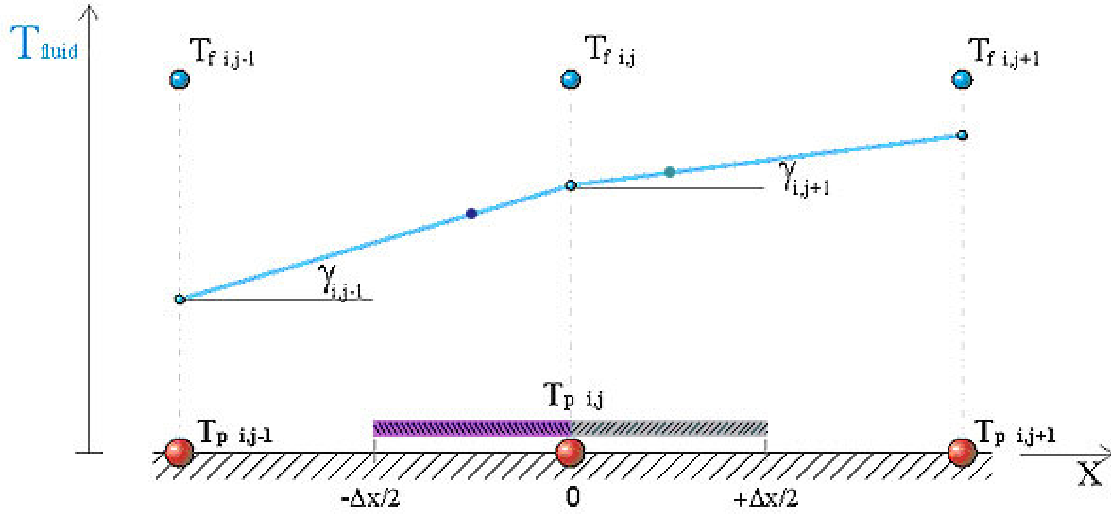

Fig. 3.13- Linear fluid temperature profile

Finally convective heat flux are expresses as

$$\Delta\Phi_1^{f\ CONV} = \alpha_{i,j}^{(1)} \frac{\Delta y - s}{2} \int_{\frac{-\Delta x}{2}}^{0} \left(T_{i,j}^{f\ W} + \frac{T_{i,j}^{f\ W} - T_{i,j-1}^{f\ W}}{\Delta x} \cdot x - T_{P\ i,j}\right) dx \qquad (3.53\ a)$$

$$\Delta\Phi_2^{f\ CONV} = \alpha_{i,j}^{(2)} \frac{\Delta y - s}{2} \int_{0}^{\frac{\Delta x}{2}} \left(T_{i,j}^{f\ W} + \frac{T_{i,j+1}^{f\ W} - T_{i,j}^{f\ W}}{\Delta x} \cdot x - T_{P\ i,j}\right) dx \qquad (3.53\ b)$$

$$\Delta\Phi_3^{f\ CONV} = \alpha_{i,j}^{(3)} \frac{\Delta y - s}{2} \int_{0}^{\frac{\Delta x}{2}} \left(T_{i,j}^{f\ E} + \frac{T_{i,j+1}^{f\ E} - T_{i,j}^{f\ E}}{\Delta x} \cdot x - T_{P\ i,j}\right) dx \qquad (3.53\ c)$$

$$\Delta\Phi_4^{f\ CONV} = \alpha_{i,j}^{(4)} \frac{\Delta y - s}{2} \int_{\frac{-\Delta x}{2}}^{0} \left(T_{i,j}^{f\ E} + \frac{T_{i,j}^{f\ E} - T_{i,j-1}^{f\ E}}{\Delta x} \cdot x - T_{P\ i,j}\right) dx \qquad (3.53\ d)$$

The total convective heat flux over a generic *(i,j)* base plate element can be obtained adding the four contributions, as each integral is calculated.

$$\Delta\Phi_1^{f\ CONV} = \alpha_{i,j}^{(1)} \frac{\Delta y - s}{2} \frac{\Delta x}{2} \left(\frac{3}{4} T_{i,j}^{f\ W} + \frac{1}{4} T_{i,j-1}^{f\ W} - T_{P\ i,j}\right) \qquad (3.54\ a)$$

$$\Delta\Phi_2^{f\ CONV} = \alpha_{i,j}^{(2)} \frac{\Delta y - s}{2} \frac{\Delta x}{2} \left(\frac{3}{4} T_{i,j}^{f\ W} + \frac{1}{4} T_{i,j+1}^{f\ W} - T_{P\ i,j}\right) \qquad (3.54\ b)$$

$$\Delta\Phi_3^{f\ CONV} = \alpha_{i,j}^{(3)} \frac{\Delta y - s}{2} \frac{\Delta x}{2} \left(\frac{3}{4} T_{i,j}^{f\ E} + \frac{1}{4} T_{i,j+1}^{f\ E} - T_{P\ i,j}\right) \qquad (3.54\ c)$$

$$\Delta\Phi_4^{f\ CONV} = \alpha_{i,j}^{(4)} \frac{\Delta y - s}{2} \frac{\Delta x}{2} \left(\frac{3}{4} T_{i,j}^{f\ E} + \frac{1}{4} T_{i,j-1}^{f\ E} - T_{P\ i,j} \right) \tag{3.54 d}$$

so

$$\Delta\Phi_{i,j}^{f\ CONV} = \frac{\Delta y - s}{2} \frac{\Delta x}{2} \begin{pmatrix} \left(\frac{3}{4}\alpha_{i,j}^{(1)} + \frac{3}{4}\alpha_{i,j}^{(2)} \right) T_{i,j}^{f\ W} + \frac{1}{4}\alpha_{i,j}^{(1)} T_{i,j-1}^{f\ W} + \frac{1}{4}\alpha_{i,j}^{(2)} T_{i,j+1}^{f\ W} + \\ + \left(\frac{3}{4}\alpha_{i,j}^{(3)} + \frac{3}{4}\alpha_{i,j}^{(4)} \right) T_{i,j}^{f\ E} + \frac{1}{4}\alpha_{i,j}^{(3)} T_{i,j+1}^{f\ E} + \frac{1}{4}\alpha_{i,j}^{(4)} T_{i,j-1}^{f\ E} + \\ - \left(\alpha_{i,j}^{(1)} + \alpha_{i,j}^{(2)} + \alpha_{i,j}^{(3)} + \alpha_{i,j}^{(4)} \right) T_{P\ i,j} \end{pmatrix} \tag{3.55}$$

3.8 Conductive heat flux between plates and vertical walls

Vertical wall exchange heat flux with base plate and cover plate, along Z direction. Such heat flux can be easily calculated according to the shape function $\vartheta(x,z)$ for the temperature profile over the fin itself, which depends on four coefficients C_i already calculated.

Therefore, conductive heat flux can be obtained by calculating the integral over the projection of the wall of the product of thermal conductivity by first derivative of $\vartheta(x,z)$ on z direction. This analysis is to be carried out both for base plate and for cover plate, and it can be done in the same way, with the same notation (using "top" for cover plate).

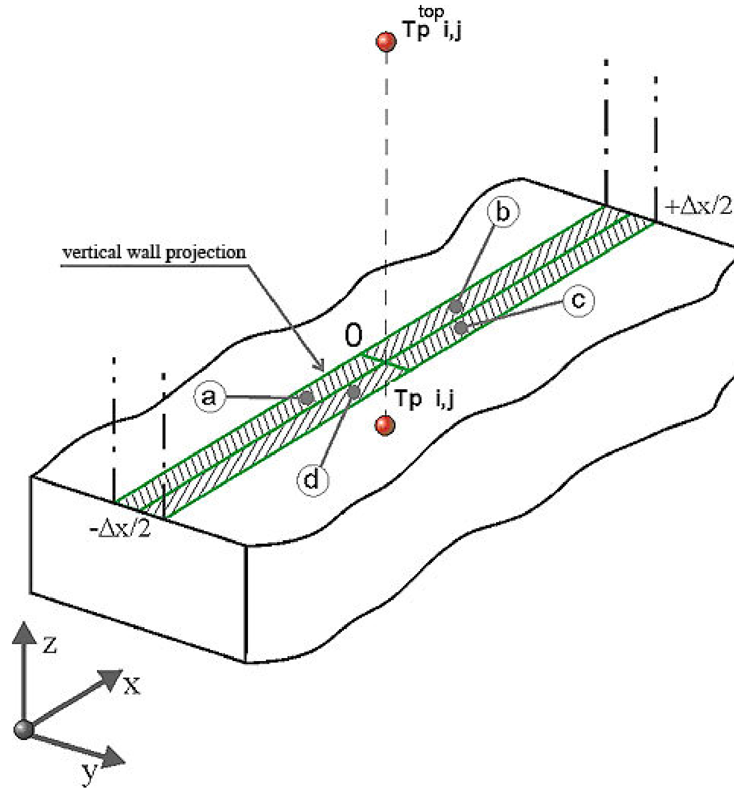

Fig. 3.14- thermal conduction area

Considering figure 3.14, total heat flux can be obtained by adding four contributes,

$$\Delta\Phi_a^{COND\,WALL} = \Delta\Phi_d^{COND\,WALL} = \int_{\frac{-\Delta x}{2}}^{0} \frac{k_w^z s}{2} \left.\frac{\partial \vartheta(x,z)}{\partial z}\right|_{z=0} dx \tag{3.56}$$

$$\Delta\Phi_b^{COND\,WALL} = \Delta\Phi_c^{COND\,WALL} = \int_{0}^{\frac{+\Delta x}{2}} \frac{k_w^z s}{2} \left.\frac{\partial \vartheta(x,z)}{\partial z}\right|_{z=0} dx \tag{3.57}$$

Integrals are two by two identical, as shape function do not depend by y. The above derivatives are calculated at $z=0$, since base plate is here analyzed. When referring to cover plate, then derivatives are to be evaluated at $z=h$, where h is fin height, i.e. fluid cell height.

So

$$\left.\frac{\partial \vartheta(x,z)}{\partial z}\right|_{z=0} = \omega(C_3\, e^{\omega z} - C_4\, e^{-\omega z})\Big|_{z=0} = \omega(C_3 - C_4) \tag{3.58}$$

Then all contributes are identical, since the derivatives calculated do not even depends on x

$$\Delta\Phi_a^{COND\,WALL} = \Delta\Phi_d^{COND\,WALL} = \frac{k_W^z s}{4}\omega(C_3 - C_4)\Delta x \tag{3.59 a}$$

$$\Delta\Phi_b^{COND\,WALL} = \Delta\Phi_c^{COND\,WALL} = \frac{k_W^z s}{4}\omega(C_3 - C_4)\Delta x \tag{3. 59 b}$$

The total conduction heat flux through vertical wall projection on the base plate element is expressed as

$$\Delta\Phi_{TOTAL}^{COND\,WALL} = 4\frac{k_W^z s}{4}\omega(C_3 - C_4)\Delta x = k_W^z s\omega(C_3 - C_4)\Delta x \tag{3.60}$$

When considering cover plate cells, the partial first derivative is to be evaluated at $z=h$:

$$\left.\frac{\partial\vartheta(x,z)}{\partial z}\right|_{z=h} = \omega(C_3 e^{\omega z} - C_4 e^{-\omega z})\Big|_{z=h} = \omega(C_3 e^{\omega h} - C_4 e^{-\omega h}) \tag{3.61}$$

Thus integrals are:

$$\Delta\Phi_a^{COND\,WALL\,TOP} = \Delta\Phi_d^{COND\,WALL\,TOP} = -\frac{k_W^z s}{4}\omega(C_3 e^{\omega h} - C_4 e^{-\omega h})\Delta x \tag{3.62 a}$$

$$\Delta\Phi_b^{COND\,WALL\,TOP} = \Delta\Phi_c^{COND\,WALL\,TOP} = -\frac{k_W^z s}{4}\omega(C_3 e^{\omega h} - C_4 e^{-\omega h})\Delta x \tag{3.62 b}$$

And finally total conduction heat flux through vertical wall projection on the cover plate element is expressed as

$$\begin{aligned}\Delta\Phi_{TOTALE}^{COND\,WALL\,TOP} &= -4\frac{k_W^z s}{4}\omega\Delta x(C_3 e^{\omega h} - C_4 e^{-\omega h}) = \\ &= -k_W^z s\omega\Delta x(C_3 e^{\omega h} - C_4 e^{-\omega h})\end{aligned} \tag{3.63}$$

3.9 Total Thermal balance

3.9.1 Gauss-Seidel procedure

An iterative procedure can be adopted for highly meshed heat exchangers: the simple Gauss-Seidel procedure. Since metal sub-domain is composed by surfaces linked together by transverse fins, it can be completely solved gathering all equations in a matrix notation. The resolution system for generic surface is most of time large enough

to suggest a reduction by adopting the Gauss-Seidel line-by-line method which divides a surface into strips.

According to this method, let us refer to a "strip" made up of elementary section as the one represented in Fig. 3.15, concordant with x direction, which coincides with the fluid flowing direction.

Gauss-Seidel Method allows to assume the selected strip temperatures as unknown values, while any other strip temperatures, including adjacent strip ones, is considered to be known, allowing to solve the entire metal sub-domain line by line, or strip by strip. To permit the first step in the SEWTLE method to be carried out, the metal sub-domain is to be initialized with a guess temperature field. Solving iteratively all the strips, with control on temperature difference on the same cell in following iteration, the entire temperature field can be evaluated.

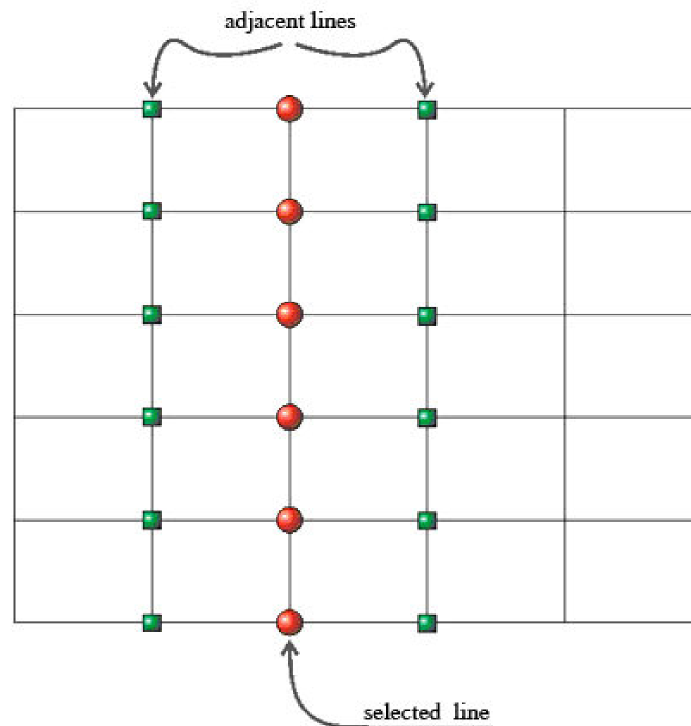

Fig. 3.15- line-by-line Gauss Siedel method

3.9.2 Total thermal balance on base plate element

Thermal balance on base plate cells can be completely calculated according to heat fluxes already evaluated. Since the analysis carried out considers a steady-state system, the sum of all contributes, both conduction, convective, heat generated and heat flux imposed, is equal to zero. Therefore, on a generic base plate cell:

$$\Delta\Phi_{i,j-1}^{COND} + \Delta\Phi_{i,j+1}^{COND} + \Delta\Phi_{i-1,j}^{COND} + \Delta\Phi_{i+1,j}^{COND} + \Delta\Phi_{i,j}^{BOTTOM} + + \Delta\Phi_{i,j}^{f\ CONV} + \Delta\Phi_{TOTAL}^{COND\ WALL} + Q_G = 0 \tag{3.64}$$

As far as the conduction heat flux, contributes can be expressed as

$$\Delta\Phi_{i,j-1}^{COND} = M(T_{P\ i,j-1} - T_{P\ i,j}) \tag{3.65 a}$$

$$\Delta\Phi_{i,j+1}^{COND} = N(T_{P\ i,j+1} - T_{P\ i,j}) \tag{3.65 b}$$

$$\Delta\Phi_{i-1,j}^{COND} = O(T_{P\ i-1,j} - T_{P\ i,j}) \tag{3.65 c}$$

$$\Delta\Phi_{i+1,j}^{COND} = P(T_{P\ i+1,j} - T_{P\ i,j}) \tag{3.65 d}$$

where

$$M = k_P^X \frac{\Delta y \cdot \Delta z}{\Delta x} \tag{3.66}$$

$$N = k_P^X \frac{\Delta y \cdot \Delta z}{\Delta x} \tag{3.67}$$

$$O = k_P^Y \frac{\Delta x \cdot \Delta z}{\Delta y} \tag{3.68}$$

$$P = k_P^Y \frac{\Delta x \cdot \Delta z}{\Delta y} \tag{3.69}$$

The possible internal heat generation is given by:

$$Q_G = S_C \cdot \Delta x\, \Delta y = S_C \cdot \Delta A \tag{3.70}$$

Heat flux imposed by a generic electronic device is simply given by $\Delta\Phi_{i,j}^{BOTTOM}$. When heat flux is uniform over the whole plate, the contribute to each single cell is calculated in the same way of (3.74), where S_c is the specific heat flux imposed per square meter. When a hot spot exists, then its heat flux is to be divided into the corresponding plate cells, and added as a new contribute. Conduction heat flux along the wall through its projection on the base cell is calculated by (3.58), thus

$$\Delta\Phi_{TOTAL}^{COND\ WALL} = W(C_3 - C_4) \tag{3.71}$$

where:

$$W = k_W^z s\omega\Delta x \tag{3.72}$$

Coefficient C_3 and C_4 can be evaluated by (3.39), so

$$\begin{Bmatrix} C_3 \\ C_4 \end{Bmatrix} = \begin{bmatrix} A & C & A & A & D & A & E & F \\ B & G & B & B & Z & B & H & L \end{bmatrix} \cdot \begin{Bmatrix} T_{P\ i,j-1}^{TOP} \\ T_{P\ i,j}^{TOP} \\ T_{P\ i,j+1}^{TOP} \\ T_{P\ i,j+1} \\ T_{P\ i,j} \\ T_{P\ i,j-1} \\ T_f^{\ E} \\ T_f^{\ W} \end{Bmatrix} \tag{3.73}$$

$$C_3 = AT_{P\ i,j-1}^{TOP} + CT_{P\ i,j}^{TOP} + AT_{P\ i,j+1}^{TOP} + AT_{P\ i,j+1} + DT_{P\ i,j} + AT_{P\ i,j-1} + ET_f^{\ E} + FT_f^{\ W} \tag{3.74}$$

$$C_4 = BT_{P\ i,j-1}^{TOP} + GT_{P\ i,j}^{TOP} + BT_{P\ i,j+1}^{TOP} + BT_{P\ i,j+1} + ZT_{P\ i,j} + BT_{P\ i,j-1} + HT_f^{\ E} + LT_f^{\ W} \tag{3.75}$$

$$\begin{aligned} \Delta\Phi_{TOTAL}^{COND\ WALL} = W\,[&(A-B)T_{P\ i,j-1}^{TOP} + (C-G)T_{P\ i,j}^{TOP} + (A-B)T_{P\ i,j+1}^{TOP} + \\ &+ (A-B)T_{P\ i,j+1} + (D-Z)T_{P\ i,j} + (A-B)T_{P\ i,j-1} + \\ &+ (E-H)T_f^{\ E} + (F-L)T_f^{\ W}\,] \end{aligned} \tag{3.76}$$

As far as for convective heat flux contributes, according to (3.52), it can be written:

$$\Delta\Phi_{i,j}^{f\ CONV} = S + RT_{P\ i,j} \tag{3.77}$$

where:

$$\begin{aligned} S = \frac{\Delta y - s}{2}\frac{\Delta x}{2}\ [&\left(\frac{3}{4}\alpha_{i,j}^{(1)} + \frac{3}{4}\alpha_{i,j}^{(2)}\right)T_{i,j}^{f\ W} + \frac{1}{4}\alpha_{i,j}^{(1)}T_{i,j-1}^{f\ W} + \frac{1}{4}\alpha_{i,j}^{(2)}T_{i,j+1}^{f\ W} + \\ &+ \left(\frac{3}{4}\alpha_{i,j}^{(3)} + \frac{3}{4}\alpha_{i,j}^{(4)}\right)T_{i,j}^{f\ E} + \frac{1}{4}\alpha_{i,j}^{(3)}T_{i,j+1}^{f\ E} + \frac{1}{4}\alpha_{i,j}^{(4)}T_{i,j-1}^{f\ E}\ \ ] \end{aligned} \tag{3.78}$$

$$R = -1 \cdot \frac{\Delta y - s}{2}\frac{\Delta x}{2}\left(\alpha_{i,j}^{(1)} + \alpha_{i,j}^{(2)} + \alpha_{i,j}^{(3)} + \alpha_{i,j}^{(4)}\right) \tag{3.79}$$

Finally, thermal balance can be written in accordance with the previous expressions as

$$
\begin{aligned}
&M(T_{P\ i,j-1} - T_{P\ i,j}) + N(T_{P\ i,j+1} - T_{P\ i,j}) + O(T_{P\ i-1,j} - T_{P\ i,j}) + \\
&+ P(T_{P\ i+1,j} - T_{P\ i,j}) + Q(T^{B}_{i,j} - T_{P\ i,j}) + S + RT_{P\ i,j} + \\
&+ W[(A-B)T^{TOP}_{P\ i,j-1} + (C-G)T^{TOP}_{P\ i,j} + (A-B)T^{TOP}_{P\ i,j+1} + (A-B)T_{P\ i,j+1} + \\
&+ (D-Z)T_{P\ i,j} + (A-B)T_{P\ i,j-1} + (E-H){T_f}^{E} + (F-L){T_f}^{W}] + Q_G = 0
\end{aligned}
\tag{3.80}
$$

or, more appropriately:

$$
\begin{aligned}
&[M + W(A-B)]T_{P\ i,j-1} + \\
&-[(M + N + O + P + Q - R - W(D-Z)]T_{P\ i,j} + \\
&+ [N + W(A-B)]T_{P\ i,j+1} + \\
&+ W(A-B)T^{TOP}_{P\ i,j-1} + \\
&+ W(C-G)T^{TOP}_{P\ i,j} + \\
&+ W(A-B)T^{TOP}_{P\ i,j+1} \\
&= -OT_{P\ i-1,j} - PT_{P\ i+1,j} - QT^{B}_{i,j} - S - W[(E-H){T_f}^{E} + (F-L){T_f}^{W}] - Q_G
\end{aligned}
\tag{3.81}
$$

Except for plate temperatures, any other factor is a known value, and depends on geometrical and physical properties.
Letting

$$\alpha^B = M + W(A-B) \tag{3.82}$$

$$\beta^B = -\left[M + N + O + P + Q - R - W(D-Z)\right] \tag{3.83}$$

$$\gamma^B = N + W(A-B) \tag{3.84}$$

$$\delta^B = W(A-B) \tag{3.85}$$

$$\varepsilon^B = W(C-G) \tag{3.86}$$

$$\varphi^B = W(A-B) \tag{3.87}$$

$$\upsilon^B = -\left\{OT_{P\ i-1,j} + PT_{P\ i+1,j} + QT^{B}_{i,j} + S + Q_G + W(E-H){T_f}^{E} + W(F-L){T_f}^{W}\right\} \tag{3.88}$$

the thermal balance can be written in vector notation

$$\begin{bmatrix}\alpha^B & \beta^B & \gamma^B & \delta^B & \varepsilon^B & \varphi^B\end{bmatrix}_{i,k} \cdot \begin{Bmatrix} T_{P\ i,k-1} \\ T_{P\ i,k} \\ T_{P\ i,k+1} \\ T^{TOP}_{P\ i,k-1} \\ T^{TOP}_{P\ i,k} \\ T^{TOP}_{P\ i,k+1} \end{Bmatrix} = \upsilon^B{}_{i,k} \quad (3.89)$$

The first vector in the left-hand member collects all the terms which are multiplied by plate temperature values (in the second vector). Index i refers to the strip selected, while index k relates to the single cell analyzed. Right-hand member assemble all known values, named as $\upsilon_{i,k}$, which relate to the temperatures of the adjacent fluid cells (both East and West of considered cell, in accordance with the notation used) and to the plate cells belonging to adjacent channels, calculated during previous steps.

3.9.3 Cover plate cell thermal balance

Thermal balance for a cover cell can be expressed in the same way as for base cells (3.63), so:

$$\begin{aligned}&\Delta\Phi^{COND,TOP}_{i,j-1} + \Delta\Phi^{COND,TOP}_{i,j+1} + \Delta\Phi^{COND,TOP}_{i-1,j} + \Delta\Phi^{COND,TOP}_{i+1,j} + \Delta\Phi_{EN} + \\ &+ \Delta\Phi^{f\ CONV\ TOP}_{i,j} + \Delta\Phi^{PARETE\ COND\ TOP}_{TOTALE} + Q_G{}^{TOP} = 0\end{aligned} \quad (3.90)$$

Similarly to what was written for base elements, it is let:

$$\Delta\Phi^{COND,TOP}_{i,j-1} = M^{TOP}(T^{TOP}_{P\ i,j-1} - T^{TOP}_{P\ i,j}) \quad (3.91\ a)$$

$$\Delta\Phi^{COND,TOP}_{i,j+1} = N^{TOP}(T^{TOP}_{P\ i,j+1} - T^{TOP}_{P\ i,j}) \quad (3.91\ b)$$

$$\Delta\Phi^{COND,TOP}_{i-1,j} = O^{TOP}(T^{TOP}_{P\ i-1,j} - T^{TOP}_{P\ i,j}) \quad (3.91\ c)$$

$$\Delta\Phi^{COND,TOP}_{i+1,j} = P^{TOP}(T^{TOP}_{P\ i+1,j} - T^{TOP}_{P\ i,j}) \quad (3.91\ d)$$

for thermal conduction with adjacent cover elements, where:

$$M^{TOP} = k_P^{X\ TOP}\frac{\Delta y \cdot \Delta z^{TOP}}{\Delta x} \quad (3.92\ a)$$

$$N^{TOP} = k_P^{X\ TOP}\frac{\Delta y \cdot \Delta z^{TOP}}{\Delta x} \quad (3.92\ b)$$

$$O^{TOP} = k_P^{Y\,TOP} \frac{\Delta x \cdot \Delta z^{TOP}}{\Delta y} \tag{3.92 c}$$

$$P^{TOP} = k_P^{Y\,TOP} \frac{\Delta x \cdot \Delta z^{TOP}}{\Delta y} \tag{3.92 d}$$

and as far as for convective heat flux with environment,

$$\Delta\Phi_{EN} = Q^{TOP}(T_{EN} - T_{P\ i,j}^{TOP}) \tag{3.93}$$

where:

$$Q^{TOP} = \alpha_{EN} \cdot \Delta x\, \Delta y \tag{3.94}$$

In the case of internal heat generation, it is to be considered the following contribute

$$Q_G{}^{TOP} = S_C{}^{TOP} \Delta x\, \Delta y = S_C{}^{TOP}\, \Delta A \tag{3.95}$$

Thermal conduction with vertical wall is expressed as

$$\Delta\Phi_{TOTAL}^{COND\,WALL\,TOP} = -W^{TOP}(JC_3 - \frac{C_4}{J}) = -\frac{W^{TOP}}{J}(J^2C_3 - C_4) \tag{3.96}$$

$$\begin{aligned}\Delta\Phi_{TOTAL}^{COND\,WALL\,TOP} = -\frac{W^{TOP}}{J}[& J^2AT_{P\ i,j-1}^{TOP} + J^2CT_{P\ i,j}^{TOP} + J^2AT_{P\ i,j+1}^{TOP} + \\ & + J^2AT_{P\ i,j+1} + J^2DT_{P\ i,j} + J^2AT_{P\ i,j-1} + \\ & + J^2ET_f{}^E + J^2FT_f{}^W - BT_{P\ i,j-1}^{TOP} - GT_{P\ i,j}^{TOP} + \\ & - BT_{P\ i,j+1}^{TOP} - BT_{P\ i,j+1} - ZT_{P\ i,j} - BT_{P\ i,j-1} + \\ & - HT_f{}^E - LT_f{}^W]\end{aligned} \tag{3.97}$$

$$\begin{aligned}\Delta\Phi_{TOTAL}^{COND\,WALL\,TOP} = -\frac{W^{TOP}}{J}[& (J^2A - B)T_{P\ i,j-1}^{TOP} + (J^2C - G)T_{P\ i,j}^{TOP} + \\ & + (J^2A - B)T_{P\ i,j+1}^{TOP} + (J^2A - B)T_{P\ i,j+1} + \\ & + (J^2D - Z)T_{P\ i,j} + (J^2A - B)T_{P\ i,j-1} + \\ & + (J^2E - H)T_f{}^E + (J^2F - L)T_f{}^W]\end{aligned} \tag{3.98}$$

where

$$J = e^{\omega h} \tag{3.99}$$

$$W^{TOP} = k_W^{z\,TOP} s\,\omega \Delta x \tag{3.100}$$

Convective heat flux with fluid cells can be expressed in a synthetic form, letting:

$$S=\frac{\Delta y-s}{2}\frac{\Delta x}{2}\ \left[\left(\frac{3}{4}\alpha_{i,j}^{(1)}+\frac{3}{4}\alpha_{i,j}^{(2)}\right)T_{i,j}^{f\ W}+\frac{1}{4}\alpha_{i,j}^{(1)}T_{i,j-1}^{f\ W}+\frac{1}{4}\alpha_{i,j}^{(2)}T_{i,j+1}^{f\ W}+\right.$$
$$\left.+\left(\frac{3}{4}\alpha_{i,j}^{(3)}+\frac{3}{4}\alpha_{i,j}^{(4)}\right)T_{i,j}^{f\ E}+\frac{1}{4}\alpha_{i,j}^{(3)}T_{i,j+1}^{f\ E}+\frac{1}{4}\alpha_{i,j}^{(4)}T_{i,j-1}^{f\ E}\ \right] \tag{3.101}$$

$$R=-1\cdot\frac{\Delta y-s}{2}\frac{\Delta x}{2}\left(\alpha_{i,j}^{(1)}+\alpha_{i,j}^{(2)}+\alpha_{i,j}^{(3)}+\alpha_{i,j}^{(4)}\right) \tag{3.102}$$

so it appears as for base cell formulation:

$$\Delta\Phi_{i,j}^{f\ CONV\ TOP}=S+RT_{P\ \ i,j}^{TOP} \tag{3.103}$$

Thermal balance for a cover elementary portion, can thus be expressed as:

$$\begin{aligned}
&M^{TOP}(T_{P\ i,j-1}^{TOP}-T_{P\ i,j}^{TOP})+N^{TOP}(T_{P\ i,j+1}^{TOP}-T_{P\ i,j}^{TOP})+O^{TOP}(T_{P\ i-1,j}^{TOP}-T_{P\ i,j}^{TOP})+\\
&+P^{TOP}(T_{P\ i+1,j}^{TOP}-T_{P\ i,j}^{TOP})+Q^{TOP}(T_{EN}-T_{P\ i,j}^{TOP})+S+RT_{P\ \ i,j}^{TOP}+Q_{G}{}^{TOP}+\\
&-\frac{W^{TOP}}{J}[(J^2A-B)T_{P\ i,j-1}^{TOP}+(J^2C-G)T_{P\ i,j}^{TOP}+(J^2A-B)T_{P\ i,j+1}^{TOP}+\\
&+(J^2A-B)T_{P\ \ i,j+1}+(J^2D-Z)T_{P\ \ i,j}+(J^2A-B)T_{P\ \ i,j-1}+\\
&+(J^2E-H)T_{f}{}^{E}+(J^2F-L)T_{f}{}^{W}]=0
\end{aligned} \tag{3.104}$$

or, properly gathering the contributes:

$$\begin{aligned}
&-\frac{W^{TOP}}{J}(J^2A-B)T_{P\ \ i,j-1}-\frac{W^{TOP}}{J}(J^2D-Z)T_{P\ \ i,j}-\frac{W^{TOP}}{J}(J^2A-B)T_{P\ \ i,j+1}+\\
&+\left[M^{TOP}-\frac{W^{TOP}}{J}(J^2A-B)\right]T_{P\ i,j-1}^{TOP}+\\
&-\left[M^{TOP}+N^{TOP}+O^{TOP}+P^{TOP}+Q^{TOP}-R+\frac{W^{TOP}}{J}(J^2C-G)\right]T_{P\ i,j}^{TOP}\\
&+\left[N^{TOP}-\frac{W^{TOP}}{J}(J^2A-B)\right]T_{P\ i,j+1}^{TOP}=\\
&=-\left\{O^{TOP}T_{P\ i-1,j}^{TOP}+P^{TOP}T_{P\ i+1,j}^{TOP}+Q^{TOP}T_{EN}+S+Q_{G}{}^{TOP}\right\}+\\
&+\frac{W^{TOP}}{J}\left[(J^2E-H)T_{f}{}^{E}+(J^2F-L)T_{f}{}^{W}\right]
\end{aligned} \tag{3.105}$$

A compact expression, with matrix notation, can be easily achieved, letting

$$\alpha^{T}=-\frac{W^{TOP}}{J}(J^2A-B) \tag{3.106}$$

$$\beta^{T}=-\frac{W^{TOP}}{J}(J^2D-Z) \tag{3.107}$$

$$\gamma^T = -\frac{W^{TOP}}{J}(J^2 A - B) \tag{3.108}$$

$$\delta^T = M^{TOP} - \frac{W^{TOP}}{J}(J^2 A - B) \tag{3.109}$$

$$\varepsilon^T = -\left[M^{TOP} + N^{TOP} + O^{TOP} + P^{TOP} + Q^{TOP} - R + \frac{W^{TOP}}{J}(J^2 C - G) \right] \tag{3.110}$$

$$\varphi^T = N^{TOP} - \frac{W^{TOP}}{J}(J^2 A - B) \tag{3.111}$$

$$\begin{aligned} \upsilon^T &= -(O^{TOP} T^{TOP}_{P\ i-1,j} + P^{TOP} T^{TOP}_{P\ i+1,j} + Q^{TOP} T_{EN} + S + Q_G{}^{TOP}) + \\ &+ \frac{W^{TOP}}{J}\left[(J^2 E - H) T_f{}^E + (J^2 F - L) T_f{}^W \right] \end{aligned} \tag{3.112}$$

Therefore thermal balance on cover cells can be written in matrix notation as

$$\begin{bmatrix} \alpha^T & \beta^T & \gamma^T & \delta^T & \varepsilon^T & \varphi^T \end{bmatrix}_k \cdot \begin{Bmatrix} T_{P\ i,k-1} \\ T_{P\ i,k} \\ T_{P\ i,k+1} \\ T^{TOP}_{P\ i,k-1} \\ T^{TOP}_{P\ i,k} \\ T^{TOP}_{P\ i,k+1} \end{Bmatrix} = \upsilon^T{}_k \tag{3.113}$$

Index k points a single analyzed cell, while index i characterized the selected strip. Left-hand member shows the product of coefficients containing geometrical and thermo-physical properties by solid sub-domain temperatures (the ones for the analyzed cell and those of the adjacent solid cell belonging to the same strip), while the right-hand member (i.e. the term $\upsilon_{i,k}$) gathers known values referred both to the adjacent fluid cells temperatures and to adjacent plate cells belonging to different strips, as shown in figure 3.15.

3.9.4 Composition of a matrix for an entire strip

Thanks to the matrix form used in (3.89) and (3.113), thermal balance for an entire strip can be easily obtained. Since each element presents unknown temperatures both for the cover and for the base, it appears more proper to gather base temperature related coefficients and cover ones in different parts of a matrix, as shown in the

following. Letting N be the number of cells by which a strip is made of, there are 2N equations and 2N unknowns, two for each cell. For example, let us consider a 5 element strip, and let us write the matrix to be used to solve the entire strip.

The system to be solved will present 10 equations and ten unknowns, i.e. five base temperatures and five cover temperatures.
Such system can be written in the following matrix notation, where coefficients are marked by B if referred to bottom plate cells, and by T if related to top plate cells.

$$\begin{bmatrix}
\alpha_1^B & \beta_1^B & \gamma_1^B & 0 & 0 & 0 & 0 & \delta_1^B & \varepsilon_1^B & \varphi_1^B & 0 & 0 & 0 & 0 \\
0 & \alpha_2^B & \beta_2^B & \gamma_2^B & 0 & 0 & 0 & 0 & \delta_2^B & \varepsilon_2^B & \varphi_2^B & 0 & 0 & 0 \\
0 & 0 & \alpha_3^B & \beta_3^B & \gamma_3^B & 0 & 0 & 0 & 0 & \delta_3^B & \varepsilon_3^B & \varphi_3^B & 0 & 0 \\
0 & 0 & 0 & \alpha_4^B & \beta_4^B & \gamma_4^B & 0 & 0 & 0 & 0 & \delta_4^B & \varepsilon_4^B & \varphi_4^B & 0 \\
0 & 0 & 0 & 0 & \alpha_5^B & \beta_5^B & \gamma_5^B & 0 & 0 & 0 & 0 & \delta_5^B & \varepsilon_5^B & \varphi_5^B \\
\alpha_1^T & \beta_1^T & \gamma_1^T & 0 & 0 & 0 & 0 & \delta_1^T & \varepsilon_1^T & \varphi_1^T & 0 & 0 & 0 & 0 \\
0 & \alpha_2^T & \beta_2^T & \gamma_2^T & 0 & 0 & 0 & 0 & \delta_2^T & \varepsilon_2^T & \varphi_2^T & 0 & 0 & 0 \\
0 & 0 & \alpha_3^T & \beta_3^T & \gamma_3^T & 0 & 0 & 0 & 0 & \delta_3^T & \varepsilon_3^T & \varphi_3^T & 0 & 0 \\
0 & 0 & 0 & \alpha_4^T & \beta_4^T & \gamma_4^T & 0 & 0 & 0 & 0 & \delta_4^T & \varepsilon_4^T & \varphi_4^T & 0 \\
0 & 0 & 0 & 0 & \alpha_5^T & \beta_5^T & \gamma_5^T & 0 & 0 & 0 & 0 & \delta_5^T & \varepsilon_5^T & \varphi_5^T
\end{bmatrix}
\begin{Bmatrix} T_0 \\ T_1 \\ T_2 \\ T_3 \\ T_4 \\ T_5 \\ T_6 \\ T_0^T \\ T_1^T \\ T_2^T \\ T_3^T \\ T_4^T \\ T_5^T \\ T_6^T \end{Bmatrix}
=
\begin{Bmatrix} v_1^B \\ v_2^B \\ v_3^B \\ v_4^B \\ v_5^B \\ v_1^T \\ v_2^T \\ v_3^T \\ v_4^T \\ v_5^T \end{Bmatrix}
\qquad (3.114)$$

Since each cell thermal balance involves the preceding cell and the subsequent cell, the temperature vector in the matrix notation shows two couples of temperatures related to the cells both previous the first one and following the last one. The system can be solved once boundary condition are imposed to the single strip analyzed. For example, T_0 and T_0^T could be considered identical to T_1 and T_1^T respectively, and analogously T_6 and T_6^T could be considered identical to T_5 and T_5^T respectively (it means conduction heat flux along x direction is neglected at the cold plate edges).

Therefore, temperature coefficients are to be modified as in the following matrix form:

$$\alpha_1^B + \beta_1^B = \beta_1^{B*} \qquad (3.115)$$

$$\alpha_1^T + \beta_1^T = \beta_1^{T*} \qquad (3.116)$$

$$\beta_5^B + \gamma_5^B = \beta_5^{B*} \qquad (3.117)$$

$$\beta_5^{\ T} + \gamma_5^{\ T} = \beta_5^{\ T*} \tag{3.118}$$

$$\delta_1^{\ B} + \varepsilon_1^{\ B} = \varepsilon_1^{\ B*} \tag{3.119}$$

$$\delta_1^{\ T} + \varepsilon_1^{\ T} = \varepsilon_1^{\ T*} \tag{3.120}$$

$$\varepsilon_5^{\ B} + \varphi_5^{\ B} = \varepsilon_5^{\ B*} \tag{3.121}$$

$$\varepsilon_5^{\ T} + \varphi_5^{\ T} = \varepsilon_5^{\ T*} \tag{3.122}$$

$$\begin{bmatrix}
\alpha_1^{\ B} & \beta_1^{\ B} & \gamma_1^{\ B} & 0 & 0 & 0 & 0 & \delta_1^{\ B} & \varepsilon_1^{\ B} & \varphi_1^{\ B} & 0 & 0 & 0 & 0 \\
0 & \alpha_2^{\ B} & \beta_2^{\ B} & \gamma_2^{\ B} & 0 & 0 & 0 & 0 & \delta_2^{\ B} & \varepsilon_2^{\ B} & \varphi_2^{\ B} & 0 & 0 & 0 \\
0 & 0 & \alpha_3^{\ B} & \beta_3^{\ B} & \gamma_3^{\ B} & 0 & 0 & 0 & 0 & \delta_3^{\ B} & \varepsilon_3^{\ B} & \varphi_3^{\ B} & 0 & 0 \\
0 & 0 & 0 & \alpha_4^{\ B} & \beta_4^{\ B} & \gamma_4^{\ B} & 0 & 0 & 0 & 0 & \delta_4^{\ B} & \varepsilon_4^{\ B} & \varphi_4^{\ B} & 0 \\
0 & 0 & 0 & 0 & \alpha_5^{\ B} & \beta_5^{\ B} & \gamma_5^{\ B} & 0 & 0 & 0 & 0 & \delta_5^{\ B} & \varepsilon_5^{\ B} & \varphi_5^{\ B} \\
\alpha_1^{\ T} & \beta_1^{\ T} & \gamma_1^{\ T} & 0 & 0 & 0 & 0 & \delta_1^{\ T} & \varepsilon_1^{\ T} & \varphi_1^{\ T} & 0 & 0 & 0 & 0 \\
0 & \alpha_2^{\ T} & \beta_2^{\ T} & \gamma_2^{\ T} & 0 & 0 & 0 & 0 & \delta_2^{\ T} & \varepsilon_2^{\ T} & \varphi_2^{\ T} & 0 & 0 & 0 \\
0 & 0 & \alpha_3^{\ T} & \beta_3^{\ T} & \gamma_3^{\ T} & 0 & 0 & 0 & 0 & \delta_3^{\ T} & \varepsilon_3^{\ T} & \varphi_3^{\ T} & 0 & 0 \\
0 & 0 & 0 & \alpha_4^{\ T} & \beta_4^{\ T} & \gamma_4^{\ T} & 0 & 0 & 0 & 0 & \delta_4^{\ T} & \varepsilon_4^{\ T} & \varphi_4^{\ T} & 0 \\
0 & 0 & 0 & 0 & \alpha_5^{\ T} & \beta_5^{\ T} & \gamma_5^{\ T} & 0 & 0 & 0 & 0 & \delta_5^{\ T} & \varepsilon_5^{\ T} & \varphi_5^{\ T}
\end{bmatrix}
\begin{Bmatrix} T_0 \\ T_1 \\ T_2 \\ T_3 \\ T_4 \\ T_5 \\ T_6 \\ T_0^{\ T} \\ T_1^{\ T} \\ T_2^{\ T} \\ T_3^{\ T} \\ T_4^{\ T} \\ T_5^{\ T} \\ T_6^{\ T} \end{Bmatrix}
=
\begin{Bmatrix} v_1 \\ v_2 \\ v_3 \\ v_4 \\ v_5 \\ v_1^{\ T} \\ v_2^{\ T} \\ v_3^{\ T} \\ v_4^{\ T} \\ v_5^{\ T} \end{Bmatrix}$$

and finally the correct matrix expression is obtained

$$\begin{bmatrix}
\beta_1^{\ B*} & \gamma_1^{\ B} & 0 & 0 & 0 & \varepsilon_1^{\ B*} & \varphi_1^{\ B} & 0 & 0 & 0 \\
\alpha_2^{\ B} & \beta_2^{\ B} & \gamma_2^{\ B} & 0 & 0 & \delta_2^{\ B} & \varepsilon_2^{\ B} & \varphi_2^{\ B} & 0 & 0 \\
0 & \alpha_3^{\ B} & \beta_3^{\ B} & \gamma_3^{\ B} & 0 & 0 & \delta_3^{\ B} & \varepsilon_3^{\ B} & \varphi_3^{\ B} & 0 \\
0 & 0 & \alpha_4^{\ B} & \beta_4^{\ B} & \gamma_4^{\ B} & 0 & 0 & \delta_4^{\ B} & \varepsilon_4^{\ B} & \varphi_4^{\ B} \\
0 & 0 & 0 & \alpha_5^{\ B} & \beta_5^{\ B*} & 0 & 0 & 0 & \delta_5^{\ B} & \varepsilon_5^{\ B*} \\
\beta_1^{\ T*} & \gamma_1^{\ T} & 0 & 0 & 0 & \varepsilon_1^{\ T*} & \varphi_1^{\ T} & 0 & 0 & 0 \\
\alpha_2^{\ T} & \beta_2^{\ T} & \gamma_2^{\ T} & 0 & 0 & \delta_2^{\ T} & \varepsilon_2^{\ T} & \varphi_2^{\ T} & 0 & 0 \\
0 & \alpha_3^{\ T} & \beta_3^{\ T} & \gamma_3^{\ T} & 0 & 0 & \delta_3^{\ T} & \varepsilon_3^{\ T} & \varphi_3^{\ T} & 0 \\
0 & 0 & \alpha_4^{\ T} & \beta_4^{\ T} & \gamma_4^{\ T} & 0 & 0 & \delta_4^{\ T} & \varepsilon_4^{\ T} & \varphi_4^{\ T} \\
0 & 0 & 0 & \alpha_5^{\ T} & \beta_5^{\ T*} & 0 & 0 & 0 & \delta_5^{\ T} & \varepsilon_5^{\ T*}
\end{bmatrix}
\cdot
\begin{Bmatrix} T_1 \\ T_2 \\ T_3 \\ T_4 \\ T_5 \\ T_1^{\ T} \\ T_2^{\ T} \\ T_3^{\ T} \\ T_4^{\ T} \\ T_5^{\ T} \end{Bmatrix}
=
\begin{Bmatrix} v_1^{\ B} \\ v_2^{\ B} \\ v_3^{\ B} \\ v_4^{\ B} \\ v_5^{\ B} \\ v_1^{\ T} \\ v_2^{\ T} \\ v_3^{\ T} \\ v_4^{\ T} \\ v_5^{\ T} \end{Bmatrix}
\tag{3.123}$$

Such system can be easily implemented in a numerical code and thus solved by inverting the 2N x 2N matrix first and multiplying it by the known value vector. It is worth noting that coefficients are placed just in particular position, and a “good”

number of 0 appears. So the solution can be quickly obtained thanks to proper numerical algorithms created for sparse matrix.

3.10 Fluid sub-domain

3.10.1 General aspects

Beside the metal sub-domain model, fluid sub-domain is to be defined to evaluate fluid thermo-physical properties and its behavior. First of all, some simplifying hypotheses are introduced, since the model purpose is to analyze the entire heat exchanger and not to solve the fluid flow field using full Navier-Stokes equations.

According to Asinari (2004), fluid sub-domain can be divided into one-dimensional streams, following the flow field, one for each channel. The possibility of a mixing region, either in the manifold to produce a generic circuit, or inside a cold plate (merging two channels), which average conditions, can be easily included.

As the fluid flow is assumed to be one-dimensional, it is not possible to calculate cross flow gradients involved in heat fluxes, so it is to be calculated by means of heat transfer coefficients given by literature. Besides, the viscous dissipation are neglected, then respective heat generation in the energy conservation equations can also be neglected.

When considering a two-phase fluid, separated fluid model is assumed and governing equations are expressed in (3.5), (3.6), and (3.7), while in the case of a single-phase fluid, equation (3.2), (3.3), and (3.4) are to be considered, but energy equation can be assumed to be decoupled from the system, and can be solved independently.

The choice of the model will depend on the kind of heat exchanger to be simulated, considering that two-phase model can be simplified compare to the equations here proposed, but anyway temperature / enthalpy field must be solved together with pressure field, making the simulation more time-consuming.

As for the plate sub-domain, FVM is chosen to discretize the fluid sub-domain, since it appears as the easiest way, and up-wind scheme is adopted.

3.10.2 Elementary fluid cell

Let us Refer to figure 3.3 which shows a plan view of a generic cold plate with both plate and fluid (arrow pikes) grid points. Let N_{ch} be the number of microchannels

by which cold plate is divided, and let N_{mesh} be the number of elementary cell by which a single channel is subdivided, then the number of fluid cell is

$$N_{fluid}^{cell} = N_{ch} \cdot N_{mesh} \tag{3.124}$$

where:

$$N_{mesh} = \frac{L}{\Delta x} \tag{3.125}$$

being L the total length of the cold plate and being Δx the size of the cell according to the fluid path direction.

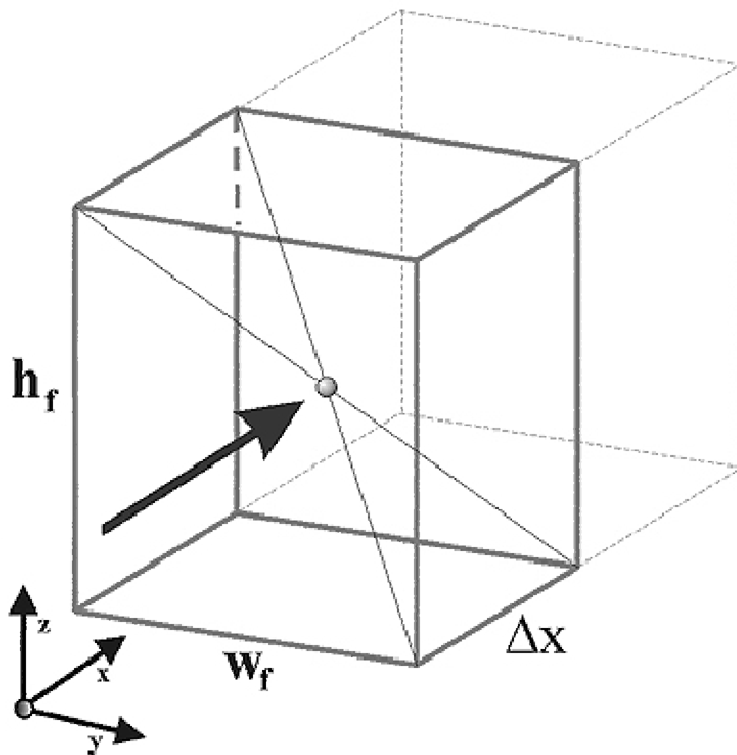

Fig. 3.16- Elementary fluid cell

As far as for the other dimensions:

$$h_f = H_{COLDPLATE} - \Delta z - \Delta z^{TOP} \tag{3.126}$$

where Δz e Δz^{TOP} are the plate thickness, both base and cover.

Finally W_f represent the microchannel width, expressed as

$$W_f = \Delta y - s \tag{3.127}$$

where Δy is the solid sub-domain cell width, and s the corresponding fin thickness.

In the following, the case of all channels fed by the same mass flow and in the same direction is considered, but it is quite easy to analyze different configurations.

3.10.3 Convective heat transfer coefficient

Let us consider a single-phase incompressible fluid, and all the channels fed in parallel, as said above, and let us write the energy conservation for this particular case with the objective to have in the end a matrix notation as for the sold sub-domain.

As far as for the convection heat transfer coefficient, several correlation allow to evaluate it according to the flow regime considered (laminar or turbulent), channel geometry and the fluid nature itself.

Local coefficients associated with laminar flow in a rectangular channel could be obtained using results proposed by Shah and London (1978). Laminar flow conditions is achieved below critical $\mathrm{Re}_{Dh,c}$, which can be evaluated as $\mathrm{Re}_{Dh,c} \approx 2300$.

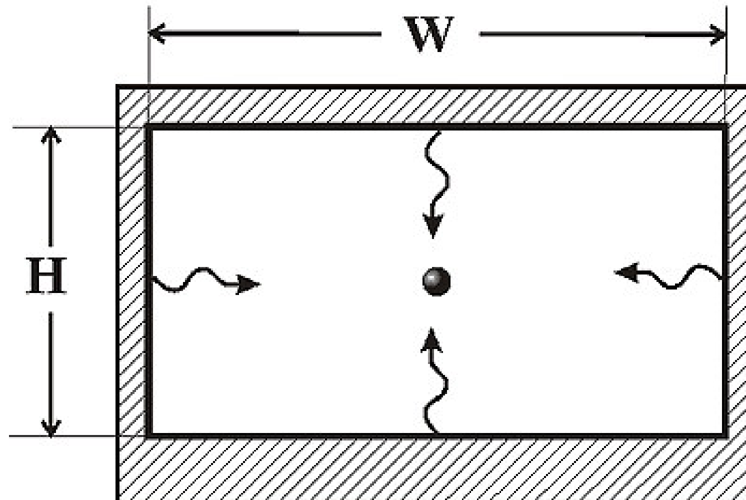

Fig. 3.17- Channel cross section

Referring to figure 3.17, the aspect ration *A* is defined as *W/H* or *H/W*, whichever is smaller

$$A = \frac{W}{H} \tag{3.128}$$

The effect of the aspect ratio on the Nusselt number was determined by Shah and London by

$$Nu_{Dh} = 8.235 \cdot \left(1 - \frac{2.0421}{A} + \frac{3.0853}{A^2} - \frac{2.4765}{A^3} + \frac{1.0578}{A^4} - \frac{0.1861}{A^5}\right) \tag{3.129}$$

where

$$Nu_{Dh} = \frac{\alpha \cdot D_h}{k} \tag{3.130}$$

where α is the convective heat flux coefficient, k is the thermal conductivity and $D_h = 4\frac{A_c}{P}$ is the channel hydraulic diameter.

In the case of a rectangular channel, it can be written:

$$D_h = 4\frac{A_c}{P} = 4\frac{WH}{2(W+H)} = 2\frac{WH}{W+H} \tag{3.131}$$

The foregoing correlation for the local heat transfer coefficient is referred to a fully developed flow condition.

When fluids enters the channel with a uniform velocity, a hydrodynamic boundary layer begin to form as the fluid meets the wall, in which fluid velocity increases starting from the wall toward the centerline, till region called inviscid, in which fluid velocity is uniform and higher than the inlet one, in order to allow the mass conservation equation to be fulfilled. The entrance region extends its limit where hydrodynamic boundary layers merge at the centerline of the channel. According to Shah and London (1978) the extent of the entrance region, from a hydrodynamic point of view, is associated with the distance at which the centerline velocity achieves 99% of its fully developed value.

According to Incropera (1999), entrance and fully developed regions are also associated with thermal conditions. If fluid enters the circular tube at a uniform temperature, lower than the walls one, also a thermal boundary layer begins to form. Fully developed condition is reached, from a thermal point of view, when either a uniform temperature or a uniform heat flux is imposed at the wall.

Since entrance region displays a radial temperature profile different from the ones occurring in the full developed region, also convective heat flux coefficients are different along x direction (i.e. the fluid path direction).

Local coefficient is in principle infinite at tube inlet, where contact is made with the wall and thermal boundary layer thickness is zero, and decreases as the layer develops till a constant value when fully developed condition is reached.

In the case there is a not heated region at the tube inlet, hydrodynamic layer forms before thermal layer, and hydrodynamic fully developed condition could occurs

before thermal layer begins to develop. This situation also happens for very large Prandtl number fluids, or in the case of a hot-spot (i.e. a local very high imposed heat flux), which is a quite common situation in electronics cooling.

Thermal entrance length is slightly larger for a simultaneously developing flow than for a thermal developing flow, and for a uniform surface heat flux than for a uniform surface temperature (Incropera, 1999). Its extent is commonly associated with the distance at which local coefficient is 5% higher the one achieved in full developed region. Shah and London (1978) defined a dimensionless form, to determine the thermal entrance region, as

$$x^*_{fd,th} = \frac{x_{fd,th}}{D_h \operatorname{Re}_{Dh} \operatorname{Pr}}. \tag{3.132}$$

For a uniform surface heat flux and square cross section (i.e. A=1), $x^*_{fd,th} = 0.066$, and decreases to $x^*_{fd,th} = 0.042$ when aspect ratio decreases to A=0.25.

For a rectangular channel, local heat transfer coefficient at a certain distance from the tube inlet x^* can be calculated according to the table proposed by Phillips (1988), which reports interpolation values of Shah and London analysis.

Tab. 3.1- Nusselt number for laminar flow in a rectangular cross section channel

	Nu$_{Dh}$				
x^*	A=1	A=1/2	A=1/3	A=1/4	$A \le 0.1$
0.0001	25.2	23.7	27	26.7	31.4
0.0025	8.9	9.2	9.9	10.4	11.9
0.005	7.1	7.46	8.02	8.44	10
0.00714	6.32	6.68	7.22	7.63	9.3
0.00833	6.02	6.37	6.92	7.32	9.1
0.01	5.69	6.05	6.57	7	8.8
0.0125	5.33	5.7	6.21	6.63	8.6
0.0167	4.91	5.28	5.82	6.26	8.5
0.025	4.45	4.84	5.39	5.87	8.4
0.033	4.18	4.61	5.17	5.77	8.3
0.05	3.91	4.38	5	5.62	8.25
0.1	3.71	4.22	4.85	5.45	8.24
1	3.6	4.11	4.77	5.35	8.23

For fully developed turbulent flow ($\operatorname{Re}_{Dh} > 10000$) in small tubes, Dittus-Boelter equation is commonly used to determined local Nusselt number:

$$\operatorname{Nu}_{Dh} = 0.023 \operatorname{Re}_{Dh}^{4/5} \operatorname{Pr}^{0.4} \tag{3.133}$$

For smaller Reynolds number, Gnielinski correlation is recommended,

$$\mathrm{Nu}_{Dh} = \frac{(f/2)(\mathrm{Re}_{Dh} - 1000)\mathrm{Pr}}{1 + 12.7(f/2)^{1/2}(\mathrm{Pr}^{2/3} - 1)} \tag{3.134}$$

where the friction factor f can be evaluated by

$$f = (1.58 \ln \mathrm{Re}_{Dh} - 3.28)^{-2} \tag{3.135}$$

Finally, it is to be pointed out that boundary layers develop much more quickly for a turbulent flow than for laminar one: fully developed condition, both hydrodynamic and thermal, is usually reached within a length corresponding to 10 D_h, so this effect can often be neglected, or it can be considered by modifying Gnielinski correlation as

$$\mathrm{Nu}_{Dh} = \frac{(f/2)(\mathrm{Re}_{Dh} - 1000)\mathrm{Pr}}{1 + 12.7(f/2)^{1/2}(\mathrm{Pr}^{2/3} - 1)}\left[1 + \left(\frac{D_h}{L}\right)^{2/3}\right] \tag{3.136}$$

3.10.4 Heat flux contributes

In the following, a single-phase fluid is considered as the coolant medium. In the case of two-phase fluid, temperature is to be replaced by enthalpy in energy balance equations.

Each fluid cell is subjected to convective heat flux over several surfaces, as shown in figure 3.18.

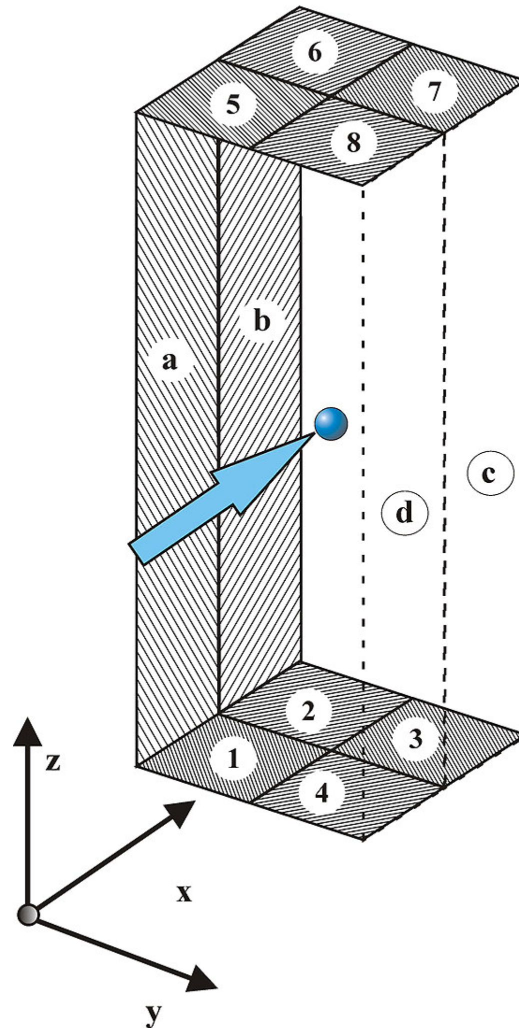

Fig. 3.18- Fluid cell surfaces through which heat flux occurs

There can be identified twelve different heat fluxes, four on the walls separating adjacent channels, *(a)-(b)* and *(c)-(d),* four on the base and four on the cover. These areas are characterized by different wall and fluid temperatures, as a linear temperature profile was chosen to interpolate fluid temperature field. Since plates and fin temperatures are known, given by the previous calculation step, heat flux over each surface can be calculated by the integral of the product of temperature difference by local convective coefficient, and thus energy conservation equation allows to determine the fluid temperature field:

$$\sum_{i=a}^{d} \Delta\Phi_i + \sum_{j=1}^{8} \Delta\Phi_j = \dot{m} c_P \Delta T_f \tag{3.137}$$

3.10.5 Heat flux over vertical walls

Thanks to the shape function already determined (3.22),

$$\vartheta(x,z) = C_1 e^{\omega x} + C_2 e^{-\omega x} + C_3 e^{\omega z} + C_4 e^{-\omega z} \qquad (3.22)$$

heat flux for the selected fluid cell, over the generic vertical wall can be calculated.
Let us consider the case of the surfaces tagged by *a* in the figure 3.18. Heat flux is of the form

$$\Delta\Phi^f{}_a = \int_0^{h_f} \int_{\frac{-\Delta x}{2}}^{0} \alpha \;\; \vartheta^W(x,z) dx dz \qquad (3.138)$$

where $\vartheta^W(x,z)$ is the difference between the wall temperature at a generic *x,z* point, and the fluid temperature. Let the fluid temperature be uniform over the surface considered, and according to the definition of the shape function for the vertical wall $\vartheta_{i-1}(x,z)$, then it can be written

$$\vartheta^W(x,z) = \vartheta_i\,(x,z) + \left[\frac{\alpha_E T_f^E + \alpha_W T_f^W}{\alpha_E + \alpha_W}\right]_i^{wall} - T_f \qquad (3.139)$$

where superscript *W* means that the West vertical wall is considered, i.e. the wall belonging to the solid element marked by *i*, when the generic *i* fluid cell is analyzed, so T_f^E and T_f^W are the West fluid temperature and East fluid temperature respectively, referring to the solid element marked by *i*.

Therefore, heat flux can be calculated by the sum of three contributes

$$\Delta\Phi^I{}_a = \int_0^{h_f} \int_{\frac{-\Delta x}{2}}^{0} \alpha \;\; \vartheta_i\,(x,z) dx dz =$$

$$\frac{\alpha h_f}{\omega_i^{wall}} \left[C_1\left(1 - \frac{1}{\sqrt{X}}\right) + C_2\left(\sqrt{X} - 1\right) + \frac{\Delta x}{2h_f} \cdot C_3\left(Y - 1\right) + \frac{\Delta x}{2h_f} \cdot C_4 (1 - \frac{1}{Y}) \right]_i^{wall} \qquad (3.140)$$

$$\Delta\Phi^{II}{}_a = \int_0^{h_f}\int_{\frac{-\Delta x}{2}}^{0} \alpha\left[\frac{\alpha_E T_f^E + \alpha_W T_f^W}{\alpha_E + \alpha_W}\right]_i^{wall} = +h_f\frac{\Delta x}{2}\alpha\left[\frac{\alpha_E T_f^E + \alpha_W T_f^W}{\alpha_E + \alpha_W}\right]_i^{wall} \tag{3.141}$$

$$\Delta\Phi^{III}{}_a = \int_0^{h_f}\int_{\frac{-\Delta x}{2}}^{0} -\alpha T_f\,dxdz = -\alpha T_f h_f\frac{\Delta x}{2} \tag{3.142}$$

And finally

$$\begin{aligned}\Delta\Phi^{f}{}_a &= \Delta\Phi^{I}{}_a + \Delta\Phi^{II}{}_a + \Delta\Phi^{III}{}_a = \\ &= \frac{\alpha h_f}{\omega_i^{wall}}\left[C_1\left(1-\frac{1}{\sqrt{X}}\right) + C_2\left(\sqrt{X}-1\right) + \frac{\Delta x}{2h_f}\cdot C_3\left(Y-1\right) + \frac{\Delta x}{2h_f}\cdot C_4(1-\frac{1}{Y})\right]_i^{wall} + \\ &+ h_f\frac{\Delta x}{2}\alpha\left[\frac{\alpha_E T_f^E + \alpha_W T_f^W}{\alpha_E + \alpha_W}\right]_i^{wall} - \alpha T_f h_f\frac{\Delta x}{2}\end{aligned} \tag{3.143 a}$$

Heat flux over the other vertical wall areas, i.e. *b*,*c*, and *d* can be evaluated in the same way:

$$\begin{aligned}\Delta\Phi_b{}^f &= \int_0^{h_f}\int_0^{\frac{\Delta x}{2}} \alpha\,\vartheta^W(x,z)dxdz = \\ &= \frac{\alpha h_f}{\omega_i^{wall}}\left[C_1(\sqrt{X}-1) + C_2\left(1-\frac{1}{\sqrt{X}}\right) + \frac{\Delta x}{2h_f}\cdot C_3\left(Y-1\right) + \frac{\Delta x}{2h_f}\cdot C_4(1-\frac{1}{Y})\right]_i^{wall} + \\ &+ h_f\frac{\Delta x}{2}\alpha\left[\frac{\alpha_E T_f^E + \alpha_W T_f^W}{\alpha_E + \alpha_W}\right]_i^{wall} - \alpha T_f h_f\frac{\Delta x}{2}\end{aligned} \tag{3.143 b}$$

$$\begin{aligned}\Delta\Phi_c{}^f &= \int_0^{h_f}\int_0^{\frac{\Delta x}{2}} \alpha\;\vartheta^E(x,z)dxdz = \\ &= \frac{\alpha h_f}{\omega_{i+1}^{wall}}\left[C_1(\sqrt{X}-1) + C_2\left(1-\frac{1}{\sqrt{X}}\right) + \frac{\Delta x}{2h_f}\cdot C_3\left(Y-1\right) + \frac{\Delta x}{2h_f}\cdot C_4(1-\frac{1}{Y})\right]_{i+1}^{wall} + \\ &+ h_f\frac{\Delta x}{2}\alpha\left[\frac{\alpha_E T_f^E + \alpha_W T_f^W}{\alpha_E + \alpha_W}\right]_{i+1}^{wall} - \alpha T_f h_f\frac{\Delta x}{2}\end{aligned} \tag{3.143 c}$$

$$\Delta\Phi_d = \int_0^{h_f} \int_{-\frac{\Delta x}{2}}^{0} \alpha\, \vartheta^E(x,z)\, dx dz =$$

$$= + \frac{\alpha h_f}{\omega_{i+1}^{wall}} \left[C_1 \left(1 - \frac{1}{\sqrt{X}} \right) + C_2 \left(\sqrt{X} - 1 \right) + \frac{\Delta x}{2h_f} \cdot C_3 (Y-1) + \frac{\Delta x}{2h_f} \cdot C_4 (1 - \frac{1}{Y}) \right]_{i+1}^{wall} +$$

$$+ h_f \frac{\Delta x}{2} \alpha \left[\frac{\alpha_E T_f^E + \alpha_W T_f^W}{\alpha_E + \alpha_W} \right]_{i+1}^{wall} - \alpha T_f h_f \frac{\Delta x}{2} \tag{3.143 d}$$

where h_f is the fin height and is defined by (4.3), $X = e^{\omega \Delta x}$ and $Y = e^{\omega h_f}$.

Finally:

$$\Delta\Phi^f{}_{a-b-c-d} = \Delta\Phi^f{}_a + \Delta\Phi^f{}_b + \Delta\Phi^f{}_c + \Delta\Phi^f{}_d \tag{3.144}$$

In the foregoing expressions, the only unknown is the fluid temperature T_f, because all other temperatures, including T_f^E and T_f^W, come from the previous step in the iterative procedure.

Letting

$$A^{FLUID} = -2\alpha h_f \Delta x \tag{3.145}$$

$$B^{FLUID} = \alpha h_f \Delta x \left[\frac{\alpha_E T_f^E + \alpha_W T_f^W}{\alpha_E + \alpha_W} \right]_i^{wall} + \alpha h_f \Delta x \left[\frac{\alpha_E T_f^E + \alpha_W T_f^W}{\alpha_E + \alpha_W} \right]_{i+1}^{wall} +$$

$$+ \frac{\alpha h_f}{\omega_i^{wall}} \left\{ \begin{array}{l} \left[C_1 \left(1 - \frac{1}{\sqrt{X}} \right) + C_2 \left(\sqrt{X} - 1 \right) + \frac{\Delta x}{2h_f} \cdot C_3 (Y-1) + \frac{\Delta x}{2h_f} \cdot C_4 (1 - \frac{1}{Y}) \right]_i^{wall} + \\ + \left[C_1 (\sqrt{X} - 1) + C_2 \left(1 - \frac{1}{\sqrt{X}} \right) + \frac{\Delta x}{2h_f} \cdot C_3 (Y-1) + \frac{\Delta x}{2h_f} \cdot C_4 (1 - \frac{1}{Y}) \right]_i^{wall} \end{array} \right\} +$$

$$+ \frac{\alpha h_f}{\omega_{i+1}^{wall}} \left\{ \begin{array}{l} \left[C_1 (\sqrt{X} - 1) + C_2 \left(1 - \frac{1}{\sqrt{X}} \right) + \frac{\Delta x}{2h_f} \cdot C_3 (Y-1) + \frac{\Delta x}{2h_f} \cdot C_4 (1 - \frac{1}{Y}) \right]_{i+1}^{wall} + \\ + \left[C_1 \left(1 - \frac{1}{\sqrt{X}} \right) + C_2 \left(\sqrt{X} - 1 \right) + \frac{\Delta x}{2h_f} \cdot C_3 (Y-1) + \frac{\Delta x}{2h_f} \cdot C_4 (1 - \frac{1}{Y}) \right]_{i+1}^{wall} \end{array} \right\}$$

$$\tag{3.146}$$

and properly rewriting B^{FLUID},

$$B^{FLUID} = \alpha h_f \Delta x \left\{ \left[Alfa*\right]_i^{wall} + \left[Alfa*\right]_{i+1}^{wall} \right\} + \\ + \frac{\alpha h_f}{\omega_i^{wall}} \left[Beta*\right]_i^{wall} + \frac{\alpha h_f}{\omega_{i+1}^{wall}} \left[Beta*\right]_{i+1}^{wall} \qquad (3.147)$$

where

$$Alfa* = \left[\frac{\alpha_E T_f^E + \alpha_W T_f^W}{\alpha_E + \alpha_W} \right] \qquad (3.148)$$

$$Beta* = \left[C_1\left(1 - \frac{1}{\sqrt{X}}\right) + C_2\left(\sqrt{X} - 1\right) + \frac{\Delta x}{2h_f} \cdot C_3\left(Y - 1\right) + \frac{\Delta x}{2h_f} \cdot C_4(1 - \frac{1}{Y}) \right] + \\ + \left[C_1(\sqrt{X} - 1) + C_2\left(1 - \frac{1}{\sqrt{X}}\right) + \frac{\Delta x}{2h_f} \cdot C_3\left(Y - 1\right) + \frac{\Delta x}{2h_f} \cdot C_4(1 - \frac{1}{Y}) \right] \qquad (3.149)$$

it can be finally written

$$\Delta\Phi^f{}_{a-b-c-d} = A^{FLUID} \; T_f + B^{FLUID} \qquad (3.150)$$

3.10.6 Convection over base and cover plate surfaces

As already done for the separating wall, integrals of the product of temperature difference by convective coefficient are to be calculated over the surfaces marked with numbers from 1 to 8. It is worth to point out that left hand surfaces are characterized by different temperature compare to the right hand ones.

Referring to expressions as the (3.48), and letting

$$\mu^{EAST} = \alpha_{k,j} \frac{\Delta y - s^{EAST}}{2} \frac{\Delta x}{2} \qquad (3.151\ a)$$

$$\mu^{WEST} = \alpha_{k,j} \frac{\Delta y - s^{WEST}}{2} \frac{\Delta x}{2} \qquad (3.151\ b)$$

where Δy is referred to the solid cell width and s^{EAST} and s^{WEST} relate to the fin thickness of the East fin and west one respectively, it can be finally written:

$$\Delta\Phi_1 = -\mu^{EAST} (\frac{3}{4} T_{f\ k,j} + \frac{1}{4} T_{f\ k,j-1} - T_{P i,j}) \qquad (3.152\ a)$$

$$\Delta\Phi_2 = -\mu^{EAST}(\frac{3}{4}T_{f\ k,j} + \frac{1}{4}T_{f\ k,j+1} - T_{P\ \ i,j}) \tag{3.152 b}$$

$$\Delta\Phi_3 = -\mu^{WEST}(\frac{3}{4}T_{f\ k,j} + \frac{1}{4}T_{f\ k,j+1} - T_{P\ \ i+1,j}) \tag{3.152 c}$$

$$\Delta\Phi_4 = -\mu^{WEST}(\frac{3}{4}T_{f\ k,j} + \frac{1}{4}T_{f\ k,j-1} - T_{P\ \ i+1,j}) \tag{3.152 d}$$

In the same way, for heat fluxes *5-6-7-8*

$$\Delta\Phi_5 = -\mu^{EAST}(\frac{3}{4}T_{f\,k,j} + \frac{1}{4}T_{f\ k,j-1} - T^{TOP}_{P\ \ i,j}) \tag{3.153 a}$$

$$\Delta\Phi_6 = -\mu^{EAST}(\frac{3}{4}T_{f\ k,j} + \frac{1}{4}T_{f\ k,j+1} - T^{TOP}_{P\ \ i,j}) \tag{3.153 b}$$

$$\Delta\Phi_7 = -\mu^{WEST}(\frac{3}{4}T_{f\ k,j} + \frac{1}{4}T_{f\ k,j+1} - T^{TOP}_{P\ \ i+1,j}) \tag{3.153 c}$$

$$\Delta\Phi_8 = -\mu^{WEST}(\frac{3}{4}T_{f\ k,j} + \frac{1}{4}T_{f\ k,j-1} - T^{TOP}_{P\ \ i+1,j}) \tag{3.153 d}$$

The minus sign means that incoming heat fluxes, given by T_p higher than T_f, are considered positive in the thermal balance. Index *(k,j)* refers to a generic fluid cell, surrounded by walls marked by *(i)* and *(i+1)*, as in figure 3.19, West and East of fluid cell respectively.

Summing all eight contributes, heat flux over base and cover plate element has the form of:

$$\begin{aligned}\Delta\Phi_{DOWN,UP} = \mu^{EAST}&\left(2T_{P\ \ i,j} + 2T^{TOP}_{P\ \ i,j} - 3T_{f\,k,j} - \frac{1}{2}T_{f\ k,j-1} - \frac{1}{2}T_{f\ k,j+1}\right) + \\ + \mu^{WEST}&\left(2T_{P\ \ i+1,j} + 2T^{TOP}_{P\ \ i+1,j} - 3T_{f\,k,j} - \frac{1}{2}T_{f\ k,j-1} - \frac{1}{2}T_{f\ k,j+1}\right)\end{aligned} \tag{3.154}$$

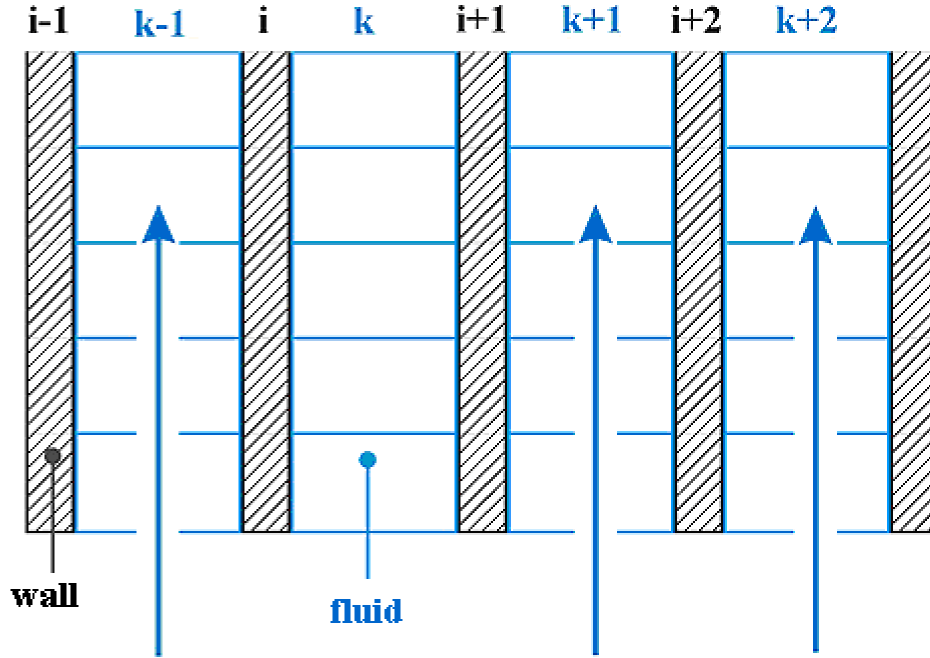

Fig. 3.19- Elementary volume indexes

3.10.7 Global thermal balance on a fluid cell

According to the simplifying hypotheses introduced, total heat flux on a fluid cell can be evaluated considering enthalpy difference (two-phase) or temperature difference (single-phase) between cell inlet and outlet. Here is considered the single-phase case, but the algorithm can be easily adapted for cases of two-phase flow.

$$\Delta\Phi_{FLUID} = \dot{m}\,\Delta i = \dot{m}\,c_P\,\Delta T_f \qquad \textit{for single phase} \tag{3.155}$$

Considering a scheme up-wind type, for a generic cell *(k,j)*, the inlet temperature fluid is the one characterizing the previous cell *(k,j-1)* while the temperature to be calculated *(k,j)* will be the inlet temperature for the subsequent cell:

$$\Delta T_{f\;k,j} = T_{f\,k,j} - T_{f\,k,j-1} \tag{3.156}$$

Thermal balance for a generic fluid cell can thus be expressed as:

$$\dot{m}\,c_P\left(T_{f\,k,j} - T_{f\,k,j-1}\right) = \Delta\Phi_{a-b-c-d} + \Delta\Phi_{DOWN,UP} \tag{3.157}$$

and making explicit:

$$\dot{m}c_P\left(T_{f\,k,j}-T_{f\,k,j-1}\right)=\mu^{EAST}\left(2T_{P\ \ i,j}+2T_{P\ \ i,j}^{TOP}-3T_{f\,k,j}-\frac{1}{2}T_{f\ \ k,j-1}-\frac{1}{2}T_{f\ \ k,j+1}\right)+$$
$$+\mu^{WEST}\left(2T_{P\ \ i+1,j}+2T_{P\ \ i+1,j}^{TOP}-3T_{f\,k,j}-\frac{1}{2}T_{f\ \ k,j-1}-\frac{1}{2}T_{f\ \ k,j+1}\right)+$$
$$+A^{FLUID}T_{f\,k,j}+B^{FLUID} \tag{3.158}$$

All temperatures marked by k index are unknown, while plate temperatures, both base and cover ones, are known because they are calculated in the previous calculation step. Also for fluid field temperature is suggested and here adopted the Gauss-Seidel line-by-line method, as for the metal sub-domain.
Gathering all known values as

$$\eta=2\mu^{EAST}T_{P\ \ i,j}+2\mu^{EAST}T_{P\ \ i,j}^{TOP}+$$
$$+2\mu^{WEST}T_{P\ \ i+1,j}+2\mu^{WEST}T_{P\ \ i+1,j}^{TOP}+$$
$$+B^{FLUID} \tag{3.159}$$

and letting

$$u=\frac{1}{2}\left(\mu^{EAST}+\mu^{WEST}-2\dot{m}c_P\right) \tag{3.160}$$

$$v=3\left(\mu^{EAST}+\mu^{WEST}\right)+\dot{m}c_P-A^{FLUID} \tag{3.161}$$

$$w=\frac{1}{2}\left(\mu^{EAST}+\mu^{WEST}\right) \tag{3.162}$$

then the thermal balance can be written in matrix notation in the form

$$\begin{bmatrix}u & v & w\end{bmatrix}\cdot\begin{Bmatrix}T_{f\,k,j-1}\\ T_{f\ \ k,j}\\ T_{f\,k,j+1}\end{Bmatrix}=\eta \tag{3.163}$$

When thermal balance is written for each fluid cell of the same channel, then it can be written for the entire strip, as it was done for the plate cells. In order to solve the system obtained, boundary conditions are to be introduced. In particular, fluid temperature at the channel entrance is known (i.e. the fluid temperature at which the heat exchanger is fed), while fluid temperature at outlet HX manifold (used for the temperature linear profile) is considered identical to the last cell outlet.

Let us consider a five cell strip and let us write the global thermal balance in matrix notation. According to the boundary conditions introduced, the first element in the known term vector gathers the inlet temperature fluid contribute, while the last row in the matrix the term *w*, usually associated to the next element temperature, is associated to the outlet temperature.

Therefore fluid sub-domain presents as many systems to be solved as the number of channels, each one is made of as many equations and unknown as the number of cells.

$$\begin{bmatrix} v_1 & w_1 & 0 & 0 & 0 \\ u_2 & v_2 & w_2 & 0 & 0 \\ 0 & u_3 & v_3 & w_3 & 0 \\ 0 & 0 & u_4 & v_4 & w_4 \\ 0 & 0 & 0 & u_5 & v_5 + w_5 \end{bmatrix} \cdot \begin{Bmatrix} T_1^f \\ T_2^f \\ T_3^f \\ T_4^f \\ T_5^f \end{Bmatrix} = \begin{Bmatrix} \eta_1 - u_1 T_{inlet} \\ \eta_2 \\ \eta_3 \\ \eta_4 \\ \eta_5 \end{Bmatrix} \qquad (3.164)$$

Thanks to the simple structure of the matrix obtained, the system can be quickly solved by the numerical code in which this model is implemented.

3.11 Global solution strategy

In the foregoing paragraphs a generic cold plate heat exchanger is analyzed by using SEWTLE method, which allows to consider also thermal conduction over the whole metal component. The calculation domain is divided into two sub-domains, a metal sub-domain and a fluid one. In the beginning a guess temperature filed is associated both to the fluid sub-domain and to the metal sub-domain.

Fluid sub-domain is analyzed by using the finite volume method, considering one dimensional flow and using convective heat transfer coefficient to evaluate heat flux over plates and walls. Each fluid channel is described by the thermal balance and temperature field along each channel can be thus calculated, considering adjacent wall temperatures and adjacent fluid channel temperatures as known values. All the channels are solved in succession, thus a new fluid temperature field over the whole fluid sub-domain is obtained and is used to calculate the new metal temperature field.

As far as for solid sub-domain, each element is made of a base plate portion, a cover element and a vertical wall which connect them, and thermal conduction is considered over the whole solid sub-domain. Vertical wall is analyzed by FEM, while FVM is adopted for the base and the cover plate. Solid temperature field is calculated using Gauss-Seidel line by

line method, thus strips made of cells connected by the same vertical wall are considered, from cold plate inlet to outlet.

Temperature field along each strip can be calculated, considering temperatures of adjacent fluid channel and of adjacent solid strip as known values. All the strips are solved in succession, thus a new solid temperature field over the whole sub-domain is obtained.

Solid sub-domain and fluid sub-domain are alternately solved till the largest temperature difference among all cells belonging to the same sub-domain between two subsequent steps is lower than a fixed error allowed.

A second check is made on the heat flux. When electronic device is cooled, heat flux is imposed to the cold plate, than it can be compared to the one rejected to the fluid.
The iteration is stopped when both error on heat flux and on temperature difference is lower than a fixed value.

When considering a two-phase flow, pressure field is to be evaluated besides temperature field. According to Corberán (2000), since all the variables mainly depend on the pressure, the momentum equation may be integrated first. Then, once the pressure at the outlet of the fluid cell is known, the energy equation can be integrated, leading to the evaluation of the enthalpy at the outlet, and of the quality and the rest of variables. Since several iteration will occur to solve the cold plate, there is no need to recalculate the new pressure drop accounting for new temperature field, because it will be calculated in the subsequent iterations.

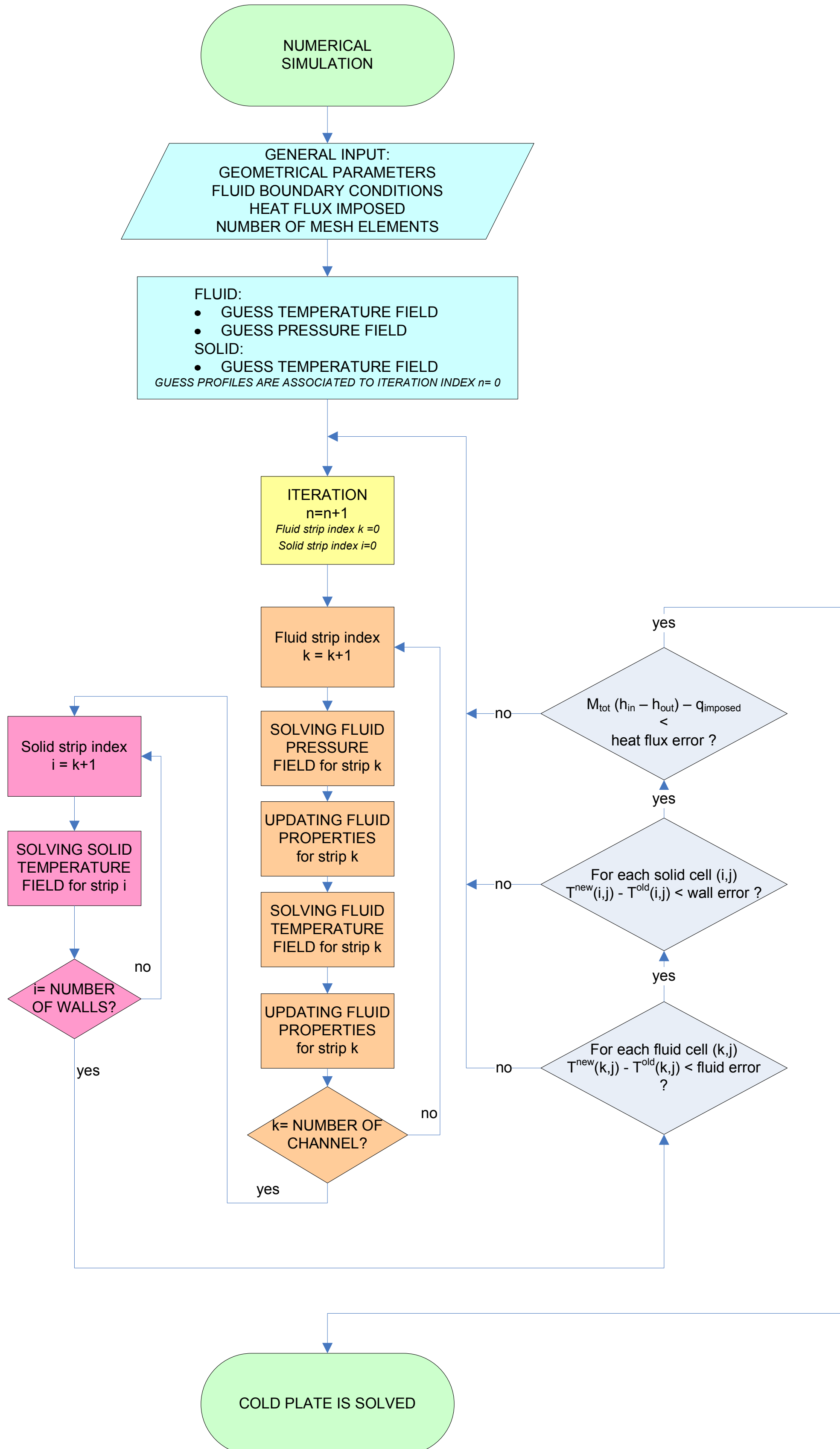

Fig. 3.20- Global solution strategy

4 FLUIDS CANDIDATED TO BE USED IN AIRCRAFT APPLICATIONS

4.1 Introduction

When considering a fluid as a candidate to be used in a system for electronics cooling purposes, several aspects need to be considered, especially when aircraft applications are evaluated. In fact, water is usually considered the best heat transfer fluid, because of the highest specific heat capacity, in comparison with all other fluids, and the high thermal conductivity (anyway, three orders of magnitude lower than copper). Furthermore, coolant requirement for electronic thermal management on aircrafts (very low soaking temperature, negligible corrosiveness, toxicity, flammability) claims for fluids (very often dielectrics ones) with specific heat capacity and thermal conductivity poorer than water. In general, these latter fluids present also a critical heat flux that is lower than for water.

Especially for direct cooling, there are some chemical, safety, and reliability constraints about the fluid:

- compatibility with materials used in electronics (e.g. silicon, solder, epoxy, assorted plastics etc.): fluid must be chemically inert.
- stability
- it must have high dielectric strength (e.g. fluorocarbons have dielectric constants around 1.7, air: 1, water around 80)
- non-toxicity, non-flammability,

Considering the convection heat transfer phenomenon between the hot surface and the cooling fluid (liquid or gas/vapor), the local thermal resistance can be defined as

$$R_{conv} = 1/(\alpha \cdot A) \quad (4.1)$$

where A is the local heat transfer area and α is the conventional Heat Transfer Coefficient. In general in forced convection,

$$\alpha = f(\rho, k, c_p, \mu, u, d) \quad (4.2)$$

where ρ is the fluid density, k is the fluid thermal conductivity, c_p is the specific heat capacity, μ is the dynamic viscosity of the fluid, u is the fluid velocity, and d is a

geometrical parameter of the heat transfer area (e.g the channel hydraulic diameter). The latter two parameters are referred to the geometrical arrangement whereas ρ, k, c_p, and μ are thermophysical properties of the fluid.

The present work considers approximately 50 fluids, most of which are already investigated or employed as secondary fluids in several applications as electronic thermal management in automotive, server and military applications, in refrigeration, and power plants. The fluids described in the following can be classified under four main categories:

- Saline aqueous solutions;
- Non-saline aqueous solutions;
- Hydrocarbon and aromatics blends (PAO);
- Fluorine compounds.

For aircraft electronic cooling purposes, pumpability at -55°C and 1 bar working pressure were considered as mandatory conditions (with the only exception for HFE-7200, for which 4 bar working pressure was assumed to avoid fluid evaporation). The investigated fluids are listed in table 4.1.

4.2 Single-phase fluids

4.2.1 Fluid properties

Thermophysical properties were reported as experimental data available in the open literature, otherwise, when no data is available, values were obtained through private communications with the manufacturers. Finally, in the case of only poor information (usually critical parameters and normal boiling point), an advanced evaluation approach was implemented as described in section 4.3.3. When possible, the temperature range -55 °C ÷ 150 °C was considered (with normal operation conditions -40 °C ÷ 90 °C).
Relevant thermophysical properties are reported in figures 4.2, 4.3, 4.4, 4.5, and 4.6.

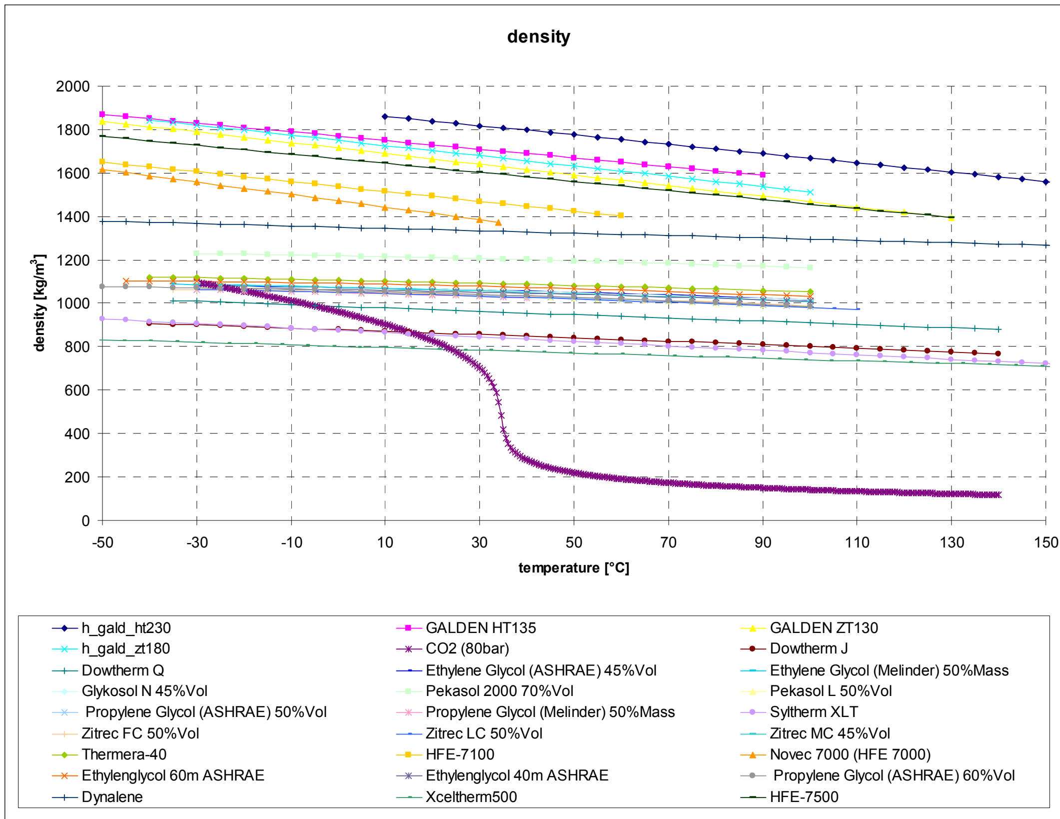

Fig. 4.1- Density vs. temperature for single phase fluids

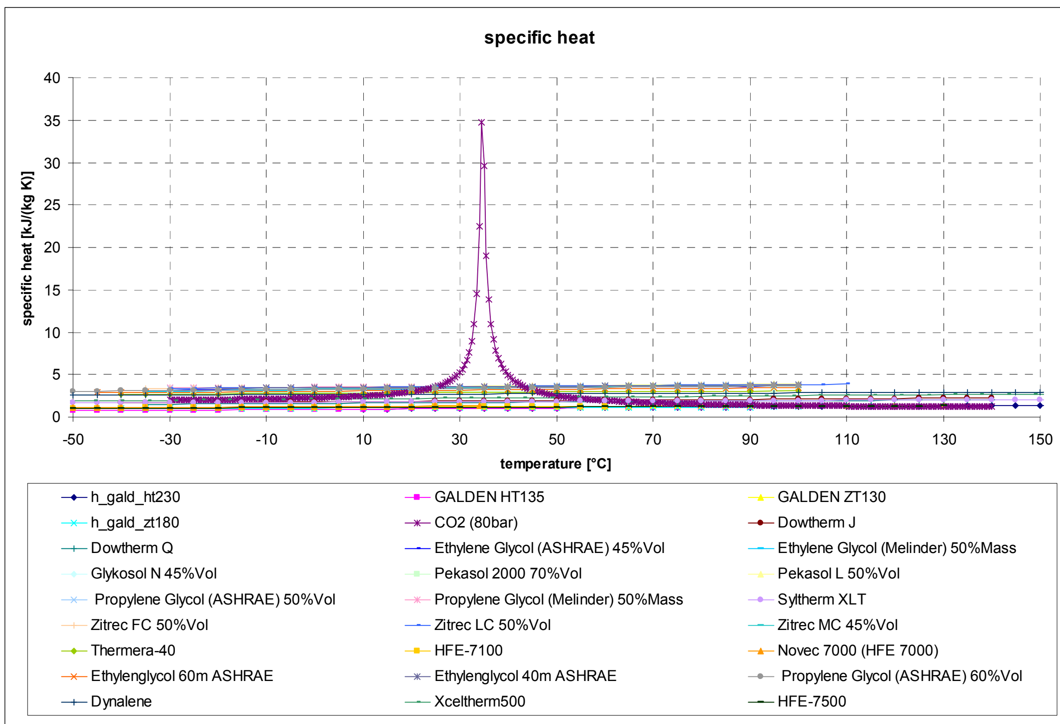

Fig. 4.2- Specific heat vs. temperature for single phase fluids

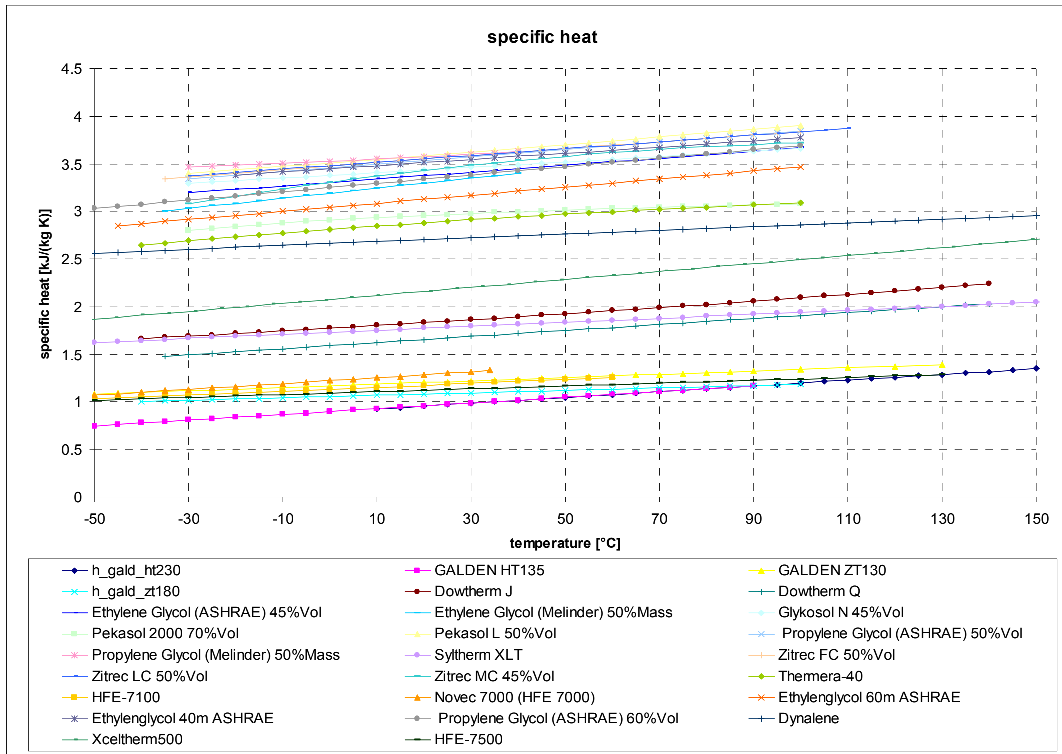

Fig. 4.3- Specific heat vs. temperature for single phase fluids (without considering carbon dioxide)

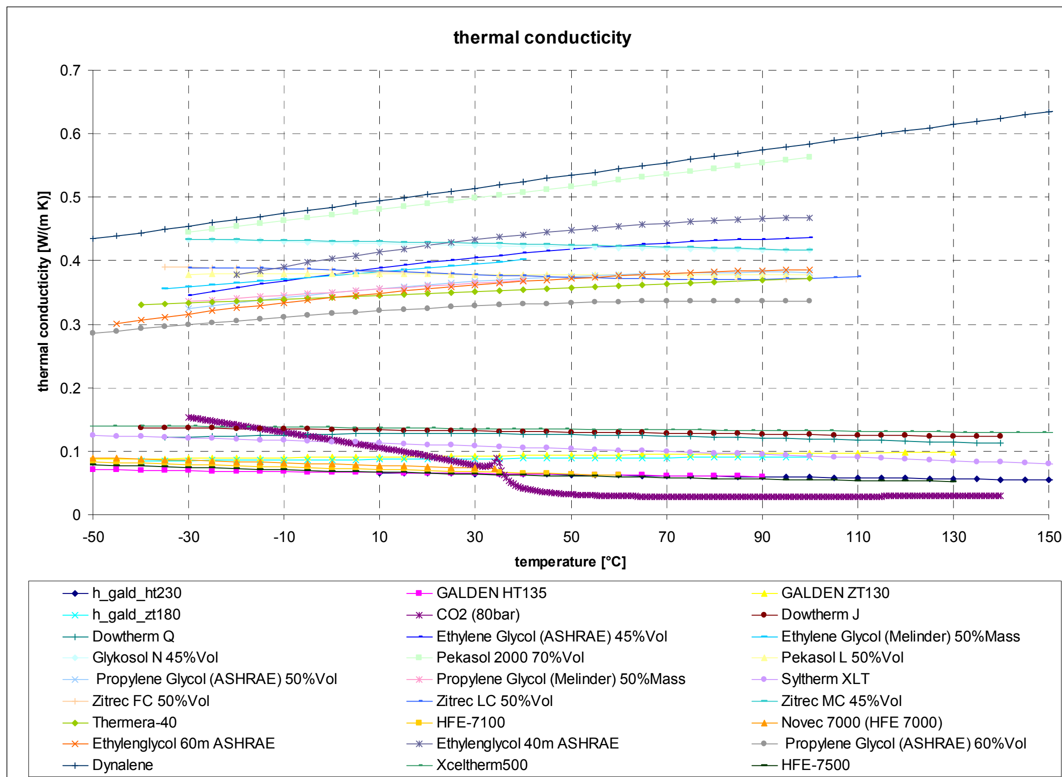

Fig. 4.4- Thermal conductivity vs. temperature for single phase fluids (without considering carbon dioxide)

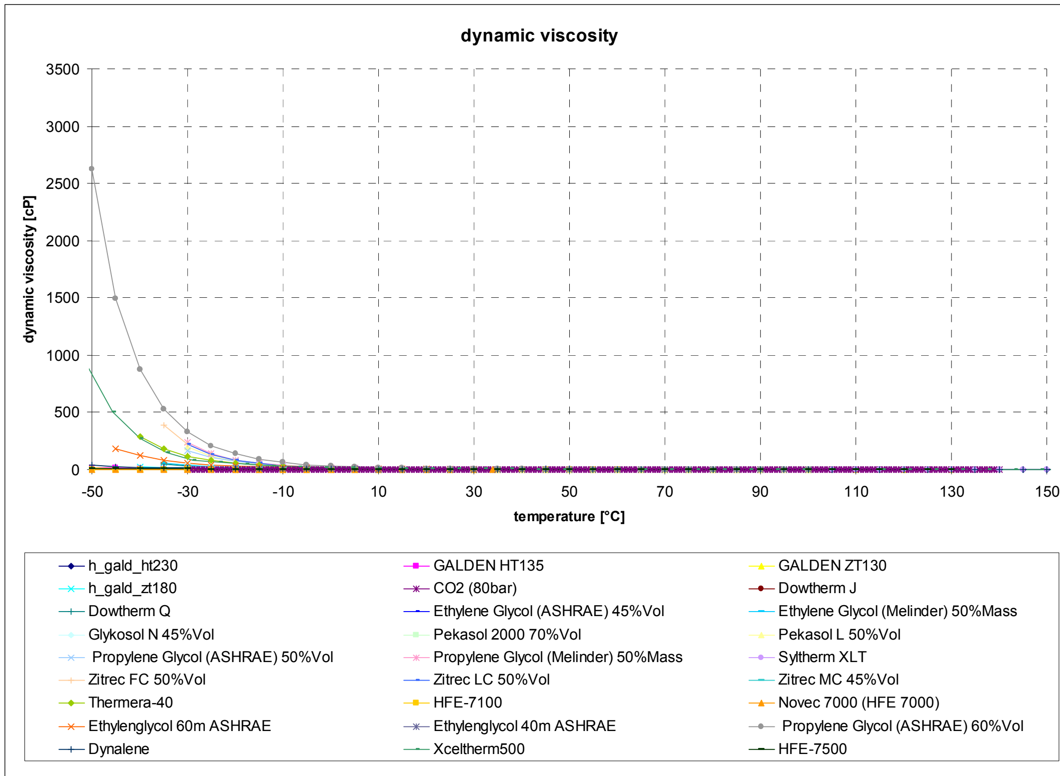

Fig. 4.5- Dynamic viscosity vs. temperature for single phase fluids

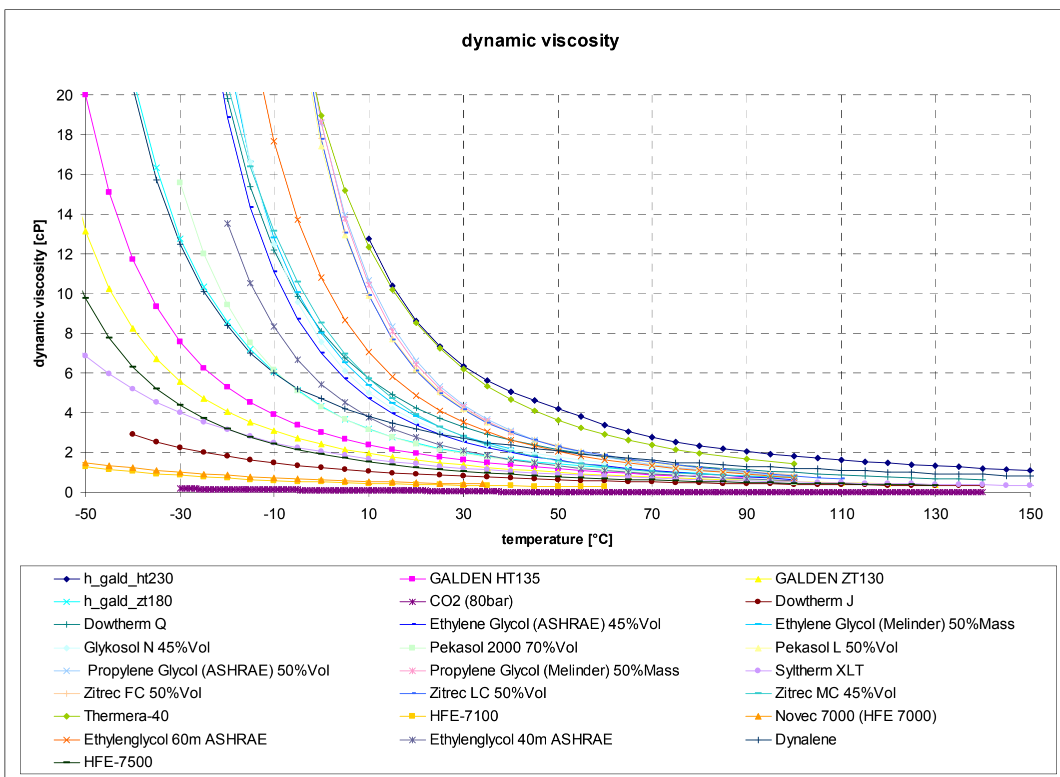

Fig. 4.6- Dynamic viscosity vs. temperature for single phase fluids (without Xceltherm500 and propylene glycol 60% vol. solutions)

Thermophysical properties reveal the fluid behavior and suitability when considering heat transfer or pressure drop issues. In fact, together with α, the other fundamental parameter is the pressure drop, which leads to pumping power consumption, and then both factors are to be taken into account when evaluating a fluid. From a general point of view, it is well known that the pressure drop in forced convection is function of dynamic viscosity, density, geometry, fluid velocity and surface roughness. When considering heat transfer equipment under fixed design constraints (such as, for example, fixed surface area or total tube length), and the performance objective is set up (such as, for example, increased heat duty, or reduction in pumping power), it is often possible to establish simple appropriate Performance Evaluation Criteria (PECs) that should allow to select the optimum fluid or, for a particular fluid, the optimum geometry for the specified operating conditions, and to establish the performance benefit relative to a reference situation (Webb, 1981).

As a general statement, in forced convection, under turbulent flow conditions, an increase in fluid velocity brings an increase both in α and in pumping power, so the ratio of α to pumping power should be considered.

Since the evaluation of α and pressure drop in turbulent forced convection is strongly linked to the particular fluid and to duct geometry, a proper PEC should be obtained for each application.

To evaluate the heat transfer coefficient, the well known Dittus-Boelter equation is considered:

$$\alpha = 0.023\,\mathrm{Re}^{0.8}\,\mathrm{Pr}^{0.33}(k/d) \qquad (4.3)$$

where Re is Reynolds number and Pr is Prandtl number, with the following validity range: Re<10000, 0.7< Pr < 100.

The frictional pressure drop *Δp* is obtained through

$$\Delta p = f\,G^2 A/(8\,\rho\,S) \qquad (4.4)$$

where G [kg/(m^{2}s)] is the mass flux, A [m^2] is the heat transfer area, S [m^2] is the duct cross section area, ρ [kg/m^3] is the fluid density.

To calculate the pressure losses, a friction factor f is to be defined, and it can be expressed as

$$f = a\,\mathrm{Re}^b \qquad (4.5)$$

In (4.5) a and b are empirical constants, and typical values for smooth “macro” tubes can be used, then a=0.148 and b=-0.2.

4.2.2 Heat transfer efficiency factor

Considering the following expression (4.6), the ratio between heat transfer coefficient and pumping power is used, but pump power is raised to a particular exponent and the ratio is multiplied by a geometric parameter:

$$HTEF = \frac{heat\ transfer\ coefficient}{(pump\ power\ per\ unit\ heat\ transfer\ area)^{0.29}} diameter^{0.14} \tag{4.6}$$

Correlation (4.6) is proposed as the performance evaluation criteria for a single-phase cooling fluid in turbulent flow, here named as heat transfer efficiency factor.
The exponents used in the previous correlation, as described in detail in the Seccool Users Manual (retrieved online on http://www.ipu.dk) allow to express HTEF as

$$HTEF = C \cdot c_p^{0.33} \cdot k^{0.67} \cdot \rho^{0.57} \cdot \mu^{-0.52} \tag{4.7}$$

where C is a constant and the other factors represent thermophysical properties already illustrated in this chapter. Equation (4.7) uses only fluid thermophysical properties, and then it can be calculated regardless of the system geometry, allowing one to compare and rank a list of fluids according to their cooling capability and required pumping power.

Calculated values of HTEF for the investigated liquids are reported in figures 4.7 and 4.8. Except for carbon dioxide, which shows a central peak linked to the supercritical condition, the other fluids behave in the same way, increasing HTEF with temperature. Furthermore, some fluids appear to be more suitable than others for high temperature applications, but not for a lower temperature range, and finally some fluids (some Galden, Dowterm fluids and Xceltherm) could be the only choice available when considering very high temperatures, above 100 °C.

Anyway, the results provided herein are limited to turbulent flow, which actually occurs in several applications, but even laminar flow is quite important in compact heat exchangers, since it leads to low pumping power. A different method is then employed and results are illustrated in the following chapters. Finally, the foregoing safety and reliability properties need to be carefully taken into account in order to carry out an exhaustive assessment, even considering the cooling system architecture. For example, saline solutions could be promising from a heat transfer capability point of view, but could be considered not the best choice because of possible detrimental saline deposits in case of leakage. Therefore, such evaluation is possible only for a well defined application, when all cooling, safety and reliability requirements are accurately determined.

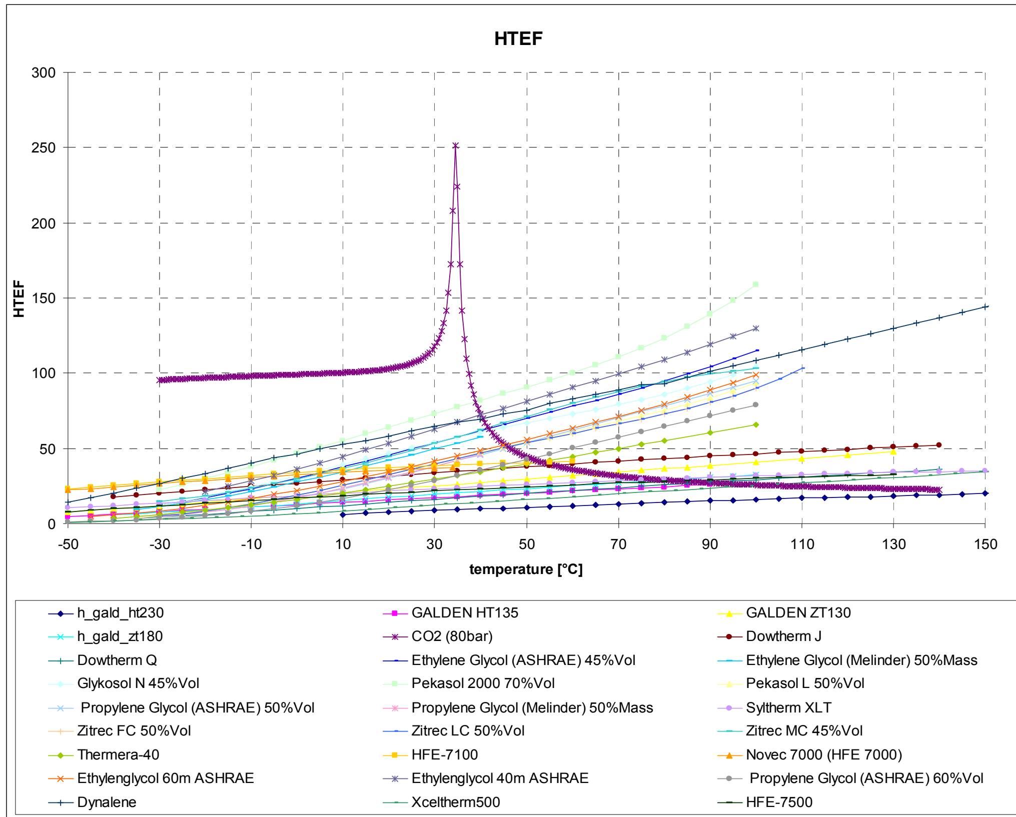

Fig. 4.7- HTEF values for the investigated single phase fluids (without considering carbon dioxide)

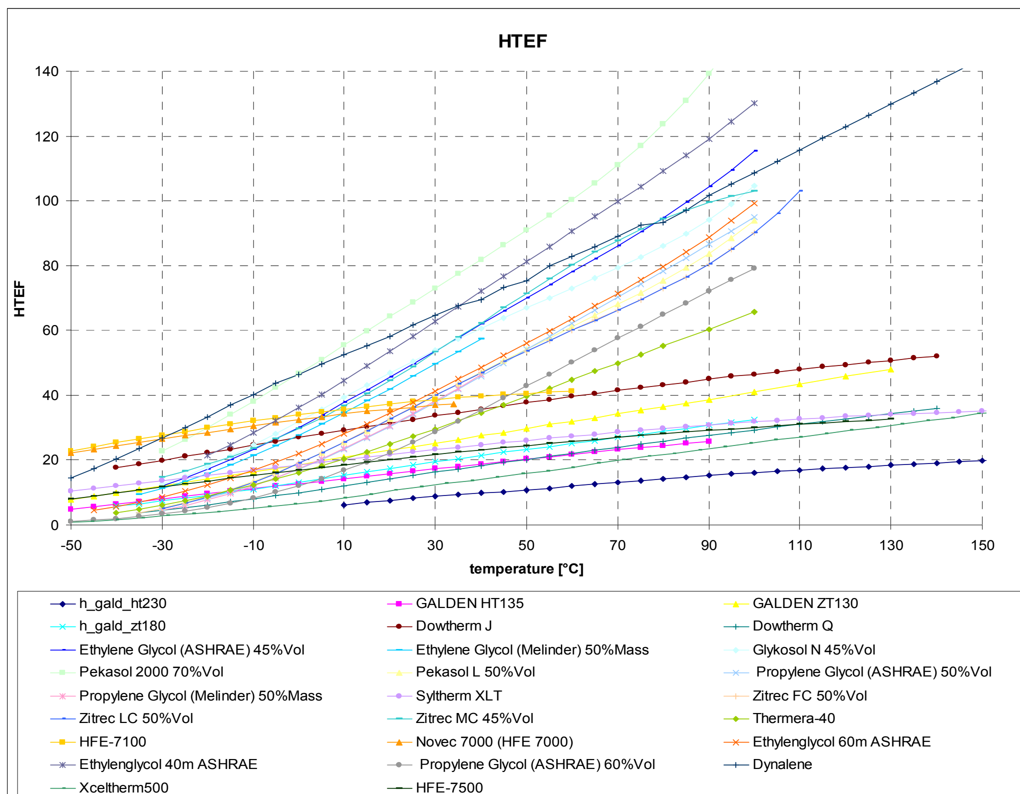

Fig. 4.8- HTEF values for the investigated single phase fluids (without considering carbon dioxide)

4.2.3 Electrical conductivity

Fluorine compounds appear suitable for direct immersion of electronics, and have already been used for several systems for years (HFC and HFE; PFCs are not considered because they don't present any advantage in comparison with Galden, which is assumed as the reference as is used in Airbus A380, and display a much higher GWP), having an electrical conductivity ~ 10^{-9} μS/cm. For the convenience of the reader, the HTEFs of selected fluids are reported in figure 4.9. By comparing figure 4.9 with figure 4.8, it can be observed that HFC and HFE display much lower HTEF values if compared with saline solutions and propylene-glycol aqueous solution (if extremely low working temperatures are not considered).

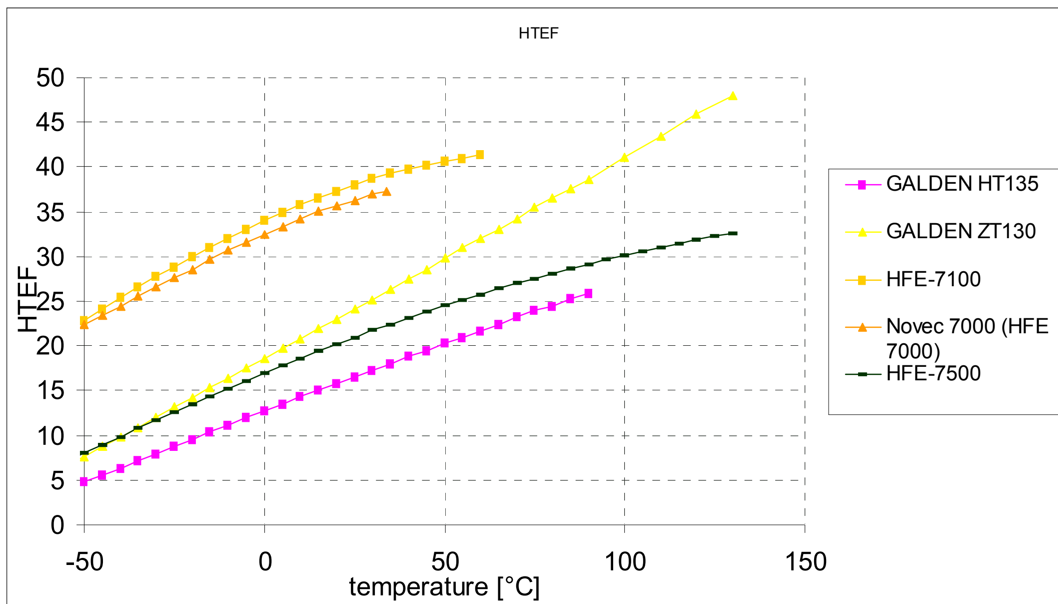

Fig. 4.9- HTEF for selected fluids suitable for direct immersion of electronics

Other fluids are considered not suitable for direct immersion of electronics purpose, but a leak or a spill will not damage the electronics. For these fluids, electrical conductivity is to be within ~ 0.05 ÷ 20 μS cm^{-1} (rough estimation, a more comprehensive approach should consider dielectric constant close to 1 and high dielectric strength). For example, de-ionized water electrical conductivity is close to 1 μS cm^{-1}, but pumpability at low temperature is to be guaranteed. Considering propylene glycol solutions, very limited data is available in open literature, then as an example, data for DoW Chemicals Dowfrost® can be considered (figure 4.10).

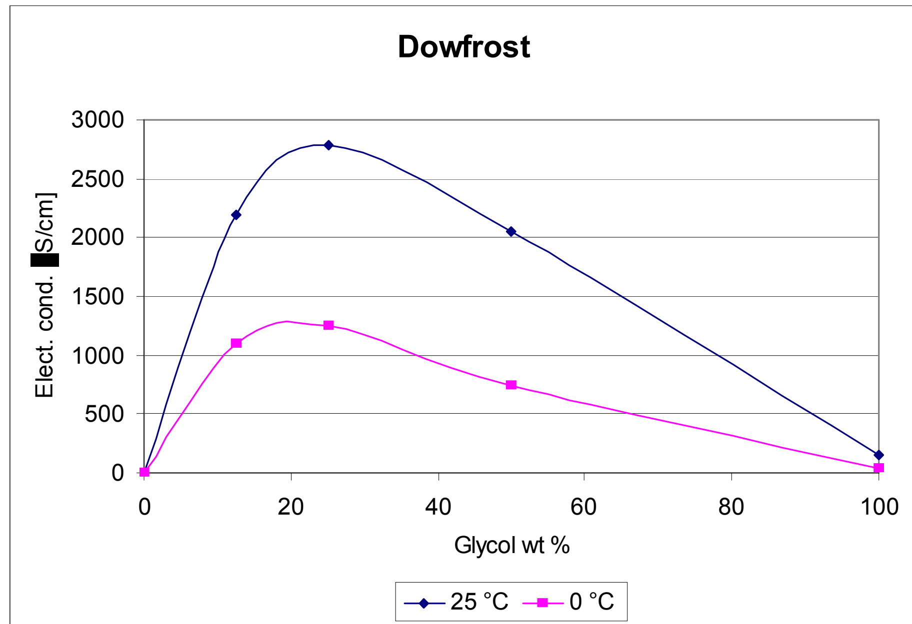

Fig. 4.10- Electric conductivity vs glycol concentration for Dowfrost® at 0 and 25 °C

It is recognised that off-the-shelf cooling liquids contain a certain amount of additives that usually are ionic substances (salt based corrosion inhibitors, carboxylic acids). This additives can greatly increase the electrical conductivity of the liquid (being ionic substances). Recently, new generation of additives where presented in scientific conferences, with the objective to significantly reduce the electrical conductivity of the liquid. An example is shown in figure 4.11 (from Mohaparta et al., 2005)

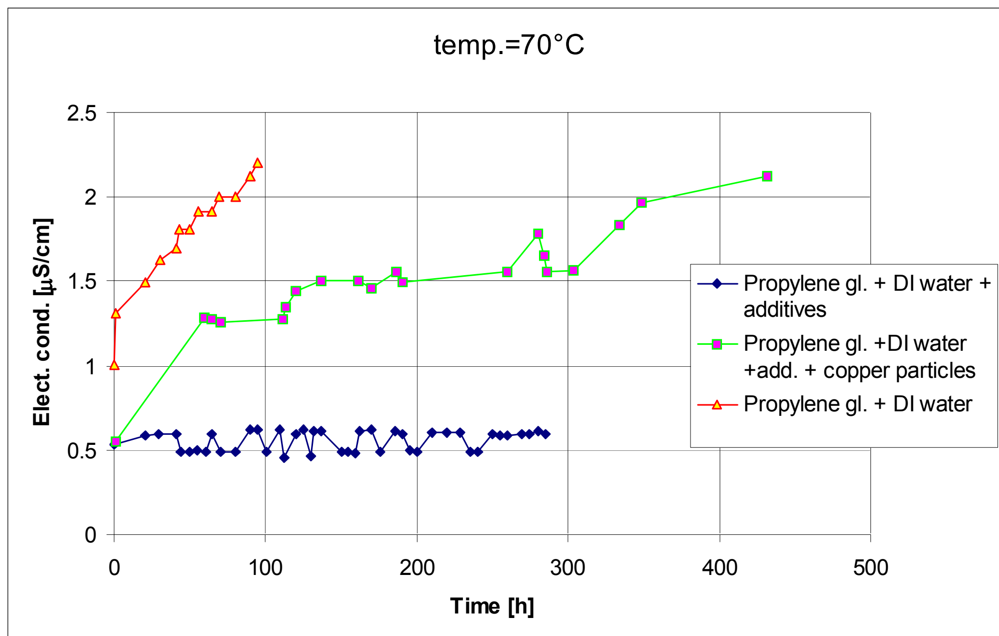

Fig. 4.11- Electrical conductivity vs time for propylene glycol solutions: effect of additives

4.2.4 Corrodibility

Most of the fluids present a certain level of incompatibility with materials usually employed for refrigeration systems, and then each case should be carefully analyzed, according to the technical datasheet (in which there is a list of materials with good or bad compatibility) given by the fluid supplier. Generally, fluorine based fluids may present some problems of compatibility with a few polymers or elastomers, aqueous solutions need suitable additives to avoid metals corrosion and finally saline solutions should be avoided (in case of dropping liquid can evaporate leaving the salt in contact with metallic parts) as described in previous sections.

4.2.5 Environmental compatibility

All the fluids considered are non Ozone Depleting (ODP=0), while low GWP is preferable. This aspect is very interesting in a perspective of synergy between aircraft, automotive and electronics industries, looking for higher standardization of products.
In fact the European Union's f-gas regulations is imposing new strict constraints about fluid GWP for automotive air conditioning. According to Regulation (EC) No 842/2006 and Directive 2006/40/EC starting from January 1, 2017 new vehicles fitted with air-conditioning can not be manufactured with fluorinated greenhouse gases having global warming potentials (GWP) greater than 150. Therefore, to allow a better integration of components coming from different industrial sectors, only low GWP fluids should be considered.

Table 4.1 reports the main flammability and environmental compatibility for most of the fluids investigated.

Tab. 4.1- Flammability and environmental compatibility values

Fluid name	GWP	ODP	Flash point [°C]	Fire point [°C]	Auto-ignition [°C]
Galden ZT130	1800	0	No	No	No
Galden ZT150	1800	0	No	No	No
Galden ZT180	1800	0	No	No	No
Galden HT55	ND	ND	No	No	No
Galden HT70	ND	ND	No	No	No
Galden HT90	ND	ND	No	No	No
Galden HT110	ND	ND	No	No	No
Galden HT135	ND	ND	No	No	No
Galden HT230	ND	ND	No	No	No
Galden HT270	ND	ND	No	No	No
Propylene Glycol –water (60% vol.)	0	0	No	No	No
Ethylene Glycol –water (up to 80% vol.)	0	0	No	No	No
Dynalene HC-50	ND	ND	No	No	ND
Xceltherm500	ND	ND	163	177	329
Xceltherm600	ND	ND	193	216	349
Xceltherm HT	ND	ND	160	170	450
Xceltherm HTR	ND	ND	200	210	371
HFE-7000	350	0	Nonflammable		
HFE-7100	280	0	Nonflammable		
HFE-7200	55	0	No	ND	ND
HFE-7500	90-210	0	Nonflammable		

Tab. 4.1- (continued) Flammability and environmental compatibility values

Fluid name	GWP	ODP	Flash point [°C]	Fire point [°C]	Auto-ignition [°C]
Dowtherm Q	ND	ND	120	124	412
Dowtherm J	ND	ND	57	60	420
Syltherm XLT	ND	ND	47	54	350
Thermera-40	ND	ND	not applicable	ND	ND
HFC-236fa	6300	0	Nonflammable		
HFC-245fa	950	0	ND	ND	412
DM-FPE	ND	ND	ND	ND	ND
Solkatherm® SES36	ND	ND	Nonflammable		
Solkane 365 mfc	890	0	-27	ND	ND
Zitrec LC	ND	ND	Nonflammable		
Zitrec FC	ND	ND	Nonflammable		
Zitrec MC	ND	ND	Nonflammable		
Dynalene BioGlycol	ND	ND	131	ND	405
Dynalene LO170	ND	ND	77	ND	ND
Dynalene 600	ND	ND	315	ND	ND
Dynalene EG	ND	ND	120	ND	ND
Dynalene HC	ND	ND	Nonflammable		
Dynalene HF-LO	ND	ND	61	72	337
Dynalene HT	ND	ND	200	ND	450
Dynalene LO-230	ND	ND	110	ND	ND
Dynalene MV	ND	ND	53	64	388
Dynalene PG	ND	ND	102	ND	ND
Dynalene SF	ND	ND	77	210	330
PEKASOL 2000	ND	ND	ND	ND	ND

4.3 Evaporation/boiling cooling

4.3.1 General aspects

Use of phase-change processes, including pool boiling and convective boiling, exploiting the latent heat of these liquids to reduce the required mass flow rates and can provide the added advantage of inherently high heat transfer coefficients.

Thermal control of operational avionic components by direct immersion in low boiling point fluids dates back to open-cycle pool evaporators developed in the late 1940s (see for example Mark et al., 1958). More recent application of open cycle evaporation thermal management of electronic disclosed in the open literature refers to Price (2003). Anyway, vapor compression systems are already used in aircraft and helicopter or galley cooling or air conditioning purposes, and the use of this cooling technique could be extended even to electronics cooling, as it is described in the following chapters. Therefore, fluid selection should be considers also two-phase fluids, as described in section 4.3.2.

4.3.2 Fluid selection for boiling/evaporation cooling

When considering avionics cooling by a two-phase process, according to the open scientific literature (further details are reported in chapter 6) the temperature level is about 50 °C. R-114 (being a CFC it is a banned substance) can be considered as the reference fluid, since it is the fluid that has been largely used for similar temperature level applications both in industrial plants and in marine units (including submarines). The candidate fluid for two-phase cooling should have a normal boiling point above 50°C, to avoid evaporation below 0.1 MPa(A), i.e. evaporation at sea level occurring at pressure below ambient pressure. Furthermore, evaporation pressure at 50 °C should not greatly exceed R114 pressure (0.39 MPa).

From an environmental point of view, no ODP substances were investigated and a GWP (100 year scenario) lower than 2000 should be advisable (see section 4.2.5 for further details). The following table reports almost all the fluids that have been considered in the last years for any kind of systems involving condensation/boiling/evaporation in a large spectrum of different applications (refrigeration, heat pumps, Organic Rankine Cycles, marine, military, electronics).

The methodology used to generate the list of potential fluids for two-phase thermal management of electronics consisted of an extensive literature search, namely:

- every issue of the International Journal of Refrigeration dating back to 1988;
- every issue of the IIR Bulletin dating back to 1994;
- every issue of ASHRAE Transactions dating back to 1998;
- every issue of HVAC&R Journal;
- United States Patents dating back to 1976;
- United States Patent Applications dating back to 2002;
- extensive online database searches.

The complete list of retrieved fluids, including critical parameters and NBP, referring to R114 (which parameters are listed in table 4.4) is reported in table 4.2.

The fluids that are shaded in darker grey in table 4.3 clearly violate one of the environmental or safety characteristics that were established as elimination criteria, namely: ODP > 0 (or a banned substance per the Montreal Protocol), GWP > 2000, or an ASHRAE Class 3 (or highly flammable fluid). The fluids shaded in lighter grey in the tables most likely violate one of the elimination criteria.

In some instances in table 4.3, the ratio F/(F+H), in which F is the number of fluorine atoms in the molecule and H is the number of hydrogen atoms in the molecule, is given to indicate the probable degree of flammability. Bivens and Minor (1998) provide the rule-of-thumb that if F/(F+H) < 0.67, then the fluid is likely to be flammable.

Tab. 4.2- Non-dimensional thermodynamic parameters for fluids that are potential candidates for electronics (two-phase) thermal management replacements (NOTE: numbers in parenthesis indicate the data sources)

Refrigerant	Formula	τ_{NBP}	τ_c	Π_c	δ_c	Cp	AF
HFE7100	CH_3O-3(CF_2)-CH_3	1.207 [1]	1.118 [1]	0.685 [1]	0.654 [1]	2.060 [2]	1.714 [2]
R-601	CH_3-3(CH_2)-CH_3	1.117 [3]	1.121 [3]	1.035 [3]	0.948 [3]	1.261 [3]	0.995 [3]
R-E347mcc	$CH_3OCF_2CF_2CF_3$	1.111 [4]	1.045 [4]	0.760 [4]	0.781 [4]	1.774 [2]	1.600 [2]
HFE7000	$CH_3OCF_2CF_2CF_3$	1.110 [1]	1.046 [1]	0.761 [1]	0.815 [1]	1.590 [2]	1.571 [2]
R-E347mmy1	$CF_3CF(OCH_3)CF_3$	1.093 [5]	1.036 [5]	0.783 [5]	0.779 [2]	1.581 [2]	1.519 [2]
R-E236ca	$CHF_2OCF_2CHF_2$	1.090 [9]	1.040 [2]	0.816 [2]	0.953 [2]	1.245 [2]	1.459 [2]
TMS	$Si(CH_3)_4$	1.083 [7]	1.071 [7]	0.866 [7]	0.814 [7]	1.312 [7]	0.977 [7]
R-601a	$(CH_3)_2CHCH_2CH_3$	1.088 [3]	1.099 [3]	1.037 [3]	0.964 [3]	1.245 [3]	0.901 [3]
R-356mff	$CF_3CH_2CH_2CF_3$	1.077 [6]	1.028 [2]	0.765 [2]	0.856 [2]	1.379 [2]	1.354 [2]
R-245eb	$CH_2FCHFCF_3$	1.070 [8]	1.051 [2]	0.905 [2]	1.070 [2]	1.085 [2]	1.152 [2]
R-245ca	$CHF_2CF_2CH_2F$	1.078 [3]	1.069 [3]	1.205 [3]	1.151 [3]	1.128 [3]	1.402 [3]
R-338mf	$CF_3CH_2CF_2CF_3$	1.052 [6]	0.990 [2]	0.677 [2]	0.791 [2]	1.494 [2]	1.400 [2]

Refrigerant	Formula	τ_{NBP}	τ_c	Π_c	δ_c	**Cp**	**AF**
$SF_5C_2F_5$	$SF_5C_2F_5$	1.034 [9]	0.981 [2]	0.698 [2]	0.854 [2]	1.472 [2]	1.312 [2]
$N(CF_3)_2(CH_3)$	$N(CF_3)_2(CH_3)$	1.025 [9]	0.985 [2]	0.804 [2]	0.923 [2]	1.300 [2]	1.316 [2]
R-245fa	$CF_3CH_2CHF_2$	1.042 [3]	1.020 [3]	1.121 [3]	1.135 [3]	1.051 [3]	1.500 [3]
R-631	$CH_3CH_2(NH_2)$	1.047 [10]	1.089 [10]	1.723 [10]	1.619 [10]	0.724 [10]	1.146 [2]
SF_5CF_2H	SF_5CF_2H	1.005 [9]	0.997 [2]	0.952 [2]	1.188 [2]	1.033 [2]	1.075 [2]
R-E236fa	$CF_3OCH_2CF_3$	1.007 [9]	0.961 [2]	0.816 [2]	0.953 [2]	1.214 [2]	1.459 [2]
R-272fb	$CH_3CH_2CHF_2$	1.017 [6]	1.026 [2]	1.149 [2]	1.263 [2]	0.855 [2]	1.074 [2]
R-E245cb1	$CH_3OCF_3CF_2$	1.007 [11]	0.971 [12]	0.886 [12]	0.999 [11]	1.158 [2]	1.417 [2]
R-E263fb	$CF_3OCH_2CH_3$	1.009 [9]	0.986 [2]	1.028 [2]	1.103 [2]	1.022 [2]	1.417 [2]
R-236ca	$CHF_2CF_2CHF_2$	1.005 [13]	0.984 [13]	1.013 [13]	1.051 [2]	1.103 [2]	1.368 [2]
R-E161	CH_2FOCH_3	1.023 [9]	1.044 [2]	1.427 [2]	1.600 [2]	0.679 [2]	1.221 [2]
R-236ea	CHF_2CHFCF_3	1.009 [3]	0.985 [3]	1.075 [3]	1.091 [3]	1.117 [3]	1.504 [3]
R-CE225e	CF_2CHFCF_2O-cyclo	0.999 [9]	0.961 [2]	0.865 [2]	0.998 [2]	1.021 [2]	1.422 [2]
R-143	CH_2FCHF_2	1.005 [13]	1.029 [13]	1.300 [13]	1.289 [2]	0.695 [2]	1.044 [2]
R-E134	CHF_2OCHF_2	1.009 [14]	1.003 [14]	1.298 [14]	1.321 [14]	0.874 [2]	1.495 [2]
R-236cb	$CH_2FCF_2CF_3$	0.983 [13]	0.963 [13]	0.957 [13]	1.015 [2]	1.109 [2]	1.274 [2]
R-254cb	$CHF_2CF_2CH_3$	0.984 [13]	1.001 [13]	1.152 [13]	1.175 [2]	0.985 [2]	0.980 [2]
R-13I1	CF_3I	0.908 [3]	0.947 [3]	1.214 [3]	1.306 [3]	0.536 [3]	0.720 [3]
R-630	CH_3NH_2	0.951 [3]	1.028 [3]	2.421 [3]	2.415 [3]	0.322 [3]	1.013 [3]
R-764	SO_2	0.897 [3]	0.960 [3]	1.633 [3]	1.656 [3]	0.585 [3]	0.763 [3]
R-E170	CH_3OCH_3	0.900 [3]	0.923 [3]	1.387 [3]	1.642 [3]	0.586 [3]	1.091 [3]
R-152a	CHF_2CH_3	0.873 [3]	0.951 [3]	1.713 [3]	1.810 [3]	0.554 [3]	0.517 [3]
R-C270	$CH_2CH_2CH_2$-cyclo	1.207 [1]	1.118 [1]	0.685 [1]	0.654 [1]	2.060 [2]	1.714 [2]
R-717	NH_3	0.867 [3]	0.968 [3]	3.480 [3]	3.894 [3]	0.281 [3]	1.015 [3]
HFE7200		1.262 [1]					
HFE7500							
R-134a	CF_3CH_2F	0.893 [3]	0.893 [3]	12.463 [3]	0.883 [3]	0.711 [3]	1.295 [3]
R-365mfc	$CF_3CH_2CF_2CH_3$	1.132 [3]	1.098[3]	1.003 [3]	0.817 [3]	1.353 [3]	1.506 [3]
R-227ea	CF_3CHFCF_3	0.928 [3]	0.895[3]	0.898 [3]	1.025 [3]	1.126 [3]	1.415 [3]
R-236fa	$CF_3CHFCHF_2$	0.982 [3]	0.950[3]	0.982 [3]	0.951 [3]	1.079 [3]	1.495 [3]
SES36		1.117					

[1] 3M (2008)
[2] Reid et al. (1987) & Poling et al. (2001)
[3] Lemmon et al. (2007)
[4] Ohta et al. (2001)
[5] Calm & Hourahan (2007)
[6] Brown (2007b)
[7] NIST (2008)
[8] ABCR (2008)
[9] Bivens & Minor (1998)
[10] CHERIC (2008)
[11] Yoshii et al. (2000)
[12] Yasumoto et al. (1996)
[13] Devotta & Penyala (1994)
[14] Defibaugh et al. (1992)

τ_{NBP} (relative normal boiling point temperature), τ_c (relative critical temperature), Π_c (relative critical pressure), δc (relative critical density), Cp (relative ideal gas specific heat at constant pressure), and AF (relative acentric factor). (Note: temperature ratios must be made using Rankine or Kelvin.).

Tab. 4.3- Environmental and safety characteristics for fluids potential for electronics two-phase thermal management

Refrigerant	Environmental & Safety Characteristics
HFE7100	GWP=390 [2] & non flam [4]
R-601	LFL=1.4% [1]
R-E347mcc	GWP=480 [2]
HFE7000	GWP=370 [4] & non flam [4]
R-E347mmy1	GWP=343 [1]
R-E236ca	
TMS	
R-601a	A3 [1]
R-356mff	LT=7.9 yrs [2]
R-245eb	
R-245ca	LFL=7.1% [1], GWP=640 [2]
R-338mf	GWP probably high
$SF_5C_2F_5$	
$N(CF_3)_2(CH_3)$	
R-245fa	B1 [1], GWP=950 [2]
R-631	LFL=3.5% [1]
SF_5CF_2H	
R-E236fa	GWP=470 [2]
R-272fb	F/(F+H)=0.25
R-E245cb1	flammable [1], GWP=580 [2]
R-E263fb	F/(F+H)=0.38
R-236ca	
R-E161	F/(F+H)=0.17
R-236ea	GWP=1200 [2]
R-CE225e	LT=26 yrs [3]
R-143	F/(F+H)=0.5, GWP=330 [2]
R-E134	GWP=6100 [2]
R-236cb	GWP=1300 [2]

Refrigerant	Environmental & Safety Characteristics
R-254cb	F/(F+H)=0.5
R-13I1	ODP<0.018 [1], GWP=1 [2]
R-630	LFL=4.9% [1]
R-764	B1 [1], GWP=300[1]
R-E170	A3 [1]
R-152a	A2 [1], GWP=120 [2]
R-C270	LFL=2.4% [1]
R-717	B2 [1], GWP<1 [1]
HFE7200	GWP=55 [4]; flammability?
HFE7500	
R-134a	GWP=1300
R-365mfc	GWP=890, flammability
R-227ea	GWP=2900 [1]
R-236fa	GWP=6300 [1]
SES36	GWP High

[1] Calm & Hourahan (2007) [2] IPCC (2001) [3] Bivens and Minor (1998)
[4] 3M (2007)
A1…A3 & B1…B3 = ASHRAE Safety Classifications (ANSI/ASHRAE Standard 34-2007)
F/(F+H) = Number of fluorine atoms relative to the number of fluorine and hydrogen atoms
LFL = Lower Flammability Limit
LT = Atmospheric Life time

Tab. 4.4- Thermodynamic Parameter Values for R-114 ($CClF_2CClF_2$) [Lemmon et al. 2007]

NBP	T_c	P_c	ρ_c	c_p^o	ω
276.74 K	418.83 K	3257 kPa	3.393 kmol m^{-3}	137.9 kJ kmol^{-1} K^{-1}	0.2523

4.3.3 Ultra low-GWP fluids

Recently, HFO-1234yf (CF_3-CF=CH_2), with a 100-year time horizon GWP of four (Nielsen et al. 2007) has been investigated (e.g., Spatz and Minor 2008) as a possible replacement fluid for R134a in automotive applications, but a scarce amount of thermodynamic and transport property data is available in the open literature.

The thermodynamic property data are generated using the approach illustrated in Brown (2007a,b,c, 2008a), while the transport property data are estimated using an originally developed methodology. Calculated properties are illustrated in figure 4.12, and have been used to an experimental test rig developed at Dipartimento di Fisica Tecnica in Padua to evaluate an automotive air conditioning system, which results are described in chapter 6.

Brown (2007a,b,c, 2008a) demonstrated how to use the Peng-Robinson (P-R) equation of state (EoS) implemented in REFPROP 8.0 (Lemmon et al., 2007) to estimate the thermodynamic properties: temperature (T), pressure (P), density (ρ), quality (x), enthalpy (h), entropy (s), and specific heat at constant pressure (c_p), whereas the group contribution methods and other simple models can be used to estimate surface tension (σ) and the transport properties: thermal conductivity (k) and dynamic viscosity (μ). These methods are particularly useful to characterize not-so-well-described refrigerants (ones where little thermodynamic or transport property data are known), such as is the case for HFO-1234yf. In order to use the P-R EoS, one must know the acentric factor (ω), the ideal gas specific heat at constant pressure (c_p^0), and the critical state properties T_c, P_c, and ρ_c. When the mentioned parameters are not known, they can be estimated through modelling.

For checking the reliability of the proposed method, in table 4.5 a comparison between the results of the calculations with REFPROP 8.0 and the approach proposed in this work for R134a.

Tab. 4.5- Mean absolute errors (ea) for R134a. The errors are between the values calculated using the approach of this work and REFPROP 8.0 (Lemmon et al., 2007).

Saturation Properties:						
P	ρ_l	ρ_v	h_l	h_v	s_l	s_v
1.2%	4.5%	2.6%	0.9%	1.4%	0.6%	1.2%
κ_l	κ_v	μ_l	μ_v	γ	$c_{p,l}$	$c_{p,v}$
12.2%	5.8%	4.9%	6.7%	2.2%	2.9%	14.5%
Superheat Properties:						
P (kPa)	ρ	h	s	c_p	κ	μ
100	0.6%	0.8%	0.6%	5.1%	5.5%	0.8%
250	0.8%	0.9%	0.7%	6.5%	5.5%	2.0%
500	0.9%	1.0%	0.8%	8.1%	4.6%	3.3%
1000	0.7%	1.1%	0.8%	10.1%	3.0%	5.2%
1750	0.8%	1.0%	0.8%	11.4%	1.9%	7.5%
2500	0.9%	1.0%	0.8%	12.7%	3.4%	9.9%

In figure 4.12, the P, h diagram for R-1234yf is reported

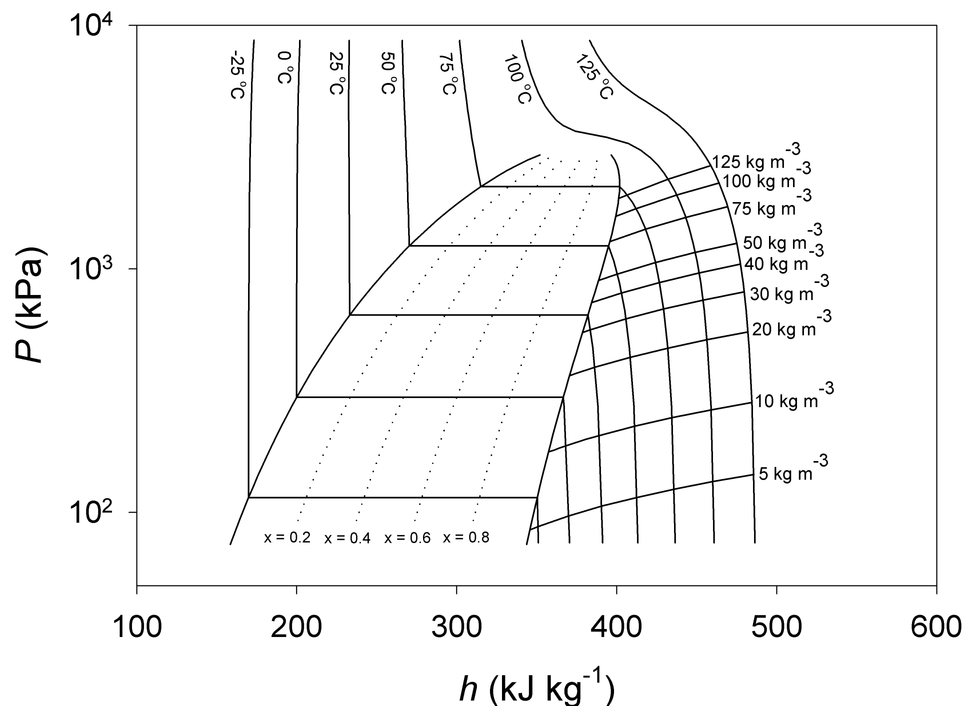

Fig. 4.12- P-h State Diagram for HFO-1234yf.

Recently, the ASHRAE proposed, for public review, several ultra-low GWP propene isomers, like the mentioned R1234yf (ASHRAE, 2008). The suitability of the proposed fluids for thermal management of electronics in airborne applications is still to be in investigated at present.

5 NUMERICAL SIMULATIONS FOR COLD PLATES WORKING WITH SINGLE PHASE FLUIDS

5.1 Introduction

The numerical method described in chapter 3 allows to carry out a critical and reliable assessment on the use of different liquid coolants, when single phase cooling is used, or even on two-phase refrigerants, and it also consents to define a suitable design for the heat exchanger and to calculate the temperature profile which occurs on the surface of the electronic device to be cooled.
In particular, both mini and micro channel cold plates can be evaluated, respectively for high power electronics (IGBT modules) and for microelectronics, such as avionic chips.
Clearly the cooling capacity to be supplied strictly depends on the electrical loss produced by the components, then power electronics will need a cooling capacity several times higher than for microelectronics, anyway the heat flux densities are extremely high in both cases and therefore an accurate design process is needed.

This chapter aims to illustrates how such process can be faced, and then an assessment on fluids and cold plate configuration will be carried out.

The cold plate here analyzed is a device with an array of channels arranged in parallel, as it is the simplest configurations and then the manufacturing cost will be as low as possible.

5.2 Heat sinks for micro electronics

The most common air-based system is here described. It mainly consists of a heat spreader (HS), with the function to reduce the heat flux density coming from the chip, a heat sink, to dissipate the heat to the ambient air, and a fan to produce a proper air flow on the heat sink surface. A thermal interface material layer is usually placed between the die and the heat spreader, and also between the heat spreader and the heat sink, in order to assure a good thermal contact between the components and thus avoid possible micro areas where air could generate high thermal resistance zones and thus reducing the heat transfer area.

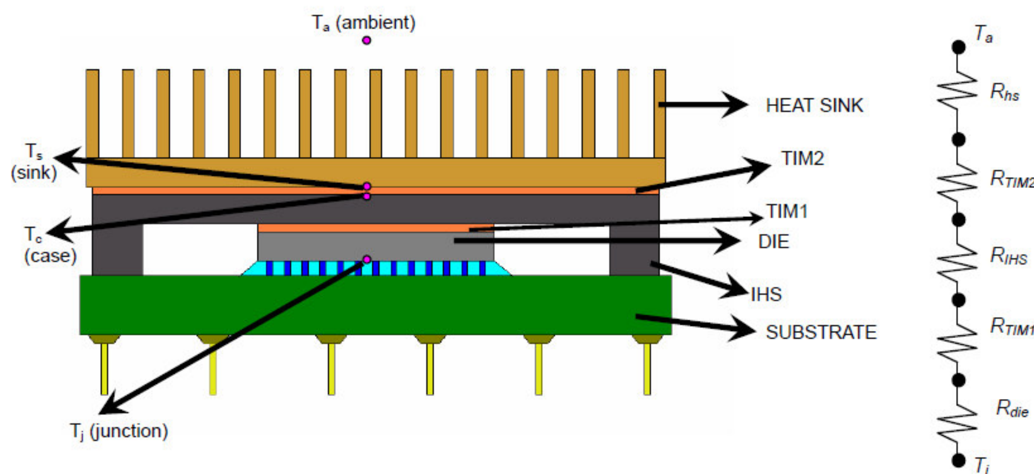

Fig. 5.1- Schematic of desktop processor packaging assembly and thermal resistance network

Figure 5.1 refers to the cooling system for an Intel Pentium® 4 processor and it corresponds to the typical air cooling heat sink. The heat spreader is integrated with the board, and a heat sink is attached to it.
As it is shown in figure 5.1, both heat sink and heat spreader are larger than the chip surface, in order to dissipate the high heat flux density coming from the chip. While the copper heat spreader decreases the heat flux density, thanks to its high thermal conductivity, the heat sink dissipates the heat coming from heat spreader to the air and it is usually produced in aluminum, with a lower thermal conductivity than HS and cheaper, since the larger thermal resistance is give by air. In fact, a finned surface is needed to compensate the low air heat transfer coefficient and give an adequate thermal resistance, but this leads to a significant increase in the system volume and may represent a problem in miniaturization processes.

Kumari, Krishnan, and Garimella suggested in their work several suitable alternatives to the baseline system, including 3 different mini channel integrated systems.

The first alternative is quite similar to the baseline from a structural point of view, and consists of a liquid minichannel cold plate attached to the heat spreader.
This can actually reduce the volume of the system, and the overall thermal resistance is considerably reduced.

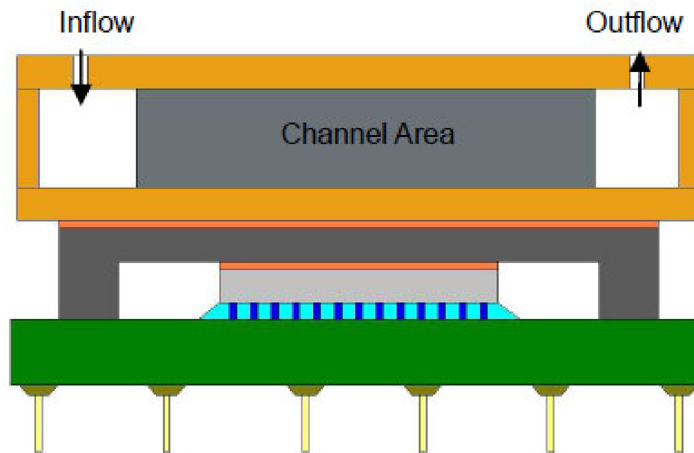

Fig. 5.2- Schematic of desktop processor packaging assembly and thermal resistance network

Anyway, since liquid heat transfer coefficients are orders of magnitude larger than air ones, higher heat flux densities can be dissipated and the heat spreader can be removed, further reducing overall thermal resistance.

In the second solution, actually spreader and heat sink are integrated in 1 component, thus having a lower packaging thermal resistance.

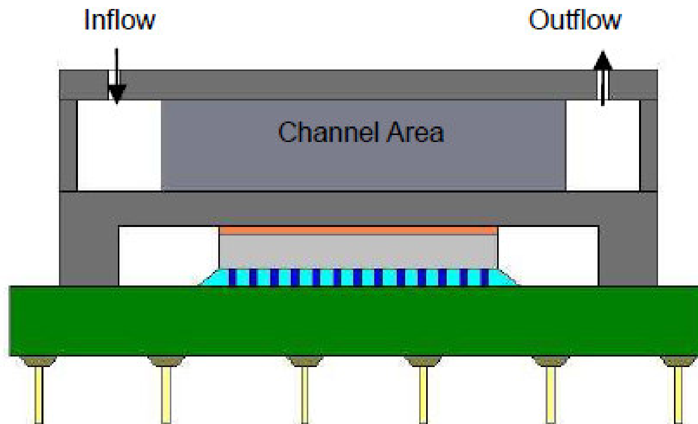

Fig. 5.3- Schematic of desktop processor packaging assembly and thermal resistance network

In this system micro channels are directly set in the spreader, and this even leads to elimination of a thermal interface material layer.

Finally, the third alternative (fig.5.4) illustrates the most integrated system, since micro channels are directly fabricated on the back side of the chip, removing the spreader and all thermal interface material layers.

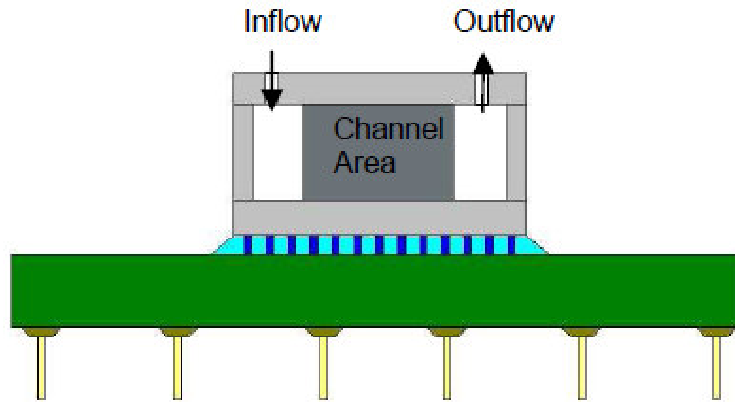

Fig. 5.4- Schematic of desktop processor packaging assembly and thermal resistance network

Clearly liquid cooling allows for the use of smaller heat transfer areas, compared with those used with air, then even if the least system is the more compact, also the second one, with micro channels fabricated on the back side of the heat spreader, appears to be very compact and easily manufacturable, indispensable condition to reduce costs, as the chip is completely separated from the liquid coolant.

5.3 Numerical simulation for a micro channel heat sink

The evaluation of a cold plate performance is often carried out assuming a uniform temperature field over the surface between the heat exchanger and the component to be cooled, because of the high thermal conductivity of the material the cold plate is made of. Anyway this assumption is acceptable only in the particular cases when the product of mass flow and specific heat, referring to the fluid flowing through the micro channels, is very high, such to give a temperature difference between inlet and outlet quite low, and in the cases there are not hot spots.

Let us consider the particular case of a component off the shelf, as it is the Intel Xeon® Processor 5000 series. According to the data provided by the supplier, the maximum thermal design power is 130 W (taken from http://www.intel.com/p/en_US/products/server/processor/xeon5000/specifications), the chip surface is about 15 mm x 15 mm, and the integrated heat spreader is 37.6 mm x 37.6 mm. At present, the product is equipped with the typical air cooling system: a heat spreader, a heat sink and a fan, with a volume of about 90 mm x 90 mm x 100 mm (taken from http://www.intel.com/Assets/en_US/PDF/datasheet/313079.pdf).

According to the product specifications, the cooling system must guarantee a maximum temperature, measured in the middle of the heat spreader surface, not higher than 69 °C.

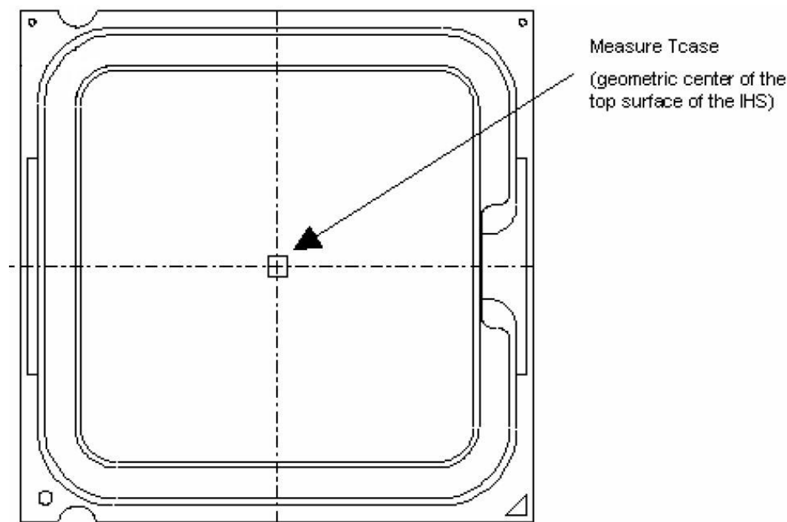

Fig. 5.5- Point of evaluation of the maximum temperature

In this case, assuming a uniform temperature over the heat spreader would certainly not be acceptable, since only a small area of the heat exchanger (in the center of the packaging) is in contact with the chip, which is a hot spot, while the remaining area works as a heat spreader, since it is subjected to conduction heat transfer from the hot spot.

In this chapter is analyzed an aluminum (thermal conductivity of 205 W/(m K)) cold plate which micro channels are set on the back side of the integrated heat spreader of the Intel system. The size of the heat exchanger corresponds to the heat spreader one, i.e. 37.6 mm x 37.6 mm (thickness of 0.9 mm), and a uniform heat flux (as suggested by Incropera, 1999) of 130 W is considered at the center of heat spreader, over an area of 15 mm x 15 mm. Micro channels are fed in parallel by the same mass flow, and the single phase fluid inlet temperature is set at 50 °C, much higher than the usual ambient air temperature, and anyway according to the value suggested by ARINC 600, in order to allow the designer to consider also a passive cooling method to dissipate the heat removed by the liquid coolant.

As regards the correlation used for the fluid, several assessments have to be considered. Several investigations both on the applicability of correlations to predict heat transfer coefficients developed for macro channels and on the friction factors have been carried out for years, but a conclusion can not yet be done because results of several studies are in disagreement.

As regards the heat friction factor, Choi (1991) and Pfahler (1991) measured values lower than those for macro channels, while Tuckerman and Pease (1981)

measured higher values than the macro channel ones. A more recent study, by Kendall and Rao (1997), confirmed the effectiveness of correlations developed for macro channels, even if their investigation was just on the range 30 – 55 μm channel height, quite lower than the height considered in the simulations of the present work.

The same situation is for the heat transfer coefficient correlations. While Peng (1994) experimentally measured Nusselt values lower than Shah and London (1978), Wang and Peng (1994), according to Incropera, measured scattered data not correlated for laminar and transitional flows. What seems to be proved is that when flowing through microchannels, the Reynolds number at which flow becomes turbulent is quite reduced compared to the traditional value of 2000, depending on the channel dimension and aspect ratio.

According to Incropera, since a clear trend is yet to be found, it is hard to evaluate fluid thermal and hydrodynamic behavior when flowing through a micro channel, and therefore the simulation of a cold plate to assess its performance have still a certain level of uncertainty, and macro channel correlations continue to be used.

5.4 Simulation results – cold plate optimization

The numerical results, relating to several cold plate configurations and fluids, are here illustrated. The first series of simulations were conducted using water as the coolant, with a velocity in the micro channels ranging from 0.1 m/s to 0.8 m/s. Input values are summarized in the following table:

Tab. 5.1- Cold plate parameters

Heat Sink	Chan.	Chan. Width [m]	Chan. Height [m]	Fin Width [m]	Chan. Length [m]	Fluid Velocity [m/s]	Mass Flow [kg/s]	Coolant	Inlet Temperature [K]
A	18	0.001	0.001	0.001	0.0376	0.1	0.0018	WATER	323
B	18	0.001	0.001	0.001	0.0376	0.2	0.0036	WATER	323
C	18	0.001	0.001	0.001	0.0376	0.4	0.0072	WATER	323
D	18	0.001	0.001	0.001	0.0376	0.8	0.0144	WATER	323
F	18	0.001	0.002	0.001	0.0376	0.2	0.0072	WATER	323
G	18	0.001	0.002	0.001	0.0376	0.4	0.0144	WATER	323
H	18	0.001	0.004	0.001	0.0376	0.4	0.0288	WATER	323
I	37	0.0005	0.001	0.0005	0.0376	0.2	0.0037	WATER	323
L	37	0.0005	0.001	0.0005	0.0376	0.4	0.0074	WATER	323
M	37	0.0005	0.002	0.0005	0.0376	0.4	0.0148	WATER	323
N	73	0.0003	0.002	0.0002	0.0376	0.2	0.00876	WATER	323
O	73	0.0003	0.002	0.0002	0.0376	0.4	0.01752	WATER	323
P	73	0.0003	0.002	0.0002	0.0376	0.8	0.03504	WATER	323

Numerical results are summarized in tables 5.2 and 5.3:

Tab. 5.2- Numerical results, part A

Heat Sink	htc [W/m^{2}k]	Thermal Resistance [K/W]	Fluid Average Temperature [K]	Reynolds [-]	Pressure Drops [Pa]
A	2320.3	0.158	332.89	212.78	67
B	2320.3	0.158	327.81	392.95	163
C	2320.3	0.160	325.37	755.36	415
D	2320.3	0.160	324.18	1481.25	1160
F	1988	0.126	325.38	503.66	112
G	1988.7	0.127	324.18	987.55	306
H	2142	0.076	323.59	419.11	965
I	3977.5	0.061	327.78	261.87	316
L	3977.5	0.061	325.34	503.35	734
M	4284	0.037	324.16	592.40	567
N	7661	0.015	325.00	195.86	512
O	7661	0.015	323.99	385.21	1119
P	7661	0.015	323.49	764.06	2573

Tab. 5.3- Numerical results, part B

Heat Sink	Fluid Average Temperature [K]	Fluid Maximum Temperature [K]	Base Average Temperature [K]	Base Maximum Temperature [K]	Base Minimum Temperature [K]
A	332.9	344.4	353.4	375.0	341.0
B	327.8	334.1	348.3	369.5	338.2
C	325.5	328.6	346.3	366.9	337.1
D	324.2	325.8	345.0	365.6	335.6
F	325.5	328.9	341.9	361.0	333.3
G	324.2	326.0	340.7	359.7	332.4
H	323.6	324.7	333.6	349.7	326.9
I	327.8	335.4	335.7	352.7	326.7
L	325.3	329.7	333.3	350.2	325.7
M	324.2	326.8	328.9	342.3	323.8
N	325.0	330.0	326.9	336.8	323.1
O	324.0	326.6	325.9	334.3	323.0
P	323.5	324.8	325.4	333.2	323.0

As a first attempt, a 18 channel configuration was analyzed, since a low number of channels allows to have low manufacturing cost, with a channel height set to 1 mm, in order to consider a very compact configuration. Heat exchanger performance is evaluated at several coolant velocities, ranging from 0.1 to 0.8 m/s.

Case named as A considers a coolant velocity of 0.1 m/s, then the average temperature difference from inlet to outlet is quite high, about 21 °C, thus the thermal resistance, calculated as the ratio between base-fluid temperature difference (using average values over the heat exchanger) and the heat flux, results to be 0.158 K/W, too high to guarantee the thermal management conditions required by the supplier.
In fact, the maximum temperature value on the base element, in particular at the center of the hot spot area (indicated by the supplier as “T case”), is about 102 °C, while the temperature allowed is 69 °C, in order to assure the integrity and correct working of the electronic component.

Configuration B is simulated with a velocity doubled compared to the case A. Since the fluid flow regime is laminar, heat transfer coefficient does not increase, in spite of a higher fluid velocity, according to Shah and London (1978) correlations, but a higher mass flow allows to decrease the outlet average temperature by about 10 °C. Even if the thermal resistance does not decrease, because both fluid and base average temperatures are lowered by the same ΔT, the positive effect results in the maximum temperature over the interface between chip and base, more than 5 °C lower in comparison with case A.

In case C, the fluid velocity is set to 0.4 m/s, then the temperature difference between inlet and outlet is just slightly higher than 5 °C. Anyway, also this configuration does not allow to meet the required specifications, since the maximum T case is about 94 °C, only 2 °C lower than the configuration B one.

It clearly appears that a new configuration is to be used, with a higher heat transfer area and a higher fluid heat transfer coefficient, in order to reduce the thermal resistance. In fact, as a confirmation of what has been said, the simulation carried out with a fluid velocity of 0.8 m/s does not lead to any significant improvement compared with previous cases, but on the contrary it implies increasing pressure drop, related to the velocity square, and increasing pumping power, related to the pressure drop and the volumetric flow.

Cold plates F and G have the same number of channels as the previous heat exchangers, but in these cases the cannel height is doubled to 2 mm, in order to increase the heat transfer area, while the fluid velocity is set at 0.2 m/s and 0.4 m/s respectively. With the same channel width but increased height, the hydraulic diameter increases and then, having the same Nusselt number, the heat transfer coefficient is about 15% lower than the 1 mm height channels. The cold plate performance is enhanced, thanks to a larger heat transfer area, and maximum base temperatures are 88 °C and 86.7 °C respectively, still higher than the required value. Since case G is just slightly better than F cold plate, a further velocity increase would not lead to any important improvement, then the next step is to enlarge again the finned surface.

Therefore the vertical wall height is brought to 4 mm for the configuration H, and the mass flow is increased in order to have the same fluid velocity. The performance is definitely better, since the T case obtained is 76.7 °C, which is 10 °C lower than case G. Also this cold plate does not meet the product specifications, and anyway a more compact heat exchanger would be better from a component miniaturization point of view.

Three heat exchangers, with 37 channels but same base area, are then analyzed. A higher number of channels allows to increase both the surface and the heat transfer coefficient, and thus the thermal resistance should significantly decrease. In the cases I, L and M there are 37 channels, with base width of 500 μm and fin width of 500 μm as well, and they differ for channel height and fluid velocity.

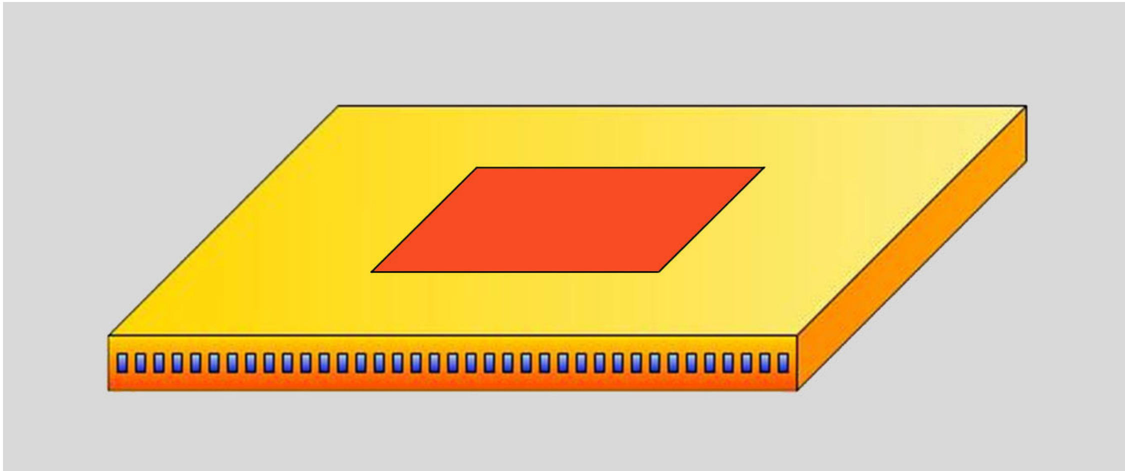

Fig. 5.6- Cold plate I

Case I has 1 mm height channels, and fluid velocity is set to 0.2 m/s, as it is in case B. Compared with case B, pressure losses associated with flow through the channel are more than doubled (123 Pa for case B, 276 Pa for case I), since channel width is halved, but this configuration allows to diminish the maximum temperature value from 96.5 °C to 79.7 °C, corroborating the effectiveness of a higher heat transfer coefficient and larger finned area. Since the temperature profile calculated is not yet suitable to meet thermal management requirements, the next step was to increase the velocity.

Case L has a velocity of 0.4 m/s, and then pressure losses doubled (585 Pa), with a quite small enhancement in terms of maximum temperature on the base, just 2.5 °C less than in case I.

Case M maintains a velocity of 0.4 m/s, while channel height is set at 2 mm (still a compact system anyway). With such configuration, the T case calculated is 69.1 °C, practically meeting electronics specifications, while pressure losses due to flow through channels is lower than in case L, as hydraulic diameter is higher, but pumping power is increased since it is in proportion to increase in the mass flow. It may be interesting to illustrate the temperature field over the base surface in contact with the chip, as depicted in figures 5.7 and 5.8.

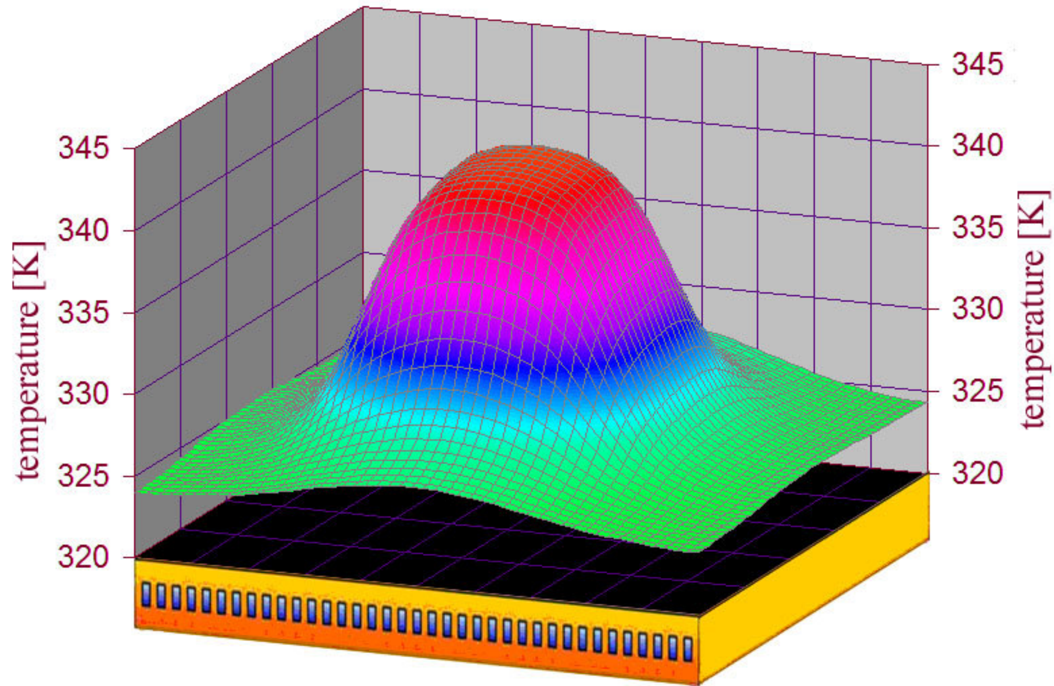

Fig. 5.7- Temperature profile for case M

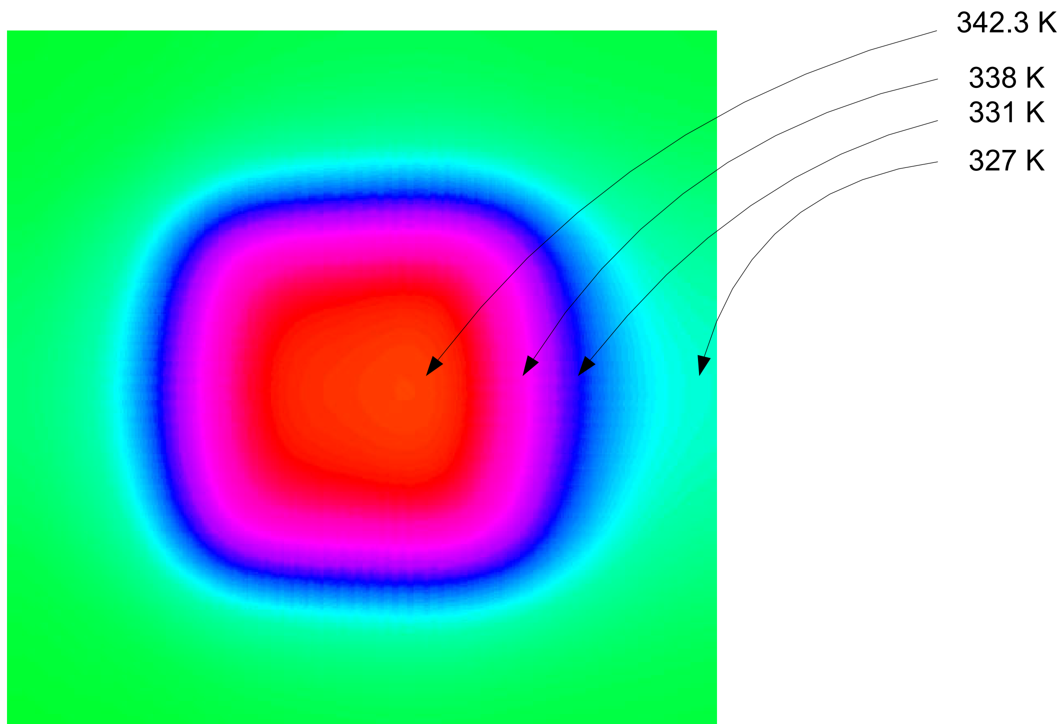

Fig. 5.8- Temperature field for case M (fluid flowing from left to right)

The red zone approximately corresponds to the chip position, and it is worth noticing that the temperature is about constant over the hot spot, even if the peak occurs about 1.5 mm beyond the geometrical center, due to the fluid temperature increase,

while in the remaining surface of the heat exchanger the temperature decreases and the thermal conduction over the metallic plate helps to dissipate the heat flux coming from the chip. While over the fluid inlet part the base temperature is very close to the fluid temperature, in the outlet part the base temperature is about 327 K, then there exist a dissymmetry along the channels, because of the increment of fluid temperature. Transversally the temperature profile is perfectly symmetric, in agreement with the choice of feeding all the channels with the same mass flow.

Finally, numerical results for 73 channel cold plates are reported in the foregoing tables, with channel height of 2 mm and fluid velocity 0.2 m/s, 0.4 m/s and 0.8 m/s for case N, O and P respectively. The strong increase of heat transfer coefficient, as well as a larger finned area, allows to get a very low T case: 63.8 °C for a velocity of 0.2 m/s (case N); 61 °C for 0.4 m/s (case O) and finally 60 °C for 0.8 m/s. The increase in fluid velocity appears not to lead to any important performance enhancement, on the contrary it implies a higher pumping power, considering pressure losses due to flow in channels, till 10 times higher.

According to the results obtained with several simulations, a configuration with large heat transfer area, gained increasing the number of channels, seems to be the only way to enhance the heat exchanger performance, and the fluid velocity is to be chosen in order to guarantee a low fluid temperature difference between inlet and outlet, but also low pressure losses and pumping power.

When using a different coolant from water, the heat exchanger is to be optimized according to the new fluid properties. Anyway, since a 37 channel cold plate was assessed to be suitable to provide proper thermal management on the chip, it was also simulated using propylene glycol (60 % vol.).

What results is that such configuration, with a fluid velocity of 0.4 m/s, is not suitable when using a different coolant from water, since the maximum temperature gain is 75.8 °C. Therefore, the number of channels was increased, and a 44 channel configuration results to meet the product specifications, as a maximum temperature of 68.4 °C can be achieved on the base plate. The temperature profile is illustrate in figure 5.9.

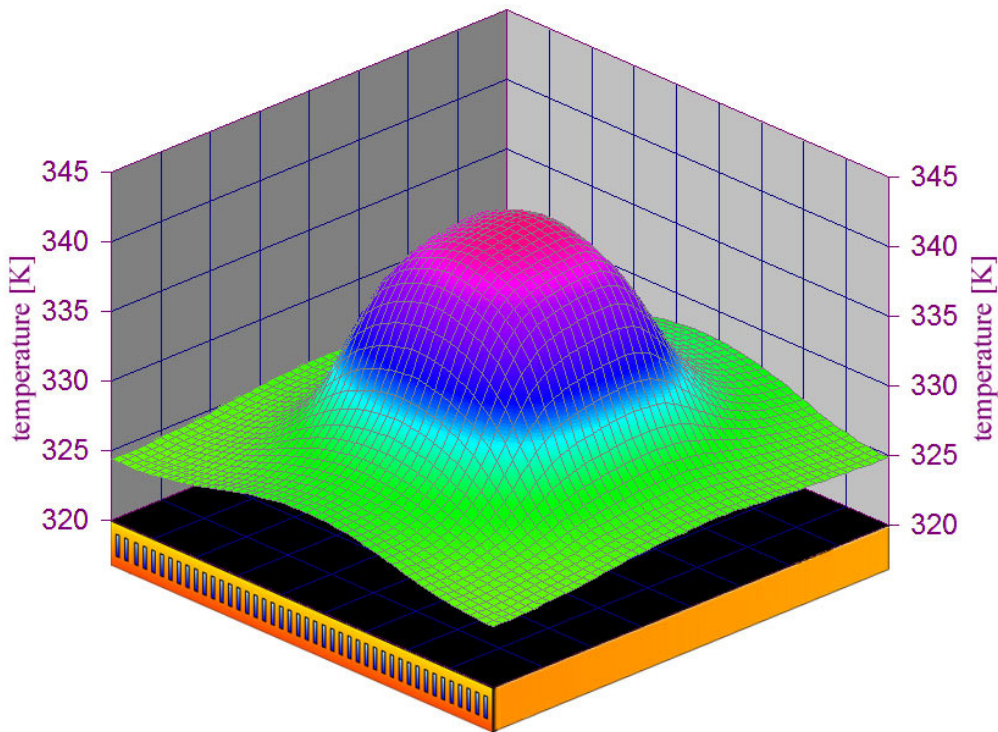

Fig. 5.9- Temperature field for a 44 channel cold plate fed with propylene glycol (60% vol.)

5.5 Simulation results – fluid assessment

When an assessment on fluids is to be carried out, fluid properties are to be considered but it is also essential to understand the configurations to be adopted in order to meet the product thermal management requirements. Considering the simulations illustrated in the foregoing section, some important considerations can be pointed out so that a first assessment on the cold plate configuration can be done.

In particular, assuming a base temperature field similar to the one calculated for a same base area heat exchanger which fulfils thermal management, then its average interface temperature can be used, together with the fluid temperature, to calculate the thermal resistance to be assured by the heat exchanger. The same is for the fluid average temperature, since the fluid temperature difference between inlet and outlet is to be low enough to guarantee a suitable thermal resistance and to provide an adequate temperature difference with the metallic surface all over the heat exchanger.

Let us consider the case illustrated in the previous section: the base average temperature, when the T case was lower than the limit value (69 °C), results 329 K. The fluid inlet temperature is set at 50 °C, while a temperature difference between inlet and outlet of 5 K was found to be suitable to assure a proper heat exchange. Finally, since the thermal power to be dissipated is 130 W, the thermal transmittance is to be at least

30 W/K. Clearly such values allow just to have a first design method to assess the channel width, height, the fin thickness and the minimum fluid velocity, while an accurate analysis is still required to evaluate the heat exchanger performance, as the heat transfer coefficient, pressure losses and surface efficiency are calculated all over the cold plate (ranging from about 650 to 2000 calculation points), and then the correct configuration can be easily obtained.

Choosing suitable configurations for the cold plate, the channel width was set to be not lower than 200 μm, as for the fin thickness, while the channel height was limited to 4 mm (a further increase did not lead to important enhancement anyway), with the only exception of carbon dioxide, which required a larger heat transfer area.

Considering the fluids illustrated in chapter 4 and evaluating both cold plate configurations to be used and the pressure losses associated with the flow through microchannels, it is possible to rank each fluid and then provide an ulterior criterion to evaluated whether a fluid can be used or not from a complete system point of view.

The following table reports the preliminary results for the cold plate to be used on the Intel chip here considered. The fluid velocity was chosen to ensure a proper mass flow and then an average temperature difference between outlet and inlet not greater than 5 K.

Tab. 5.4- Preliminary results

Fluid	Chan. [-]	Height [mm]	Chan. Width [µm]	Mass Flow [kg/s]	Velocity [m/s]	Nu [-]	htc W/(m^{2}K)	Re [-]	Area x htc [W/K]	Pressure Losses [Pa]
Pekasol 2000	53	2	500	0.0086	0.14	5.33	3464.6	101.7	34.5	349.4
Dynalene	53	2	500	0.0094	0.13	5.33	3579.6	70.9	35.6	528.4
Ethylen Glycol (40%) (ASHRAE)	57	2	450	0.0071	0.13	5.53	3384.3	81.5	35.5	397.5
Ethylene Glycol (ASHRAE)	57	2	450	0.0074	0.14	5.53	3156.0	70.0	33.1	488.8
Glykosol N	57	2	450	0.0073	0.14	5.53	3169.9	62.6	33.2	534.9
Zitrec MC	62	2	400	0.0072	0.14	5.74	3656.0	65.2	40.9	586.7
Ethylen Glycol (60 %) (ASHRAE)	62	2	400	0.0079	0.15	5.74	3211.0	55.2	35.9	813.7
Pekasol L	62	2	400	0.0070	0.14	5.74	3260.0	43.1	36.4	835.3
Zitrec FC	62	2	400	0.0070	0.14	5.74	3215.3	43.6	35.9	843.8
Zitrec LC	62	2	400	0.0070	0.14	5.74	3215.7	43.9	35.9	844.2
Propylene Glycol (60% vol) (ASHRAE)	62	2	400	0.0074	0.15	5.74	2876.2	36.1	32.1	1123.5
Thermera 40	62	2	400	0.0087	0.16	5.74	3081.4	34.2	34.4	1541.2
Xceltherm 500	68	4	350	0.0113	0.15	6.94	1455.0	22.8	32.3	1526.1
Galden ZT 130	83	4	250	0.0207	0.16	7.28	1451.5	123.1	38.5	850.5
Gald ZT 180	83	4	250	0.0231	0.17	7.28	1380.7	96.0	36.6	1319.8
CO_2	93	7	200	0.0113	0.41	7.77	625.2	1669.3	31.4	103.0

HFE 7100	93	4	200	0.0210	0.20	7.46	1241.7	376.3	36.4	527.3
HFE 7500	93	4	200	0.0222	0.19	7.46	1188.5	151.9	34.9	1249.2
Galden HT 135	93	4	200	0.0246	0.20	7.46	1235.8	111.3	36.3	1932.9
Dowtherm J	93	2	200	0.0135	0.43	6.79	2428.5	216.3	37.3	2540.7
Syltherm XLT	93	2	200	0.0141	0.46	6.79	1933.9	157.2	29.7	3869.4
Galden HT 230	93	4	200	0.0247	0.19	7.46	1229.0	31.6	36.1	6256.3
Dowtherm Q	93	2	200	0.0148	0.42	6.79	2350.0	70.8	36.1	7975.3

The fluids are ranked in the table according to the channel number which the cold plate is to be manufactured (it can be consider as a parameter of cost), and this ranking corresponds even to the pressure losses which occurs in the heat exchanger, with the only exceptions of carbon dioxide, because of the particular fluid properties in the transcritical process, and HFE 7100, since dynamic viscosity indicated by the producer is very low.

To control if the predictions reported in table 5.4 could be acceptable, several cases were simulated and the results are illustrated in the following. In particular, Dynalene, Propylene glycol (vol. 60%), Galden ZT 130, Xceltherm, and HFE 7100 were considered both to evaluate if the fluid are suitable and to analyze the effectiveness of different heat transfer area.

The case of Dynalene gives a maximum temperature of 70 °C over the base plate, therefore meeting the thermal management constraint. The temperature field is symmetric when considering a longitudinal central axis, while it is asymmetric in the other direction, because after the hot spot the base temperature increases as the fluid temperature rises, since a low mass flow was consider to have low pressure losses and pumping power. The base temperature profile is illustrated in figure 5.10, and figure 5.11 shows the cover plate temperature profile, assuming the cold plate thermally insulated from the ambient air.

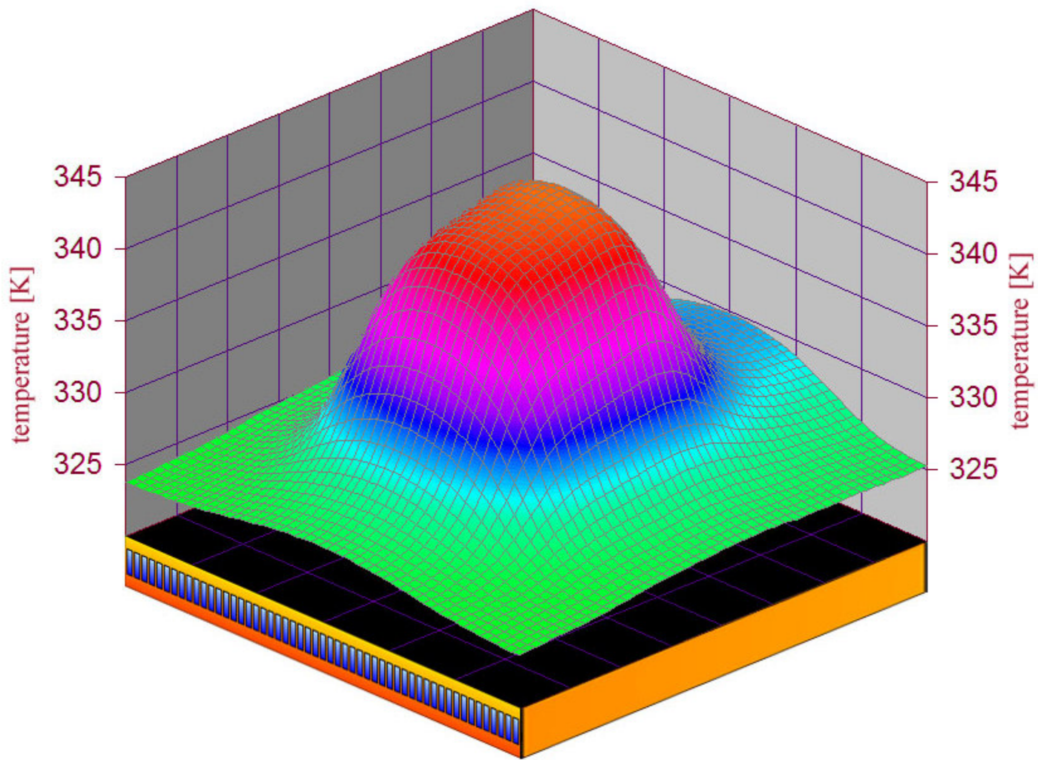

Fig. 5.10- Base temperature profile using Dynalene

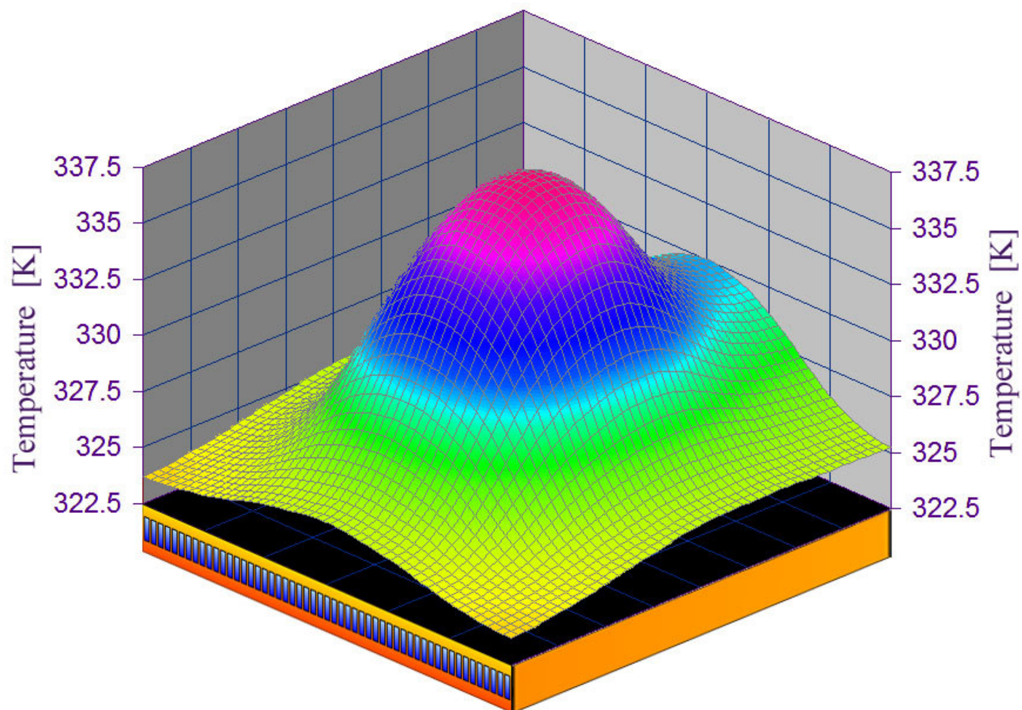

Fig. 5.11- Cover temperature profile using Dynalene

Also the cover plate element works as a sort of spreader, and the temperature field is more homogeneous than the base one, even if the temperature increase after the hot spot clearly appears.

Galden ZT 130 requires a high channel number, i.e. 83 channels, and a channel height of 4 mm, since a really high heat transfer area is needed to compensate for the low heat transfer coefficient. The temperature profile over the base is shown in figure 5.12.

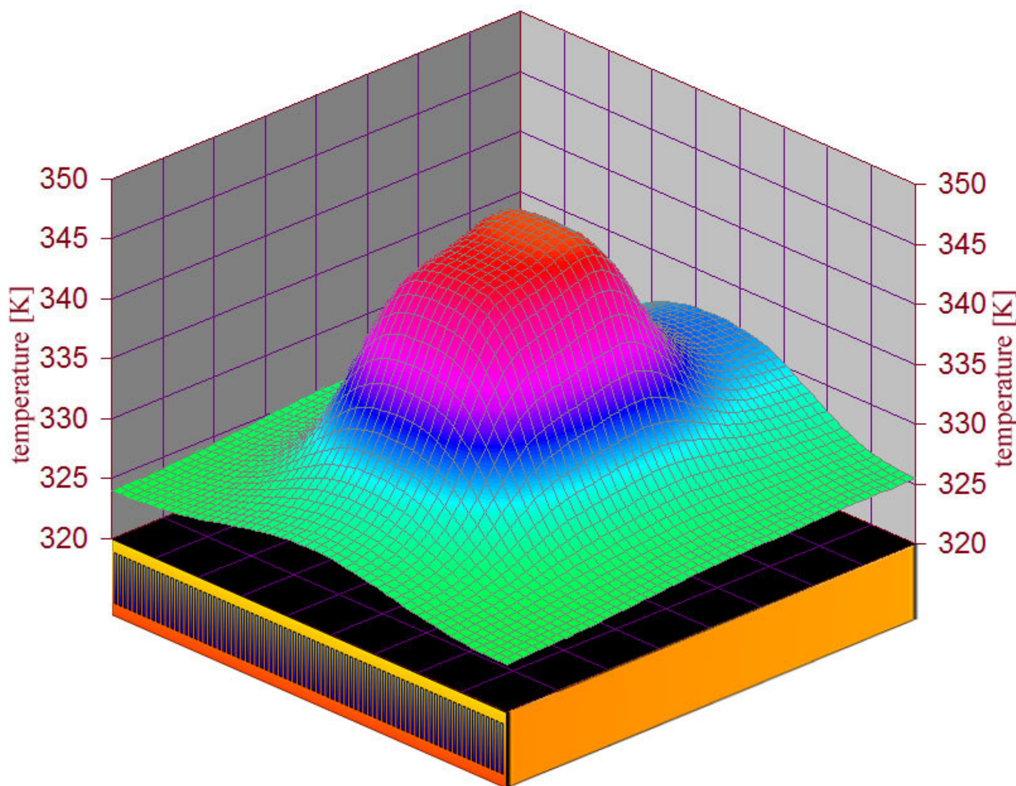

Fig. 5.12- Base temperature profile using Galden ZT 130

Even for this case, the same remarks as for Dynalene can be expressed referring to the temperature profiles. Anyway, the maximum temperature calculated in this case is 72.5 °C, then too high to fulfil the thermal specifications, and then the cold plate to be used must have a larger heat transfer area, because of the finned surface effectiveness, which is quite important in this case as it is characterized by a very large surface.

Temperature profile for Propylene Glycole (60% vol.), relating to the cold plate size reported in table 5.4 is illustrated in the figure 5.13.

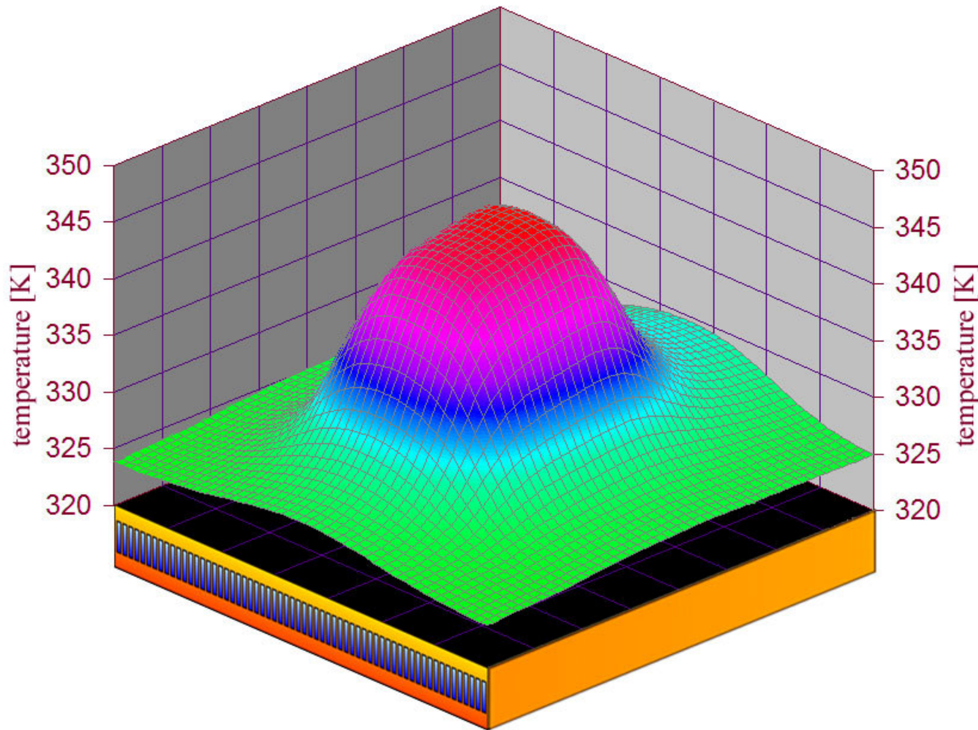

Fig. 5.13- Base temperature profile for Propylene Glycol (60% vol)

The profile is in agreement with the previous ones, and the maximum temperature is 72 °C, then slightly higher than the required value. Anyway, even configurations with a lower number of channels could be suitable, as the 44 channel cold plate illustrated in figure 5.9, in which the channel width was set to 350 μm, height set to 2 mm, and velocity 0.4 m/s. This cold plate gives a maximum temperature of 68.4 °C, which represents a significant improvement since the temperature difference between fluid and surface is quite modest. Nevertheless, the 44 channel cold plate requires an elevated velocity, then pressure losses (5.2 kPa) are 5 times higher compared with the case reported in table 5.4 (1.1 kPa), and pumping power is 10 times increased, as the mass flow results almost doubled.

Also HFE 7100 and Xceltherm 500 cold plates were simulated, and the maximum temperature calculated over the base resulted to be 72.5 °C and 74 °C respectively. Therefore further simulations should be carried out to understand which parameters can be modified to enhance the cold plate performance, and a suggestion can be derived from figure 5.14, which shows the temperature profile for fluid HFE 7100 through the channels. It can be clearly seen that even if the average temperature

difference between inlet and outlet is only 5 K, the maximum temperature reached is almost 332 K, and the fluid temperature corresponding to the maximum base plate temperature is 329 K, then the temperature difference between fluid and base plate is about 13 °C (considering 342 K as the maximum temperature allowed over the base plate). This is why the actual maximum base temperature occurs slightly after the geometrical center of the cold plate (and of the hot spot), and therefore a velocity increase is the easiest way to improve the thermal performance, still having low pressure drop and pumping power (as the value reported in the table is the lowest calculated on several simulations).

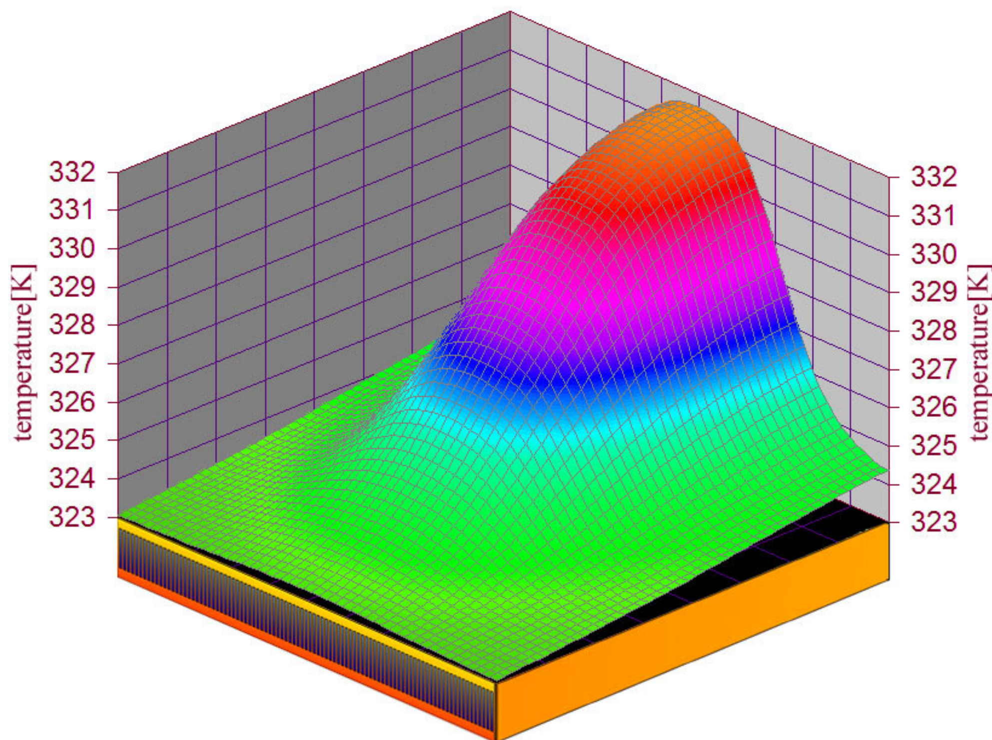

Fig. 5.14- Fluid temperature profile for HFE 7100

In conclusion, the predicted parameters reported in table 5.4 are very close to the proper cold plate configuration, but simulations are still required in order to analyze the correct heat transfer coefficient and pressure drop relating to the actual cell temperature value and surface efficiency.

5.6 Channel side walls efficiency

The foregoing results for cold plates are subjected to a level of uncertainty due to the heat transfer coefficient evaluation in mini and micro channels. As it was pointed out, several authors focused their attention on this issue, but a general trend is yet to be found. In the previous section the same correlation, developed by Shah and London (1978) for laminar flow, was used for all the simulations, and no enhancement associated with the entrance region since this region was really small relative to the length of each channel.

Anyway, one more uncertainty factor could be relevant in the performance calculation. In fact, in the previous section, several channel aspect ratios were used, increasing the fin height when, at a given fluid velocity, the cold plate could not meet the thermal management requirement. This often leads to channels with very low base width compared with the fin height, as it can be seen in the figures here proposed (relating to actual heat exchangers for electronics cooling), so the surface efficiency often becomes important to correctly calculate the heat flow rate in each heat exchanger element.

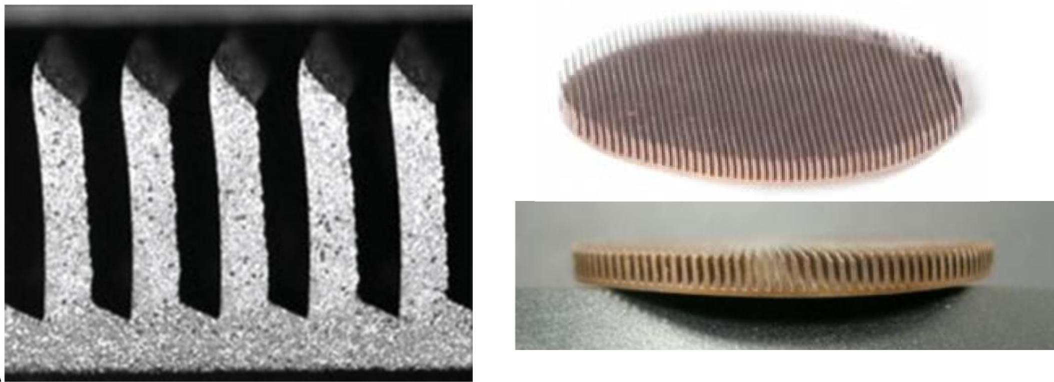

\

Fig. 5.15- Cross section and heat transfer surface (www.microcooling.com, by Wolverine Tube Inc.)

The model described in chapter 3 provides a two-dimensional temperature profile over each fin surface, allowing then a higher accuracy in evaluating the temperature difference between the surface and the fluid.

Let us consider a cold plate with the same overall size as the ones in the previous section, with water as the coolant fluid in laminar flow, and let us consider the temperature profile on the fin surface for the element placed in the HX center, over the hot spot (heat flow rate 130W).

Tab. 5.5- Test condition for four simulations

CASE		A	B	C	D
fin thickness	[mm]	1	0.5	0.5	0.2
fin height	[mm]	2	2	4	4
fin thermal conductivity	[W/(m K)]	200	200	200	200
fluid htc	[W/(m^{2}K)]	1988	2224	2224	14480
fluid inlet temperature	[°C]	50	50	50	50

In the first simulation test, namely A, the cold plate is quite compact, with thick short fins, relative to the aspect ratios illustrated in figure 5.16, and also with a low heat transfer coefficient associated with the fluid.

Considering a linear profile joining the two edge temperatures, the maximum difference from the calculated profile is just 0.4 °C (at 50% of fin length), then even a linear profile would be suitable for calculating the HX performance.

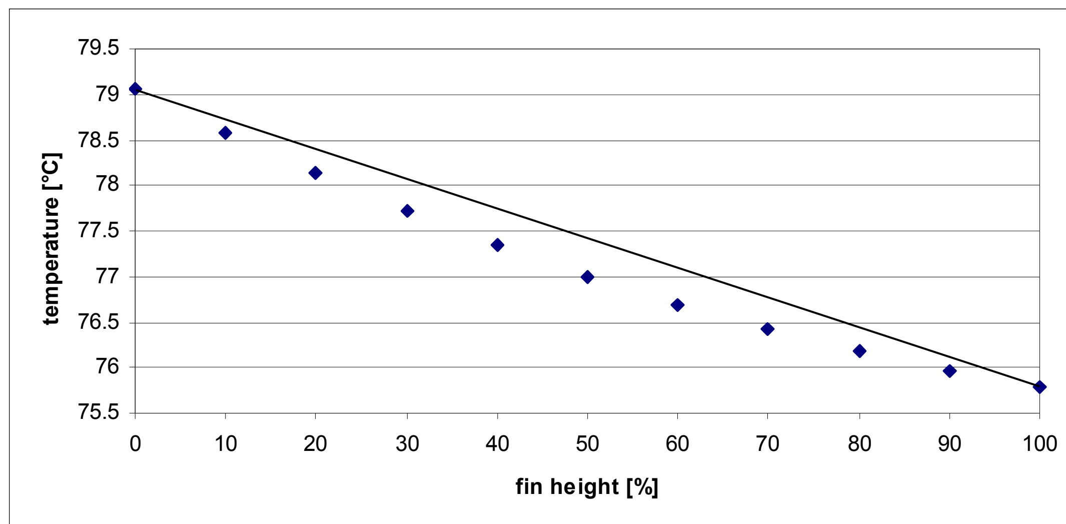

Fig. 5.16- Temperature profile over the fin center element, compare to a linear profile, (case A)

In the second simulation test, namely B, the fin thickness was reduced, as the number of channels was increased, while the heat transfer coefficient is slightly higher compared with case A, because of the different channel aspect ratio.

Considering a linear temperature profile, the maximum difference from the calculated one is slightly higher than 0.4 °C, so a linear profile would be suitable also in this situation.

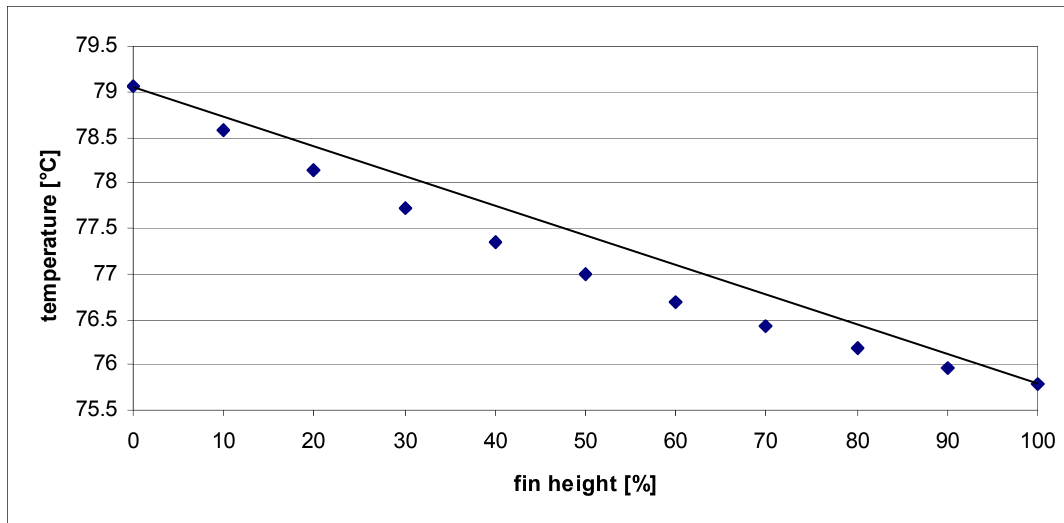

Fig. 5.17- Temperature profile over the fin center element, compare to a linear profile, (case B)

When finally the fin height is increased till 4 mm, producing a cold plate cross section similar to the ones often employed in miniaturized systems, the maximum difference between the linear temperature profile and the calculated one becomes significant since it is 1.4 °C when the temperature difference between the base and the fluid (fluid cell temperature is 52.1°C) is 17°C, leading to a maximum deviation of 8.2%. On average, the fin calculated temperature is 0.98 °C lower than when considering a linear profile, then the heat flow rate in this particular fluid cell is almost 93% than the one calculated using a linear profile. Therefore, a proper evaluation of the temperature along the walls separating adjacent channels appears to be quite important when evaluating a cold plate performance for electronics cooling.

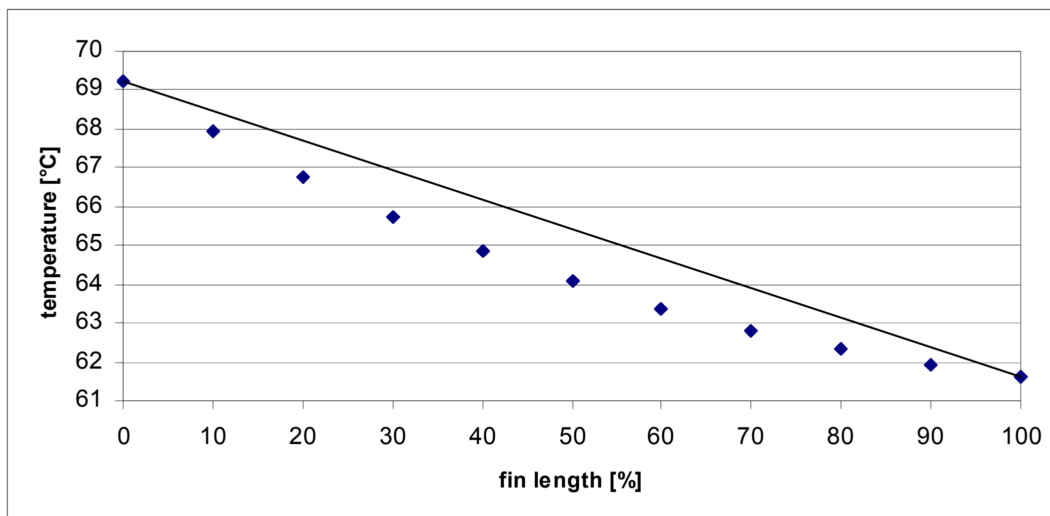

Fig. 5.18- Temperature profile over the fin center element, compare to a linear profile, (case C)

All the simulations carried out in this chapter consider a laminar fluid flow, in order to keep pressure losses low. Anyway, several researchers have investigated even turbulent flow in cold plates, achieving higher heat transfer coefficient. Moreover, cold plates are also used as evaporators in mini vapor compression systems, in which a two-phase process occurs and the heat transfer coefficient obtained is really high.
For these reasons, a further simulation with a turbulent flow (heat transfer coefficient calculated by Gnielinski correlation) was carried out, and the results are concordant with the classic fin efficiency theory.
In fact in this case, namely D, the temperature difference between the calculated profile and the linear one reaches about 6°C, when the temperature difference between base and fluid is about 14°C. In the center of the fin, the temperature difference is just 2.2 °C, while the fin temperature increases by the fin top to 54.2 °C.

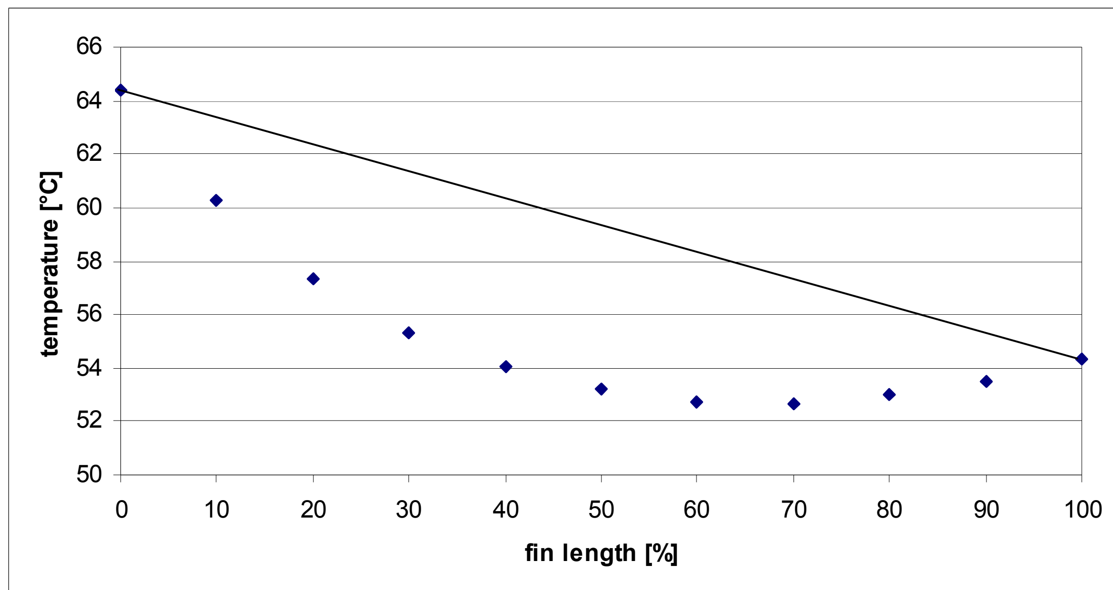

Fig. 5.19- Temperature profile over the fin center element, compare to a linear profile, (case D)

In conclusion, a careful calculation of the temperature profile on the fin surfaces appears to be very important, at least as much as the heat transfer coefficient, when evaluating cold plate performance, since a rough estimation could lead to significant errors. In laminar flow a linear profile could be used when considering thick short fins, while a correct evaluation is preferable when the separating walls have the same usual ratio as in the miniaturized HX for electronics cooling purpose.
When the heat transfer coefficient is increased, considering turbulent flow or two-phase conditions, a linear profile would lead to large errors, which would invalidate the performance evaluation process.

6 A NEW TWO-PHASE REGRIGERANT PROPOSED

6.1 Introduction

Two-phase fluids have already been investigated as working fluids in several applications both for airborne systems and for general electronics cooling.

Mongia et al. (2006) studied (for a notebook application) a small scale refrigeration system, made of a mini vapor compression system with a microchannel cold plate as the evaporator, a microchannel condenser, a capillary tube as the throttling device and a 12 V Embraco miniature compressor.

Fig. 6.1- Embraco compressor used by Mongia et al.

This system was integrated in a laptop to cool a hot spot, and more than 40 refrigerants were evaluated. Finally isobutane was used, and the evaporator temperature was set to 50 °C; the reader may recall that the same temperature was chosen for the inlet single phase fluid temperature for cold plates in chapter 5. The miniature vapor cycle system was analyzed in order to provide a "negative" thermal resistance to the heat flow path, and a COP of 2.25 was achieved, according to the authors.

Anyway, the use of two-phase fluids can also be very important in particular applications, such as new generation electronic devices for defense purpose, where heat dissipation could reach even 1000 W/cm^2. Lee and Mudawar (2008) investigated an evaporator micro channel heat sink in a conventional compression cycle, with R134a as the working fluid, and also an indirect cooling system in which HFE 7100 was pumped in a primary loop, then heat was rejected to a secondary refrigeration loop, made of a vapor compression cycle. Besides achieving high heat transfer coefficients, fluid temperature does not significantly change along a micro channel, as it is equal to the

saturation temperature, differently from the cases analyzed in chapter 7, and then a more uniform temperature can be obtained on the surface. Anyway, pressure losses can be greatly increased compared with the single phase fluids, and micro channels could be subjected to different types of flow, and then to sensible pressure and temperature variations.

Finally, as it is pointed out in chapter 2, the environmental control system could be completely re-designed in perspective of a more electrical aircraft, and vapor compression cycle system should provide the cooling capacity required. Cavallini et al. (2005) proposed an investigation on a carbon dioxide transcritical cycle to be integrated in a conventional air cycle machine for airborne applications.

The choice of the refrigerant to be used could depend on several aspects, as the evaporation temperature level, the quantity (weight assessments) of refrigerant needed, the kind of system (mini vapor cycles or primary loop vapor cycles), and also the safety characteristics as flammability or toxicity.

Recently, a new type of refrigerant has been introduced, as R134a is to be phased out from automotive air conditioning systems starting from 2011 due to environmental problems relating to its high GWP. Even if carbon dioxide was considered by some motor builder as a suitable solution to design a new generation of automotive air conditioning systems, others focused on drop in fluid solutions, in order to use the same technology also for the new systems. In the last year, an intensive experimental test series was carried out at laboratory facilities of Dipartimento of Fisica Tecnica on the use of new low GWP refrigerant HFO-1234yf, and the results are illustrated in the following.

6.2 Fluids proposed to substitute R134a

Over the last several years, much research and development effort has been focused on potential refrigerants possessing low Global Warming Potentials (GWPs). As discussed by Brown (2009), the catalyst for much of this effort can be attributed to European regulations regarding the use of R-134a [GWP relative to CO_2 based on a 100-year time horizon, which is the reference that will be used throughout this work, is 1430 (IPCC, 2007)] in automotive applications. In particular, the European Union's F-gas regulations (Regulation (EC) No 842/2006 and Directive 2006/40/EC) specify that beginning on January 1, 2011 new models and on January 1, 2017 new vehicles fitted with air conditioning cannot be manufactured with fluorinated greenhouse gases having global warming potentials (GWP) greater than 150. Possible candidate refrigerants that

possess GWP < 150, and that are being considered, include R-152a, R-744 (CO_2), and R-1234yf. R-152a, if used, would likely be implemented in a secondary loop system because of its flammability. R-744, if used, would likely be implemented in a transcritical cycle requiring significant modifications to the currently used automotive air conditioning systems because of its considerably different thermophysical properties when compared to R-134a. Among the fluorinated propene isomers which have normal boiling point temperature data published in the public domain, several have low GWP and normal boiling temperatures relatively close to R-134a (from about 3.7 ºC lower to about 8 ºC higher); however, among them, R-1234yf is the one closest to commercialization (its normal boiling temperature is approximately 3.7 ºC lower than that of R-134a). It has a GWP of 4 (Nielsen et al. 2007) and is being widely considered as a possible replacement for R-134a in automotive applications.

To date, researchers and manufacturers have focused their R-1234yf research and development efforts primarily on characterizing its flammability, toxicity, environmental impact, materials compatibility, oil compatibility, air conditioning system performance, thermophysical property data, and in the developing of simple equations of state. Excluding thermophysical property data and equation of state modeling, much of the remaining published work has been presented by chemical manufacturers and vehicle manufacturers through organizations such as VDA (German Association of the Automotive Industry), SAE International, and JAMA (Japan Automobile Manufacturers Association). For example, VDA organizes an annual alternative refrigerant winter meeting where chemical manufacturers and vehicle manufacturers have presented some of their R-1234yf work beginning with its February 2008 meeting. SAE International through its Cooperative Research Program CRP 1234-1 and CPR 1234-2 has focused its research efforts on safety and risk assessment, air conditioning system performance, and materials compatibility, with much of this work having been presented at an annual automotive alternate refrigerant systems symposium beginning with its June 2008 meeting. In the previously mentioned work, the researchers, for the most part, have concluded that R-1234yf appears to be a promising candidate to replace R-134a in automotive applications, with several issues still being investigated through ongoing research and development work. R-1234yf, for example, has somewhat lower thermodynamic performance (e.g., Bang (2008) showed that the cooling capacity of R-1234yf is 3 – 7 % lower and its COP is 1 – 3 % lower than R-134a when used as a “drop-in” replacement for R-134a. As a second example, however, Meyer (2008) showed that with simple system modifications the cooling capacity and COP of R-1234yf could be made approximately equal to the baseline R-134a values). A second issue is the flammability of R-1234yf, where testing has shown

that, while flammable, a significantly larger amount of energy is required to ignite the refrigerant than for other common Class 2 refrigerants (Spatz and Minor, 2008). In recognition of this, a Committee Draft version of ISO 817 (see, e.g., ISO/CD 817:2007) proposes to add a 2L Subclass defined as those refrigerants that meet the conditions for Class 2 refrigerants and, in addition, have a burning velocity ≤ 0.10 m/s when tested at 23.0 ºC and 101.3 kPa. A third issue is the toxicity of R-1234yf. Testing to-date has shown that R-1234yf has similar toxicity as R-134a (e.g., Koban, 2009), though long term toxicity testing is still underway. A fourth issue is the environmental performance of R-1234yf. Koban (2009) performed Life Cycle Climate Performance (LCCP) simulations and has shown under her assumptions that R-1234yf results in reductions of 17 – 20 % when compared to R-134a. Finally, the compatibility of R-1234yf with common materials and oils appears promising (e.g., Spatz and Minor, 2008).

Recently, several research groups have begun publishing R-1234yf thermophysical property data. For example, Tanaka and Higashi (2009) measured its critical properties, saturation pressure from 310 to 360 K, and surface tension from 373 to 340 K. Tanaka et al. measured its liquid isobaric heat capacity and its liquid density from 310 to 360 K at pressures up to 5 MPa. Then, Akasaka et al. (2009) developed both a Patel-Teja EoS and an Extended Corresponding State EoS based on their research group's data. Di Nicola et al. (2009) measured saturation pressures from 224 to 366 K. Brown et al. (2009a,b) developed a simple Peng-Robinson (P-R) Equation of State (EoS) model coupled with group contribution estimation techniques to easily and relatively accurately predict thermophysical property data, which were then used to make performance predictions in a typical automotive air conditioning system (Zilio et al., 2009). Leck (2009) used his employer's data to develop a Martin-Hou EoS and then used it to predict the performances for several refrigeration examples. Hulse et al. (2009) measured its critical temperature, saturation pressure, liquid density, ideal gas heat capacity, liquid viscosity, and surface tension, and then developed a corresponding states EoS using their data.

In this work, the performance potentials of R-134a and R-1234yf are compared in a typical European compact automobile. In particular, experimental data from the baseline R-134a system are compared to data from four systems: (i) the baseline system operating with an optimal charge of R-1234yf with the baseline TXV setting, (ii) the system of *i* with an optimal charge of R-1234yf with a TXV setting optimized for R-1234yf, (iii) the system of *ii* with the variable displacement compressor control valve deactivated, and (iv) the system of *ii* with the condenser replaced by one having 40 % more external surface area.

6.3 Experimental apparatus

The experimental apparatus consists of four basic systems: (1) a closed-loop air circuit for the evaporator, including centrifugal fan, electric resistance heater, humidification equipment, and associated controls, (2) a closed-loop air circuit for the condenser, including centrifugal fan, chiller, electric resistance heater and associated controls, (3) the refrigerant circuit, including a mini-channel evaporator, a mini-channel condenser, a variable volume swashplate compressor, and a TXV, all components from the air conditioning system of a typical European compact automobile, and (4) the instrumentation system.

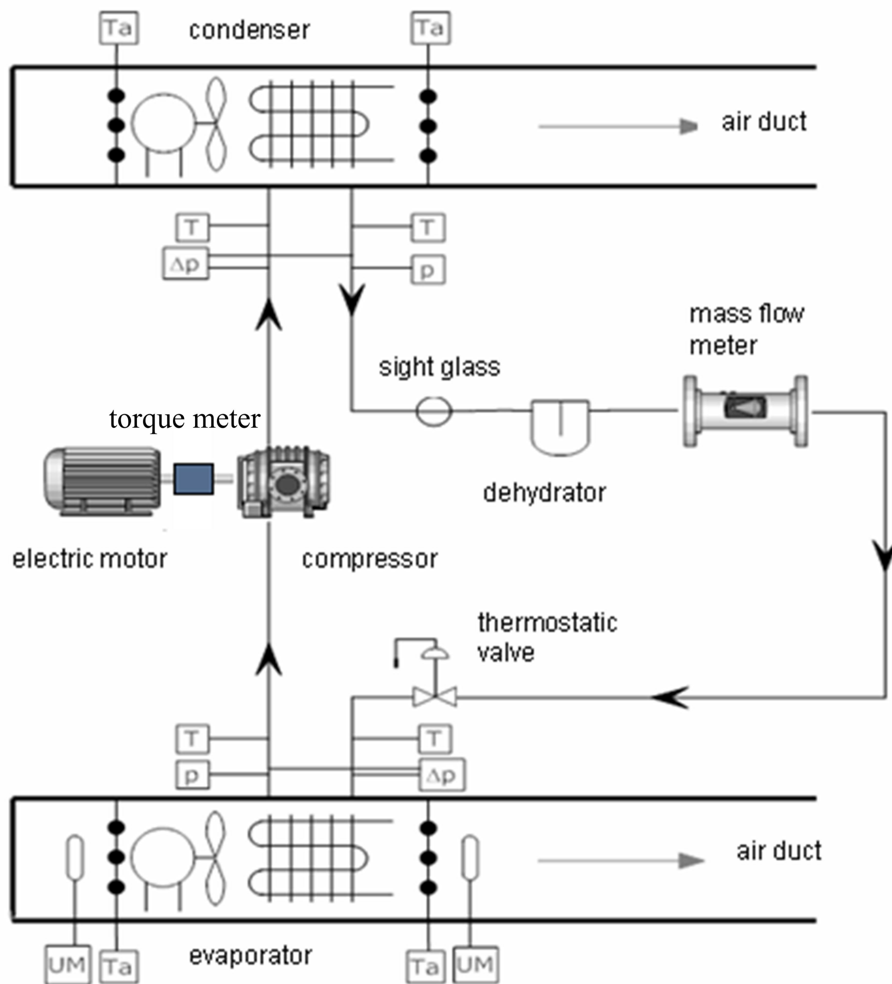

Fig. 6.2- Schematic of experimental apparatus

The inlet air temperatures to both the evaporator and the condenser are controlled using two closed-loop air circuits, whose ductwork configurations provide uniform temperature and velocity profiles at the inlet faces of the heat exchangers. The volumetric air flowrates are measured using ISA 1932 nozzles per ISO 5167-4:2003 to accuracies of ± 0.8 % of the measured values. A chiller supplies conditioned water to a cross-flow heat exchanger to maintain the condenser inlet air temperature to near the desired value. Then, a PID-controlled electric resistance heater located upstream from the condenser controls the inlet air temperature to the desired value. A separate, but similar, system controls the evaporator inlet dry-bulb air temperature to the desired value. An industrial vapor generator located sufficiently far upstream of the evaporator to ensure uniform conditions at the evaporator inlet face controls the relative humidity. A grid of nine evenly spaced type T thermocouples for the condenser and six for the evaporator are used to measure the mean inlet air temperature for the respective heat exchanger. The air downstream from each heat exchanger is well-mixed prior to its temperature being measured by separate grids of nine evenly spaced type T thermocouples. For both air circuits and for the refrigerant system, a PT-100 platinum resistance thermometer with an accuracy of ±0.02 °C was used to calibrate the temperature measuring system (consisting of thermocouple, electronic ice point and multimeter) to an accuracy of ± 0.05 °C. The relative humidity (RH) of the evaporator air circuit is measured in two ways: (1) using a capacity transducer with an accuracy of ± 3 % RH and (2) using a load cell that measures the amount of water condensed in a specified time with an accuracy of ± 0.5 g.

Type T thermocouples calibrated to ±0.05 °C measure the refrigerant temperature immediately before and after each major component. Diaphragm-type differential pressure transducers measure the pressure drop across both the evaporator and the condenser to accuracies of 0.1 kPa. Strain gauge pressure transducers measure the absolute pressures in the evaporator to ± 0.8 kPa and in the evaporator to ± 1.6 kPa.

The refrigerant enthalpies are determined from measured temperature and pressure values, where the refrigerant quantities are calculated using an improved version of the P-R EoS of Brown et al. (2009a,b). Note: the original P-R EoS predictions of Brown et al. are lower by -6 % to -4 % when compared to the saturation data of Di Nicola et al. (2009) over the temperature range from 220 to 360 K. These original predictions are based on the normal boiling point temperature and critical state property data of Spatz and Minor (2008). The predictions from the improved version of the P-R EoS used in this work are from -1 % lower to +1 % greater when compared to the saturation data of Di Nicola et al. (2009) over the temperature range from 220 to 360 K. This improved

version is based on using the normal boiling point temperature of Di Nicola et al. (2009) and the critical state property data of Tanaka and Higashi (2009).

A Coriolis flow meter located in the liquid line measures the refrigerant mass flow rate to an accuracy of ± 0.1 % of the measured value.

An asynchronous electric motor drives the compressor. An optical system measures the compressor speed to an accuracy of ± 0.01 % of the measured value and a torsiometer located on the shaft that couples the electric motor with the compressor measures the torque to an accuracy of ± 0.2 N-m. The expanded uncertainty on the mechanical power delivered to the refrigerant is less than 2 % for compressor speeds of 900 and 2500 RPM and less than 3 % for compressor speeds of 4000 RPM.

A desiccant-based drier and a sight glass are located between the condenser and the mass flow meter.

The total expanded uncertainties for the air-side heat transfer rate measurements are ± 1%. The total expanded uncertainties for the refrigerant-side heat transfer rate measurements are ± 4 % for the evaporator and ± % 3 for the condenser, with the largest contributor being the uncertainties in the thermodynamic property estimates calculated using a modified version of the P-R EoS of Brown et al. (2009b).

6.4 Test conditions

The system tested is a typical R-134a based compact European automobile, which had a nominal cooling capacity of 5.8 kW at a compressor volumetric flow rate of 7.8 m^3 h^{-1}. Five systems were tested: (i) the baseline R-134a system, (ii) the same system as *i* operating with an optimal charge of R-1234yf with the baseline TXV setting, (iii) the system of *ii* operating with a TXV setting optimized for R-1234yf, (iv) the system of *iii* operating with the variable displacement compressor control valve deactivated, and (v) the system of *iii* with the condenser replaced by one having 40 % more external surface area. While the operating conditions were not meant to exactly duplicate actual in-vehicle conditions, they were chosen to cover typical European conditions. In particular, they covered three compressor speeds, three ambient temperatures (the inlet air temperature of both the evaporator and the condenser), and two relative humidity values for the evaporator inlet air stream. The evaporator and condenser fan speeds (air mass flow rates) were held constant throughout the tests (while this is not the case in a real vehicle, it reduced the complexity of the test matrix while still allowing for a comparison of the performance potential of R-1234yf relative to R-134a). Table 6.1 provides the operating conditions. Note: data were collected for only four operating

conditions for case (v), i.e., the system with the condenser with the increased external surface area.

Tab. 6.1- Operating conditions

Test Conditions	1st set			2nd set			3rd set		
Evaporator air inlet	35 ºC & 40 % RH			25 ºC & 80 % RH			15 ºC & 80 % RH		
Evaporator air volumetric flow rate (m^3 h^{-1})	400 ± 3 %			400 ± 3 %			400 ± 3 %		
Condenser air inlet	35 ºC			25 ºC			15 ºC		
Condenser air volumetric flow rate (m^3 h^{-1})	1580 ± 3 %			1580 ± 3 %			1580 ± 3 %		
Compressor speed (rpm)	900	2500	4000	900	2500	4000	900	2500	4000

6.5 Results and discussion

More than 140 tests were run. In each case, the system was allowed to reach steady-state before data were collected. The energy balances on the airside and refrigerant side for both the evaporator and the condenser differed by a maximum of 5 %.

Figures 6.3 – 6.8 show the evaporator refrigerant inlet temperatures, the evaporator refrigerant outlet temperatures (or compressor suction temperatures), the compressor discharge temperatures, the condenser subcooling values, the refrigerant mass flow rates, and the compressor powers, respectively, for the five systems described in the previous section. Then, Figure 6.9 compares the cooling capacities and Figure 6.10 compares the COPs for the same systems. Note: Figures 6.3-6.6 are shown in dimensional terms; whereas, Figures 6.7-6.10 are shown in relative terms (i.e., the particular system is compared to the baseline R-134a system). In particular, in the figures, the variable $\varepsilon = \left(\frac{Y_{R\text{-}134a} - Y_{R\text{-}1234yf}}{Y_{R\text{-}134a}} \right) \text{x}\,100$, where Y represents refrigerant mass flow rate, compressor power, cooling capacity, and COP. In the next paragraphs, the figures will be discussed in more detail.

Figure 6.3 shows that the evaporator refrigerant inlet temperatures for the four R-1234yf systems, excluding the one with the compressor control valve deactivated, are some 1.5 ºC to 3.5 ºC lower than the baseline R-134a system; whereas, the system with the compressor control valve deactivated has temperatures that are more or less equal to approximately 1 ºC lower than the baseline R-134a system for higher ambient temperatures and has values that are some 2 ºC to 2.5 ºC lower for the lowest ambient temperature. Given the generally lower R-1234yf evaporator saturation temperatures, if all else were to be equal, one would expect the COPs for the R-1234yf systems to be lower than the baseline R-134a system, except for the R-1234yf systems with the deactivated compressor control valve at the higher ambient temperatures.

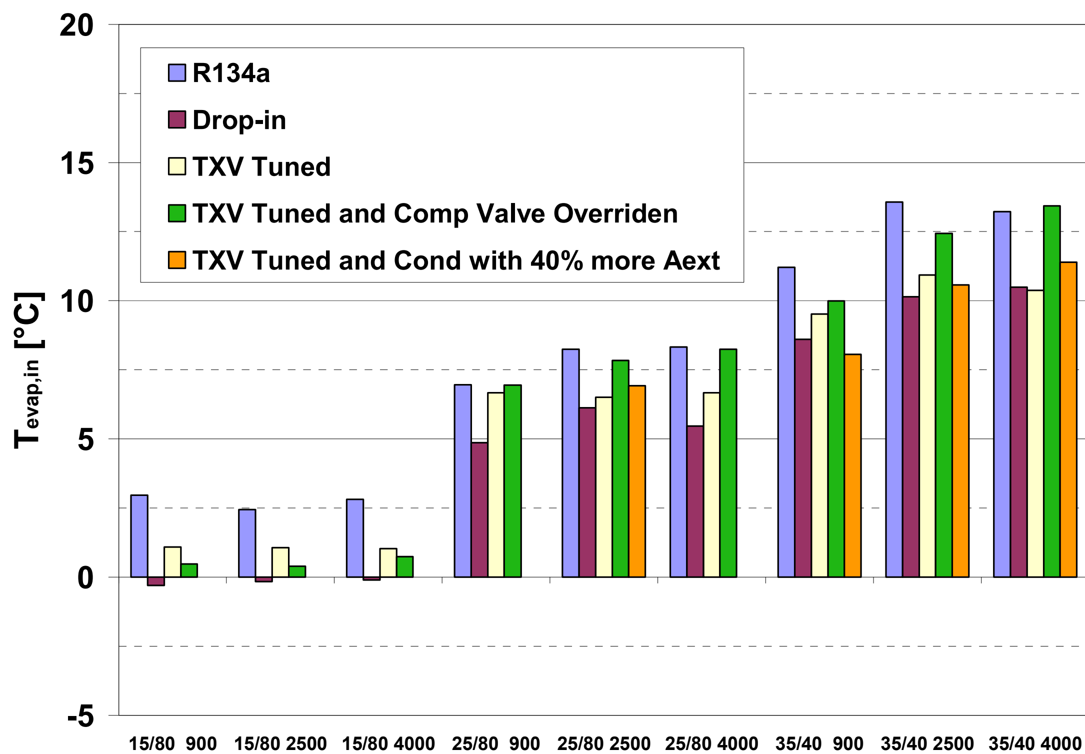

Fig. 6.3- Evaporator refrigerant inlet temperatures. Note: for a given label along the abscissa, the first number is the ambient temperature in ºC, the second number is the relative humidity in percent, and the third number is the compressor speed in RPM.

Figure 6.4 shows that the evaporator refrigerant outlet temperatures for the R-1234yf systems are similar to the baseline R-134a system, except for the lowest ambient temperatures for the systems with a tuned TXV, where the temperatures are roughly 1 ºC to 2.5 ºC lower for the R-1234yf systems, and for the higher compressor speeds at an ambient temperature of 35 ºC, where the temperatures are roughly 2 ºC to 4 ºC higher for the R-1234yf systems, except for the system with the modified condenser, which has similar values to the baseline R-134a system.

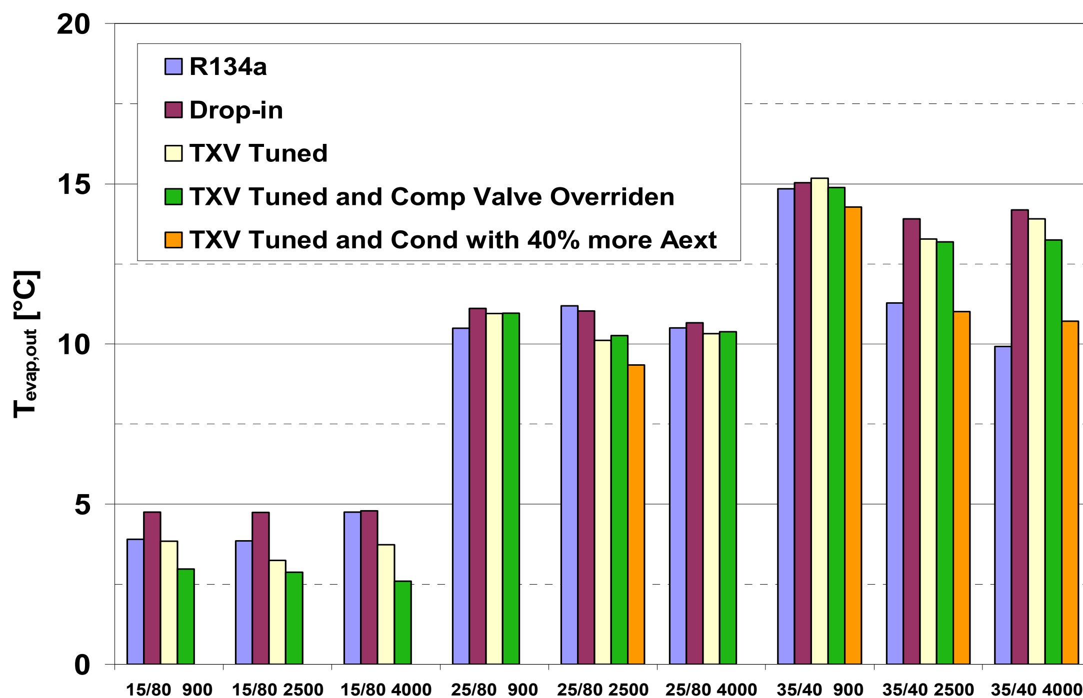

Fig. 6.4- Evaporator refrigerant outlet temperatures. Note: for a given label along the abscissa, the first number is the ambient temperature in ºC, the second number is the relative humidity in percent, and the third number is the compressor speed in RPM.

Figure 6.5 shows that the compressor discharge temperatures for the R-1234yf systems when compared to the baseline R-134a system are roughly 1 ºC to 5 ºC higher at the lowest ambient temperature, 3 ºC to 10 ºC lower for the medium ambient temperature and for the higher ambient temperature for the lowest compressor speed, and 10 ºC to 20 ºC lower for the higher ambient temperature for higher compressor speeds. The reduction in the compressor discharge temperature for the R-1234yf systems operating at higher ambient temperatures, particularly at higher compressor speeds, should lead to longer lifetimes for the R-1234yf compressors when compared to the R-134a compressors.

Figure 6.6 shows that the subcooling values for the R-1234yf condensers compared to the baseline R-134a system are approximately 5 ºC to 9 ºC higher for the lowest ambient temperature, 2 ºC higher for the medium ambient temperature, excluding the system with the modified condenser, and 1 ºC to 3 ºC higher for the highest ambient temperature, again excluding the system with the modified condenser. For the systems with the modified condensers, the subcooling values for the R-1234y systems are approximately 7 ºC to 12 ºC higher than the baseline R-134a system. Achieving larger subcooling values is more important for R-1234yf than for R-134a since the throttling losses are larger for R-1234yf due to the shallower slope of its saturated liquid line on a temperature-entropy state diagram. Another way of

expressing this observation would be that an R-1234yf would benefit more than R-134a from the use of a liquid-line/suction-line heat exchanger (Zilio et al., (2009).

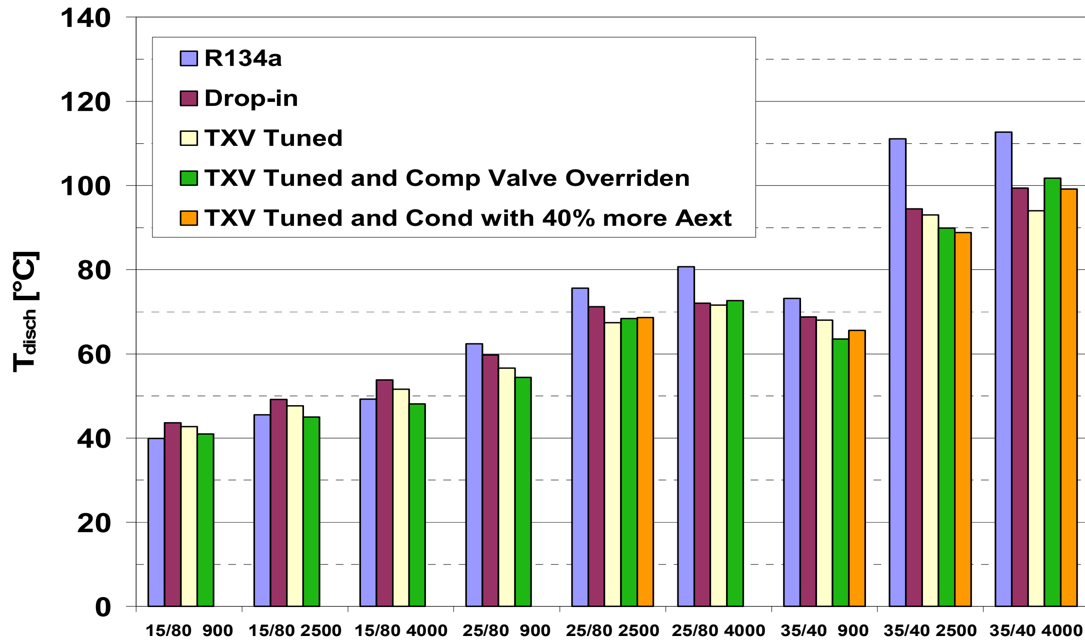

Fig. 6.5- Compressor discharge temperatures. Note: for a given label along the abscissa, the first number is the ambient temperature in ºC, the second number is the relative humidity in percent, and the third number is the compressor speed in RPM.

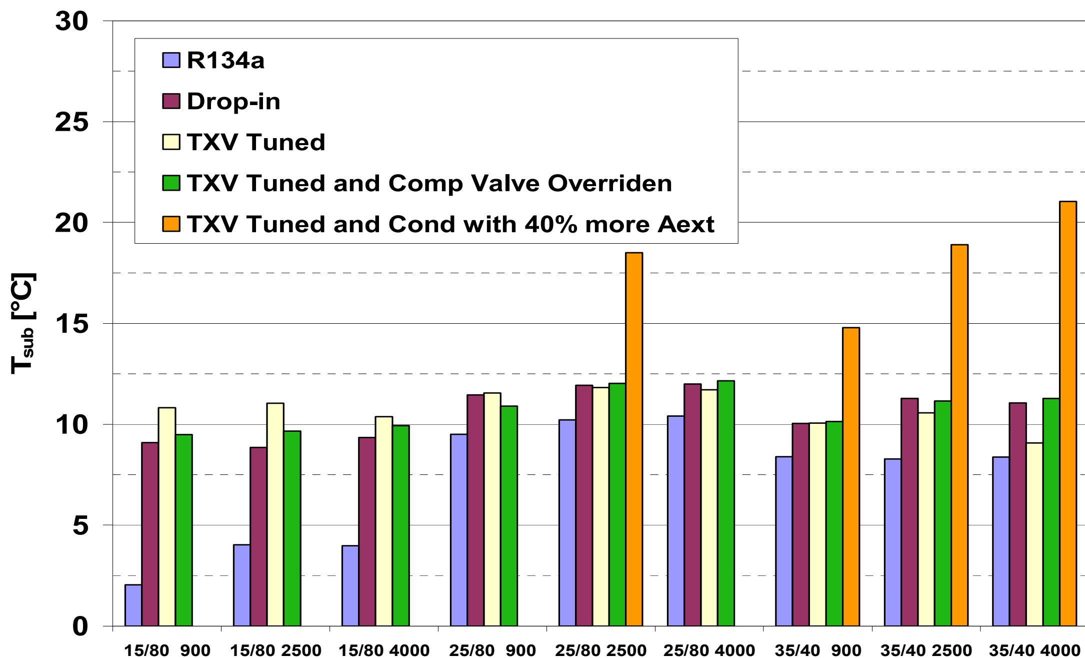

Fig. 6.6- Condenser subcooling values. Note: for a given label along the abscissa, the first number is the ambient temperature in ºC, the second number is the relative humidity in percent, and the third number is the compressor speed in RPM.

Figure 6.7 shows that the refrigerant mass flow rates for the “drop-in” R-1234yf systems are approximately 10 % to 20 % lower than for the baseline R-134a system, except for three of the operating conditions. The reduction in the mass flow rate is due to the lower compressor suction density for R-1234yf (Zilio et al., 2009). Simply tuning the TXV, however, increases the R-1234yf mass flow rates to being 10 % to 30 % higher than the baseline R-134a system, except for higher ambient temperatures and compressor speeds where the R-1234yf values still remain some 5 % to 15 % lower than the baseline R-134a value. If in addition to tuning the TXV, the compressor control valve is deactivated, the R-1234yf mass flow rates significantly increase to being approximately 40 % to 50 % higher than the baseline R-134a values at the lowest ambient temperature, 20 % to 25 % higher at the medium ambient temperature, and 5 % to 15 % higher at the highest ambient temperature. Finally, while there are only four data points for the system with the improved condenser, its mass flow rate values are similar to the systems with the compressor control valve deactivated.

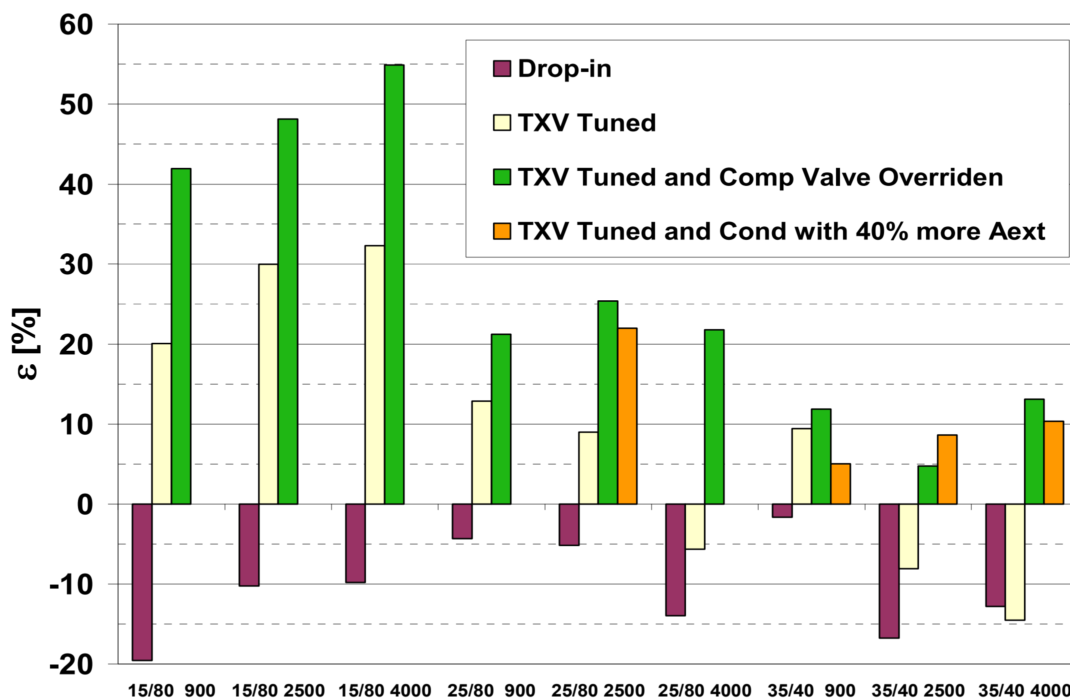

Fig. 6.7- Relative refrigerant mass flow rates. Note: for a given label along the abscissa, the first number is the ambient temperature in ºC, the second number is the relative humidity in percent, and the third number is the compressor speed in RPM.

Figure 6.8 shows the compressor powers for the “drop-in” R-1234yf systems are approximately 4 % to 15 % higher than the baseline R-134a system for the lowest ambient temperature, 2 % to 16 % higher for the medium ambient temperature, and 4 % to 23 % higher for the highest ambient temperature. The compressor powers for the TXV tuned R-1234yf systems are approximately 18 % to 30 % higher than the baseline

R-134a system for the lowest ambient temperature, 2 % higher to 11 % lower for the medium ambient temperature, and 2 % to 26 % lower for the highest ambient temperature. The compressor powers for the R-1234yf systems with the compressor valve deactivated are approximately 28 % to 34 % higher than the baseline R-134a system for the lowest ambient temperature, 2 % to 18 % higher for the medium ambient temperature, and 2 % higher to 6 % lower for the highest ambient temperature. While there are few data for the system with the enhanced condenser and they are available only for the higher ambient temperatures, the compressor powers are approximately 1 % to 7 % higher than the baseline R-134a system, except for the medium ambient temperature where the compressor power is some 15 % lower than the baseline R-134a system.

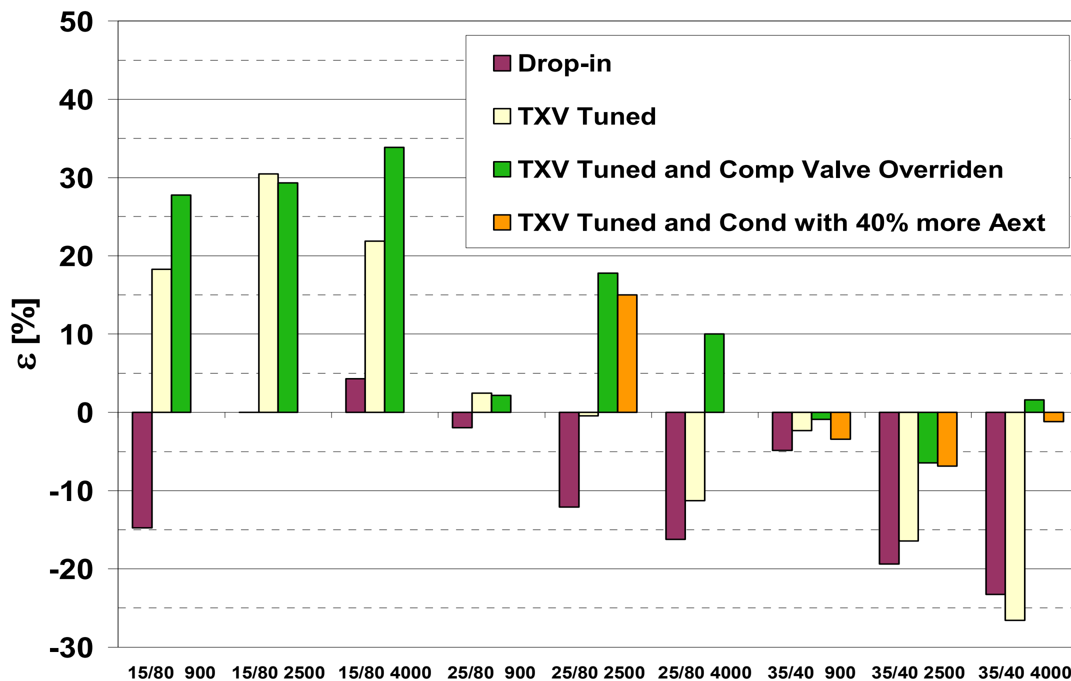

Fig. 6.8- Relative compressor powers. Note: for a given label along the abscissa, the first number is the ambient temperature in ºC, the second number is the relative humidity in percent, and the third number is the compressor speed in RPM.

Figure 6.9 shows the cooling capacities for the "drop-in" R-1234yf systems are approximately 20 % to 30 % lower than the baseline R-134a system for all ambient temperatures. The cooling capacity of R-1234yf, however, can be improved by simply tuning the TXV. After doing so, the cooling capacities are some 2 % to 9 % higher than the baseline R-134a system for the lowest ambient temperature and some 10 % to 25 % lower for the higher ambient temperatures. If in addition to tuning the TXV, the compressor control valve is deactivated the cooling capacities improve again to being some 19 % to 25 % higher for the lowest ambient temperature, some 1 % to 2 % lower

for the medium ambient temperature and some 10 % to 15 % lower for the highest ambient temperature. While there are few data for the system with the enhanced condenser and they are available only for the higher ambient temperatures, the cooling capacities are approximately 2 % higher to 4 % lower than the baseline R-134a system, except for the highest ambient temperature at the lowest compressor speed where the cooling capacity is some 11 % lower than the baseline R-134a system.
Figure 6.10 shows that the COPs for the "drop-in" R-1234yf systems are approximately 10 % to 25 % lower than the baseline R-134a system for all ambient temperatures. Tuning the TXV improves the R-1234yf systems to being approximately 10 % to 17 % lower than the baseline R-134a system for all ambient temperatures. If in addition to tuning the TXV, the compressor control valve is deactivated, the COPs of the R-1234yf systems improve again to being approximately 5 % to 7 % lower for the lowest ambient temperature, 3 % to 15 % lower for the medium ambient temperature, and 8 % to 11 % lower for the highest ambient temperature. While there are few data for the system with the enhanced condenser and they are available only for the higher ambient temperatures, the COPs are approximately 5 % higher to 10 % lower than the baseline R-134a system.

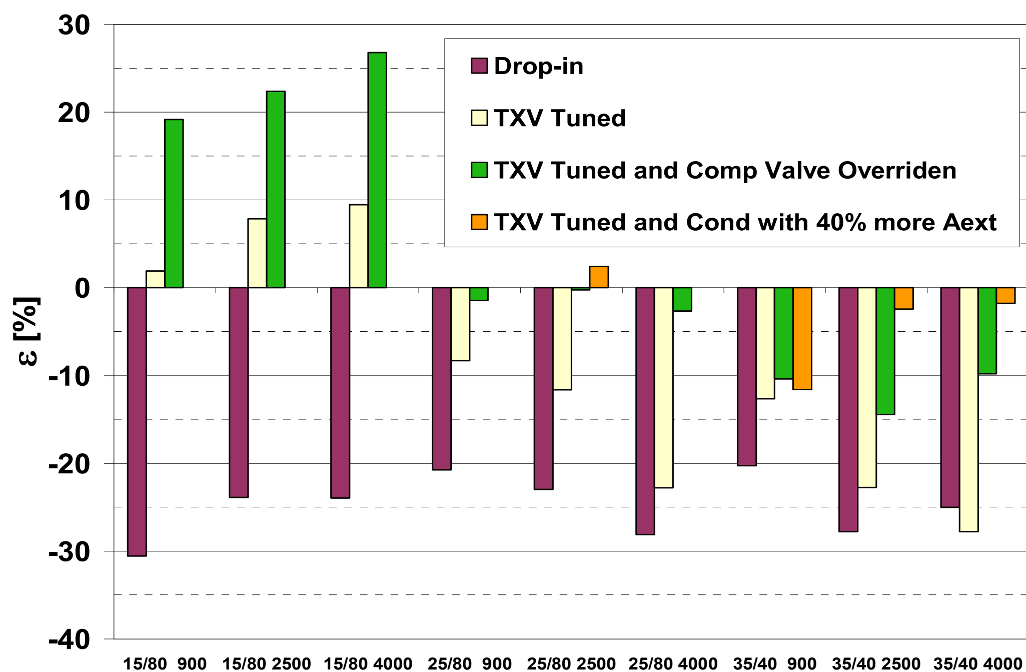

Fig. 6.9- Relative cooling capacities. Note: for a given label along the abscissa, the first number is the ambient temperature in ºC, the second number is the relative humidity in percent, and the third number is the compressor speed in RPM.

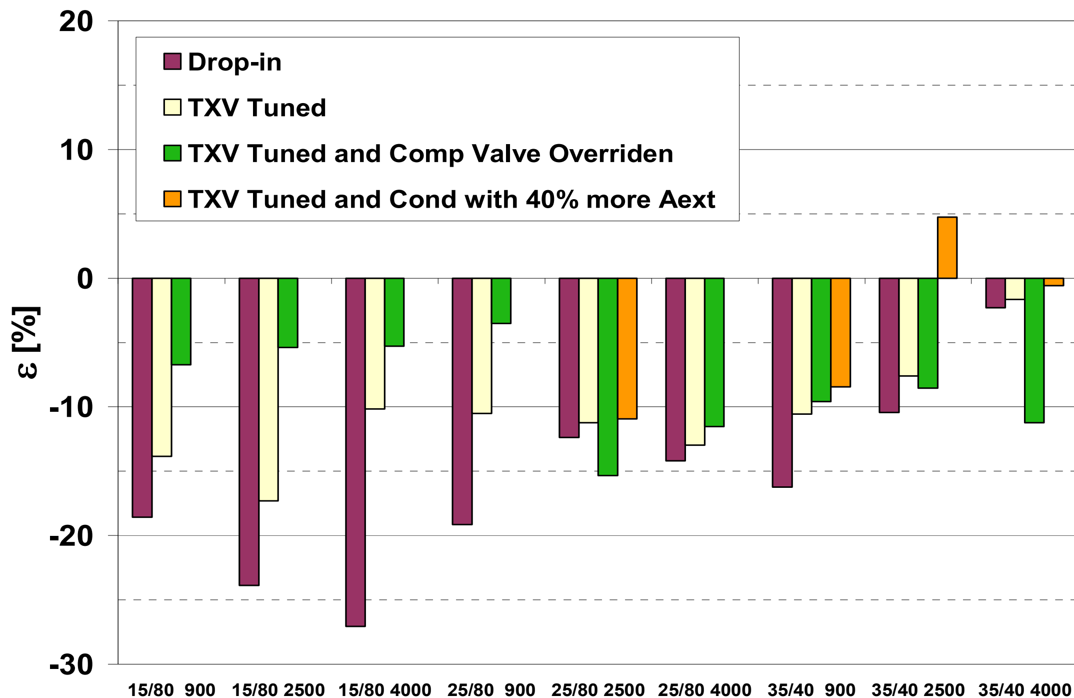

Figure 6.10- Relative COPs. Note: for a given label along the abscissa, the first number is the ambient temperature in ºC, the second number is the relative humidity in percent, and the third number is the compressor speed in RPM.

In conclusion, the cooling capacity and COP of the "drop-in" R-1234yf system are considerably lower than the baseline R-134a system. However, their values can be improved significantly, even approaching or for some operating conditions exceeding, the baseline R-134a values with some simple hardware modifications: (1) tuning the TXV setting for R-1234yf and (2) optimizing the variable displacement compressor control valve. The performance can be improved further by using an enhanced condenser with additional external surface area. Furthermore, the condenser refrigerant circuitry could be optimized to improve the R-1234yf performance (Zilio et al., 2009) and, although not explicitly a part of this study, both R-134a and R-1234yf systems would benefit from the use of a liquid-line/suction-line heat exchanger; however, R-1234yf would benefit somewhat more from its use than would R-134a because of the larger throttling losses for R-1234yf (Zilio et al., 2009).

Therefore, the results and analyses presented in this work demonstrate the attractiveness of pursuing R-1234yf as a potential replacement for R-134a.

CONCLUSIONS

In the present work, several promising thermal control techniques were presented, with the perspective of eventual use in the aeronautics industry. Furthermore, an extensive review of fluids as possible candidates both in single phase and two phase flow in electronics cooling systems has been undertaken.

Cold plate heat exchangers have been carefully analyzed through the use of a custom developed numerical code, in order to evaluate thermal behavior and performance. This analysis has allowed for the evaluation of a particular case of chip cooling, examining the geometrical characteristic a mini channel cold plate has to have in order to meet thermal control requirements, when using a laminar single phase flow (to keep pressure drops and pumping power low). First, the geometric design was optimized for a cold plate using water as the coolant fluid, while afterwards some indications, based on the first cold plate designed, are illustrated to approximately set the geometrical parameters for a cold plate using any single phase fluid. Subsequent simulations carried out on cold plates designed using such indications confirmed the effectiveness of this method, but they also pointed out that careful design is needed to thoroughly meet the thermal requirements, as in several cases the cold plate performance was lower than the one predicted by the numerical code. Such difference is partially due to the heat transfer surface effectiveness: while in the cold plate whose channel side walls are short and thick, the temperature profile over their surfaces is nearly linear, from base plate to cover plate, in the fins with significant ratio between height and thickness, and particularly when the flow is characterized by high heat transfer coefficients, the temperature profile is to be carefully calculated to allow a correct evaluation of the heat exchanger performance, giving reason for the use of finite element technique.

Finally, relating to several laboratory tests carried out for an air conditioning system both with R134a and R1234yf, experimental results are proposed. The comparison between the performance of the two cases is illustrated in detail, as R1234yf is the candidate fluid proposed to substitute R134a in applications subjected to limitations on the GWP of the fluid employed. At present, R1234yf is expected to be used only in automotive air conditioning systems, but the need for synergies between industries and the possible use of refrigerating vapor compression systems, claim for deep analysis of systems using R1234yf, together with the prediction of its thermophysical properties in order to allow a proper comprehension of the experimental measurements. For the case examined, a simple drop-in does not allow to attain the

same performance of the R134a system, anyway better results are possible by correctly setting the throttling device and properly designing the heat exchangers, confirming R1234yf as a suitable fluid for cooling applications, even if further tests need to be carried out for high evaporation temperature applications.

APPENDIX

A1 - Heat transfer through fins in a fin-and-tube gas-cooler

Introduction

According to the necessity of decreasing greenhouse effect, as pointed out in chapter 6, new fluids need to be investigated as refrigerants. Carbon dioxide is one of the fluids candidate as substitute for high GWP refrigerants, because of its environmental friendliness, and some excellent thermodynamic and transport properties, such as high specific heat, high thermal conductivity and low viscosity. When considering a CO_2 transcritical cycles, the gas cooling process needs to be investigated taking into account two points of view: the great variation of thermophysical properties and the large decrease in temperature occurring along the heat exchanger.

In the present work a set of tests was conducted and experimental results were compared with numerical predictions obtained trough a finite volume simulation software. Although simulation results gained by our software has been found to be in agreement with experimental results for a large number of refrigerants and test conditions, a systematic deviation was seen using CO_2, and the heat conduction along the heat exchanger, which has not been considered by above mentioned software, was deemed to be the most important cause of the disagreement in results. Actually, very poor evidence is given to this problem by papers available in the open literature. Furthermore, it seems to be relevant just to finned coil heat exchangers, since it was shown to be not important in microchannel heat exchangers (Asinari et al, 2004).

Test rig description and uncertainty analysis

The CO_2 circuit (Fig. A1.1) carries out a double compression with gas intercooling between the two compression stages and single throttling, and it is equipped with an internal heat exchanger. The compressor is a two-stage semi-hermetic reciprocating unit running at 1450 rpm (50 Hz). The nominal volumetric flow rate of the low pressure stage (one cylinder) is 3.0 m^3/h, while of the second stage is 1.74 m^3/h (vol. ratio 1.7). The lubricant is a PAG oil 46 ISO grade.

The compressor power input is recorded with an electronic transducer (with an accuracy ±0.5 % of the reading value).

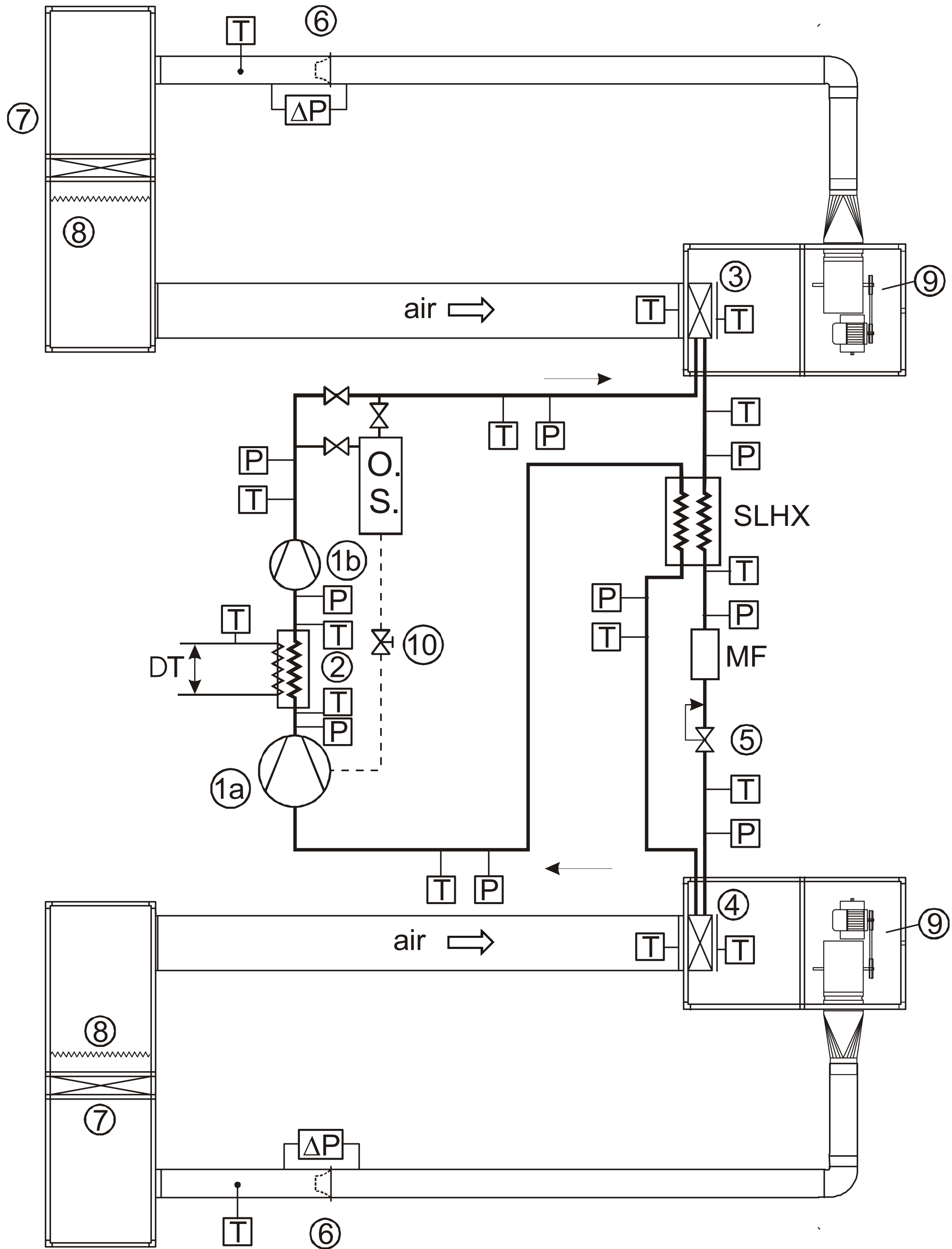

Fig. A1.1- Test rig lay-out. 1a,b two-stage compressor, 2 intercooler, 3 gas-cooler, 4 evaporator, 5 back-pressure valve, 6 nozzle, 7 auxiliary finned coil, 8 electrical heater, 9 centrifugal fan, 10 metering valve, MF Coriolis mass flow meter, OS oil separator, SLHX suction line heat exchanger, P pressure transducer, T thermocouple, ΔT thermopile

The intercooler (IC) heat flow is rejected to a water-loop. The cooling water inlet temperature and flow rate are controlled through an auxiliary circuit (temperature stability ±0.05°C). The IC is a copper tube-in-tube heat exchanger with the CO_2 flowing inside three pipes (ID 4 mm, OD 6 mm) fed in parallel and inserted into a 20 mm ID (22 mm OD) copper tube. The water flows inside the outer tube in counter-current to the CO_2. The IC was designed for 1°C temperature approach between the two fluids. The water volumetric flow rate is measured with an electromagnetic flow-meter (accuracy ±0.2 % of the reading value).

The internal heat exchanger used is a copper-steel 10 m long tube-in-tube heat exchanger with the high pressure fluid flowing inside three pipes (ID 6 mm, OD 8 mm) fed in parallel and inserted into a 21 mm ID (26.7 mm OD) steel tube. The low pressure CO_2 flows inside the outer tube in counter-current to the high pressure CO_2. The internal heat exchanger was designed for 2°C temperature approach between the two fluids. The throttling device used in the tests is a back-pressure valve: this allows the operator to set and keep constant the gas-cooler (GC) outlet pressure.

The CO_2 circuit is equipped with an oil separator. A special accumulator with sight glasses is inserted for visual inspection of the oil returning to the compressor crankcase. A metering valve is also installed to control the lubricant level in the compressor and to avoid any hot gas by-pass through the oil drainage.

Air is the external fluid for both the gas-cooler and the evaporator. For the tests here reported finned coils with round copper tubes (8.22 mm ID and 9.52 mm OD) are employed. The aluminium fins are louvered with 2.1 mm fin spacing. The face area for both exchangers is 500x500 mm. Air temperature at the inlet of each heat exchanger is controlled by way of two separated closed-loop wind tunnels. The air ducts lay-out was designed through CFD simulation targeted at getting very uniform velocity and temperature distribution over the entire heat exchanger face area. The centrifugal fans are equipped with inverter to adjust the volumetric flow rate that is measured with ISA 1932, AISI 316L nozzles with pressure taps integrated in the nozzle body. The nozzles were installed according to EN-ISO Standard 5167. Air pressure drop through the nozzles is measured by a strain gauge pressure transducer, with an accuracy of ±1 Pa while air temperature downstream the nozzles is recorded with a thermocouple. In this way, according to EN-ISO Standard 5167, the estimated accuracy in volumetric flow rate $\dot{V}$ measurement is ± 0.8 % of reading.

The air in the closed loop serving the GC is re-conditioned by a cooling finned coil fed with water kept at an inlet constant temperature in an auxiliary circuit equipped with a commercial chiller and control system. The air inlet temperature to the GC is then kept at the desired value by electrical heaters, PID controlled. Another PID feedback loop is

used to control the air dry bulb temperature at the evaporator inlet by compensating the CO_2 system cooling power with electrical heating. The air temperature stability thus achieved in steady-state conditions was ±0.05°C. Nine thermocouples are placed, evenly distributed, just before the GC inlet. Since the large temperature change of the CO_2 through the gas cooling process leads to a scattered distribution of the air temperature accross the outlet section (depending on the CO_2 pipe arrangement in the finned coil), an air mixer is placed after the GC and the air temperature is measured again by nine thermocouples placed after the air mixer. The same thermocouple arrangement was used for the evaporator.

CO_2 temperatures are measured with thermocouples placed inside mixing chambers at the inlet and outlet of each heat exchanger. A thermocouple is also placed at the IC water inlet, whereas the water temperature change across the IC is measured with a four junctions type T thermopile.

All the thermocouples for air and CO_2 are T type: the complete measuring chain, including multimeter and the ±0.01°C reference ice point was calibrated against a ±0.02°C accuracy Pt100 thermometer. Thus a ±0.05°C accuracy is estimated for all the temperature measurements.

R744 pressures are recorded with strain-gauge transducers at the outlet of each heat exchanger and inside the compressor 2nd-stage (high pressure) suction chamber. The accuracy is ±1 kPa for evaporator and compressor chamber pressures and ±2 kPa for gas-cooler pressures, according to the calibration report from the manufacturer. Differential pressure transducers were used for pressure drop recording across GC, evaporator and IC (accuracy ±400 Pa).

CO_2 mass flow rate is measured by a Coriolis mass flow meter placed upstream of the throttling valve. The claimed accuracy is ±0.1 % of reading. IC water volumetric flow rate was measured by an electromagnetic meter (accuracy ±0.2 % of reading).

All the measurements are real time acquired and elaborated. The particular lay-out of the air tunnels and the accuracy of the instruments led to a heat balance error for each component and for the complete system lower than ±1 %.

According to Moffat (1988), a “single sample uncertainty analysis” was considered for the air velocity u and for the heat flux q.

In general, the uncertainty in a variable “y” depending on “N” independent variables (x_i) with uncertainties “δx_i”, is estimated through eq. 1:

$$\delta y = \left[\sum_{i=1}^{N} \left(\frac{\partial y}{\partial x_i} \delta x_i \right)^2 \right]^{0.5} \tag{A1.1}$$

In particular, being

$$u = \dot{V} / S \tag{A1.2}$$

where $\dot{V}$ is the volumetric flow rate and S is the frontal area, it is

$$\delta u = \left[\left(\frac{1}{S} \delta \dot{V} \right)^2 + \left(- \frac{\dot{V}}{S^2} \delta S \right)^2 \right]^{0.5} \tag{A1.3}$$

Regarding the heat flux q, air side, it is

$$q = \rho \dot{V} c_p \left(t_{air,out} - t_{air,in} \right) \tag{A1.4}$$

Since a gas-cooling application is considered, air can be treated as dry air (no dehumidification) so the air density ρ is evaluated through the following ideal gas relationship (ASHRAE, 2001):

$$\rho = \frac{p}{0.2871(t + 273.15)} \tag{A1.5}$$

Furthermore, a constant value for the specific heat capacity c_p = 1006 J kg-1 K-1 was considered.

So it comes out that:

$$\delta\rho = \left[\left(\frac{1}{0.2871(t+273.15)} \delta p \right)^2 + \left(- \frac{0.2871 p}{\left(0.2871(t+273.15)\right)^2} \delta t \right)^2 \right]^{0.5} \tag{A1.6}$$

and therefore,

$$\delta q = \left[\left(\dot{V} c_p \left(t_{air,out} - t_{air,in} \right) \delta\rho \right)^2 + \left(\rho c_p \left(t_{air,out} - t_{air,in} \right) \delta \dot{V} \right)^2 + \left(\sqrt{2} \rho \dot{V} c_p \delta t \right)^2 \right]^{0.5} \tag{A1.7}$$

The “single point” estimated uncertainties are listed in Tables A1.1 and A1.2.

The heat flux, CO_2 side, can be expressed as follows:

$$q_{CO_2} = \dot{m}_{CO_2} \left(i_{CO_2,out} - i_{CO_2,in} \right) \tag{A1.8}$$

By using equation (A1.1), the related uncertainty is:

$$\delta q_{CO_2} = \left[\left(\left(i_{CO_2,out} - i_{CO_2,in} \right) \delta \dot{m}_{CO_2} \right)^2 + \left(\dot{m}_{CO_2} \delta \left(i_{CO_2,out} - i_{CO_2,in} \right) \right)^2 \right]^{0.5} \tag{A1.9}$$

As already mentioned, a Coriolis mass flow meter with 0.1% of the reading accuracy is used for $\dot{m}_{CO_2}$. REFPROP v. 8.0 (NIST, 2007) is used for enthalpy calculations. It is well known that

$$i_{CO_2} = f(p, t) \tag{A1.10}$$

so, in general enthalpy calculation uncertainty is affected by:

- Temperature measurement accuracy;
- Pressure measurement accuracy;
- Accuracy of the enthalpy calculation approach used for equation (A1.10).

The evaluation of the last contribution is outside the purpose of this work: reference should be made to Span and Wagner (1996) data, since REFPROP v.8.0 modelling is based on the Span and Wagner measurements for the implementation of the Helmholtz approach to equation (A1.10). In the present work only the effects of T and p accuracy on δi are kept into account. According to Moffat (1998), a “sequential perturbation” method is applied by using the REFPROP code. Considering a temperature measurement accuracy of ± 0.05°C and a pressure measurement accuracy of ±2 kPa, the estimated accuracy for the CO_2 side heat flow rate is reported in Table A1.2. The reader may appreciate that the difference between air side and CO_2 side heat fluxes is always below 1% of the air side heat flux.

The simulation model for the finned coil

The heat transfer analysis has been applied to the case of a finned coil gas-cooler, by developing a dedicated simulation model. Since the flow configuration of a finned coil does not conform to the elementary and well known parallel or counter flow patterns, the heat transfer area is subdivided into a three-dimensional array of cells that conforms to the true flow pattern of the air and of the refrigerant streams. Each tube is divided into cells and the total volume, in the form of a parallelepiped, is subdivided into individual nodes, each including a small stretch of tube and the related fins.

The numerical approach to the definition of the circuits is accomplished by means of two arrays, one for the refrigerant [PR(N)] and one for the air [PA(N)]. Each element of the PR vector (Preceding Refrigerant) indicates the index of node preceding the N-node, along the refrigerant flow.

As described for the refrigerant, the PA(N) value (preceding air) represents the air-side node preceding the N-node according to the air flow direction.

This simple approach allows a finned coil to be solved regardless of how complicated is the lay-out of the tube circuits. For thermal performance determination, the refrigerant temperature and pressure at the gas cooler outlet are calculated by an iterative procedure, being known the air flow rate, its inlet temperature as well as the refrigerant pressure, temperature and flow rate at the gas cooler inlet. The well known method of the secant is employed.

The refrigerant and air-side heat transfer coefficients are also input parameters in the program. The model can deal with carbon dioxide in transcritical conditions; in this case the heat transfer coefficient is calculated from equations described in literature, such as Gnielinski's equation (1976), Pitla et al. equation (2002) and also Dang and Hihara's equation (2004).

The friction factor is calculated by the Colebrook-White's equation, while pressure drops in the curves are locally accounted for by adding an equivalent tube length equal to 50 times the tube diameter.

The air side heat transfer coefficient, including surface efficiency was evaluated experimentally, by feeding the coils with a water flow at temperature higher than ambient air temperature. An overall heat transfer coefficient U was evaluated from equation (A1.11), being q the measured heat flux, A_0 the external heat transfer area and ΔT_{lm} the counter- current logarithmic mean temperature difference. U is defined by equation (A1.12):

$$q = UA_0 \Delta T_{lm} \tag{A1.11}$$

$$\frac{1}{U} = \frac{A_0}{A_1}\frac{1}{\alpha_i} + \frac{A_0}{A_1}\frac{r_i}{k}\ln(r_0 / r_i) + \frac{1}{\eta_0}\frac{1}{\alpha_0} \tag{A1.12}$$

(r radius, α heat transfer coefficient, η finned surface efficiency, k tube thermal conductivity, ans the subscripts i: internal, o: external). α_i was evaluated with the Gnielinski equation, so it was possible to obtain $\eta_o\alpha_o$ from equation (A1.12).

It's worth noting that, the investigated finned coils display four passes tube side, with air flowing in cross flow. According to Kays and London (1998) the efficiency of this configuration is almost identical to pure counterflow configuration. The consistency of the $\eta_o\alpha_o$ experimental values obtained through equations (A1.11) and (A1.12) was evaluated by comparison with the $(\eta_o\alpha_o)_{calc}$ values calculated according to Wang et al. (1999) model. All the experimental values were predicted by Wang et al. (1999) model within ±10% (deviation defined as $100 \cdot [(\eta_o\alpha_o)_{exp} - (\eta_o\alpha_o)_{calc}] / (\eta_o\alpha_o)_{calc}$).

The thermodynamic and thermophysical properties of R744 in the calculations are obtained from the database REFPROP 8.0 by NIST (2007).

A more detailed description of the simulation model is provided in (Casson et al., 2002).

Gas cooler description

Three different devices were tested, marked as "A", "B" and "C". The main characteristics of the three finned coils are listed in Table A1.3.

Tab. A1.3- Specifications of the heat exchangers

Heat exchanger		Gas-cooler	Row pitch	[mm]	19
Type		Finned coil	Geometry		staggered tubes
Dimension (W x H)	[mm]	500 x 500	Fin pitch	[mm]	2.1
Number of circuits		2	Fin thickness	[mm]	0.1
Number of tubes per row		20	Fin type		louver aluminium (Fig. A1.4)
Number of rows		4			
Refrigerant path		vertical, counter-current	Tube outside diameter	[mm]	9.52
			Tube thickness	[mm]	0.65
Tube pitch	[mm]	25	Tube type		Smooth

"A" and "B", as depicted in Fig. A1.2, are identical but for the fins. Referring to Fig. A1.4, in coil "B", the fins insisting on adjacent tube rows are separated (cut) along line DE. This expedient contributes in reducing heat conduction between adjacent tube rows. Coil "C" presents the same fin arrangement as for coil "B", with different tubes lay-out, as in Fig A1.3. A simple scheme of the fin type used is given in Fig. A1.4.

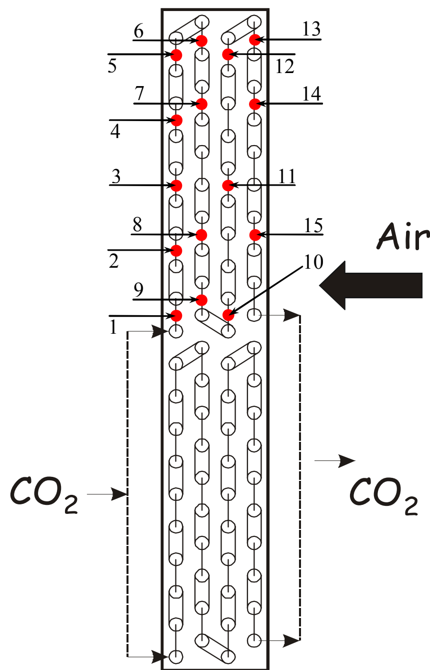

Fig. A1.2- Coils A and B (numbered points indicate thermocouples position)

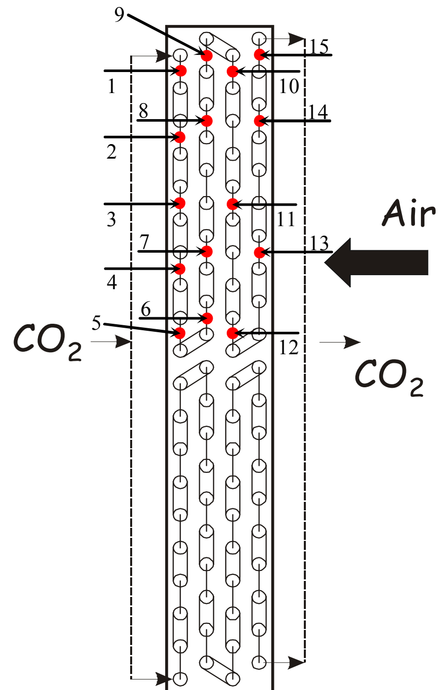

Fig. A1.3- Coil C (numbered points indicate thermocouples position)

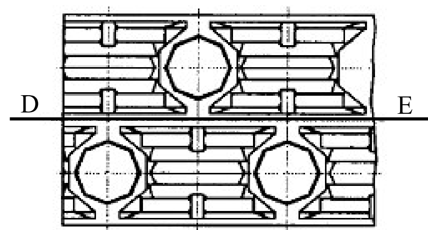

Fig. A1.4- Simple scheme of the investigated fin type

Comparison between numerical and experimental results

The gas-cooler "A" performance was compared with "B" and "C" at several operating conditions. In this work three different working pressure are analysed from 7.9 MPa up to 9.1 MPa. The mentioned pressure range was considered particularly meaningful because in these working conditions the R744 Prandtl number is recognized to undergo the most "dramatic" variation. The test conditions to evaluate the gas-cooler performance are listed in Table A1.1.

Tab. A1.1- Test conditions

Test	CO_2 inlet pressure	CO_2 inlet temperature [°C]	CO_2 mass flow rate [kg/h]	Air inlet temperature [°C]	Air inlet velocity [m/s]
1	7.911±0.002	87.0±0.05	169.0±0.2	20.3±0.05	1.59±0.01
2	8.599±0.002	97.6±0.05	167.1±0.2	21.5±0.05	1.59±0.01
3	9.102±0.002	107.8±0.05	166.4±0.2	23.0±0.05	1.61±0.01

Three sets of tests were conducted at the mentioned conditions, and the experimental results obtained are summarized in Table A1.2.

Tab. A1.2- Experimental results

Finned coil	Test	CO_2 outlet temperature [°C]	Air outlet temperature [°C]	Approach [°C]	Heat flow rate (CO_2 side) [kW]	Heat flow rate (Air side) [kW]
A	1	33.0±0.05	39.5±0.05	12.7±0.05	9.0±0.05	9.0±0.1
	2	33.1±0.05	42.7±0.05	11.6±0.05	10.1±0.06	10.2±0.1
	3	33.1±0.05	45.1±0.05	10.1±0.05	10.9±0.06	10.8±0.1
B	1	32.1±0.05	40.6±0.05	11.8±0.05	9.5±0.05	9.5±0.1
	2	31.1±0.05	43.7±0.05	9.6±0.05	10.6±0.06	10.6±0.1
	3	30.9±0.05	46.0±0.05	7.9±0.05	11.3±0.07	11.2±0.1
C	1	32.1±0.05	40.8±0.05	11.8±0.05	9.5±0.05	9.5±0.1
	2	31.0±0.05	43.8±0.05	9.5±0.05	10.7±0.06	10.6±0.1
	3	31.0±0.05	46.2±0.05	7.9±0.05	11.1±0.07	11.2±0.1

In order to analyse the fluid temperature distribution in the heat exchangers, a set of thermocouples was inserted along one circuit of the finned coil, as it is illustrated in Fig. A1.5. The thermocouples were attached to the outside surface of fifteen U-bends, using a silicone based heat transfer compound to improve the thermal contact to the surface. The thermocouple distribution is reported in figure A1.2 for coils "A" and "B" and in figure A1.3 for coil "C". Then every single thermocouple and its corresponding U-bend were suitably insulated towards the environment. Referring to test number 3, for the gas-cooler A, the temperature profile is shown in Fig. A1.5, where the temperature measurements are numbered according to what shown in figure A1.2.

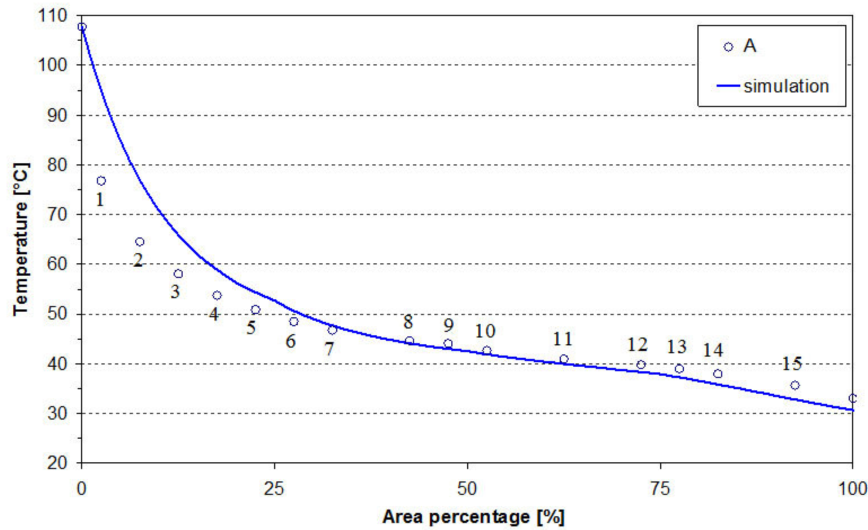

Fig. A1.5- Temperature profiles at 9.1 MPa (test conditions 3, finned coil "A", temperature measurements numbered as in figure A1.2). Note: the temperature error bars are not visible because of the large scale of the y-axis

The "solid" line shown in the figure relates to the temperature profile obtained by the numerical simulation. In each test a significant difference, between the predicted temperatures and values measured on coil A, was observed. Although the approach and the temperature values are different between tests at different refrigerant and air inlet conditions, in the first row (0 % - 25 % of the total surface) of the heat exchanger the measured temperature values are always lower than the calculated ones, while they are higher in the last three rows (25 % - 100 %).

Several CO_2 heat transfer coefficient correlations were tested, but without any significant change in the prediction (see Table A1.4).

Tab. A1.4- Simulation results by using three different correlations

	Gnielinski		Pitla et al.		Dang and Hihara	
Test	**CO_2 outlet temperature**	**Heat flow-rate [kW]**	**CO_2 outlet temperature [°C]**	**Heat flow-rate**	**CO_2 outlet temperature**	**Heat flow-rate [kW]**
1	32.2	9.5	32.2	9.5	32.3	9.5
2	31.0	10.6	31.0	10.6	31.2	10.6
3	30.7	11.3	30.7	11.3	30.9	11.2

All CO_2 specific correlations usually refer to the Gnielinski's one that was chosen as the reference to be used in the simulation software to evaluate the temperature profile and the heat flux. The other correlations were selected considering the different approach to the heat transfer coefficient evaluation. Pitlas's correlation makes use of an average between Nusselt numbers referred to bulk and wall temperatures, while Dang and Hihara's correlation uses a film temperature to evaluate CO_2 properties and therefore the heat transfer coefficient.

Different correlations don't give rise to different results because the heat transfer resistance is chiefly concentrated on the air side in finned coils. Therefore the reason of the difference between predicted and measured values must lie in a phenomenon associated with the gas cooling process and not modelled by the numerical code.

Unlike condensation or evaporation processes, in which the fluid temperature is almost uniform in a large part of the heat exchanger, the gas cooling process involves a significant temperature glide along the heat exchanger. In particular, the CO_2 temperature gradient is higher in the first 20 % (following the R744 flow direction) of the heat transfer area. Therefore it seems reasonable to consider the thermal conduction from the first high temperature tubes to the adjacent low temperature tubes through the continuous fins as the most important factor responsible for performance penalization and temperature profile disagreement in finned coils. As a consequence of the conduction heat transfer from hotter to colder tubes, the efficiency of the heat exchanger deviates from the ideal counter-flow behaviour.

To confirm this hypothesis, the continuous fins were cut to eliminate the thermal conduction from any tube row to the adjacent ones. In this way a separated row finned coil was tested (dubbed as "B" in Table A1.2). A 3.7 % to 5.6 % heat flow rate improvement was gained, as it can be seen in Table A1.2, while Fig. A1.6 shows a better agreement of the "B" temperature profile as compared with the "A" profile.

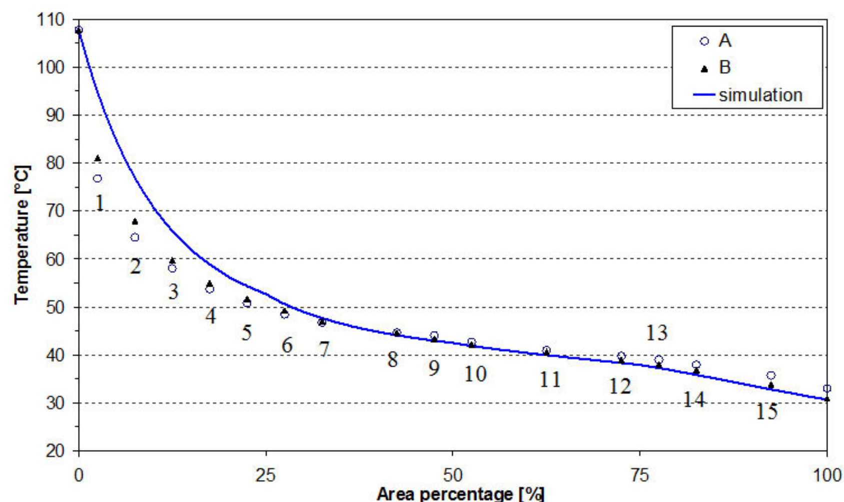

Fig. A1.6- Improvement of the temperature profile obtained by using the finned coil B (test conditions 3). Note: the temperature error bars are not visible because of the large scale of the y-axis

In the first row of the coil (0 % - 25 %) the temperature values increased while in the second part of the heat exchanger the temperatures decreased approaching the simulation profile. That is consistent with a decrease in thermal conduction.

This improvement can be clearly transferred in terms of COP, since a low value of the CO_2 temperature at the gas cooler outlet increases the cooling capacity. Using the “cut-configuration”, a 5.7 % to 6.6 % increase in coefficient of performance can be obtained, considering a reference cycle with the same operating conditions. The considered reference cycle is the simplest kind of a transcritical CO_2 system using single stage compression, without the presence of a Suction Line Heat Exchanger. The compressor is simulated with constant isentropic efficiency equal to 0.6. Isobaric processes except for compression and throttling were considered, with -10 C evaporation temperature and 5 C vapour superheating. Furthermore, a higher COP improvement can be reached by an optimization of the gas-cooler pressure.

The “C” configuration represented in Fig. A1.3 was chosen in a second set of tests to limit the thermal conduction between the two circuits along the vertical direction. Basically, from a geometric point of view, the two circuits were symmetrically fed, to reduce the thermal conduction in the horizontal middle cross section of the heat exchanger.

Referring to the comparison between the “C” configuration and the “B” one, Fig. A1.7 shows a slightly better approach just in the first tube row (high temperature zone), while in the other three tube rows the measured temperatures are almost the same, and the same is also the overall thermal performance.

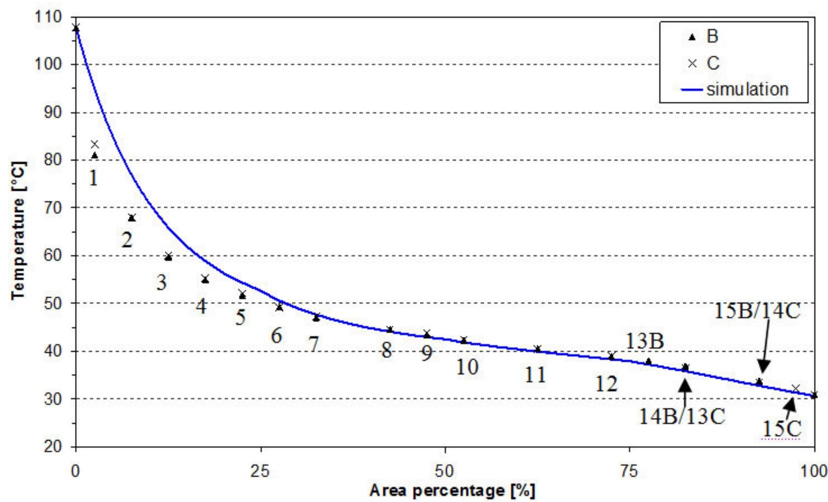

Fig. A1.7- Comparison of the temperature profiles of the two different circuit arrangements in the same finned coil. Note: the temperature error bars are not visible because of the large scale of the y-axis

These experimental results are evidence that the thermal bridge through fins contributes to penalize heat transfer because of the thermal conduction between different tube rows, not between tubes in the same row.

Asinari et al. (2004) pointed out a negligible effect of conduction through fins in minichannel air cooled gas coolers. It is worth noting that the flow arrangement plays a

key role in this respect. Usually minichannel gas coolers are arranged as a single slab heat exchanger with CO_2 flowing in multi-stream with several pipes in parallel (in Asinari et al. 2004 a three passes in the unique rank with respectively 13-11-10 tubes in parallel was analyzed). In this configuration the heat conduction through fins is only significant in the region of flow inversion caused by the manifolds. In fact a marked wall temperature difference is only present between the adjacent pipes in the flow inversion portion of the heat exchanger, whereas the other tubes fed in parallel within the same CO_2 pass are interested by very similar temperature fields, if the air velocity is supposed fairly uniform over the whole face area. According to temperature measurements presented in this work, in the investigated finned coil at least 12 tubes of the first rank are directly set into contact through the fins with tubes having wall temperature lower by at least 15 C (and in some cases up to 35 C), according to figures A1.5 – A1.7. From the same figures it is evident that the largest temperature change occurs in the first tube rank: the temperature profile is much more "flat" starting from the second down to the fourth rank. So the "cut configuration" (coils "B" and "C") interrupts the thermal bridge between the "higher wall temperature" first rank and the "lower wall temperature" part of the finned coil. The "separated" first rank behaves like a single slab heat exchanger, from the point of view of conduction through fins. In the "cut-configuration" only the first three tubes of each circuit (following the CO_2 flow from the entrance) in the first rank are in direct contact through the fins with tubes having wall temperature difference higher than 5 °C from the preceding pipe. Thus the effect of thermal conduction of the first rank arrangement on the overall efficiency of the heat exchanger is expected (and proved experimentally by comparison of coil "B" and coil "C" performance) to be negligible.

Therefore, experimental tests and numerical analysis on two identical finned coils, one with continuous fins, the other with separated fins per each tube row, indicates that "internal" heat conduction through the fins is an important factor even in finned coils when used as CO_2 gas-coolers. This fact is strictly linked to the high temperature variation of carbon dioxide during the gas cooling process in a transcritical refrigeration cycle. The improvement in temperature approach between CO_2 outlet temperature and air inlet temperature was found to increase the efficiency of the refrigerating cycle. This point offers a quite promising technological opportunity, since it is easy to build a coil with fins separated among the different rows. Furthermore, a new numerical code needs to be developed in order to teke conduction into account, as it has been done for the cold plate heat exchangers.

A2 - Prediction of the mass flow rate of carbon dioxide through capillary tubes in transcritical cycles

Introduction

Capillary tubes are widely used in small size refrigeration (including the mini vapor compression systems illustrated in the previous chapters) and air conditioning systems as throttling devices, because of their low cost, reliability and the low torque needed at the compressor during start-ups. Beginning early in the 1990s, capillary tube performance with HFC refrigerants has been reported by many investigators (Fiorelli et al., 2002; Yana Motta et al., 2000; Melo et al., 1999). Recent developments brought researchers' attention to CO_2, because of its environment compatibility and safety. Practical applications of CO_2 as refrigerant in vapour compression inverse cycle have been so far restrained by very high operating pressures and by the low thermodynamic efficiency of the idealised cycle, due to the low value of the critical temperature. It is not definitely ascertained if the good fluid properties connected to the heat transfer and compression processes can compensate for the drawback arising from poor thermodynamic properties (Pettersen et al., 2004; Lorentzen et al., 1994). A CO_2 inverse cycle is in general very different from a traditional one since the upper pressure is often supercritical and the resulting refrigerating cycle, of transcritical type, does not entail condensation, but a simple cooling process of dense fluid accomplished in the so-called 'gas cooler'. As a consequence, unlike the common subcritical cycle, the flow factor of the capillary tube determines the gas cooler pressure, which is no more related to the temperature of the heat transfer process. Then for the best utilization of such a technology it is necessary to design the capillary tube in order to find the optimal value of the cycle upper pressure, that is the one which leads to the maximum COP (Kim et al., 2004; Lorentzen et al., 1994).

Recently Zimmermann and Maciel (2006) and Cecchinato et al. (2007) presented test results on capillary tube optimization for commercial bottle coolers, aimed at keeping the upper cycle pressure always close to the optimal one at different ambient temperatures. Madsen et al. (2005) carried out theoretical and experimental studies of capillary systems in a transcritical CO_2 refrigeration system testing tubes with different lengths and diameters. They developed a numerical model which is in a quite good agreement with the mass-flow rate experimental results. The authors demonstrated that with CO_2, the dependence on the tube roughness of the friction factor of capillary tubes

should be accounted, unlike with synthetic refrigerants (Kuehl and Goldschmidt, 1991). Agrawal and Bhattacharyya (2008) developed a numerical model to evaluate the performance of a capillary tube based transcritical CO_2 heat pump system. Capillary tubes of various diameters, lengths and internal surface roughness were simulated. The authors developed a normogram to be employed as a guideline to select the optimum capillary tube. All the authors (Zimmermann and Maciel, 2006; Cecchinato et al., 2007; Madsen et al., 2005; Agrawal and Bhattacharyya, 2008) are in agreement stating that the capillary tube demonstrates an intrinsic capability of matching the flow rate imposed by the compressor. The capillary tube varies the upper pressure thus adjusting it close to the optimal value in response to changes of gas cooler heat sink temperature.

Unfortunately, only few experimental data of CO_2 mass flow rate through capillary tubes appear in the open literature. Hence in this work the experimental results obtained using capillary tubes of different diameter and length are presented. A test rig was developed to test capillary tubes with different temperature and pressure boundary conditions. Finally the experimental results are compared to the predicted values of open literature numerical models and approximate analytic solutions of the capillary tube equations.

Equations and models used

Many scientists have investigated the performance of capillary tubes using experimental data or theoretical models to predict the refrigerant flow rate. Most of the models and empirical correlations have been validated against experimental data of synthetic refrigerants. It is worth investigating whether common correlations might predict values in good agreement with CO_2 experimental data. Experimental correlations have been derived from Whitesel (1957) for R12 and R22, from Bittle et al. (1998) for R134a and recently from Kim et al. (2002), Choi et al. (2003; 2004) and then Yang and Wang (2008) for R-407C and R-410A. These authors developed dimensionless correlations, applying the Buckingham Π theorem, and rating charts to predict refrigerant mass flow rate through adiabatic capillary tubes (ASHRAE Handbook, 2002). Some of these dimensionless correlations are generalized for different refrigerants considering the refrigerant properties in the dimensionless parameter. Unfortunately none of the correlations is useful to predict CO_2 flow rate entering the capillary tube in transcritical conditions. In fact there wasn't any correlation developed using dimensionless parameters that account for transcritical state of the refrigerant at the capillary tube inlet but only for sub-cooled or two-phase inlet.

Continuity, energy and momentum equations applied to the capillary tube define a two point boundary value problem. A numerical solution with a shooting or a relaxation method (using a finite difference or finite volume approach on a distributed grid) is the most popular approach of researchers because of its generality (Kuehl and Goldschmidt, 1991; Stoecker and Jones, 1982; Li et al., 1990; Escanes et al., 1995; Bittle and Pate, 1996; Chung, 1998; Garcia-Valladares et al., 2002; Jung et al., 1999; Bansal and Wang, 2004). Madsen et al. (2005) and Agrawal and Bhattacharyya (2008) already demonstrated that such a numerical approach can be used to predict CO_2 flow rate. In this work Madsen et al. (2005) and Stoecker et al. model (1982) is validated against experimental data. However the numerical solution of the problem is somewhat time-consuming and the needed programming skills are not easily available to most engineers.
To balance generality of numerical models and simplicity of the empirical correlations, a novel approximate analytical approach to the solution of capillary tube equations was first introduced by Yilmaz and Unal (1996). Their work is valuable to simplify the numerical approach to the solution of the adiabatic capillary tube and it can still be used to predict CO_2 flow rate. The up-to-date model using this kind of approach is that of Zhang and Ding (2004) and it is validated against experimental data.
Both in Stoecker et al. and in Zhang and Ding model, the suggested friction factor correlations don't account for the tube roughness. Two modified models in which the friction factor is calculated with Miller (1996) equation are considered together with the original models and marked as "modified". In Zhang and Ding model, the M-predictor flow rate (equations 23 and 25 of Zhang and Ding, 2004) solution is calculated as in the original model without accounting for roughness while the M-corrector (equations 27 and 28 of Zhang and Ding, 2004) solution is obtained calculating the friction factor with Miller correlation.

Test rig description

The test rig (Figure A2.1) mainly consists of a pressure vessel, filled with carbon dioxide, a copper tube-in-tube heat exchanger, the capillary tube section and a metering valve (Whitey 31RS4). The pressure vessel is made of carbon steel and its capacity is 0.07 m^3. It is equipped with a cooling system and with an electrical heater which allow respectively the filling operation and the achievement of the test conditions. Carbon dioxide flows inside the inner pipe (internal diameter 4 mm, external diameter 6 mm) of the tube-in-tube heat exchanger and cooling water flows inside the outer tube (internal

diameter 10 mm) in counter-flow to CO_2. Water inlet temperature and flow rate are controlled through an auxiliary circuit (temperature stability ±0.05°C).

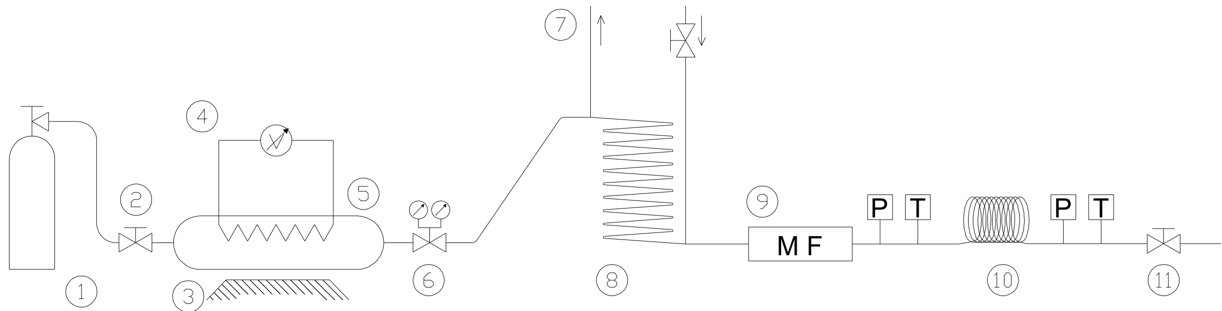

Fig. A2.1-Test rig lay-out: 1 CO_2 bottle, 2 shut-off valve, 3 cooling system, 4 electrical heater, 5 pressure vessel, 6 pressure regulator, 7 water auxiliary circuit, 8 tube-in-tube heat exchanger, 9 Coriolis mass flow meter, 10 capillary tube, 11 metering valve, P: pressure transducer, T: thermocouple.

CO_2 temperatures are measured by thermocouples placed inside adiabatic mixing chambers at inlet and outlet of the capillary tube. The thermocouples are T type: the complete measuring chain, including multimeter and the ±0.01°C Peltier reference ice point was calibrated against a ±0.02°C accuracy Pt100 thermometer. Thus a ±0.05°C accuracy is estimated for all the temperature measurements.

R-744 pressures are measured by strain-gauge transducers both at inlet and outlet of the capillary tube. The accuracy is ±1 kPa for low-pressure side and ±2 kPa for high-pressure side. CO_2 mass flow rate is measured by a Coriolis mass flow meter placed upstream of the throttling valve (accuracy ±0.1 % of reading). The water volumetric flow rate through the tube-in-tube heat exchanger was measured by an electromagnetic flow meter (accuracy ±0.2 % of reading). Four capillary tubes, different in diameter, length and roughness, were tested and their characteristics are listed in table A2.1.

Lengths of capillary tubes were measured with an uncertainty of 1.0 mm. Tubes diameter were measured using a precision plug gauge set with an uncertainty of 0.005 mm. The roughness values are listed in Table A2.1.

Tab A2.1- Capillary tube geometric parameters

Material	length [m]	diameter [10^{-3} m]	roughness [10^{-6} m]
Copper	3.5	0.66	1.5
Copper	6	0.8	1.5
Stainless Steel	2.78	0.76	0.5
Stainless Steel	1.29	0.51	0.5

Experimental measurements

Inlet pressure was varied from 75 10^5 Pa to 110 10^5 Pa, inlet temperature was ranged from 20 °C to 40 °C, and most of tests were carried out with outlet pressure varying from 24 10^5 Pa to 27 10^5 Pa. These test conditions were chosen to realize the typical operating conditions of bottle coolers and retail systems, which usually adopt capillary tubes as throttling devices. Notwithstanding this, different outlet pressures, from 15 10^5 Pa to 30 10^5 Pa, were also considered in order to investigate the variation of the mass flow rate as the choking condition wasn't gained. In fact, chocking pressure was assessed as about 10 10^5 Pa for the test boundary conditions. This pressure was not achievable because of instability problems occurring at the metering valve relating to the solid CO_2 deposition. The pressure vessel was filled up with 50 kg of carbon dioxide before each test. This quantity of CO_2 assured reaching suitable conditions and also recording for 10 minutes the main parameters during experimental measurements when steady state conditions were achieved. After the filling procedure was completed, the bottle was disconnected and the vessel cooler was turned off. The electrical heater was turned on in order to increase the carbon dioxide pressure over the critical value and afterward the capillary inlet pressure was fixed by using a pressure regulator. The temperature was adjusted by using a tube in tube heat exchanger. Figure A2.2 shows all the processes which occur during any experimental set of tests. Point 1 corresponds to the carbon dioxide condition in the pressure vessel, and the process 1-2 represents the heating process and it takes place along an isochoric curve. The isenthalpic process 2-3 displays the pressure decreasing due to the pressure regulator, while the process 3-4 shows the heat rejection that occurs to the gas cooler at almost constant pressure. Point 4 represents the capillary tube inlet condition. As each test was running, the CO_2 mass quantity in the pressure vessel decreased and therefore the heating process took place at higher values of specific volume. This entails a higher temperature value of the carbon dioxide at the outlet of the regulating pressure valve (point 3'). The heat exchanger was designed to set the CO_2 outlet temperature as the test was carried out, being the water temperature controlled by a PID regulation system.

Capillary tube inlet conditions were thus set to those required in each test, while the outlet pressure was adjusted by a metering valve. This system has several advantages when compared to those based on mechanical compression, as swiftness to achieve steady conditions and accurate control of the inlet pressure at the capillary tube. Furthermore, since the system is not equipped with any compressor, it does not require any lubrication, therefore all the tests in this study are not influenced by the presence of refrigeration oil. The achieved values of temperature and pressure, as well as the mass

flow, were real time displayed in order to provide an immediate feedback to the operator. After steady state conditions were reached, all parameters were acquired every five seconds.

Comparison between experimental results and predicted values

The consistency of experimental data is analyzed against Madsen et al. (2005), Stoecker et al. (1982) and Zhang and Ding (2004) models. Stoecker et al. and Zhang and Ding modified models account for tube roughness influence on the pressure drop calculating the friction factor with Miller (1996) correlation. All required thermophysical properties are evaluated by using REFPROP 7.0 database (Lemmon et al., 2002). Despite four capillary tubes were investigated under several conditions, any significant discontinuity in the results trends wasn't pointed out and all data were merged together on the same charts and tables.

In Figures A2.3, A2.4 and A2.5 the comparison between predicted mass flow rate as calculated by Zhang-Ding's, by Stoecker et al. and by Madsen's et al. model, and experimental data are shown respectively.

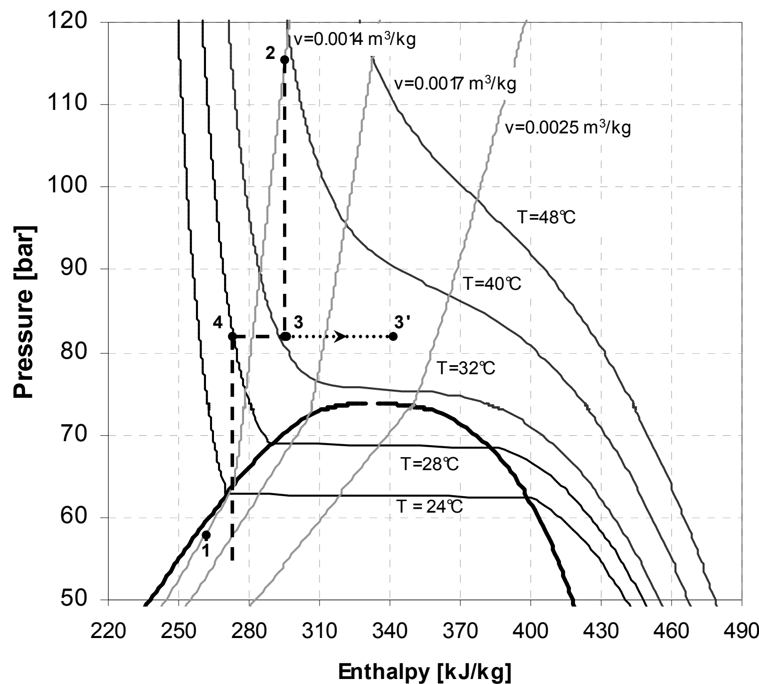

Fig A2.2- Processes which occur during tests

From Figure A2.5 it can be pointed out that approximately 88.5% of Madsen's *et al.* predicted mass flow rates are consistent with the measured data within a relative deviation of ±10%, Instead only 33.1% and 23% data fall within a relative deviation of ±10% for Zhang-Ding's et al. and Stoecker's et al. equations respectively.

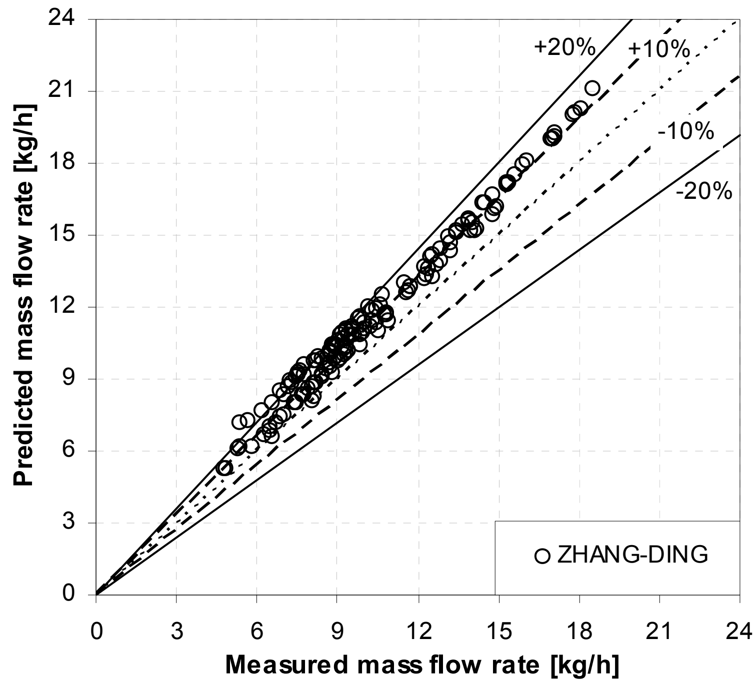

Fig. A2.3-Comparison between predicted mass flow rate as calculated by Zhang-Ding's et al. equation and experimental data. Note: the mass flow rate error bars are not visible because of the large scale of the x-axis.

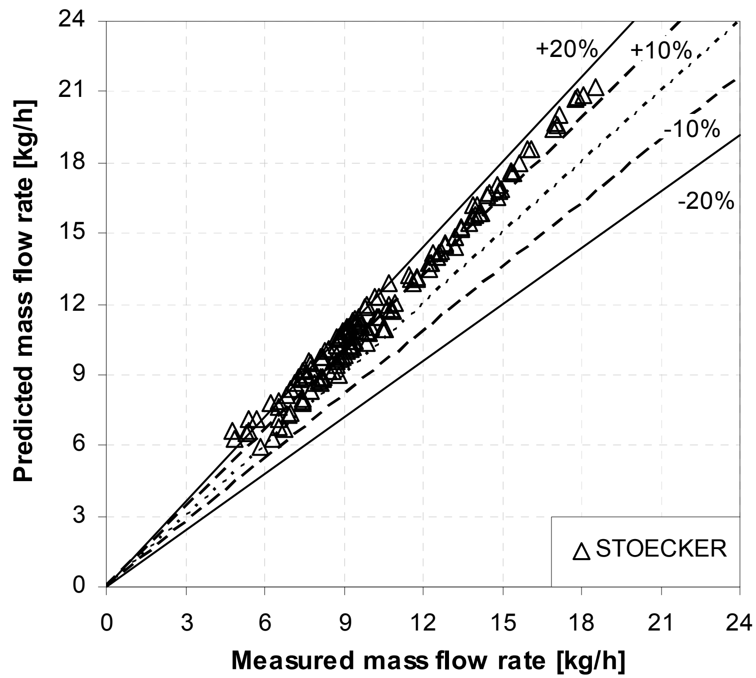

Fig. A2.4- Comparison between predicted mass flow rate as calculated by Stoecker's equation and experimental data. Note: the mass flow rate error bars are not visible because of the large scale of the x-axis.

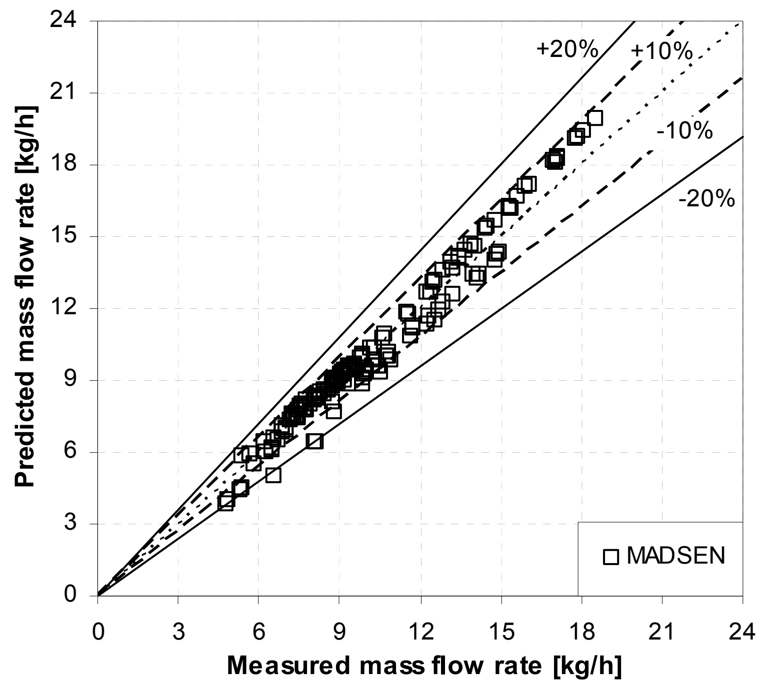

Fig. A2.5- Comparison between predicted mass flow rate as calculated by Madsen's et al. equation and experimental data. Note: the mass flow rate error bars are not visible because of the large scale of the x-axis.

Considering roughness in the calculation of friction factor, Zhang-Ding's and Stoecker's et al. models agreement with experimental result strongly improves, as it can be seen in Figures A2.6 and A2.7.

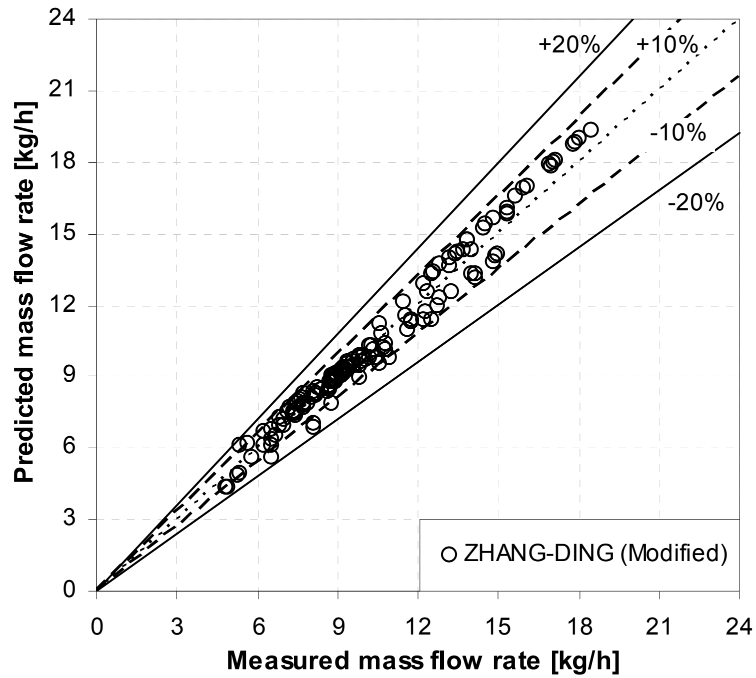

Fig. A2.6- Comparison between predicted mass flow rate as calculated by Zhang-Ding's modified correlation and experimental data. Note: the mass flow rate error bars are not visible because of the large scale of the x-axis.

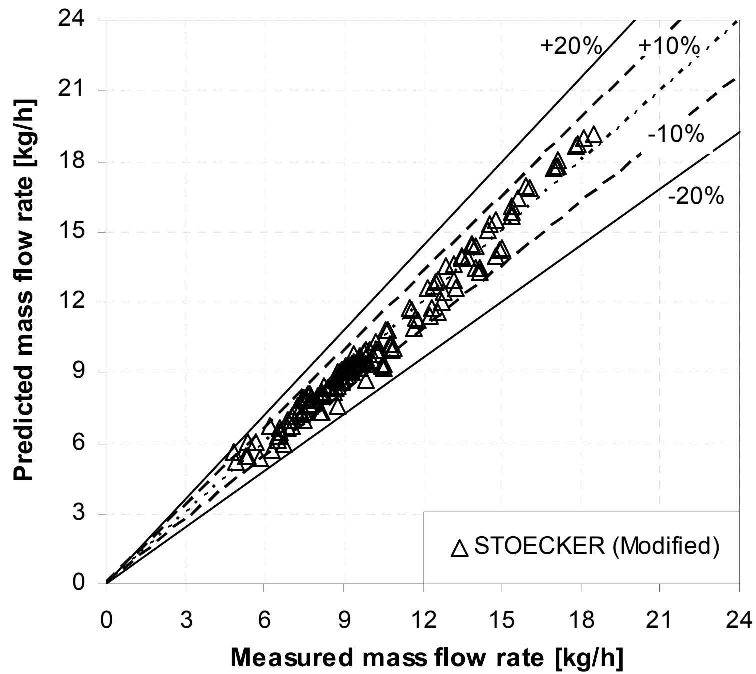

Fig. A2.7- Comparison between predicted mass flow rate as calculated by Stoecker's modified correlation and experimental data. Note: the mass flow rate error bars are not visible because of the large scale of the x-axis.

Figure A2.8 and A2.9 show relative deviations of the predicted data from the experimental data using Stoecker's et al. modified, Zhang-Ding's modified and Madsen's model. It can be pointed out that all predicted data are included between -25% and +16% at any test conditions.

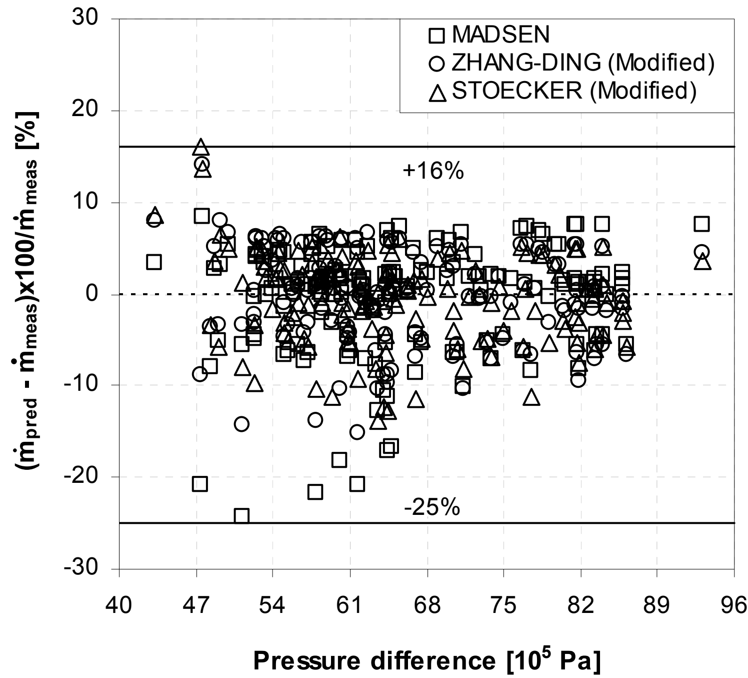

Fig. A2.8- Deviations of predicted mass flow rate from experimental data related to pressure difference.

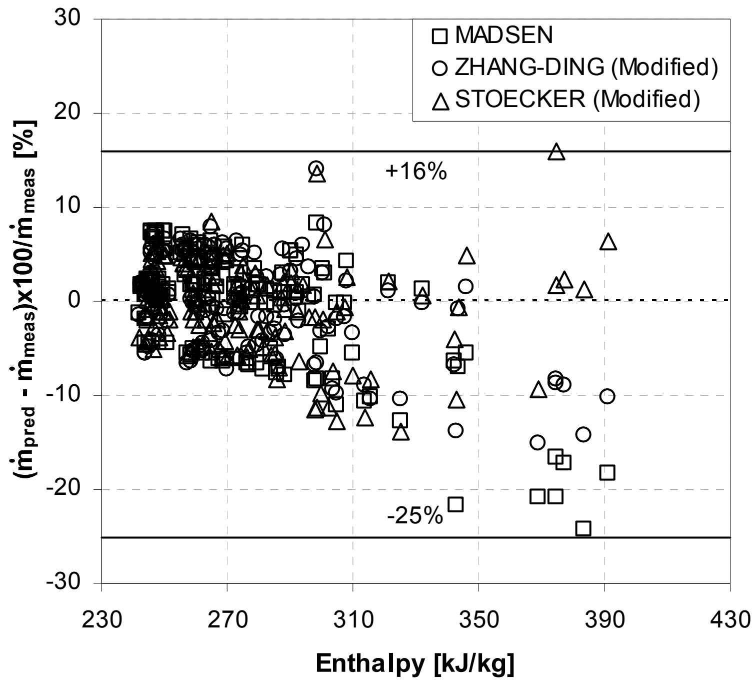

Fig. A2.9- Deviations of predicted mass flow rate from experimental data related to inlet enthalpy (reference IIR).

However, considering only Stoecker's et al. and Zhang-Ding's modified models, the maximum underprediction is equal to -14%. It is worth noticing that considering Figure A2.8, the deviation in the prediction is almost uniform unrelated to pressure difference, it appears just slightly higher at lower values. If the deviation is plotted against inlet enthalpy as in Figure A2.9, it appears that the higher is the enthalpy, and the outlet quality, the bigger is the prediction error. The model used for calculating the two-phase properties, the assumed two-phase flow model and liquid generation phenomena (i.e. vapour quality decreases by lowering the pressure along an isoenthalpic process) during expansion for inlet enthalpy greater than the critical one (Figure A2.10) could influence the prediction accuracy. Nevertheless for the most part of CO_2 transcritical cycle applications, working conditions set inlet enthalpy much lower than the critical one and the prediction errors keep below 10%.

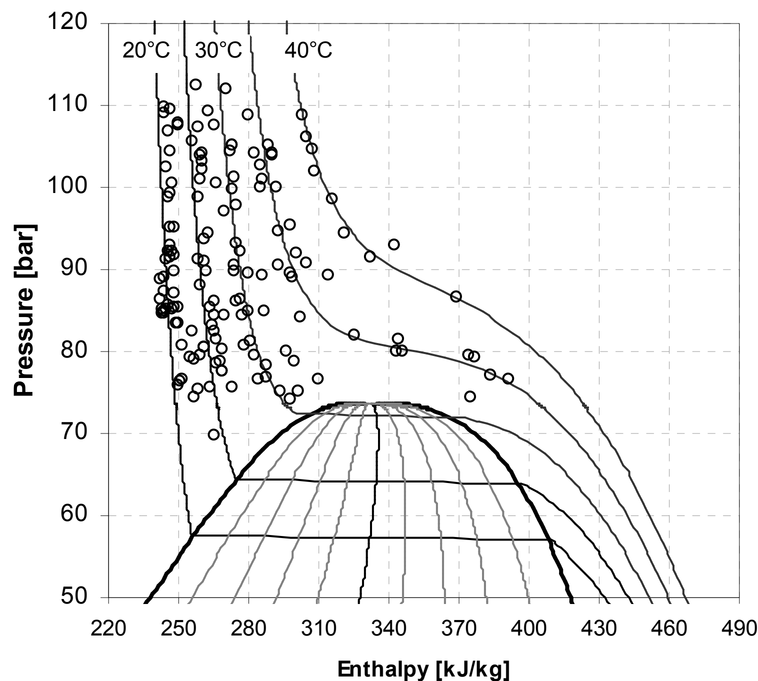

Fig. A2.10- Experimental capillary inlet points on the p-h diagram.

Table A2.2 reports average and standard deviations for all the used correlations and the number of predicted values within ± 10 % of experimental data. Stoecker's et al. modified method shows the highest number of predicted data within ± 10 % of experimental ones and even the lowest standard deviation. Finally, all experimental points are listed in Table A2.3 by inlet pressure together with inlet temperature, outlet pressure and mass flow rate

Tab A2.2- Comparison between experimental measurements and models.

Correlation	Ave. Dev.a	Stan. Dev.b	Points predicted within ± 10% of exp. data
	[%]	[%]	[%]
Stoecker	14.1	38.2	23.0
Zhang-Ding	12.2	28.7	33.1
Stoecker (modified)	-0.6	23.8	90.5
Zhang-Ding (modified)	-0.2	25.7	89.9
Madsen	-0.7	39.8	88.5

[a] $Ave.\,dev. = \frac{1}{n}\sum_{1}^{n}\left[\left(\dot{m}_{pred} - \dot{m}_{meas}\right)\times 100 / \dot{m}_{meas}\right]$

[b] $Stan.\,dev. = \frac{1}{n}\sum_{1}^{n}\left[\left(\dot{m}_{pred} - \dot{m}_{meas}\right)\times 100 / \dot{m}_{meas}\right]^2 - Ave.\,dev.^2$

To summarize, the performances of different adiabatic capillary tubes with CO_2 in transcritical conditions were experimentally investigated under a wide range of inlet pressures and temperatures, in order to evaluate the accuracy in the prediction of the mass flow rate. Madsen et al. (2005), Stoecker et al. (1982) and Zhang and Ding (2004) models were validated against experimental data. Approximately 88.5% of Madsen's et al. predicted mass flow rates are consistent with the measured data within a relative deviation of ±10%, instead only 33.1% and 23% data fall within a relative deviation of ±10% for Zhang-Ding's et al. and Stoecker's et al. equations respectively. Both in Stoecker et al. and in Zhang and Ding model, the suggested friction factor correlations don't account for the tube roughness. If the model friction factor correlation is calculated with Miller (1996) equation to consider roughness influence, Zhang-Ding's and Stoecker's et al. agreement with experimental result strongly improves, 89.9% and 90.5% data fall within a relative deviation of ±10% respectively.

Tab. A2.3- Detailed experimental measurements.

p_{in} [10^5 Pa]	T_{in} [°C]	p_{out} [10^5 Pa]	Mass flow rate [kg/h]	p_{in} [10^5 Pa]	T_{in} [°C]	p_{out} [10^5 Pa]	Mass flow rate [kg/h]
Material (steel), diameter (0.51 [10^{-3} m]), length (1.29 [10^{-3} m])							
75.6	24.7	23.2	6.89	91.3	25.0	26.1	8.45
76.6	29.3	27.5	6.54	91.7	21.4	26.6	8.77
76.6	21.1	21.0	7.41	92.9	41.2	22.4	6.53
76.7	32.1	25.5	5.83	95.2	21.2	27.0	9.12
77.5	26.3	22.5	7.02	99.9	33.9	20.8	8.62
78.9	32.1	26.6	6.30	100.4	28.5	24.7	9.05
80.5	24.5	24.5	7.47	101.1	30.8	20.7	8.96
80.8	21.6	24.6	7.74	102.3	26.7	30.5	9.26
83.5	21.3	26.2	8.05	102.7	34.4	22.1	8.72
84.2	34.0	24.8	6.72	103.2	26.7	30.5	9.34
84.5	26.3	24.1	7.74	104.2	33.9	22.2	8.90
85.4	21.5	25.1	8.21	104.2	26.6	30.3	9.43
87.2	21.2	24.8	8.44	105.1	30.9	23.7	9.25
88.0	24.8	26.0	8.18	108.9	33.8	23.0	9.32
90.5	34.0	26.2	7.47	109.2	28.2	23.3	9.85
90.6	29.4	28.3	7.93				
Material (steel), diameter (0.75 [10^{-3} m]), length (2.78 [10^{-3} m])							
75.1	30.3	20.8	10.61	93.2	30.1	24.2	14.47
75.4	23.1	20.7	12.52	94.5	39.6	30.3	12.41
75.9	20.7	25.8	12.85	94.7	34.7	27.8	13.71
78.4	30.3	21.7	11.48	95.0	21.6	29.5	15.93
78.5	25.7	23.4	12.58	97.0	28.9	26.9	15.35
79.1	23.1	21.6	13.20	98.7	21.0	21.5	16.94
80.1	34.9	23.8	9.37	98.8	25.7	27.7	16.09
80.7	29.0	27.4	12.23	100.4	21.9	22.1	17.10
81.4	35.6	19.0	10.00	101.9	39.6	29.4	14.04
82.5	23.2	22.2	13.87	103.8	35.8	24.1	15.34
83.1	25.7	24.1	13.46	104.2	35.9	24.1	15.39
85.1	20.8	26.9	14.51	105.7	25.4	29.1	17.14
85.4	25.7	23.8	13.87	106.9	21.6	22.8	18.06
86.0	29.0	24.3	13.44	107.5	23.3	26.0	17.79
90.9	25.8	26.0	14.80	107.5	28.7	28.8	17.02
91.4	39.6	29.4	11.56	107.8	23.2	26.2	17.86
91.5	20.7	27.0	15.62	109.5	22.2	16.4	18.51
91.9	35.7	21.6	13.21				
Material (copper), diameter (0.66 [10^{-3} m]), length (3.50 [10^{-3} m])							
69.8	24.1	26.5	6.22	85.6	20.2	25.8	8.79
74.1	30.4	26.5	5.36	86.1	26.5	18.7	8.28
74.3	32.0	26.8	4.81	86.4	19.0	26.3	9.07
74.4	22.5	25.7	7.16	87.4	19.7	26.6	9.19
75.2	31.0	26.1	5.70	88.7	19.1	25.7	9.60
75.7	26.9	16.8	6.86	89.0	19.6	25.7	9.62
76.6	35.4	16.6	4.89	89.4	30.8	19.6	8.15
79.2	22.6	16.6	7.76	89.7	29.4	26.2	8.46

79.3	35.9	14.8	5.32	89.8	21.2	25.1	9.40
79.5	29.6	26.0	7.02	91.2	20.2	26.5	9.38
79.5	24.0	26.4	7.52	92.2	21.3	25.9	9.59
79.6	35.9	14.8	5.36	92.2	20.7	26.0	9.61
80.1	32.0	26.2	6.57	94.4	26.6	19.7	9.21
80.3	26.5	27.7	7.26	95.4	36.0	17.5	8.22
80.4	24.5	26.0	7.58	97.7	30.7	20.8	9.13
81.5	26.0	29.0	7.45	99.4	21.3	26.5	10.30
83.5	21.0	23.9	8.74	100.0	35.7	18.4	8.79
84.3	27.4	26.7	7.66	103.8	26.4	20.5	10.19
84.5	29.5	26.1	7.74	104.4	21.7	20.4	10.68
84.5	19.0	26.1	8.88	104.5	30.9	21.9	9.80
84.8	19.5	26.7	8.90	104.6	40.0	21.4	8.74
84.8	31.6	26.5	7.36	105.1	35.5	19.3	9.38
84.9	19.5	26.7	8.91	105.2	31.0	21.8	9.86
85.0	19.1	25.8	8.92	106.1	39.8	21.7	8.95
85.1	19.7	26.6	9.18				
Material (copper), diameter (0.80 [10^{-3} m]), length (6.00 [10^{-3} m])							
76.3	21.0	23.9	10.32	89.8	26.0	25.4	11.77
76.8	30.0	28.5	8.75	90.8	36.2	26.3	10.55
77.1	34.8	25.8	6.57	92.1	30.3	21.4	11.63
77.6	26.1	20.4	9.92	93.0	21.0	26.0	12.83
78.7	26.1	23.4	10.05	93.6	25.9	26.0	12.31
79.9	34.7	21.9	8.16	98.4	40.0	27.0	10.94
81.1	29.6	24.3	9.84	99.8	30.4	23.0	12.72
81.9	35.1	18.3	8.80	100.9	34.3	26.9	12.23
82.5	25.9	21.4	10.81	100.9	26.1	27.4	13.25
84.8	30.0	29.8	10.24	102.4	21.1	27.4	14.01
85.4	21.0	24.6	11.77	107.3	26.4	25.5	14.18
86.3	29.5	25.5	10.74	108.8	40.0	26.9	12.55
86.5	40.0	24.8	8.09	108.9	21.0	25.4	14.90
89.1	34.7	11.6	10.50	109.6	21.0	25.7	14.98
89.2	37.0	25.0	9.86	112.0	30.9	28.7	14.16
89.3	32.2	26.0	10.83	112.4	26.4	26.2	14.80
89.5	34.7	22.5	10.46				

NOMENCLATURE

p	Pressure
ρ	Fluid density
c_p	Specific heat
T	Temperature
k	Thermal conductivity
i, h	Enthalpy
u	Fluid velocity
μ	Dinamic viscosity
D_h	Hydraulic diameter
f	Friction factor
$\Delta\Phi$, Q	Heat flow rate
Φ_f^2	Two-phase friction multiplier
Ω	Three dimensional domain
σ	Border surface of three-dimensional discretized domain
Σ	Border surface of three dimensional domain
ϑ	Temperature difference between wall and fluid
J	Specific thermal flux
n	Unit vector
$x^*_{fd,th}$	Thermal entrance region, dimensionless
g	Gravity
α	Heat transfer coefficient
A_c	Channel cross section
ΔS_i	Heat transfer surface of a generic element
ε_v	Void fraction
x_r	Fluid quality
x, y, z	Space coordinates
s_w	Fin thickness
$\nabla^2(T)$	Two dimensional gradient of T
$\nabla^3(T)$	Three dimensional gradient of T
δy	Uncertainty in the result, generic

x_i	Generic i-th variable
δx_i	Uncertainty in x_i
$\dot{V}$	Volumetric air flow rate
U	Overall heat transfer coefficient
ΔT_{lm}	Log mean temperature difference
r	Tube radius
η_0	Finned surface efficiency
Ra	Rayleigh number
Re	Reynolds number
Pr	Prandtl number
Gr	Grashof number
Bi	Biot number

Subscripts and superscripts

l	Liquid phase
v	Vapor phase
w	Wall
f	Fluid
CP	Cold plate
i, j	Cell index
in	Inlet
out	Outlet

Note: units are reported in the full text. In case that other symbols are used in a specific equation, this is directly mentioned in the full text.

REFERENCES

3M. 3M Novec™ 7000 Engineered Fluid Product Information. Retrieved October 20, 2008, from http://www.mmm.com

Agrawal J., Bhattacharyya S., 2008, "Optimized transcritical CO_2 heat pumps: performance comparison of capillary tubes against expansion valves", Int. J. Refrigeration 31, 388-395

ANSI/ASHRAE Standard 34-2007, Designation and safety classification of refrigerants, Proposed addendum z, available on-line at www.ashrae.org

Arik M.,Bar-Cohen A., 2003, "Effusivity-based correlation of surface property effects in pool boiling CHF of dielectric liquids", Int. J. Heat Mass Transfer. vol. 46, pp. 3755–3765

ARINC SPECIFICATION 600-16 - Air transport avionics equipment interfaces, aeronautical radio, inc. 2551 Riva road, Annapolis, Marylamd 21401-7435

ASHRAE Fundamentals, 2001, Atlanta: S:I Edition.

ASHRAE. ASHRAE Handbook, 2002 – Refrigeration. American Society of Heating, Refrigerating and Air-Conditioning Engineers, Atlanta (Chapter 45)

Asinari P., Cecchinato L., Fornasieri E., 2004 "Effects of thermal conduction in microchannel gas coolers for carbon dioxide. Int. J. Refrig., 27(6): 577-586.

Asinari P., 2004, "Finite-volume and finite-element hybrid technique for the calculation of complex heat exchangers by semiexplicit method for wall temperature linked equations (SEWTLE)", Numerical Heat Transfer, Part B: Fundamentals, v 45, n 3, p 221-248, ISSN: 10407790

Bang S., 2008, "Evaluation result of HFO-1234yf as an alternative refrigerant for automotive air conditioning" In Proceedings of the VDA Alternative Refrigerant Winter Meeting, Saalfelden, Austria.

Bansal P.K., Wang G., 2004, "Numerical analysis of choked refrigerant flow in adiabatic capillary tubes", Applied Thermal Engineering 24, p.851-863.

Bar-Cohen A., Arik M., Ohadi M., 2006, "Direct Liquid Cooling of High Flux Micro and Nano Electronic Components", Proceedings of the IEEE |Vol. 94,No. 8

Bittle R.R., Pate M.B., 1996, "A theoretical model for predicting adiabatic capillary tube performance with alternative refrigerants", ASHRAE Transactions 102(2), 52–64.

Bittle R.R., Wolf D.A., Pate M.B., 1998, "A generalized performance prediction method for adiabatic capillary tubes", Int. J. HVAC & Refrigeration Research, 4 (1), 27-43.

Bivens D.B., Minor. B.H., 1998. "Fluoroethers and other next generation fluids", International Journal of Refrigeration 21(7): 567-576.

Brown J.S., 2007a. “Predicting performance of new refrigerants using the Peng-Robinson Equation of State”, Int. J. Refrigeration 30 (8), 1319-1328.

Brown J.S., 2007b. “A methodology to evaluate R114 replacement refrigerants using thermodynamic properties”, HVAC&R Research 13 (5): 697-709.

Brown J.S., 2007c. “Evaluation of potential R-22 substitute refrigerants using fundamental thermodynamic parameters”, In: Proceedings of the 22nd International Congress of Refrigeration, Beijing, China.

Brown J.S., 2008a. “Methodology for estimating thermodynamic parameters and performance of alternative refrigerants”, ASHRAE Transactions 114 (1).

Brown, J.S., 2009 “HFO’s: New, low global warming potential refrigerants”, ASHRAE Journal 51(8): 22-29.

Brown, J.S., Zilio C., Cavallini A., 2009a “Thermodynamic properties of eight fluorinated olefins”, International Journal of Refrigeration doi:10.1016/j.ijrefrig.2009.04.005

Brown J.S., Zilio C., Cavallini A., 2009b. “Estimations of the thermodynamic and transport properties of R-1234yf using a cubic equation of state and group contribution methods”, In: Proceedings of the 3rd IIR Conference on Thermophysical Properties and Transport Processes of Refrigerants, Boulder, CO, USA.

Calm J.M., Hourahan G.C., 2007. “Refrigerant data update”, Heating/Piping/Air Conditioning Engineering 79(1): 50-64.

Casson V., Cavallini A., Cecchinato L., Del Col D., Doretti L., Fornasieri E., Rossetto L., Zilio C., 2002 “Performance of finned coil condensers optimized for new HFC refrigerants” ASHRAE Transactions, 108 (2): 517-528.

Cecchinato L., Corradi M., Schiochet G., Fossati C., 2007, “Development of a transcritical R744 bottle cooler”, In: 22th IIR Int. Cong. of Refrigeration, Beijing, China, August 21-26.

Choi S. B., Barron R. R., Warrington R. O., 1991 “Liquid flow and heat transfer in microtubes” Micromechanical sensor, actuator and systems, ASME DSC-32, 123-134.

Choi J., Yongchan K., Kim H.Y., 2003, “A generalized correlation for refrigerant mass flow rate through adiabatic capillary tubes”, Int. J. Refrigeration 26, 881–883.

Choi J., Kim Y., Chung J.T., 2004, “An empirical correlation and rating charts for the performance of adiabatic capillary tubes with alternative refrigerants”, Appl. Therm. Eng. 24, 29–41.

Chung M., 1998, “A numerical procedure for simulation of Fanno flows of refrigerants or refrigerant mixtures in capillary tubes”. ASHRAE Transactions 104(2), 1031–1042.

Corberan, J.M., Fernández De Córdoba P., Ortuño S., Ferri V., Gonzálvez J., Setaro T., Boccardi G., 2000 , “Modelling of compact evaporators and condensers”, Computational Studies, v 3, p 487-496, Advanced Computational Methods in Heat Transfer VI

Corberan J. M., Fernandez de Cordoba P., Gonzalvez J., Alias F., 2001, "Semiexplicit method for wall temperature linked equations (SEWTLE): a general finite-volume technique for the calculation of complex heat exchangers", Numerical Heat Transfer, Part B: Fundamentals, Volume 40, Issue 1, pages 37 - 59

Dang C., Hihara E., 2004, "In-tube cooling heat transfer of supercritical carbon dioxide Part 1. Experimental measurement". Int. J. Refrig., 27(7): 736-747.

Davis S., 2008, "Cooling Techniques Attack MPU Processing Heat", electronicdesign.com, ID #19882

Defibaugh D.R., Gillis K.A., Moldover M.R., Morrison G., Schmidt J.W., 1992, "Thermodynamic properties of CHF_2-O-CHF_2, bis(difluoromethyl) ether", Fluid Phase Equilibrium 81: 285-305.

Devotta S., Penyala V.R., 1994. "Thermodynamic screening of some HFCs and HFEs for high-temperature heat pumps as alternatives to CFC114", International Journal of Refrigeration 17(5):338-342.

Di Nicola G. D., Polonara F., Santori G., 2009, "Saturated Pressure Measurements of 2,3,3,3 Tetrafluoroprop-1-ene (HFO-1234yf)", Journal Chemical Reference Data doi:10.1021/je900306v.

Directive 2006/40/EC of The European Parliament and of the Council of 17 May 2006 relating to emissions from air-conditioning systems in motor vehicles and amending Council Directive 70/156/EC, 2006. Official Journal of the European Union. Retrieved online at: http://eur-lex.europa.eu/LexUriServ/LexUriServ.do?uri=OJ:L:2006:161:0012:0018:EN:PDF, November 3, 2009.

EN-ISO Standard 5167-1, 2005, Measurement of fluid flow by means of pressure differential devices.

Ellsworth M.J., Simons R.E., "High Powered Chip Cooling - Air and Beyond" available on-line at www.electronics-cooling.com, Volume 11, Number 3, August 2005

Escanes F., Perez-Segarra C.D., Oliva A., 1995, "Numerical simulation of capillary-tube expansion devices", Int J Refrigeration 18(2), 113–122.

Estes K. A., Mudawar I., 1995 "Comparison of two-phase electronic cooling using free jets and sprays" ASME Journal of Electronic Packaging, Vol. 117, pp. 323-332.
Fiorelli F., Huerta A., Silvares O., 2002, "Experimental analysis of refrigerant mixtures flow through adiabatic capillary tubes", Exper. Therm. Fluid Sci. 26, 499–512.

Fourie F., Andriamisana M., 2009, "Large aircraft integration rig and tests results", Moet forum, Barcelona. Retrieved online at http://www.eurtd.com/moet/proceedings.html

Galzin G., Gomez V., Mevenkamp C., Brunswig H., 2009, "Electrical Environmental Control System", Moet forum Barcelona. Retrieved online at http://www.eurtd.com/moet/proceedings.html

Garcia-Valladares O., Perez-Segarra C.D., Oliva A., 2002, "Numerical simulation of capillary tube expansion devices behavior with pure and mixed refrigerants considering metastable region. Part I: mathematical formulation and numerical model", Applied Thermal Engineering 22(2), 173–182.

Gnielinski V., 1976, "New equations for heat and mass transfer in turbulent pipe and channel flow" Int. Chem. Eng., 16(2): 359-367.

Hulse R., Singh R., Pham H., 2009, "Physical properties of HFO-1234yf", In Proceedings of the 3rd IIR Conference on Thermophysical Properties and Transport Processes of Refrigerants, Boulder, CO, USA.

Huang D., Quack H., Ding G.L., 2007, "Experimental study of throttling of carbon dioxide refrigerant to atmospheric pressure", Appl. Thermal Eng., 27, 1911-1922
Jung D, Park C, Park B, 1999 "Capillary tube selection for HCFC22 alternatives", Int J Refrigeration 22(8), 604–614.

Ing P., Sperry C., Philstrom R., Claybaker P., Webster J., Cree R., 1993, "Supercomputer cooling system", 43rd Electronic Components Technology Conf., pp. 218–237.

Incropera F. P., 1999, "Liquid cooling of electronic devices by single-phase convection", Wiley-Interscience.

International Standards Organization, 2004, ISO 5167-4:2003, Measurement of fluid flow by means of pressure differential devices inserted in circular cross-section conduits running full—Part 4: Venturi Tubes.

International Standards Organization, 2007, ISO/CD 817: 2007, Refrigerants – Designation and Safety Classification. Retrieved online at: http://isotc.iso.org/livelink/livelink/fetch/2000/2122/138198/756301/1060103/ISO_CD_817_-_2007.pdf?nodeid=6427209&vernum=0, November 3, 2009.

IPCC, 2007, Climate Change 2007: The Physical Science Basis – Contribution of Working Group I to the Fourth Assessment Report of the Intergovernmental Panel Climate Change. Intergovernmental Panel on Climate Change of the World Meteorological Organization and the United Nations Environment Programme (UNEP). Edited by S.S. Solomon, et al. Cambridge, U.K.: Cambridge University Press.

Kandlikar S., Grande W., 2004, "Evaluation of single phase flow in microchannels for high flux chip cooling – Thermodynamic performance enhancement and fabrication technology" 2nd Int. Conf. On Microchannels and Minichannels, Rochester, NY, p. 67-76

Kays W. M., A. L. London, 1984, "Compact Heat Exchangers", McGraw-Hill, New York

Kendall S. R., Rao H. V., 1997, "Experimental study of flow through micro-passages", Procedures Fourth international conference on experimental heat transfer, fluid mechanics and thermodynamics, vol. 4 2423-2430

Kim S.G., Kim M.S., Ro S.T., 2002, “Experimental investigation of the performance of R22, R407C and R410A in several capillary tubes for air-conditioners”, Int. J. Refrigeration 25, 521–531.

Kim M.H., Pettersen J., Bullard C.W., 2004, “Fundamental process and system design issues in CO_2 vapor compression systems”, Progress in Energy and Combustion Science 30(2), 119-174.

Koban M., 2009 “HFO-1234yf low GWP refrigerant LCCP analysis”, In Proceedings of 2009 SAE World Congress, Detroit, MI, USA.

Kumari N., Krishnan S., GarimellaS.V., 2007, “Analysis and performance comparison of competing desktop cooling technologies”, Proceedings of IPACK2007 ASME InterPACK '07, Vancouver, British Columbia, CANADA

Kuehl S.J., Goldschmidt V.W., 1991, “Modeling of steady flows of R-22 through capillary tubes”, ASHRAE Transactions 97(1),139–148.

Leck T.J., 2009, “Evaluation of HFO-1234yf as a replacement for R-134a in refrigeratioin and air conditioning applications”, In: Proceedings of the 3rd IIR Conference on Thermophysical Properties and Transport Processes of Refrigerants, Boulder, CO, USA.

Lee J., Mudawar I., 2008, “Low-temperature two-phase micro-channel cooling for high-heat-flux thermal management of defense electronics”, Thermal and Thermomechanical Phenomena in Electronic Systems, ITHERM 2008. 11th Intersociety Conference 28-31 May 2008 Page(s):132 - 144

Lemmon, E.W., Huber M.L., and McLinden, M.O., 2007, NIST reference fluid thermodynamic and transport properties-REFPROP. NIST standard reference database 23-Version 8.0.

Li R.Y., Lin S., Chen Z.H., 1990, “Numerical modeling of thermodynamic non-equilibrium flow of refrigerant through capillary tubes”, ASHRAE Transactions 96(1), 542–549.

Lorentzen G., 1994, “Revival of carbon dioxide as a refrigerant”, Int. J. Refrigeration 17(5), 292-301.

Madsen K.B., Poulsen C.S., Wiesenfarth M., 2005, “Study of capillary tubes in a transcritical CO_2 refrigeration system”, Int. J. Refrigeration 28, 1212–1218.

Marchionni G., Avataneo M., De Patto U., Maccone P., Pezzin G., 2005, “Physical properties of four α,ω-dimethoxyfluoropolyethers”, Journal of Fluorine Chemistry, 126, 465–473

Mark M., Stephenson M., Goltsos C. E., 1958, “An evaporative-gravity technique for airborne equipment cooling” Trans. IRE, vol. ANE-5, pp. 47–52

Martinez M., 2009, “130 kW / 200 kVA Starter – Generator and Associated Power Electronics”. Moet forum, Barcelona. Retrieved online at http://www.eurtd.com/moet/proceedings.html

Melo C., Ferreira R.T.S., Boabaid Neto C., Goncalves J.M., Mezavila M.M., 1999, "An experimental analysis of adiabatic capillary tubes", Appl. Therm. Eng. 19, 669–684.

Meyer J., 2008, "R1234yf system enhancements and comparison to R134a". In Proceedings of the 2008 SAE Alternative Refrigerant Systems Symposium, Phoenix, AZ, USA.

Miller R.W., 1996, "Flow Measurement Engineering Handbook (3rd ed)", chapter 5. McGraw-Hill, New York, USA.

Moffat R. J., 1988, "Describing the uncertainties in experimental results", Exp. Thermal Fluid Sc., 1: 3-17.

Mohapatra S. C., Loikits D., 2005, "Advances in liquid coolant technologies for electronics cooling", Annual IEEE Semiconductor Thermal Measurement and Management Symposium, 21st Annual IEEE Semiconductor Thermal Measurement and Management Symposium, p 354-360

Mongia R., Masahiro K., DiStefano E., Barry J., Chen W., Izenson. M., Possamai F., Zimmermann A.; Mochizuki M., 2006, "Small scale refrigeration system for electronics cooling within a notebook computer." Thermal and Thermomechanical Phenomena in Electronics Systems, 2006. ITHERM apos;06. The Tenth Intersociety Conference on Volume , Issue , May 30 2006-June 2 2006 Page(s):751 – 758

Moran M. E., Wesolek D. M., Berhane N. T., Rebello K.J., "Microsystem Cooler Development", 2nd International Energy Conversion Engineering Conference, 16 - 19 August 2004, Providence, Rhode Island

Morten J.S., 2005, SecCool Properties Users Manual, retrieved online on http://www.ipu.dk

Mudawar I., 2000, "Assessment of high heat flux thermal management schemes", Inter Society Conference on Thermal Phenomena

Nielsen O.J., Javadi M.S., Sulback Andersen, Hurley M.P.,, Wallington M.D., Singh R., 2007, "Atmospheric chemistry of $CF_3CF{=}CH_2$: Kinetics and mechanisms of gas-phase reactions with Cl atoms, OH radicals, and O_3". Chemical Physical Letters 439: 18-22.

Ohta H., Morimoto Y., Widiatmo J.V., Wantanabe K., 2001, "Liquid-phase thermodynamic properties of new refrigerants: pentafluoroethyl methyl ether and heptafluoropropyl methyl ether" Journal of Chemical Engineering Data 46(5): 1020-1024.

Pfahler J. N., Harley J., Bau H. H., Zemel J., 1991, "Gas and liquid flow in small channels" Micromechanical sensors, actuators and systems, ASME DSC-32, 49-60

Peng X. F., Peterson G. P., Wang B. X., 1994, "Heat tranfer characteristic of water flowing through microchannels" Experimental heat transfer, 7, 265-283

Pitla S.S., Groll E.A., Ramadhyani S., 2002, "New correlation to predict the heat transfer coefficient during in-tube cooling of turbulent supercritical CO_2", Int. J. Refrig, 25(7): 887-895.

Poling B.E., Prausnitz J.M., O'Connell J.P., 2001, "The Properties of Gases and Liquids", 5th ed. New York: McGraw-Hill, p. 1.6-1.9, 2.2-2.27, 3.1-3.50.

Price D. C., 2003, "A Review of Selected Thermal Management Solutions for Military Electronic Systems", IEEE Trans. on components and packaging technologies, 26, 1

Reeber M.D., Frieser R.G., 1980, "Heat transfer of modified silicon surfaces", IEEE Trans., Vol. 3, pp. 387- 391

Reid R.C., Prausnitz J.M., Poling B.E., 1987, "The Properties of Gases and Liquids", 4th ed. New York: McGraw-Hill, p. 8-10, 12-24, 150-204.

Sathe A. A., Groll E. A., Suresh V. G., 2008, "Experimental evaluation of a miniature rotary compressor for application in electronics cooling", International Compressor Engineering Conference at Purdue, July 14–17, 2008

Scott A.W., 1974, "Cooling of Electronic Equipment", John Wiley and Sons, pp. 204-227.

Shah R. K., London A. L., 1978, "Laminar flow forced convection in ducts", Academic Press, New York

Skuriat R., Johnson C.M., Dietl K., Vasel J., Schmitz G., 2009 , "Thermal Management of Power Electronics in the More Electric Aircraft", Moet forum, Barcelona. Retrieved online at http://www.eurtd.com/moet/proceedings.html

Span R., Wagner W., 1996, "New Equation of State for Carbon Dioxide Covering the Fluid Region from the Triple-Point Temperature to 1100 K at Pressures up to 800 Mpa" J. Phys. Chem. Ref. Data, 25(6):1509-1596.

Spatz M., Minor B., 2008, "HFO-1234yf low GWP refrigerant update". In: Proceedings of the International Refrigeration and Air Conditioning Conference at Purdue, West Lafayette, Indiana, USA.

Stoecker W.F., Jones J.W., 1982, "Refrigeration and air conditioning (2nd ed)", McGraw-Hill, New York, USA.

Suwat Trutassanawin, Eckhard A. G., 2004, "Numerical analysis of a miniature scale refrigeration system (MSRS) for electronics cooling", International Refrigeration and Air Conditioning Conference at Purdue, July 12-15, 2004

Suwat Trutassanawin, Groll, E. A., Garimella S. V., Cremaschi L., 2006, "Experimental investigation of a miniature-scale refrigeration system for electronics cooling" IEEE Transactions on Components and Packaging Technologies, v 29, n 3, p 678-687, September 2006

Tanaka K., Higashi Y., 2009, "Thermodynamic properties of HFO-1234yf (2,3,3,3-Tetrafluoropropene)" In: Proceedings of the 3rd IIR Conference on Thermophysical Properties and Transport Processes of Refrigerants, Boulder, CO, USA.

Tanaka K., Higashi Y., and Akasaka R., 2009, "Measurements of the isobaric specific heat capacity and density for HFO-1234yf in the liquid phase" Submitted to Journal Chemical Engineering Data

Tian J, Kim T, Lu T.J., Hodson H.P., Queheillalt D.T., Sypeck D.J., Wadley H.N.G. 2004, “The effect of topology upon fluid-flow and heat-transfer within cellular copper structures”, Int. J. of Heat and Mass Transfer, 47: 3171-3186.

Tuckerman D.B., Pease R.F.W., 1981, “High performance heat sinking for VLSI”, IEEE Electr. De. Lett. 2, p. 126-129

Wang C.-C., Lee C.-J., Chang C.-T., Lin S.-P., 1999, “Heat transfer and friction correlation for compact louvered fin-and-tube heat exchangers” Int. J. Heat and Mass Transfer, 42: 1945-1956.

Webb L. R., 1981, “Performance evaluation criteria for use of enhanced heat transfer surfaces in heat exchanger design”, Int. J. Heat and Mass Transfer, vol. 24, pp 715-726

Webb R., 2007, “Next generation devices for electronic cooling with heat rejection to air”, ASME Journal of Heat Transfer, vol.127, p. 2-9

Whitesel H.A., 1957, “Capillary two-phase flow”. Refrig. Eng. 65 (9), 35–47.

Wei X., Joshi Y., Patterson M.K., 2007, “Experimental and numerical study of stacked microchannel heat sink for liquid cooling of microelectronic devices”, ASME Journal of Heat Transfer., vol.129, p.1432-1444

Yana Motta S., Braga S.L., Parise J.A.R., 2000, “Critical flow of refrigerants through adiabatic capillary tubes: experimental study of zeotropic mixtures R-407c and R-404a”, ASHRAE Trans. 106 (1), 534–549.

Yang L., Wang W., 2008, “A generalized correlation for the characteristics of adiabatic capillary tubes”, Int. J. Refrigeration 31, 197–203.

Yasumoto M., Ito H., Yamashita S., 1996, “Critical properties of fluorinated ethers”, Journal of Chemical Engineering Data 41(4): 802-805.

Yilmaz T., Unal S., 1996, “General equation for the design of capillary tubes”, ASME J. Fluids Eng. 118 (2), 150–154.

Yoshii Y., Mizukawa S., Widiatmo J.V., Watanabe K., 2000, “Measurements of saturation densities in critical region of pentafluoroethyl methyl ether (245cbEβγ)” Proceedings of the Fourteenth Symposium on Thermophysical Properties, Boulder, Colorado.

Zhang C.L., Ding G.L., 2004, “Approximate analytic solutions of adiabatic capillary tube”, Int. J. Refrigeration 27 (1), 17–24.

Zilio C., Brown J.S., Cavallini A., 2009, “Simulation of R-1234yf performance in a typical automotive system” In: Proceedings of the 3rd IIR Conference on Thermophysical Properties and Transport Processes of Refrigerants, Boulder, CO, USA.

Zimmermann A.J.P., Maciel R.A., 2006, “Discharge pressure optimization for CO_2 transcritical cycle using capillary tube”, In: Proceedings of 11th International Refrigeration and Air Conditioning Conference, Purdue, Indiana, USA, July 15-20.

ACKNOWLEDGEMENTS

This thesis would not have been possible without the kind and significant support and the remarkable patience of my thesis supervisor, Dr Claudio Zilio, to whom I am sincerely grateful for the inspiration and the scientific guidance.

I would like to express sincere gratefulness to a very helpful person, Dr. J. Steven Brown, for all the assistance, patience and important suggestions.

I would also like to thank Professor Fornasieri, Dr. Marco Corradi, and Dr. Luca Cecchinato. Part of this thesis draws from papers co-authored with them and with Dr. J. Steven Brown and Dr. Claudio Zilio.

I wish to thank the many friends I knew during my doctoral course, Manuel Chiarello (I have spent almost 10 years with him, talking about everything, above all about soccer!), Paolo, Wilmer, Valeria, Martina, Giuseppe, Luca, Simone and Manuela: I will miss their company.

Finally, and most importantly, I thank my family for providing support and for the patience through the difficult times. To them I dedicate this thesis.